Imaging and analysis of natural and manufactured nanoparticles

by

Emilia Cieślak

A thesis submitted to
The University of Birmingham
for the degree of
DOCTOR OF PHILOSOPHY

supervisors:
Professor Jamie R. Lead
Professor Roy M. Harrison

School of Geography, Earth and Environmental Sciences
University of Birmingham

~ October 2010 ~

UNIVERSITY OF BIRMINGHAM

University of Birmingham Research Archive

e-theses repository

Abstract

Nanotechnology, a new science discipline, which studies design, characterization, production and applications of materials with sizes 1-100 nm, has marked a new breakthrough in technological development. It promises to revolutionise many aspects of modern life. However, with increasing markets and industrial scale of production, nanomaterials (NMs) became a potential, but largely unknown, risk to human health and the environment. Carbon based NMs including carbon nanotubes (CNTs) and fullerenes are an important class of NMs and are further studied in this thesis.

Potential fate and behaviour of single-walled CNTs (SWCNTs) was investigated in natural waters using transmission electron microscopy (TEM) and atomic force microscopy (AFM). There was a focus on CNT interactions with natural aquatic colloids along with the impacts of other solution conditions at environmentally relevant levels. Similar research on fullerenes C_{60} was also undertaken, as a part of a wider study investigating fish ecotoxicology of fullerenes. Nanoscale atmospheric particles were imaged and analysed with AFM. Additionally, a pilot study on metal speciation in $SWCNT_{aq}$ was conducted to determine partitioning of Ni, Y, Cd, Cu and Cr between particle-bound, labile and dissolved fractions with a view to better understand the role of SWCNTs in trace metals binding (and thus influencing their transport, chemistry and bioavailability).

The results indicate that SWCNTs in aquatic systems are likely to interact with natural nanoscale material. The experiments showed that SWCNTs in aqueous suspensions are stabilised with humic acid (probably by surface coating formation) and precipitated by divalent cations, while monovalent cations did not exhibit such destabilising effects. 95-100 % of yttrium (catalyst residue) was retained by the ultrafiltration membrane at all studied conditions indicating its particulate or particle-bound speciation. On the other hand, the majority of chromium was dissolved. In general, the presence of humic acid decreased dissolved and labile metal species whereas Ca^{2+} had the opposite effect. Comparison of TEM and AFM results showed that both techniques are suitable to study suspended SWCNTs and produced consistent and complementary quantitative and qualitative results. An improved protocol (involving ultracentrifugation) for TEM specimen preparation was tested with aqueous suspensions of SWCNTs and nC_{60}. It shortened the analysis time and improved reproducibility.

The results show that fullerenes form very stable aqueous suspensions. However, the majority of the dispersed C_{60} occurs in microscale, rather than nanoscale aggregates, with only ca. 2% of material by mass between 1 and 100 nm. Visualisation of C_{60} in the presence of natural aquatic colloids did not show such strong interactions as in case of SWCNTs.

Two analysed size fractions of atmospheric nanoparticles collected with an inertial impactor proved to be significantly contaminated with particles in the size range of 1-10 nm, which was attributed mainly to the diffusive mechanism of impaction for the imaged material.

Acknowledgements

Firstly, secondly and thirdly, I would like to thank my supervisor Professor Jamie Lead. To the best of my knowledge, you've been the only person who always believed that this thesis will see its successful viva. You provided me with ideas, scientific expertise, guidance, help, support and encouragement.
Thank you.

Great thanks to many people who lent me their brains. Mohammed Baalousha, Nadia Palaniswamy, Anna de Momi, Julia Fabrega, Adriana Manciulea, Sue Cumberland... I am very happy I've met you. (And your brains.)

Table of Contents

LIST OF FIGURES

Chapter 2

Chapter 3

Chapter 5

Chapter 6

LIST OF TABLES

NOMENCLATURE

Acronym	Definition
AFM	atomic force microscopy
CCD	charge coupled device
CNTs	carbon nanotubes
DBL	diffusive boundary layer
EDL	electric double layer
EM	electron microscopy
ETEM	environmental transmission electron microscopy
IHSS	International Humic Substances Society
LIBD	laser induced breakdown detection
MOUDI^{TM}	micro-orifice uniform-deposit impactor
NAC	natural aquatic colloids
NMs	nanomaterials
NMWL	nominal molecular weight limit
NOM	natural organic matter
NPs	nanoparticles
NW	natural water
PEC	predicted environmental concentration
PHA	Pahokee peat humic acid
PNEC	predicted no effect concentration
QD	quantum dots
SEM	scanning electron microscopy
SG	succinoglycan
SRFA	Suwannee River fulvic acid
SRHA	Suwannee River humic acid
SWCNTs	single-walled carbon nanotubes
TEM	transmission electron microscopy
TOC	total organic carbon
UHP	ultra high purity
UHV	ultra high vacuum

Symbol	Definition
C	concentration of metal in the bulk solution
d	diameter
D	diffusion coefficient
$d_{\pm}$	half-width of the confidence interval
d_{ae}	aerodynamic diameter

dC/dx	concentration gradient
F	force
f_0	resonant frequency
$f_{non\text{-}contact}$	vibration frequency of the cantilever in the non-contact mode
$f_{tapping}$	vibration frequency of the cantilever in the tapping mode
J	flux of ions
k	spring constant of the cantilever
n	count
n_{min}	minimum sample size
r_{max}	distance from the rotor axis to the bottom of the sample
r_{min}	distance from the rotor axis to the surface of the sample
s^2	estimate of the population variance
t	time
$t_{\alpha(2),(n-1)}$	two-tailed critical value of Student's t with n-1 degrees of freedom
x	deflection of the cantilever
$\Delta A_{non\text{-}contact}$	decrease in the oscillation amplitude of the cantilever in the non-contact mode
$\Delta A_{tapping}$	increase in the oscillation amplitude of the cantilever in the tapping mode
Δg	thickness of the diffusive gel

Greek characters	**Definition**
ŋ	solution viscosity
δ	thickness of the diffusive boundary layer
ρ	density of the particle
ρ_0	density of the suspension

1 INTRODUCTION

1.1 Introductory remarks

Nanoparticles (NPs), defined as entities with more than one dimension in the range 1-100 nm [ASTM, 2006], have been present in the environment for millions of years [Christian et al., 2008]. They are produced in large numbers in commonplace natural processes such as weathering of rocks, volcanic eruptions, biodegradation of organic matter in soils and water [Nowack and Bucheli, 2007]. For the last few decades, substantial quantities of fine particles have been released into the atmosphere as by-products of fossil fuel burning and other industrial processes [SCENIHR, 2006].

Recently NPs have become scientifically and technologically very topical and have been regarded as a foundation of the 'Third Industrial Revolution' [Yih and Talpasanu, 2008]. The reason for this is that only recently science has matured enough to study and, most importantly, manipulate matter at the nanoscale [SCENIHR, 2006]. Engineered NPs emerged as a new type of materials with a multitude of fascinating and desired properties. Novel properties of nanomaterials (NMs), such as high reactivity and large specific surface area, are a result of their nanoscale dimensions. These unique characteristics can be (and in some cases already are) utilised in countless applications in cutting-edge technology and medicine. Potential benefits of nanotechnology are impressive and widely recognised [EPA, 2007]. Moreover, some NMs and their applications promise new significant advances in environmental sustainability of technological development [Council for Science and Technology, 2007].

However, concern has been raised that release of NPs in the environment will pose significant risks to human health and ecosystems [Roco, 2005]. This risk is hugely

unknown and poorly characterised. Very little is known about toxicity, ecotoxicity and fate and behaviour of NPs in the atmosphere, water and soil [National Nanotechnology Initiative, 2006]. Nevertheless, the apprehension towards potential negative effects of nanotechnology is additionally fuelled by what is already known about natural and incidental anthropogenic fine particles. Although extremely small, they play a vital role in natural waters, by controlling nutrients, pollutants and pathogens [Lead et al., 1999; Buffle, 2006; Lead and Wilkinson, 2006A]. Through epidemiological studies atmospheric particulate matter has been correlated with respiratory and cardiovascular mortality [Samet et al., 2000; Brook et al., 2004].

Consequently, research and development on applications of NPs has to be coupled with toxicological, environmental and exposure studies. Human and environmental health implications of nanotechnology are among the most important research priorities of the scientific community, governments and industry in order to protect health and to underpin a sustainable nanotechnology industry [EPA, 2007].

Properties of NPs depend on many parameters (chemical composition, size, shape, synthesis protocol, surface coating, etc.). Even materials sold under the same product name can significantly differ among various batches. For this reason, there is a general consensus that particles used in toxicological and environmental experiments have to be carefully characterised [EPA, 2007; SCENIHR, 2009]. Solid and reliable information on particle characteristics is also crucial to explain and underpin the mechanisms of observed effects and behaviour. Careful characterisation of a studied material allows comparison between (eco)toxicological data among various types of NPs, which is expected to aid future research and legislation by NPs categorisation [Stone et al., 2010].

Characterisation of NMs that could properly serve the aforementioned purposes is a challenging analytical task. Examination of nanoscale particles requires sensitive techniques with powerful resolution or very low limits of detection. NPs tested in toxicological and environmental studies are usually bound in complex matrices (such as exposure media or body tissues), which strongly depend on sample physicochemistry and which behaviour may be dynamic (e.g. govern by aggregation/disaggregation processes) [Domingos et al., 2009C]. The majority of existing techniques for NP characterisation and quantification have been adapted from studies on aquatic colloids or atmospheric fine particles. However, most of these techniques still require further development, optimisation and verification to overcome their limitations, e.g. sample modification by the analytical protocol [Lead and Wilkinson, 2006]. In general, to advance the risk assessment of emerging NMs, there is an urgent need for a standardised characterisation methodology including the list of properties to be examined, choice of analytical methods and their protocols as well as data processing and interpretation.

In this work various characterisation techniques (such as TEM, AFM, ICP-MS, etc.) were successfully employed to characterise natural and engineered NPs. Single-walled carbon nanotubes (SWCNTs) and fullerene C_{60} were extensively imaged in aqueous suspensions to study their morphologies qualitatively and quantitatively. To the best of my knowledge, this thesis is the first to present detailed morphological characterisation of different size fractions of water-stirred fullerenes. Additionally, the imaging techniques have been applied in an extensive study of engineered − natural aquatic NPs interactions in natural aquatic systems to advance the knowledge on the fate and behaviour of engineered NPs in the environment. Moreover, an improved

protocol for TEM specimen preparation for these samples has been proposed and successfully tested to provide more accurate analysis, better reproducibility of the results and additional quantitative information. Furthermore, one of the chapters addresses the issue of metal contamination in aquatic environment as influenced by the presence of carbon nanotubes. A protocol has been proposed and tested to determine how SWCNTs may impact the amounts of dissolved and bioavailable trace metals.

1.2   Aims and objectives

The overall aim of this project is to examine the interactions of engineered and natural NPs to better understand the fate and behaviour of engineered NPs in the environment and thus advance the knowledge on possible risks of nanotechnologies to human health and ecosystems. This goal is to be achieved by application of existing techniques to characterise engineered NPs and study them in environmentally relevant matrices. These techniques should be tested for their suitability to study engineered NPs in environmental studies and optimised to provide best possible quality of the data.

The specific objectives of this study include:

1)

Visualisation and quantification of engineered NPs (SWCNTs, fullerene C_{60}), natural aquatic NPs (such as humic substances, polysaccharides, natural water) and atmospheric incidental[*] NPs at environmentally relevant conditions (including a range of pH values, presence of ubiquitous cations)

2)

Examination of engineered NPs (SWCNTs, fullerene C_{60}) in aqueous suspensions in the presence and absence of natural aquatic colloids (such as humic substances, polysaccharides, natural water) and under environmentally relevant conditions (including a range of pH values, presence of ubiquitous cations) to better understand the impacts of ubiquitous natural water components on engineered NPs behaviour (e.g. stability)

---

[*] Incidental (adventitious) atmospheric NPs are released as by-products of human activities such as combustion of fossil fuels (in vehicles and energy generation) and industrial processes. More information on natural and incidental atmospheric NPs is provided in sections 2.2.1 and 2.2.1.2.

3)

Testing and optimisation of existing microscopy protocols to assist characterisation of engineered NPs in natural waters with a view to providing possibly most reliable and reproducible quantitative and qualitative data

4)

Analysis of metal speciation in aqueous suspensions of NPs (SWCNTs) to better understand the role of NPs in trace metal chemistry (bioavailability, toxicity and transport) in natural waters

1.3   Thesis synopsis

Chapter 2 contains an introduction to the issue of NPs and nanoscience. The most popular types or NMs, such as carbonaceous, metal, metal oxides NPs and quantum dots, are presented with an emphasis on their most important properties as well as present and proposed future applications. A separate section (2.1.3) is devoted to currently known toxic and ecotoxic effects of NPs, mainly carbon nanotubes, fullerenes and silver NPs. Later engineered NPs are put in the context of natural and incidental particulate matter. A summary of the current knowledge on environmental fate and behaviour of NPs follows.

The details of materials used throughout the experimental work are gathered in chapter 3. This chapter also explains the protocol used to obtain the stock suspensions and solutions. Further dealing with these stock materials depended on the laboratory work so remaining protocol details are distributed among the chapters with the results accordingly to their relevance. Also in chapter 3 all used analytical techniques are presented and discussed in detail.

The subsequent six chapters present the experimental results with their interpretation. Chapter 4 presents the results of AFM characterisation of atmospheric NPs collected with a cascade inertial impactor. AFM height measurements were used to obtain size distribution histograms.

Chapter 5 contains a study on the interactions between single-walled carbon nanotubes (SWCNT) and natural aquatic colloids (NAC) including Suwannee River humic acid, Pahokee peat humic acid, succinoglycan and natural lake water at different values of pH as well as the presence/absence of sodium and calcium cations. Samples

were analysed with TEM and average bundle thicknesses for all samples were calculated. The formation of nanoscale films is discussed.

TEM specimen preparation protocol was expanded by adding an ultracentrifugation step and tested on aqueous suspensions of SCWNTs and fullerenes C_{60} in the presence/absence of NAC. The results are presented in chapter 6.

TEM analysis of SWCNTs in natural waters from chapter 5 was complemented with AFM imaging. The results are discussed in chapter 7. To quantify the comparison between the two techniques, average bungle heights were measured and weighed against TEM bundle thicknesses. Additionally, comparison between AFM tapping and non-contact modes is presented.

Chapter 8 is devoted to a pilot study into metal speciation in aqueous suspensions of SWCNTs. Five metals (Ni, Y, Cu, Cd, and Cr) were measured in 3 different size fractions: in the original samples, in 1.2 μm filtrates and in 1 kDa ultrafiltrates. To measure the labile metal fraction, the diffusive gradients in thin films (DGT) technique was employed.

Chapter 9 presents the particle characterisation which was conducted for the water-stirred $C_{60.}$ This characterisation underpinned a toxicogenomics study after exposure to fish. Concentrations of 4 different size fractions were estimated with UV-Vis absorption spectra. TEM imaging was used to study morphologies and size distribution of five size fractions and number concentrations were estimated where feasible.

Chapter 10 contains final conclusions and recommendations for future work.

Appendix (companion CD) contains all TEM and AFM images used throughout the experimental work.

2   BACKGROUND

2.1   Applications and implications of engineered nanomaterials

2.1.1   Introduction to nanotechnology and nanomaterials

Being just a few decades old, nanoscience has already revolutionised almost all traditional science disciplines, including chemistry, engineering, physics, materials science, biology, medicine and environmental sciences [Yih and Moudgil, 2007]. It is also referred to as a key scientific discipline, which will help to launch the Third Industrial Revolution [Yih and Talpasanu, 2008].

Nanoscience studies matter at the nanoscale, i.e. when at least one dimension is in the range 1-100 nm [PAS, 2005; ASTM, 2006; ISO, 2008]. Nanoscience has led to the emergence of nanotechnology, which is claimed to be the basis of the most important technological innovations of the 21st century [Roco, 2006]. This promising prognosis derives from the fact that already well known materials show completely different and often fascinating properties when studied at the nanoscale.

To illustrate such changes, gold NPs will be used as an example here. The way of preparation of 'two-phase aqueous gold' (and other metals) colloids was introduced by the pioneering studies of Faraday as early as in 1857, when he studied optical properties of gold [Faraday, 1857]. The subject of colloidal gold received substantial scientific attention, especially in the last 10-20 years [Dykman et al., 1996; Hernández-Santos et al., 2000; Dobrovolskaia et al., 2009]. Gold NPs proved to be an effective catalyst, although in bulk gold is one of the most inert elements in the periodical table. For instance, when immobilised on a surface of TiO_2, nanosize gold particles can serve as a very active and selective catalyst for carbon monoxide oxidation at room

temperature, as long as the size of gold NPs does not exceed 8 nm in diameter [Campbell, 2004]. The chemical reactivity of gold is strongly size dependent and for this reaction the best performance is seen for particles 2-3 nm in size [Lopez et al., 2004]. Not only does the reactivity of gold change considerably when entering the nanoregime but its colour turns from yellow to pink, red or blue indicating major changes in optical properties [Cortie, 2004]. What is more, non-toxic bulk gold can become potentially harmful when the particle size reaches 2 nm because such small NPs have been proved to bind to the DNA groove potentially affecting its structure and function (Fig. 2.1) [Tsoli et al., 2005].
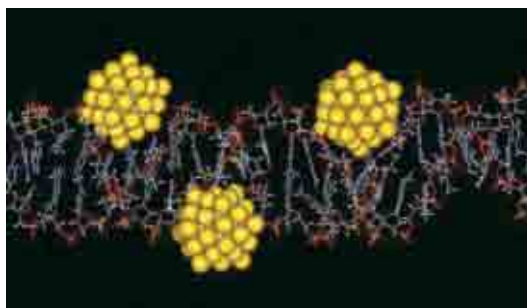
Figure 2.1. Molecular model of B-DNA combined with Au55 clusters irreversibly attached to the major grooves [Tsoli et al., 2005].

Such drastic changes in properties can be explained by an extremely large specific surface area per unit mass, e.g. 1000 m^2g^{-1} for nanoporous crystalline MgO [Dohnálek et al., 2002], 866 m^2g^{-1} for aerogel silica NPs [Wang et al., 2005A]. Secondly, at the nanoscale, quantum phenomena govern the behaviour of materials, resulting in different chemical, mechanical, electrical, optical, thermal and magnetic properties. Quantum effects are characteristic for matter at atomic and subatomic scale and cannot be explained by the laws of Newtonian mechanics and classical electromagnetism. They include:

- discretization of certain physical quantities, e.g. energy of electrons on atomic orbitals;

- detectable wave-particle duality, i.e. particles can behave like waves and waves can behave like particles;

- Heisenberg uncertainty principle, i.e. a position and momentum of an electron cannot be calculated precisely but only with certain probability, the more accurate calculation of momentum, the less accurate calculation of the position and vice versa;

- quantum entanglement, i.e. quantum states of two or more objects have to be described with reference to each other, even though the individual objects may be spatially separated.

Due to novel properties, so far NMs have found numerous industrial and commercial applications including production of sunscreens and cosmetics, home care products, food packaging, paints and textiles, computers and electronic devices, composites, clays, coatings and surfaces, tougher and harder cutting tools and others. The number of nanotechnology consumer products already on the market worldwide rocketed in the last 5 years and in 2009 exceeded a thousand [Rejeski, 2009 A; Project on Emerging Nanotechnologies, 2009]. Future applications of NMs are expected to be in a broad range of industries such as electronics and communications, chemicals and materials (especially as catalysts improving energy and combustion efficiency), pharmaceuticals, healthcare, precision engineering, energy technologies (batteries, solar cells), space exploration, remediation and water purification [Allianz & OEDC, 2005; Council for Science and Technology, 2007].

Nano-related products sold worldwide in 2009 were worth an estimated $224 billion [PCAST, 2010]. It is undoubtedly one of the most rapidly expanding markets predicted to reach $ 1 trillion/year worldwide by 2015 [Aitken et al., 2006] and $3 trillion/year by 2018 [Global Industry Analysts, Inc., 2008]. Global consumption already in millions of tonnes per annum (over 9 million metric tonnes in 2005) is expected to rise dramatically in the coming years [BCC Research, 2005; Powell et al., 2008; Delgado, 2010].

2.1.2   Types of manufactured nanomaterials

Manmade NMs come in a variety of shapes and forms:

- with one dimension in the range 1-100 nm (e.g. Fig. 2.2 g): nanostructured films, coatings and nanosheets e.g. titanium nitride coating used for cutting tools to improve their performance and durability [Nanofilm Technologies International Pte Ltd.], polymer reactive self-assembling nanofilms used as protective coatings for ophthalmic lenses [Nanofilm Company].

- with two dimensions in the range 1-100 nm (e.g. Fig. 2.2 a-d): nanowires (metallic, semiconducting or insulating) and nanotubes (single-, double- or multi-walled) made of carbon or inorganic materials such as oxides, nitrides, carbides, chalcogenides, phosphides and others [Rao et al., 2004].

- with three dimensions in the range 1-100 nm (e.g. Fig. 2.2 e, f and h): spheres, cubes, rods, capsules, pyramids and many others [Nagarajan and Hatton, 2008].
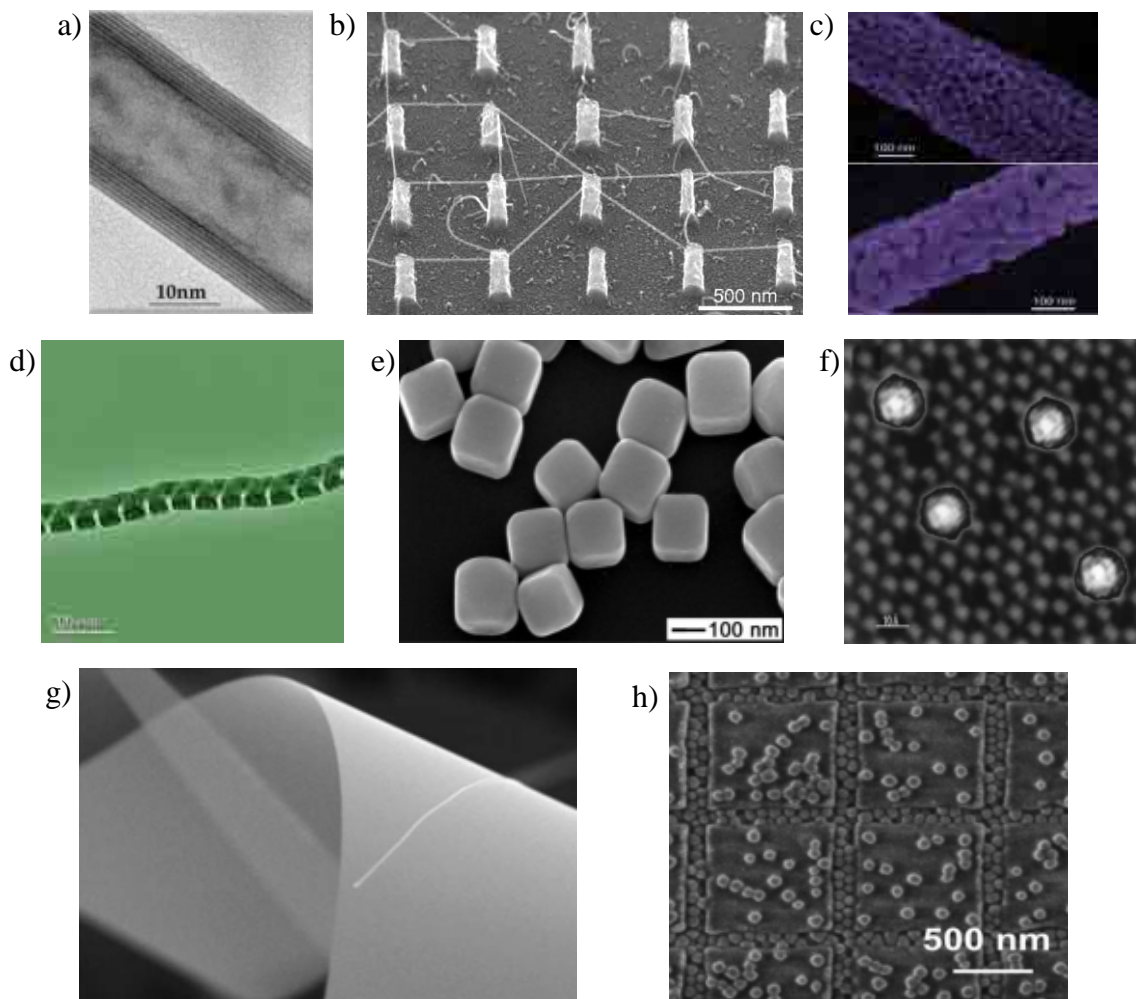
Figure 2.2. Examples of engineered NMs: a) TEM image of a tungsten sulphide multi-walled nanotube [Rosentsveig et al., 2002]; b) SEM image of CNT grown on Si pillars [Homma et al., 2002]; c) SEM image of porous gold nanowires [Ji and Searson, 2002]; d) TEM image of a helical SiO_2 nanospring [Zhang et al., 2003]; e) SEM image of silver nanocubes [Sun and Xia, 2002]; f) STM image of fullerene C_{60} molecules on Si surface [Hou et al., 1999]; g) SEM image of ZnO nanosheet [Park and Park, 2006]; h) SEM image of SiO_2 NPs [Maury et al., 2008].

However, most commonly manmade NPs are categorised according to the core material they are made of. Nevertheless, diversity of NPs and their physico-chemical properties within the same material group can be astonishing. Differences usually encompass different size ranges and their homogeneity/heterogeneity, varied shapes and crystal or amorphous structure. Additionally, properties of the same NPs can be significantly altered by means of surface coating (e.g. polymer-coated magnetic NPs for

biomedical applications [Figuerola et al., 2010]), surface functionalization (e.g. surface carboxylation of CNTs to improve solubility in polar solvents [Foldvari and Bagonluri, 2008]), and chained capping agents (e.g. long-chain acids used in the synthesis of cobalt NPs [Lu et al., 2008A]).

Depending on the material they are made from, there are two main groups of NMs:

• carbon-based NPs: carbonaceous NPs (e.g. fullerenes, carbon nanotubes) and nano-polymers.

• inorganic NPs: metal (e.g. silver, gold , iron) and metal oxides (e.g. iron oxide, titanium dioxide, zinc oxide, cerium oxide) as well as quantum dots (e.g. cadmium sulphide or selenide) [Ju-Nam and Lead, 2008].

Some of the most common and well-studied NPs will be discussed in more detail below.

Carbon-based nanoparticles

The discovery of a new carbon allotrope (in addition to diamond and graphite), a buckminster fullerene molecule (C_{60}) in 1985 was awarded the Nobel Prize in Chemistry in 1996 (the prize went to H. Kroto, R. Curl and R. Smalley). Also known as a buckyball or fullerene C_{60}, it is built of exactly sixty atoms of carbon organised in interlocking hexagons and pentagons arranged in a symmetrical spherical shape (Fig. 2.3 a). From the very beginning the molecule of C_{60} attracted substantial scientific attention and subsequently fullerenes with different numbers of carbon atoms were synthesised. Among different ring sizes ranging from C_{20} (buckyball clusters) to C_{120} [Cozzi et al., 2005] the most common include C_{60}, C_{70} (Fig. 2.3 b), C_{76}, C_{78} and C_{84}.

Many promising practical applications of fullerenes have been suggested in the scientific literature, including formulation of superlubricants, drug delivery systems, new fuels, superconductors, new classes of rechargeable batteries [Wilson et al., 1992; Hughes, 2005]. Most of these proposals are still in the early stages of development. Current commercial fullerene products include mainly cosmetics where fullerenes act as antioxidants [Project on Emerging Nanotechnologies, 2009].
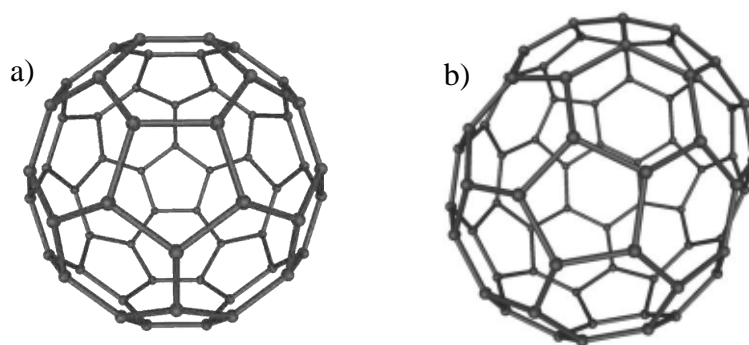
Figure 2.3. a) fullerene C_{60} b) fullerene C_{70} [by Michael Ströck]

CNTs are another very important and well-studied group of carbonaceous NPs. Due to their distinctive properties such as fluorescence [O'Connell, 2002], extremely high tensile strength (even over 60 GPa) [Yu et al., 2000] elastic modulus in the range of 1 TPa [Esaw and Farag, 2006], electric conductivity many times higher than copper or, depending on structure, comparable with silicon (i.e. semi-conductive) [Hamada et al., 2002] CNTs have found numerous potential industrial and commercial applications as well as biomedical applications in diagnostics and therapeutics [Paradise and Goswami, 2006; Tran et al., 2009].

CNTs (also called fullerene nanotubes) are long thin cylinders made of one-atom thick graphene sheets consisting of carbon atoms laid in hexagons. The graphene sheets can be rolled in 3 different directions: along the two symmetry axes or along non-

symmetrical axis. In the two former cases either an armchair or zigzag nanotube will be formed (Fig. 2.4 a and b), in the latter case a chiral nanotube will be obtained (Fig. 2.4 c). According to their structure carbon nanotubes can be also classified into two groups: single-walled CNTs (SWCNTs) and multi-walled CNTs (MWCNTs). The former are composed of a single graphene cylinder (Fig. 2.4 d) while multi-walled contain two or more concentric graphene layers (Fig. 2.4 e). Additionally, nanotubes can be closed or opened at the ends. Diameters usually range from 1-2 nm for SWCNTs to 8-50 nm for multi-walled ones. Diameter-to-length ratio can be as high as over 100 million [Wang et al., 2009].
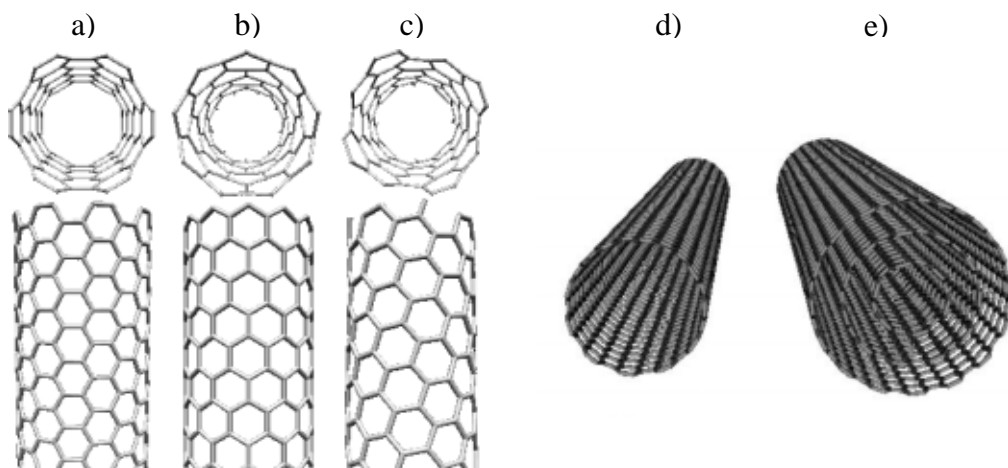
Figure 2.4. Carbon nanotubes. a) armchair b) zigzag c) chiral d) single-walled e) multi-walled (sources: http://www.nano-enhanced-wholesale-technologies.com and http://www-ibmc.u-strasbg.fr).

Currently CNTs are used in composite materials to increase their strength while maintaining low mass at the same time. The most popular applications include bicycle parts, sports equipment, aircraft components and electronics for computers [Project on Emerging Nanotechnologies, 2009].

Other forms of carbonaceous NPs include nano-diamond [Grichko and Shenderova, 2006], nano-onions [Bing-she, 2008], capsules [Sun and Li, 2005], C_{60} rings [Li et al., 2001], C_{60} dimers [Hingston et al., 2006].

Metal nanoparticles

Being presently used in over 300 consumer products, silver NPs are the most commonly exploited NM at the moment [Rejeski, 2009 B; product inventory of the Project on Emerging Nanotechnologies, 2010]. The primary function of silver NPs in these applications is antimicrobial activity of colloidal Ag. Possible future utilization of silver NPs in medicine is very promising, especially in the light of the rising number of pathogens that have developed resistance to antibiotics, which in case of silver NPs seems unlikely thanks to their broad range of targets attacked in microbes [Rai et al., 2009]. On the other hand, high volumes of produced silver NPs and low concentrations in antimicrobial applications may promote resistance against Ag NPs [Percival et al., 2005; Chopra, 2007]. Most often the proposed applications in the healthcare sector embrace coating of tools, devices and implants, dental alloy and wound dressings [Chen and Schluesener, 2008].

Although the disinfectant properties of silver and its ions have been known for centuries and silver NPs have been extensively studied by numerous researchers in the last two decades, their exact mechanism of action is still a subject of scientific debate [Rai et al., 2008]. Very limited information on human toxicity is available, which raises concerns on the safety of the still growing number of commercial products already on the market [Chen and Schluesener, 2008].

Apart from bactericidal action, there are also other proposed applications, which make use of the unique properties of silver NPs such as conductivity, catalytic activity, chemical stability and non-linear optical behaviour [Capek, 2004].

Zero-valent iron (ZVI) NPs have earned a reputation of a useful agent in bioremediation. Because of their large surface area they are very reactive. In the presence of water and oxygen they are easily oxidised (i.e. a thin iron oxide coating is formed) and act as reducing agents (mainly towards organic pollutants) and adsorbing agents (towards metals and other pollutants) [Zhang, 2003; Noubactep, 2009; Cundy et al., 2008; Dickinson and Scott, 2010]. The list of harmful chemicals that could be removed from soil and groundwater with the help of iron NPs includes polychlorinated biphenyls, chlorinated and brominated organic solvents, organochlorine pesticides and dyes [Zhang, 2003; Cundy et al., 2008; Huang et al., 2008]. These technologies offer in-situ treatment at relatively low costs [EPA, 1998].

Earlier in this chapter (section 2.1.1) colloidal gold was used as an example of how entering the nanoregime changes properties of materials. Size-dependent properties of nanogold are of interest in many scientific disciplines, such as electronics, magnetism, optics, medicine, biology and material science [Daniel and Astruc, 2004]. Gold NPs are the most stable among metal NPs. Possible future applications, which have attracted most attention and publicity, include cancer diagnosis and therapy [Service, 2005; Peng et al., 2009]. Oncological uses for gold NPs encompass photothermal therapy of malignant tumours, bioimaging and nuclear targeting [Huang and El-Sayed, 2010; Kang et al., 2010]. Bio-conjugated gold NPs can be used for highly

sensitive and selective DNA detection, which could revolutionise biodiagnostics of hundreds of pathogens such as anthrax, small pox and HIV [Panyala et al., 2009].

Metal oxide nanoparticles

There are a number of types of iron oxide NPs: magnetite Fe_3O_4, hematite α-Fe_2O_3, maghemite γ-Fe_2O_3, ε-Fe_2O_3, β-Fe_2O_3, ferrous oxide (wüstite) FeO, etc. [Wu et al., 2008]. Although they occur in nature in high concentrations [Ju-Nam and Lead, 2008], many efficient ways to synthesise shape specific, monodisperse and stable iron oxide NPs have been proposed [Cushing et al., 2004; Park et al., 2004; Wang et al., 2005B]. Superparamagnetic, ferromagnetic and magneto-resistive properties of iron oxide NPs attracted extensive scientific interest [Xiong et al., 2008]. Magnetic properties combined with generally low toxicity makes them ideal for biomedical applications as contrast agents in magnetic resonance imaging, cell delivery systems and gene therapy [Mornet et al., 2006; Barnett et al., 2007; Medarova et al., 2007].

Titanium dioxide occurs in nature in three main polymorphs: anatase, rutile and brookite. Due to its excellent opacifying and light refraction properties it is most widely used as a white pigment in food, cosmetics, paints, paper and plastic industries. Nanosize anatase TiO_2 received much attention for its potential applications in photocatalysis, gas sensors, solar cells and electronic devices, while the rutile form, thanks to its high dielectric constant and high electrical resistivity, can be the material of choice for capacitors, filters, power circuits and temperature compensating condensers [Huang et al., 2006; Qiu and Kalita, 2006]. One of the most common use of titanium dioxide NPs in commercial products already on the market results from their excellent

ultraviolet radiation filtering properties, which are utilized in sun-blocking cosmetics [Project on Emerging Nanotechnologies, 2010]. The introduction of TiO_2 (and ZnO) NPs instead of their bulk counterparts was an important breakthrough in the sunscreen industry [Nohynek et al., 2008]. Retaining high UV protection but at the same time offering high visible light transparency, NPs solved the problem of unsightly white smudges left by traditional lotions as well as improved their viscosity and blending into the skin [Newman et al., 2009].

As has been mentioned above, along with TiO_2, zinc oxide NPs are widely used in cosmetics as sun blocking agents [Mitchnick et al., 1999; Nohynek et al., 2008]. Semiconducting properties of nanosize ZnO, with a band gap that can be tuned with particle size, aggregation behaviour, shape and surface modifications, could find many useful applications in design and manufacturing of optoelectronic devices [Carnes and Klabunde, 2000; Andelman et al., 2005; Moleski et al., 2006]. Antibacterial action of ZnO NPs is used in creams, lotions and ointments [Li et al., 2008C] and is more effective in case of smaller diameters [Padmavathy and Vijayaraghavan, 2008]. ZnO NPs have also been proposed as a catalyst in the remediation process of water contaminated with petrol additives [Eslami et al., 2008]

Cerium oxide (ceria) NPs are known for their catalytic properties. $Cu-CeO_2$ nano-composites are used in air pollution control (CO oxidation) with better efficiency than platinum and Cu/Au/Ni-ceria catalyst systems are employed in hydrogen production processes [Liu, 2005]. Similarly to titanium and zinc oxides, CeO_2 NPs show excellent UV radiation absorption activity and UV-Vis transparency and were

proposed to be used in sunscreens (doped with different metals) [Yabe and Sato, 2003; Song et al., 2006]. There are also numerous reports that nanosize CeO_2 protects cells against oxidative stress [Schubert et al., 2006; Das et al., 2007, Niu et al., 2007].Very exciting findings were published for possible protection and treatment of photoreceptor cells (in retina), whose light-induced degeneration causes vision loss [Chen et al., 2006].

Quantum dots

With sizes below 10 nm (usually 1-2 nm), quantum dots (QDs) are among the smallest NPs and are sometimes called artificial atoms. They are made of semiconductor materials, usually chalcogenides (selenides or sulphides) of metals like cadmium or zinc. QD are expected to be used in the future in quantum computing, which could be applied to some calculations unfeasible for the traditional computer [Dong and Cao, 2009]. Another potential useful application is proposed in photovoltaic cells technology, where QDs may improve their efficiency and lower the costs [Conibeer et al., 2008]. In biomedical disciplines QDs could be exploited in diagnostic, imaging and drug delivery [Azzazy et al., 2007]. However, applicability of QDs in life sciences at the moment is limited by the toxicity of the metals they contain and poor solubility in water [Jamieson et al., 2007].

2.1.3 Toxicity and ecotoxicity of engineered nanoparticles

Recent advances in nanoscience and nanotechnology have aroused hopes for revolutionary technological developments and attracted massive investments from both governmental and private sectors. Consequently, NMs, already produced on an

industrial scale, are likely to enter the environment. In its report from March 2007, the UK Council for Science and Technology emphasises that many NMs do not pose new risks for human health and the environment. Nevertheless, there have been numerous studies giving evidence that some NPs may be toxic to humans or to environmental biota.

Carbon nanotubes

No more than 10 years after their discovery, CNTs were first compared to carcinogenic asbestos because of their similar fibrillar shape [Service, 1998; Sealy, 2008; Poland et al., 2008]. Indeed, there are numerous studies showing adverse respiratory health effects of CNTs. Lam et al. (2003) found that when they reach the lungs, SWCNTs can be significantly more toxic to mice than carbon black and quartz particles. Three different types (in terms of production process and contamination with residues of metallic catalysts) of nanotubes in two doses (0.1 and 0.5 mg per animal) were administered by a single intratracheal instillation and lung tissue was histopathologically examined 7 or 90 days after the exposure. All studied CNT products caused dose-dependent epithelioid granulomas and in some cases they also induced an inflammatory reaction, which was even more profound after 90 days. In another study SWCNTs have been found toxic to rats when intratracheally instilled [Warheit, 2004]. Mortality of 15 % within 24 hours after 5 mg/kg dose exposure was observed and was explained by the mechanical blockage of the upper airways rather than inherent pulmonary toxicity of the nanotubes themselves. However, there were concerns that the intratracheal instillation (and high dose) as an exposure method is physiologically irrelevant and can produce artifactual results due to high aggregation of nanotubes being

delivered to the respiratory tract [Donaldson et al., 2006]. Nevertheless, inhalation studies in rodents confirmed the previous results. In fact, aerosolized SWCNTs used in exposure studies in mice proved to be even more effective in causing inflammatory response, oxidative stress, collagen deposition, fibrosis and gene mutations than the same dose of SWCNTs administered by aspiration [Shvedova et al., 2008]. Pathogenic, length-dependent behaviour (inflammation and granulomatous lesion) towards mesothelial lining of the body cavity of mice (used to mimic human chest tissue, where malignant mesothelioma, cancer caused by asbestos, occurs) was also reported for long (> 20 µm) MWCNTs [Poland et al., 2008]. No effect was observed in case of short MWCNTs (< 5 µm). Nevertheless, although long MWCNTs caused inflammation and asbestos-like behaviour, the study does not answer the question if CNT exposure could result in lung cancer. This question was addressed by another research group in a 24-month bioassay study in rats, whose peritoneal cavity was injected with a single dose of two kinds of MWCNTs and blue asbestos [Muller et al., 2009]. After two years, only the group exposed to asbestos developed tumours and both groups treated with nanotubes did not show a clear carcinogenic response, which may possibly be attributed to the fact that both kinds of nanotubes used in the study were relatively short (< 1 µm on average). In conclusion, the hypothesis of CNTs being the next asbestos is still under investigation and it is still unclear what is their exact respiratory toxicity and carcinogenic status.

A number of studies have shown dermal toxicity of CNTs and this toxicity was caused by accelerated oxidative stress. Cultured human skin cells were treated with SWCNTs, which resulted in ultrastructural and morphological changes and reduced cell viability [Shvedova et al., 2003]. Water-soluble purified functionalised SWCNTs at

concentrations of 0.05-50 mg L^{-1} caused inflammatory response in human epidermal keratinocytes and penetrated intracytoplasmic vacuoles at the higher dose [Zhang et al., 2007]. More recently, in-vitro (engineered skin, murine epidermal cells) and in-vivo (mice) dermal toxicity of purified and unpurified (containing 30% of iron) SWCNT has been investigated [Murray et al., 2009]. Inflammation and oxidative stress were reported for both purified and unpurified products but the presence of metal impurities elevated the observed toxicity.

Functionalising CNTs to improve their solubility in water makes them more biocompatible and may significantly lower their toxicity. SWCNT treated by dipolar cycloaddition and oxidation/amidation, although up taken by the immune cells, did not affect their viability (even though the oxidised CNTs induced proinflammatory response in macrophages, which was connected with the presence of CNTs aggregates, i.e. lower solubility than in the case of CNTs modified with dipolar cycloaddition) [Dumortier et al., 2006]. Harmful effects can also be a function of the degree of functionalization (functionalization density), e.g. the more the surface is modified, the less cytotoxicity is induced [Sayes et al., 2006]. Nevertheless, with the abundance of possible functional groups and chemistries it is not possible to generalise and it should be noted that some functionalised nanotubes could be more toxic than pristine ones [Firme and Bandaru, 2010].

There is also some evidence that CNTs are a source of adverse effects in natural aquatic environments. SWCNTs were shown to cause a range of deleterious effects including respiratory toxicity, subtle neurotoxicity, cardiovascular problems and organ pathologies (including gill, brain and liver) in chronic exposure assay to rainbow trout [Smith et al., 2007]. Unlike carbon black, SWCNTs at concentrations >120 mg L^{-1} and

MWCNTs at concentrations >240 mg L^{-1} were reported to cause a significant hatching delay in zebrafish embryos [Cheng et al., 2007]. Microscopic results showed that nanotubes aggregates were too big to penetrate the chorion (no individual nanotubes were reported for the experimental conditions) and the hatching delay was attributed to metal (Co and Ni) impurities in nanotubes. Larvae of African clawed frog exposed to aqueous suspensions of double-walled CNTs in concentrations of 10-500 mg L^{-1}, experienced acute toxicity expressed by physical blockage of the gills and/or digestive tract after 12-day exposure [Mouchet et al., 2008]. At the same time no genotoxicity was found in erythrocytes of the larvae. Ecotoxicity of SWCNTs to estuarine meiobenthic crustaceans was tested on copepod *Amphiascus tenuiremis* during its entire life cycle [Templeton et al., 2006]. The highest analysed dose of laboratory synthesised impurified SWCNTs (10 mg L^{-1}) significantly increased life-cycle mortality, reduced fertilization rates and worsened moulting success. Since the purified SWCNTs did not cause the same effect, the authors suggested that the observed toxicity was induced by the smallest fraction of by-products.

C_{60} fullerene

Toxicity of fullerenes, the next most common example of carbonaceous NMs, has been examined in a number of studies on cells, bacteria, crustaceans, invertebrates, fish and rodents [Lyon et al., 2005; Oberdorster et al., 2006; Markovic et al., 2007; Sayes et al., 2007]. Generally speaking, there is no consensus in the literature whether fullerenes are toxic or not. Poor water solubility of fullerenes (estimated at 1.3×10^{-11} µg L^{-1} [Heymann, 1996]) hampers toxicological tests since, similarly to CNTs, different protocols for preparation of fullerene water suspensions result in different C_{60}

conformations in aquatic environment. The first proposed method of dispersing C_{60} in water utilised tetrahydrofuran (THF) as an intermediate solvent [Deguchi et al., 2001]. Such a preparation method was used in a study by Oberdorster (2004), which showed that fullerenes induce oxidative stress in brain of juvenile largemouth bass. Lack of growth and decreased aerobic respiration rates were reported for two bacteria species exposed to low concentrations (up to 4 ppm) of C_{60} in water prepared in the same way [Fortner et al., 2005]. Antibacterial properties of fullerenes (using THF as an intermediate solvent) were demonstrated in low-saline water with *Escherichia coli* and *Bacillus subtilis* as indicator species at concentrations of 0.5 to 1 mg L^{-1} and 1.5 to 3.0 mg L^{-1} respectively [Lyon et al., 2005]. It has been proposed that bactericidal action of such fullerene suspensions towards Gram-negative and Gram-positive bacteria can be explained by photocatalytic generation of reactive oxygen species (ROS), which result in abnormalities in cell wall morphology (lipid composition and phase behaviour) [Fang et al., 2007]. A later study, which looked into ROS production and ROS-mediated damage in bacteria did not find evidence for such mechanism in case of fullerenes and the authors proposed that aqueous C_{60} exerts ROS-independent oxidative stress (acts as an oxidant itself) [Lyon et al., 2008]. Toxicity studies with *Daphnia magna* produced LC_{50} values for THF water fullerenes at a range of 460 – 800 ppb [Lovern and Klaper, 2006; Zhu et al., 2006]. 100 % mortality in fathead minnow was reported 6-18 hours after exposure to THF-solubilised C_{60} at 0.5 ppm [Zhu et al., 2006] as well as delayed and impaired embryo and larval development of zebrafish [Zhu et al., 2007]. Aqueous fullerenes suspended according to the THF protocol were also shown to be toxic to human cells (dermal, neuronal and liver) [Sayes et al., 2005].

Nevertheless, the results raised concerns that the observed toxicity was attributable to the residual THF as opposed to the fullerenes themselves [Andrievsky et al., 2005]. The authors argue that pristine hydrated C_{60} (also called $C_{60}HyFn$, nC_{60} or nano-C_{60}) which form very stable aqueous suspensions, are completely non-toxic and that previously reported toxicity resulted both directly from the presence of THF (at least one molecule of THF accounts for one molecule of C_{60}) and products of its catalytic degradation and from the way in which organic solvents may change interaction between C_{60} and water (interference in the formation of ordered water shells around a C_{60} molecule). In fact, non-modified pristine C_{60} in water medium have been shown to protect against oxidative damage and ionizing radiation (towards DNA in an in-vitro study and in-vivo in mice) [Andrievsky et al., 2009]. $C_{60}HyFn$ in drinking water administered to rats at concentration of ~20 mg mL^{-1} protected their central nervous system from oxidative stress during chronic ethanol exposure [Tykhomyrov et al., 2008]. Pristine nC_{60} were also found a powerful liver protection agent against free-radical damage in mice exposed to tetrachloride [Gharbi et al., 2005].

To better understand the toxicology of nC_{60}, other methods of suspending fullerenes in water have been tested: using alternative solvents to THF (toluene, hexane, ethanol) or solubilising agents, through milling, (ultra)sonification and extended mixing [Fortner et al., 2005; Lyon et al., 2006; Markovic et al., 2007; Endoh et al., 2009; Yang et al., 2009]. Indeed, there are a number of reports supporting the hypothesis that it is the solvents used to disperse fullerenes in water rather than C_{60} themselves that cause the observed adverse effects. THF and water-stirred nC_{60} were used in-vitro (with human epithelial cells) and in-vivo (with *Daphnia magna*) to provide more insight into the influence of the NP sample preparation protocol [Spohn et al., 2009]. Acute toxicity

was found only in the case of THF aqueous fullerenes, no effects were observed in water-stirred samples and in THF sample after careful purification (removal of THF residue and THF hydroperoxide). Additionally, adding water-stirred fullerenes to the THF-dissolved ones, resulted in reduction of the oxidative stress and prevention of ROS formation, which confirms previous reports that pristine C_{60} act as radical scavengers. THF-C_{60} and water-stirred solutions of fullerenes were also tested by other authors for ecotoxicity towards *Daphnia magna* and fathead minnow [Zhu et al., 2006]. The former led to 100 % mortality within 18 h whereas the latter produced no observable effects after 48 h.

Nonetheless, there are also quite a few publications concerning the toxicity of water-stirred nC_{60}. Different fullerenes suspensions (including THF-C_{60}, C_{60} sonicated in toluene, water-stirred C_{60} and C_{60} dispersed in water with the aid of a solubilising agent) were used to examine their antibacterial properties [Lyon et al., 2006]. The study showed relatively strong antibacterial activity towards *Bacillus subtilis* for all four studied suspensions, especially for THF-C_{60} (minimal inhibitory concentration one order of magnitude smaller than in case of all the other preparation methods). Another study used several aquatic species (crustaceans *Daphnia magna* and *Hyalella azteca*, marine harpacticoid copepod, fathead minnow and Japanese medaka) to investigate acute ecotoxicity of water-stirred nC_{60} [Oberdorster et al., 2006]. The authors reported a significant delay in moulting and reduced offspring production in *Daphnia* at concentrations of 2.5 and 5 ppm. Nonetheless, no characterisation analyses were undertaken to address possible toxicity mechanisms. Mortality of 24 % among *Daphnia magna* was recorded for 0.45 ppm sonicated nC_{60} and LC_{50} value was estimated at 7.9 ppm [Lovern and Klaper, 2006].

Generally, toxicity testing for carbonaceous NPs is hampered by problematic experiment design. Pristine fullerenes and nanotubes are poorly dispersed in aqueous media. Different protocols either modify the NPs themselves (e.g. by means of functionalization) or introduce additional substances into the system (e.g. solvents, surfactants), which raises questions if observed effects are caused by the product or by other components added to or formed in the solution matrix. Additionally, commercial products are often contaminated with impurities (e.g. metal catalyst residues), which may be toxic themselves. On the other hand, additional purification might not reflect realistic environmental exposure scenarios. Moreover, depending on the type of product, dispersion method and exposure conditions, NPs show different aggregation behaviour, which may significantly influence toxicity (e.g. ability to penetrate cell organelles).

Silver nanoparticles

Many applications of silver utilize its effective antimicrobial action. Indeed, silver ions are among the most toxic species of heavy metals [Cornfield, 1977], especially towards bacteria but also towards small aquatic invertebrates [Ratte, 1999]. The mechanism of Ag^+ toxicity, although only partially understood, includes inhibition and deactivation of cellular enzymes, electrostatic sorption to the negatively charged cell walls and disruption of membrane permeability, which lead to cell lysis and death [Ratte, 1999; Sambhy et al., 2006]. Current and expected commercialisation of silver NPs has raised concerns that uncontrollable release of tonnes of nano-silver into the environment may cause undesirable effects on human health as well as in ecosystems.

Some studies indicated that toxicity exerted by Ag NPs is mainly (if not entirely) caused by dissolution of silver ions, which is facilitated by large surface area, increasing with smaller particle sizes [Lok et al., 2007]. Ag^+ mediated toxicity of silver NPs was also used to explain their inhibitory effects towards photosynthesis in single cell green algae [Navarro et al., 2008].

Nevertheless, most researchers agree that antimicrobial properties of nano-silver cannot be attributed exclusively to Ag^+ formation but also to a range of mechanisms characteristic to silver NPs in aqueous media. Thanks to their minute size, nano-Ag was shown to penetrate the *E. coli* cell membrane reducing its permeability [Sondi and Salopek-Sondi, 2004]. Damaged cell walls impair transport through the plasma membrane and ultimately lead to cell death. Four types of Gram-negative pathogenic bacteria (*E. coli, V cholera, P. aeruginosa* and *S. typhus*) were treated with faceted silver NPs and showed size-dependent response [Morones et al., 2005]. Apart from membrane damage and Ag^+ formation, antimicrobial action also included the penetration inside the cell, which possibly results in nanoparticle-DNA interaction. Nanosilver toxicity was also linked to photocatalytic ROS generation and their intracellular accumulation in a study with nitrifying bacteria with particle sizes < 5 nm [Choi and Hu, 2008]. Cell membrane damage was explained by free radicals formation, which can destroy membrane lipids [Kim et al., 2007].

Most of microbial toxicity test with silver NPs concentrate on pathogenic bacteria in view of their future applications in medicine and germ control. Very few studies deal with potential implications of nano-silver to natural communities of microorganisms. To the best of my knowledge, only a few publications have investigated harmful effects of silver NPs to environmentally relevant single-cell

organisms including advantageous bacteria - autotrophic nitrifying species used in water treatment plants [Choi and Hu, 2008; Choi et al., 2008], *Chlamydomonas reinhardtii*, green algae species [Navarro et al., 2008], *Paramecium caudatum* [Kvitek et al., 2009], planktonic *Pseudomonas fluorescens* and *Pseudomonas putida* biofilms [Fabrega et al., 2009A, Fabrega et al., 2009B]. There are some data on nano-Ag effects in invertebrates and vertebrates. The bioassay with freshwater zebra fish discriminated the effect of silver ions from particulate silver – significantly more metal was found in the gill and in the whole body in the latter case [Griffitt et al., 2009]. NPs were attached to the gill but did not cause morphological changes even though soluble silver did. Gene profiling showed little similarity between nano and dissolved silver indicating that they interact with the gill in different manners.

Silver has been considered harmless to people (especially via dermal application or oral consumption) [ATSDR, 1990; Soto et al., 2006]. Only high doses (at least a couple of grams) usually administered over extended periods of time (months or years) may cause argyria – general or localised permanent blue discoloration of the skin [ATSDR, 1990; Brandt et al., 2005]. Argyria is regarded as merely a cosmetic problem since no other health effects are observed. Nevertheless, uncontrolled availability of colloidal silver advertised as a universal cure to a range of illnesses (including cancer and AIDS) may result in the increase of argyria cases [Brandt et al., 2005].

Even though human toxicity of silver is low there are new reports describing adverse effects of nano-silver in mammals. For instance, livers of mice fed with Ag NPs showed lymphocyte infiltration, inflammatory response and genotoxic effects (inducers of apoptosis and inflammation) [Cha et al., 2008]. Inhalation toxicity of nano-silver was studied in rats, which were exposed to up to 1.32×10^6 particles per cm^3 and did not

experience significant changes in body weight, haematology and blood biochemical values after 28 days of exposure [Ji et al., 2007]. However, prolonged exposure (90 days) to 2.9 x 10^6 particles per cm^3 affected lung function and caused inflammatory response [Sung et al., 2008].

Titanium dioxide and zinc oxide nanoparticles

Widely produced titanium dioxide NPs used in sunscreens have been recently linked to an increased risk of cancer due to DNA strand breakage and chromosomal damage [Trouiller et al., 2009]. This new finding will surely add to an already heated debate whether nano-TiO_2 is safe. Generally speaking, TiO_2 is regarded as a harmless pigment with no adverse health effects (not dangerous or hazardous in sense of the EEC Directive 67/548). In 2006 the Australian Government published a literature review on the safety of nanosize TiO_2 and ZnO as UV filters in skincare products, in which it stated that, although there is some evidence of toxicity from isolated studies (reporting free radical formation and genotoxicity), TiO_2 and ZnO NPs do not penetrate beyond the outer layer of skin, do not reach viable cells and thus are safe to be used in sunscreens [TGA, 2006]. This report was up-dated in May 2009 without changing its recommendations.

Quantum dots and other nanoparticles

QDs are made of a metalloid core and shell (e.g. CdSe/ZnS) and for biomedical applications are coated with a layer of bioactive "cap" (e.g. protein, peptide) to enhance their bioavailability [Hardman, 2006]. QDs are a very diverse group of NPs and their toxicity depends on many factors including their inherent chemical and physical

properties as well as test conditions (material, size, concentration, charge, coating, oxidative, photolytic, and mechanical stability) [Hardman, 2006]. Most common QDs contain cadmium and selenium, both of which are known to cause acute and chronic toxicity and are listed as hazardous substances [EU Dangerous Substances Directive 67/548/EEC]. Release of Cd^{2+} in uncoated CdSe QDs was found responsible for acute cytotoxicity towards liver cells but adding a protective shell (ZnS) to prevent core metalloid from leaching rendered QDs non-toxic [Derfus et al., 2004]. However, other studies reported toxicity despite the presence of the coating. Carboxyl and amine surface shell did not protect mice injected with CdSe/ZnS QDs from harmful effects (vascular thrombosis in the lung) [Geys et al., 2008]. Freshwater mussels exposed to CdTe QDs experienced oxidative stress and DNA damage in gills [Gagne et al., 2008]. CdTe QDs also showed effective bactericidal action towards *Escherichia coli* by causing oxidative damage in biomolecules such as protein and lipid [Lu et al., 2008B].

Toxicological status of ceria NPs is also a controversial issue, especially with regard to their oxidant/antioxidant effects. Independently of size (6 and 12 nm diameter) CeO NPs showed neuroprotective properties by reducing the amount of reactive oxygen species [Schubert et al., 2006]. Another study reports similar neuroprotective action of CeO NPs towards rat spinal cord neurons [Das et al., 2007] and cardioprotective effects in mice [Niu et al., 2007]. At the same time there are a number of reports that CeO NPs induce oxidative stress and cell death in *Escherichia coli* and human lung cells [Lin et al., 2006; Thill et al., 2006; Park et al., 2008].

Fig. 2.1 showed gold NPs interacting with DNA molecules. Au NPs have also been found to penetrate cytoplasm and nucleus [Patra et al., 2007; Li et al., 2008A].

Due to potential applications of Au NPs to cancer diagnosis, some studies concentrate on cytotoxicity in human carcinoma cells [Patra et al., 2007]. However, most researchers report lack of toxic effects of gold NPs [Shukla et al., 2005; Patra et al., 2007].

Overall, the same fascinating properties of NMs that promise revolutionary technological advances may cause undesired consequences for human health and the environment when released uncontrollably. For instance, large surface area, which drastically enhances reactivity of the material, may, on the other hand, generate harmful oxyradicals and show high affinity for heavy metals and poisonous organic compounds. Secondly, the ability of NPs to cross cell membranes and interact with organelles, which was welcomed with great enthusiasm for new drug delivery systems, can possibly turn out fatal if unintended exposure occurs.

Although much attention has been paid in the past few years to better understand the health and environmental implications of nanotechnology, available data is still fragmentary, often inconclusive, and in some cases contradictory. Some issues, like toxicity of NPs to plants, have hardly been addressed. Possible toxic properties of NMs, potential entry points and likely pathways in the human body may be largely predicted on the basis of already available extensive knowledge in the field of pharmaceutical research and particle toxicology. Much discussion is based on extrapolation from fairly well examined nanosize substances like quartz, asbestos and ultrafine atmospheric particles. All these theories need to be verified experimentally before safe ways of production, handling, use and disposal of NMs are established. It may also be necessary to develop completely new toxicity testing protocols to address unique properties of NPs.

At the moment, in view of remaining knowledge gaps precautionary approach is advised, i.e. individual risk assessment for new NMs on a case-by-case basis [SCENIHR, 2006]. Currently no reliable and comprehensive risk assessment of NMs is possible. All important risk assessment stages suffer from limited, inconclusive or questionable data, in some areas there is no data at all [Savolainen et al., 2010]. With search terms "nanomaterials" and "toxicity" Science Direct database produces over 1900 documents published since 2000. Many efforts have been made to advance hazard identification, hazard characterization, exposure assessment and risk characterization in nano-science. (Eco)toxicological implications of NMs are subjected to scrutiny and have become priority for governments, manufacturers and the general public [Roco, 2005; Helland, 2006; Siegrist, 2007]. Still, the majority of questions about toxic effects, their mechanism, conditions under which they take place and realistic exposure concentrations to humans and ecosystems, remain unanswered.

With extensive lack of knowledge and extremely wide range of products to be tested, the scientific community and regulatory bodies are challenged to level nano-products commercialisation and rapid increase in production output with providing toxicological database for NMs and legal regulations concerning placing NMs on the market. As a consequence a priority list of recommendations for research has been proposed [Alvarez et al., 2009]:

- development of structure-activity relationships to predict toxicity, bioavailability and bioaccumulation of NPs on the basis of their key properties;

- development of standardised toxicity test protocols;

- development of multiphase models for predicting fate and behaviour of NPs in the environment to estimate forms and concentrations for exposure studies.

2.2   Nanoparticles in the environment

2.2.1   Natural and anthropogenic nanoparticles

Although in the centre of recent research efforts, nanosize particles as such are nothing new to the environment and science. There is a group of nano- and microscale naturally occurring materials in aquatic systems known as natural aquatic colloids (NAC). They include a range of organic and inorganic solid-phase material with at least one dimension between 1-1000 nm [Buffle, 2006]. Colloids are distinguished from the dissolved and particulate matter. Particles have sizes > 1 μm, whereas the dissolved fraction is often defined operationally as compounds that pass through a filter, usually with a pore size of 0.45 μm, 0.1 μm or an ultrafilter ~ 1nm [Lead and Wilkinson, 2006A; Nowack and Bucheli, 2007].

Natural nanosize particles occur also in the atmosphere. Weathering processes, volcanic eruptions, dust storms, forest fires or sea spray are all sources of natural fine particles in the air [Nowack and Bucheli, 2007; Murr and Garza, 2009]. However, an estimated 15 % of atmospheric particulate matter (PM) and its gaseous precursors are produced inadvertently as by products of human activities [Anastasio and Martin, 2001]. Incidental (adventitious) sources of anthropogenic atmospheric PM encompass mainly combustion of fossil fuels (in vehicles and energy generation) and industrial processes. Typical size fractions of atmospheric particles are classified as PM_{10} (with sizes < 10 μm), $PM_{2.5}$ (with sizes < 2.5 μm) and ultrafine particles UFP (with sizes < 100 nm, i.e. $PM_{0.1}$).

Types of NPs, their source and examples are summarised in table 2.1.

natural		anthropogenic	engineered	origin
inorganic	**organic**	**wear & corrosion products**	**standard industrial products**	
- silicates (e.g. clays)	- macromolecules	- from tire & brakes	- polymers	
smectites	humic acids	- from catalysts (e.g. Pt, Pd)	- surfactants	
montmorillonite	fulvic acids	- metals (wear in bearings)	- dyes & pigments	
nontronite	polysaccharides	- metal oxides (roof run-off)	- metal oxides	
hectorite	proteins	- additives to lubricants	**NP metals & metal oxides**	
chlorites	peptides		- metals (Au, Ag, Fe)	composition
mica	exo-polymers, EPS	**waste & combustion products**	- metal oxides (of Ti, Zn, Zr, Ce...)	
kaolinite	- bio-colloids	- soot	- metal tubes and wires	
- oxides / hydroxides	bacteria	- "anthropogenic" humic acids	**carbon based**	
Fe-oxohydroxides	viruses	from e.g. waste dumps	- fullerenes	
Mn-oxides	fungi	- tar leachates in plumes	- single & multi walled nanotubes	
- carbonates	- coal/soot/black carbon	- fly ash	**hybride structures**	
- phospates	- cellular debris	- fine dust (inorganic & organic)	- quantum dots	
- metal sulfides			- functionalized materials	
- polym. silicic acid			- core-shell structures	

Table 2.1. Classification of micro- and nanoparticles [modified from Christian et al., 2008].
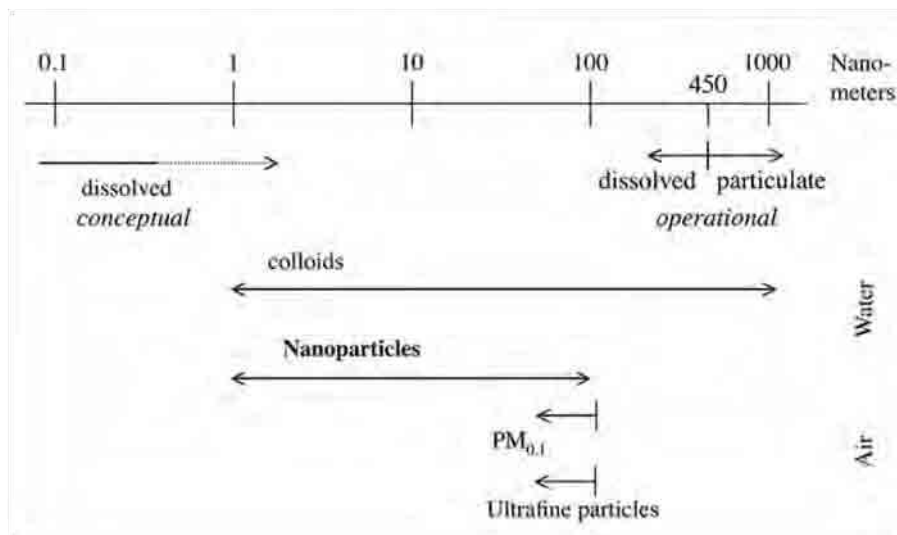
Figure 2.5. Size classes of natural and anthropogenic (incidental and engineered) nanoparticles [modified from Nowack and Bucheli, 2007].

With dimensions between 1-100 nm, the size fraction of engineered NPs overlaps with natural aquatic colloids and atmospheric particulate matter, especially UFP (Fig. 2.5).

Aquatic colloids and atmospheric particulate matter have been intensively studied for the last years. Experience and knowledge gathered through these investigations is of great value in current efforts to advance applications and implications of nanotechnologies. Many analytical methods, approaches and protocols can be directly transferred or modified or provide a good starting point in nanoscience research [Oberdorster et al., 2005; Lead and Wilkinson, 2006A].

2.2.1.1   Natural aquatic colloids

Defined in the previous section as particles in the size range 1-1000 nm, NAC encompass humic substances, polysaccharides, proteins, cellular debris, viruses, metal oxides and sulphides, etc., naturally occurring in aquatic environments (Fig. 2.6). Important fraction of NAC is constituted by natural organic matter (NOM), e.g. humic and fulvic substances: macromolecular, polymeric, polyfunctional and polydisperse materials [Guo and Santschi, 1997].

In the past few decades NAC received substantial amount of scientific attention and much has been done to better understand their properties, fate and behaviour. NAC have been broadly recognised to play multiple key roles in the environment because they interact with pollutants, nutrients and pathogens influencing their chemistry transport and bioavailability in natural waters [Lead et al., 1999; Buffle, 2006; Lead and Wilkinson, 2006A]. There is much evidence that natural colloids play an important role in trace metal speciation [Martin and Dai, 1995; Lead et al., 1999; Tipping et al., 2002; Koukal et al., 2003]. Metal complexation by chemically heterogeneous colloids is based

on a large charge density of humic substances and inorganic colloids and on a high number of binding site types [Buffle, 2006].
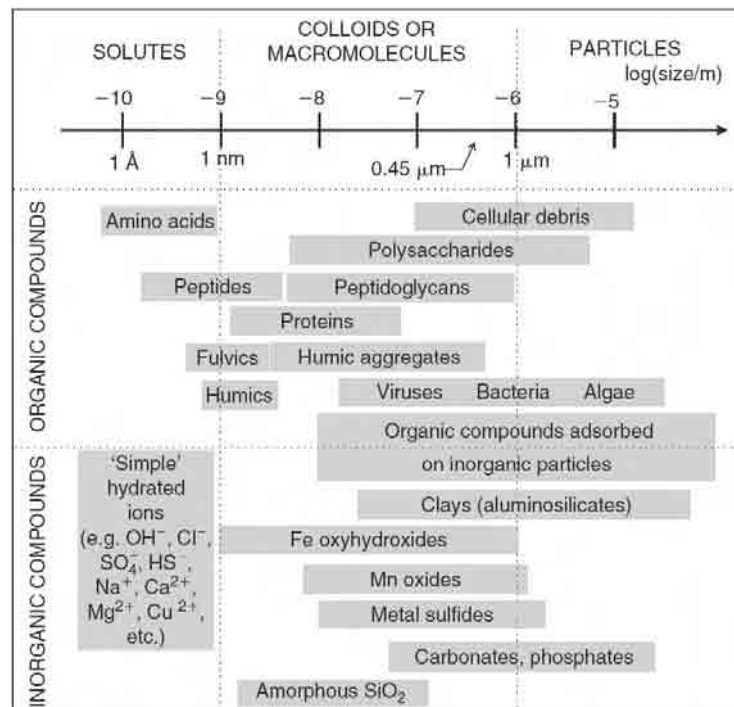
Figure 2.6. Types and sizes of natural aquatic colloids [Lead and Wilkinson, 2006].

Although techniques for fractionation and characterisation of the structure and morphology of NAC have been developed and established to a certain extent, there is still much to be done to understand and quantitatively describe their environmental role [Lead and Wilkinson, 2006A].

2.2.1.2 Atmospheric nanoparticles

Natural particulate matter is found in abundance in the atmosphere. Number concentrations significantly differ between remote and polluted regions. For instance, in remote areas there are usually under 100 ultrafine particles per cm^3 [Weber et al., 1995;

Covert et al., 1996; Weber et al., 1997], whereas in urban areas number concentrations are in order of magnitude of 10^4 particles per cm^3 [Shi et al., 1999, McMurry et al., 2000] and between 10^4 and 10^6 particles per cm^3 in a roadside background [Kittelson et al., 2001]. As has been mentioned in the previous section, these particles are usually addressed as PM_{10} and $PM_{2.5}$. The smallest fraction of $PM_{2.5}$ − ultrafine particles, usually defined as < 100 nm, has come under particular scrutiny because of its high toxicity per unit mass. Fractions and sizes of atmospheric particulate matter are shown in Fig. 2.7. Since atmospheric particles can have different shapes, this classification is based on aerodynamic diameter, which accounts for different morphologies and densities. Aerodynamic diameter is defined as a diameter of an ideal sphere with unit density having the same aerodynamic properties (such as sedimentation velocity) as the particle in question. This way the same aerodynamic diameter defines particles having the same inertial properties. Such a definition is especially valid in case of ultrafine particles, which tend to show fractal or irregular morphologies [Barone and Zhu, 2008]. Nevertheless, it should be noted that there is no consistent definition of ultrafine atmospheric particles and their upper cut-off diameter cited in literature can significantly differ from 10 nm [McMurry et al., 2000], 50 nm [Donaldson et al., 1998], 180 nm [Eiguren-Fernandez et al., 2003] to 560 nm [Yao et al., 2005].

Aerosol size distribution, as its most important physical parameter, is a crucial issue in airborne pollution and atmospheric science. Depending on their sizes, micro- and NPs behave differently and are governed by different phenomena [Willeke and Baron, 1993]. Understanding size distributions of atmospheric aerosols is vital for understanding the radiation budget as well as air quality and its influence on human health [IPCC, 2001].

Ultrafine particles are believed to be mainly anthropogenic in source. They are generated during combustion of fuels, when particles are formed by condensation of gases [The Royal Society & the Royal Academy of Engineering, 2004]. There is evidence that in urban areas the smallest UFPs (< 10 nm) originate from road traffic and stationary combustion sources [Shi et al., 2001].
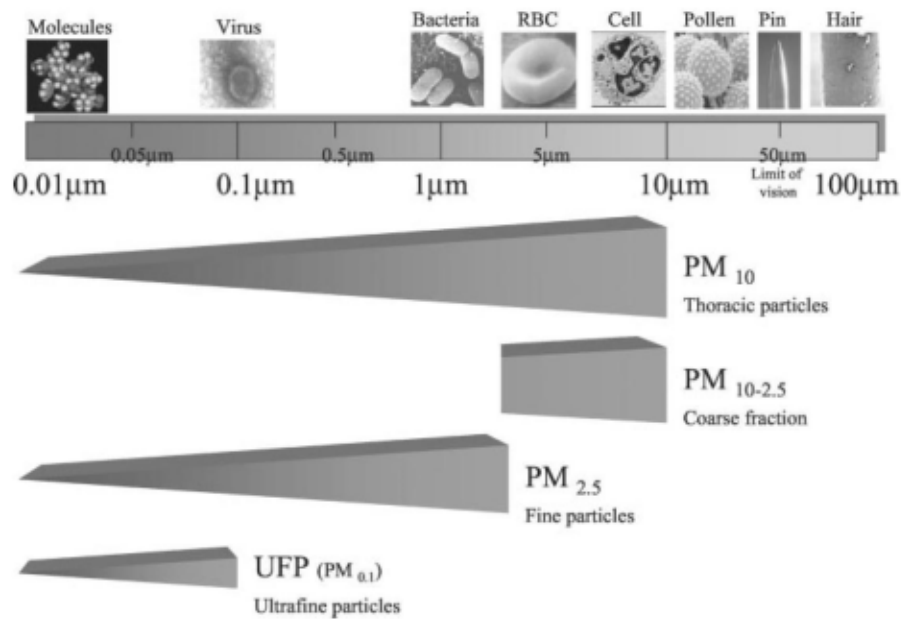
Figure 2.7. Fractions and sizes of atmospheric particulate matter [Brook et al., 2004].

PM_{10} has been linked to cardiac and respiratory morbidity and mortality through worldwide epidemiological studies [Samet et al., 2000; Brook et al., 2004; Dockery and Stone, 2007]. Since 1980s numerous studies have provided evidence for toxic properties of atmospheric particles causing heart and lung diseases despite the fact that they are strongly diluted even in urban environments (tens of $\mu g\ m^{-3}$) [Brook et al., 2004; Seaton et al., 1995]. However, low mass concentration of tens of $\mu g\ m^{-3}$ translates into high number concentrations, for instance 10^{4}-10^{6} particles per cm^{3} of air [Kittelson et al.,

2001]. Toxicity of such small amounts of inhaled pollutants, which mainly contain regarded as non-toxic carbon and simple ammonium salts, has been thus associated with the extremely small sizes of particles resulting in high surface area and enhanced reactivity. Similarly, engineered nanoscale particles of titanium dioxide and carbon black are more toxic than their larger counterparts [Oberdorster, 1996]. It can be explained by larger surface for binding toxic air pollutants (organic compounds, transition metals) [Sioutas et al., 2005], which may lead to enhanced ability to cause oxidative stress [Donaldson et al., 2001]. Additionally, due to their extremely small size, UFPs are especially effective at entering tissues by evading and impairing macrophage phagocytosis, the body's main defence against constant exposure to airborne particles [Renwick et al., 2000]. This phenomenon determines pulmonary toxicity of UFPs in the first place because deposited particles cannot be removed from airways by normal pathways. Foreign particles remaining and accumulating in the pulmonary interstitial sites cause chronic toxicity to the cells. Moreover, from the lung tissue PM can enter cardiovascular system causing further damage.

In-vivo studies carried out to date used very high concentrations of UFPs and with the exact mechanism of their toxicity still unknown, it is impossible to extrapolate the results to relevant environmental concentrations. Additionally, observations of respiratory and cardiovascular effects were made in susceptible patients and it appears that healthy subjects are not likely to develop the symptoms if the concentrations of UFPs are not artificially elevated [Oberdorster et al., 2005].

Although there has been enough evidence to believe that the ultrafine fraction is the most responsible for morbidity and mortality linked to atmospheric PM, it is still unclear which particular size fractions (concentrations and components) cause which

deleterious health effects and what are the mechanisms of PM toxicity. Given the fact that air pollution is a heterogeneous and extremely complex mixture of gases, liquids and solid particles, there is still much to be done to address remaining scientific questions in the field.

2.2.2 Fate & behaviour of engineered nanoparticles

As discussed in one of the previous sections (2.1.3), some of the (eco)toxicological properties of certain NMs have been quantified in laboratory conditions. Whether and how these findings will translate into actual adverse effects for humans and the environment hugely depends on environmental exposure, as affected by fate and behaviour of manmade NPs after they are released into soil, water or atmosphere. However, the fate and behaviour of engineered NPs is largely unknown. Key issues that need better understanding include mobility, reactivity, ecotoxicity and persistence of NMs in the natural and anthropogenic environment. Dependable data on probable production, usage and disposal scenarios for manmade NMs is essential for hazard characterisation, exposure assessment and risk characterisation.

A number of NMs are already produced on an industrial scale but very little data on current or predicted occurrence of engineered NPs in the environment is available. Monitoring and tracing of NMs in the environment requires reliable and accurate detection methods. Unfortunately, to this day detection of NMs is one of the most underdeveloped domains in nanoscience [NPCA, 2008]. The main reasons why detecting and quantifying NPs in complex environmental matrices is such a challenge include:

- extremely low expected concentrations (Table 2.2) [Boxall et al., 2007; Mueller and Nowack, 2008; Tiede et al., 2009]

- interference with background material, e.g. relatively high concentrations of natural NPs, which cannot be distinguished from engineered NPs with available laboratory techniques (background levels of organic compounds for carbonaceous NPs and background levels of trace metals for metal and metal oxide NPs) [Handy et al., 2008].

Type of nanomaterial	Water [µg/L]	Soil [µg/kg]	Air [µg/m^3]
Ag	0.010–0.03	0.02–0.43	0.0017–0.0014
AlO$_3$	0.0002	0.01	
Au	0.14	5.99	
Carbon nanotubes	0.0005–0.0008	0.001–0.02	0.0015–0.0023
CeO$_2$	<0.0001	<0.01	
Fullerenes	0.31	13.1	
Hydroxyapatite	10.1	422	
Latex	103	4307	
Organo-silica	0.0005	0.02	
SiO$_2$	0.0007	0.03	
TiO$_2$	0.7–24.5	0.4–1030	0.0015–0.042
ZnO	76	3194	

Table 2.2. Predicted concentrations of engineered NPs in the environment [Boxall et al., 2007; Mueller and Nowack, 2008; Perez et al., 2009].

With no data on current measured concentrations of NPs in the environment, efforts have been made to estimate them using information on production output and most probable usage and disposal scenarios. Life-cycle modelling has been used to predict expected concentrations in water, air and soil for a range of NMs, including

fullerenes, CNTs, silver, zinc oxide, titanium dioxide and other NPs (Table 2.2) [Boxall et al., 2007; Mueller and Nowack, 2008]. Life-cycle inventory for products containing NPs is built as a mass-balanced material flow spanning over manufacturing, usage and disposal stages. An example of such modelling for CNTs in Switzerland is presented in Fig. 2.8. Most CNTs from commercial products are expected to end up in waste incineration plants, 75% of which is then transferred to landfills (as slag). Based on calculations presented in Fig 2.8, risk quotients, RQ, (ratio between predicted environmental concentration and predicted no effect concentration, PEC/PNEC) for carbon nanotubes were in order of magnitude $10^{-3} – 10^{-5}$ for water and air indicating that CNTs pose no or very low risk to the environment (soil was excluded from calculations due to lack of data). However, the relatively large release was allocated to air, where CNTs raise most toxicological concerns (as discussed in chapter 2.1.3). Similar models were used for silver and titanium dioxide NPs and only in case of nano-TiO_2 in water systems was significant exposure recorded (RQ of $0.73 – 16$) [Mueller and Nowack, 2008].

Such estimates are of great value since they provide a basis for more detailed and accurate analysis, a reference point for further investigations and most of all they support decision making process for policy makers. However, with so many knowledge gaps and high uncertainty of the data, life-cycle modelling of NMs has to hugely rely on assumptions, simplifications and extrapolations such as:

- environment compartments (air, water and soil) are treated as homogenous and well mixed (which neglects local effects);
- rough estimates on global and regional production of NMs including a list of products containing NPs;

- percentage of particles that become airborne during waste incineration has to be assumed;

- efficiency of particle removal in sewage treatment plants has to be assumed;

- many material flows have to be neglected (e.g. degradation, bioaccumulation, NPs in groundwater, etc.).
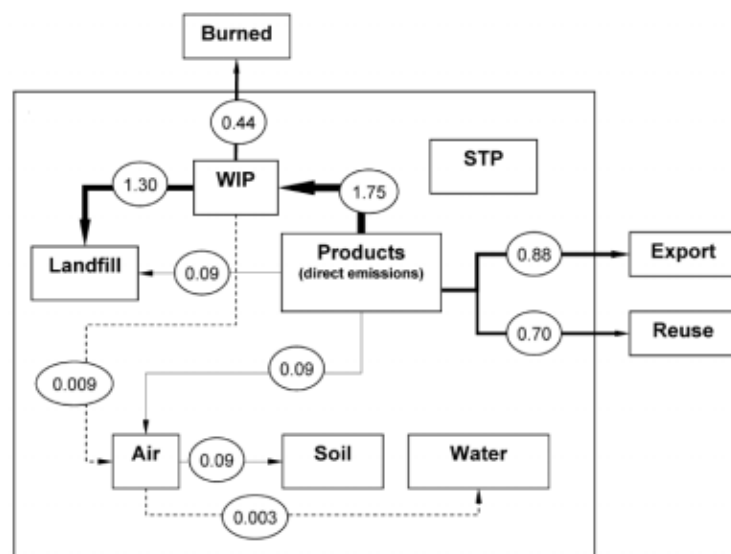
Figure 2.8. Carbon nanotubes from commercial products circulation in the environment in Switzerland according to high risk scenario. Figures are in tonnes/year. STP – sewage treatment plant, WIP – waste incineration plant. Thickness of lines corresponds with volume they represent; dashed line is used for the smallest flows [Mueller and Nowack, 2008].

Interactions with NAC, pollutants and aquatic biota

Engineered NPs entering the aquatic systems are a new challenge in the field as they are likely to interact with natural colloids [Lead and Wilkinson, 2006A]. A schematic model of these interactions is presented in Fig. 2.9. Depending on a range of environmentally relevant parameters (pH, ionic strength, concentration of cations and

pollutants, etc.) the fate and behaviour of NPs in aquatic environment will be controlled by aggregation and disaggregation, surface coating with NOM and interaction with pollutants [Christian et al., 2008]. Contaminants can be adsorbed on the surface of NPs or trapped inside NPs aggregates (absorbed). There is evidence that humic substances (HS) form a few nanometre thick films on microsurfaces and particles [Lead et al., 2005]. Such coating on NPs may significantly change surface properties and thus influence their behaviour and interaction with pollutants.
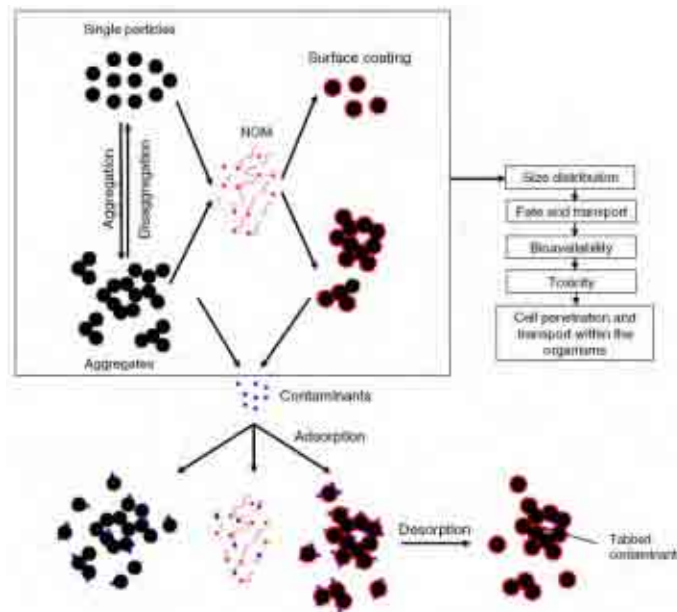
Figure 2.9. Model of interactions between engineered nanoparticles, pollutants and aquatic colloids in natural waters [Christian et al., 2008].

There has already been a small body of work supporting the hypothesis that the fate and behaviour of engineered NPs in natural waters will be hugely dependent on interactions with NAC. Coating with humic acid has been reported for iron containing NPs, ZVI [Giasuddin et al., 2007] and iron oxide [Baalousha, 2009]. Previous reassurance about lowered mobility of fullerenes in water suspensions caused by

sedimentation (and hence removal from bulk water) [Brant et al., 2005] has been recently weakened by evidence of fullerene stabilisation in the presence of Suwannee River humic acid at certain concentrations of NaCl and $MgCl_2$ [Chen and Elimelech, 2007]. This effect was explained by steric repulsion of humic acid particles adsorbed on C_{60}. The environmental implication is that soft waters, rich in NOM will probably suffer from C_{60} persistence. Similar behaviour has been observed in case of CNTs. NAC were found to stabilise MWCNTs even better than sodium dodecyl sulphate, synthetic surfactant commonly used to stabilise water suspensions of nanotubes [Hyung et al., 2007]. Analysed samples remained stable for over a month implying that dispersal of CNTs in natural waters may happen to an unexpected extent.

Interaction of NPs with pollutants in the environment may alleviate negative effects. CNTs in aqueous media can act as powerful adsorbents for a range of organic pollutants: dioxin [Long and Yang, 2001], polycyclic aromatic hydrocarbons [Yang et al., 2006B], DDT and its metabolites [Zhou et al., 2006] and many others. Functionalised CNTs (hydroxylated and oxidised) efficiently adsorb metals from aqueous solutions including Cd, Mn, Ni, Cu and Pb [Li et al., 2002; Liang et al., 2004; Liang et al., 2005]. On the other hand, in some instances pollutant-nanoparticle interaction may amplify toxicity. The presence of TiO_2 NPs has been shown to increase bioavailability of arsenic to carp by means of adsorption and facilitated transport [Sun et al., 2007].

Aquatic organisms were also found to be able to modify suspended nanotubes. *Daphnia magna* digested lipid coating on SWCNT, which resulted in aggregation and precipitation of NPs [Roberts et al., 2007].

Ionic strength and specific counterions

Surface charge is a very important parameter influencing the stability of NPs in aqueous suspensions. Electrostatic stabilisation of suspended particles depends on the balance between two kinds of forces: repulsive forces exerted by ionic groups on the particle surface, which form electric double layer (EDL) and attractive Van der Waals forces. The DVLO theory quantitatively describes the balance of these repulsive and attractive forces for particles interacting in a liquid medium as a function of interparticle distance [Derjaguin, and Landau, 1941; Verwey, and Overbeek, 1948]. If the repulsive force produced by the EDL is sufficient, mutual repulsion between same charged particles keeps them apart and provides stabilising mechanism. If, however, the EDL is compressed (e.g. by accumulation of salt ions) the electrostatic repulsion becomes too weak to counterbalance Van der Waals attraction and precipitation occurs. This phenomenon governs the stability of charged particles at higher ionic strengths. A number of NPs have been found to destabilise and sediment out of the suspension when moving from freshwaters to seawater. Relatively weak NaCl solutions (0.001 M) were reported to destabilise and precipitate nC_{60} clusters in suspensions and in porous media [Brant et al., 2005]. Divalent cations (such as Ca^{2+} and Mg^{2+}) are more efficient in surface charge neutralisation on nC_{60} aggregates and thus act as stronger coagulation agents [Chen and Elimelech, 2007]. These results suggest that in hard waters C_{60} are likely to be removed and transferred to sediment. Similarly to fullerenes, positively charged cations (especially divalent, e.g. Ca^{2+}) cause CNTs to rapidly aggregate and precipitate [Sano et al., 2001]. Similar observations have been made for TiO_2 [Domingos et al., 2009B; French et al., 2009; Jiang et al., 2009] and silica [Singh and

Song, 2007]. Particles which exhibit such behaviour stay stable in freshwaters but sediment out in the marine environment [Stolpe and Hassellov, 2007].

pH

Another important parameter in the stability of NP suspensions in aqueous media is often pH value. A number of NPs are negatively charged over a large range of pH values, e.g. hydroxylated SWCNTs [Hu et al., 2005], nC_{60} [Chang and Vikesland, 2009]. Oxides, carbonates and other NPs tend to show positive surface charge at low and neutral pH values (polysaccharide NPs [Jallouli et al., 2007], ZVI NPs [Sun et al., 2006], iron oxide NPs [Baalousha, 2009], ceria NPs [Patil et al., 2007]). Generally, at pH far from point of zero charge (i.e. when the electrical charge density on the surface is relatively high), NPs form stable suspensions [Guzman et al., 2006; Baalousha, 2009].

Nanoparticles in soil

Transport of NPs in porous media such as soil has been hardly addressed by researchers yet. Initial studies examining possible uses of iron NPs in remediation show that nanoscale iron was transported with underground water for a distance of 20 m and remained reactive towards chlorinated organic solvents for periods even longer than 4-8 weeks [Zhang, 2003]. Lecoanet et al. (2004) carried out experiments on a porous filter medium (comparable to groundwater aquifer and water treatment plant filters) to study the mobility of 8 types of NPs including: hydroxylated C_{60} (fullerol), nC_{60}, SWCNTs, silica NPs with 2 different diameters, alumoxane, ferroxane and anatase. Transport behaviour for studied NPs turned out to be different in all cases and the authors

concluded that environmental risk of NMs cannot be treated in a uniform fashion. Functionalised fullerenes and SWCNTs have been found to be the most mobile with theoretical migration distance in unfractured sand aquifers of 10 m. On the other hand, unmodified nC_{60} showed the lowest mobility probably due to its relatively high hydrophobicity. It is conceivable that fullerenes may be functionalised in natural environments through photolytic and bioprocesses leading to increase in their mobility.

2.2.3   Characterisation of nanoparticles

The properties of NPs depend on many parameters: core material, production technique, dimensions, shapes, presence of coating and surface functionalization, concentration, solution matrix, etc. Chemical, physical and biological properties within the same group of NMs can be drastically different. For instance, pristine SWCNTs are virtually insoluble but after surface functionalization can be easily suspended in water [Zhang et al., 2009]. Moreover, 5 nm gold NPs strongly inhibit DNA hybridisation, whereas 17 nm ones do not show any effect [Yang, 2006A], and the toxicity of fullerenes has been regarded to be dependent on the dispersion protocol used [Spohn et al., 2009]. Consequently, any experiments in environmental nanoscience have to be accompanied by precise and accurate characterisation of the material under study. It is widely accepted that physicochemical characterisation is essential to understand the implications of NPs and that much work is still needed to advance existing knowledge and techniques [The Royal Society & the Royal Academy of Engineering, 2004; SCENIHR, 2009; Stone et al., 2010].

Although there is no agreement on what exactly a standard characterisation of NMs should involve to ensure reliable risk assessment, these are the main parameters of interest [SCENIHR, 2009]:

- physical properties: size, shape, specific surface area, aspect ratio, agglomeration/aggregation state, size distribution, surface morphology/topography, structure including crystallinity and defect structure and solubility.

- chemical properties: structural formula/molecular structure, composition of nanomaterial (including degree of purity, known impurities or additives), phase identity, surface chemistry (composition, charge, tension, reactive sites, physical structure, photocatalytic properties, zeta potential) and hydrophilicity/lipophilicity.

Additionally, characterisation should ideally comprise analysis of NPs in their original form and in the experimental media [Stone et al., 2010].

A broad range of techniques have been used to characterise NPs (Table 2.3). Heterogeneous samples usually require size fractionation to determine size distribution and properties of individual fractions. Centrifugation, flow field fractionation, filtration and chromatography are most popular techniques to perform this task. Visualisation with microscopy techniques is used in most studies to describe sizes, shapes and morphological characteristics of NPs. Some newer advances in microscopy allow examination of wet samples (environmental scanning electron microscopy and atomic force microscopy). The surface of NPs can be analysed with nitrogen adsorption (to

technique	property	sample requirements	LOD/spatial resolution/separation range	limitations
atomic force microscopy (AFM)	morphology, size, aggregation state, surface properties	fixing particles on a surface	~ 0.5 nm to several µm	time consuming especially to get representative and robust statistics
electron microscopy (EM)	morphology, size, aggregation state, surface properties, elemental analysis	dry sample, preferably high electron density of the sample	~ 0.3 nm to several µm	not suitable for wet samples, time consuming
environmental scanning electron microscopy (ESEM)	morphology, size, aggregation state	wet samples	40 nm to several µm	low resolution
N_2 adsorption, BET	specific surface area, porosity	solid sample	~ 1 nm to several µm	not suitable for aggregated materials, complex microporous structures or materials reacting with nitrogen
electrophoretic mobility	zeta potential (surface charge)	liquid sample		limited information on charge heterogeneity
X-ray spectroscopy, scattering	surface chemical and structure analysis	powder samples	µg to mg	poor spatial resolution
centrifugation	size distribution	liquid sample, whole sample		low size resolution
dynamic light scattering (DLS)	size distribution	liquid monodisperse samples	3 nm to several µm	not suitable for polydisperse samples
flow field fractionation (FFF)	size distribution	liquid polydisperse samples, complex media	1 nm to several µm	errors may arise due to particle shape or density, for low concentrations a pre-concentration step may be required
filtration	size distribution	liquid sample, whole sample	down to 1 kDa	charging, clogging, etc.
hydrodynamic chromatography	size distribution	liquid polydisperse samples, complex media	5-1200 nm	low separation efficiency
size exclusion chromatography	size distribution	liquid polydisperse samples	dependent on pore size	risk of sample loss in the column, non-size interactions in the column, and molar mass calibration can be problematic
voltammetry	free metal ions, concentration, metal speciation	liquid samples	ng range	preferably metals
diffusive gradients in thin films (DGT)	free metal ions, concentration, metal speciation	liquid samples	down to ppb	metals, phosphate, sulphide and radionuclides.

Table 2.3. Requirements and application range of most common analytical techniques for environmental testing of nanoparticles [Handy et al., 2008; Hassellov et al., 2008; Tiede et al., 2009].

technique	property	sample requirements	LOD/spatial resolution/separation range	limitations
gravimetry	bulk particle concentration	liquid samples	depending on the filtration membrane	large sample volumes, particles smaller than the cut-off are lost
turbidimetry	bulk particle concentration	liquid samples	mg/L	interference from dissolved organic carbon
nephelometry	bulk particle concentration	liquid samples	ppb-ppm	signal dependent also on particle size, refractive index and shape
total organic carbon (TOC) analysis	bulk particle concentration	liquid samples		background carbon levels in the sample
laser induced breakdown detection (LIBD)	bulk particle concentration, particle size	dilute liquid samples	below 1 mg/L	careful calibration critical to particle size measurement
UV-Vis spectrometry	bulk particle concentration	liquid samples		interference from turbidity generated by particles

Table 2.3. continued.

measure surface area and porosity), electrophoretic mobility (surface charge) or spectroscopy (chemical and structural analysis). Metal speciation can be studied with techniques such as voltammetry, diffusive gradients in thin films, spectroscopy and spectrometry.

Due to the complexity of nanoparticle behaviour and properties (in as-produced state as well as in exposure media) and a requirement for state-of-the-art methodology in characterisation and (eco)toxicological testing, a need for interdisciplinary collaboration has been widely recognised [Defra, 2007]. As outlined in Table 2.3, there are many instruments and analytical methods available for NPs characterisation. Most of these methods are very sensitive and provide sufficient resolution to study materials at the nanoscale. Many techniques are well developed and validated and have been routinely used for fine particle examination (in atmospheric and aquatic studies and in material science) [Hassellov et al., 2008]. However, all analytical tools have their

limitations and may produce artifactual results [Handy et al., 2008; Hassellov et al., 2008; Tiede et al., 2009]. There is an international consensus that development of improved standardised methods for nanoparticle characterisation is among the research priorities required to address knowledge gaps in risk assessment of nanotechnologies [SCENIHR, 2006; Defra 2007; EPA, 2007].

It is pertinent to stress that, detection techniques to identify and measure NPs in the environment are currently in their infancy and require substantial development. Such techniques are urgently needed to monitor NPs in the environment, to characterise their nature in complex media and to help understand fate and behaviour and toxicity mechanisms. This is a crucial issue to understand the fate and behaviour of NPs. For instance, realistic environmental concentrations of NPs are essential to correctly design toxicity protocols and advance risk assessment of NPs by providing data on expected exposure to NMs. Moreover, efficient detection techniques in biological matrices, such as body tissues, would help to underpin the mechanisms of observed toxic effects [Handy et al., 2008; NPCA, 2008].

Another major analytical challenge in NP analysis for environmental studies is development of standardised rapid and statistically reliable methods to measure particle size and size distribution. Existing techniques such as microscopy are expensive and time consuming and methods measuring mean dimensions in bulk samples (such as dynamic light scattering) neglect particle shapes and aggregation behaviour [National Nanotechnology Initiative, 2006]. Additionally, available microscopy techniques and specimen preparation protocols inherently introduce artefacts caused by dehydration of the sample (such as shrinkage, aggregation or evaporation of volatile components). In case of microscopy techniques, which can analyse only extremely small fractions of a

sample, unrepresentative nature of images is a problematic issue. Similarly, analytical methods and protocols need to be established to address the issues of surface properties and modifications, assessing the purity of the studied material, their shape, structure, surface area, stability and aggregation behaviour [National Nanotechnology Initiative, 2006; EPA, 2007]. The development of improved sample handling, preparation and metrology is crucial to the development of understanding of NP environmental behaviour.

3 MATERIALS AND METHODS

3.1 <u>Materials</u>

This chapter gives information on the protocols used to prepare materials and stock samples throughout the experimental work. These stock suspensions were used to prepare all the test samples, details of which are given in subsequent chapters in accordance with experimental procedures used in these chapters.

3.1.1 Natural aquatic colloids

Suwannee River Humic Acid

Suwannee River humic acid standard (SRHA) was purchased from the International Humic Substances Society (IHSS). Stock solutions of either 20 or 100 ppm were prepared by diluting the appropriate amount of powdered SRHA in ultrapure water. Solutions were stored refrigerated at 4° C and used within two days.

Peat Humic Acid

Pahokee peat humic acid standard (PHA) was purchased from the International Humic Substances Society (IHSS). Stock solutions of either 20 or 100 ppm were prepared by diluting the appropriate amount of powdered PHA in ultrapure water after adjusting pH with 1M NaOH to ~10 to facilitate dissolution. Rapid stirring prevented any localised effects and the pH was reduced quickly mitigating any oxidation. Solutions were stored refrigerated at 4° C and used within two days.

Succinoglycan

Succinoglycan (SG), a polysaccharide relevant to natural waters, was purchased from CarboMer Inc. Stock solutions of either 20 or 100 ppm were prepared by adding

succinoglycan to ultrapure water followed by gentle stirring for 12 h at room temperature. The resulting solution was filtered through a 0.2 μm Isopore membrane filter (Millipore) and stored refrigerated at 4° C for two days.

Natural lake water

Water samples were collected from the Vale Lake, Birmingham University campus, Birmingham, UK. The volume of 1L was collected in a polyethylene bottle washed with ultrapure water and with the sample prior to sampling. Sampling was performed at ~0.5 m from the bank and a few cm below the surface of the water. Samples were returned to the laboratory immediately and filtered through a 0.1 μm pore size membrane filter to remove the biggest size fraction. Transport and storage time prior to experiments was always less than 24 hours and samples were stored refrigerated at 4° C.

3.1.2 Engineered nanoparticles

Single walled carbon nanotubes

Carboxylic acid functionalized SWCNTs, produced by the electric arc discharge technique [Journet et al., 1997] were purchased from Sigma Aldrich. Manufacturer's specifications are as follows:

- average diameter of individual SWCNT 1.4 nm ± 0.1 nm;

- bundle dimensions: diam. × length at 4-5 nm × 500-1500 nm;

- purity: 80 - 90%;

- total impurities: 5-10 % metals (Ni and Y)

- solubility in H_2O: 0.1 mg mL^{-1}

Stock solutions of either 20 or 100 ppm were prepared at room temperature by sonication for 90 minutes to disperse nanotubes in ultrapure water. The short sonication period prevented excessive breakage of nanotubes at the same time [Yang et al., 2005; Hennrich et al., 2007; Smith et al., 2009]. Stock suspensions were stored refrigerated at 4° C and used within one week.

Fullerenes C$_{60}$

Sublimed fullerenes C$_{60}$ were purchased from Materials and Electrochemical Research (MER) Corporation and used without any further purification. Manufacturer's specifications are as follows:

- purity: 99.9 %

- production method: chromatography

- visual properties: black crystalline powder with powder density of about 0.8 g cm^{-3}

- impurities: traces of C$_{70}$ and C$_{60}$ oxide.

Water-stirred fullerene aggregates (nC$_{60}$) were prepared by magnetic mixing of 250 mg of the powder at room temperature for 65 days in 500 mL of ultrapure water giving a nominal concentration of 500 ppm. To avoid microbiological contamination during the long stirring, ultrapure water was filtered over 0.2 μm (cellulose nitrate membrane, Whatman) and sterilized in an autoclave prior to stirring. Stirred solutions were exposed to natural light (but not to direct sunlight). The stock solution was then stored refrigerated at 4° C and diluted accordingly for the experiments.

The water-stirring technique was previously used and reported in the literature [Cheng et al., 2004; Lyon et al., 2006; Oberdorster et al., 2006; Baun et al., 2008; Spohn et al., 2009; Hyung and Kim, 2009]. This approach allows the preparation of well dispersed suspensions while avoiding the introduction of organic solvents. In such methods, tetrahydrofuran (THF) is most commonly used for solubilisation [Deguchi et al., 2001; Sayes et al., 2005; Spohn et al., 2009]. However, other solvents such as toluene, acetone and ethanol have been used [Brant et al., 2006; Dhawan et al., 2006; Hyung and Kim, 2009]. An extended mixing protocol was chosen for this study due to its simplicity and environmental relevance.

3.1.3 Ancillary solutions and substances

HCl

Hydrochloric acid solution 2M bench reagent was purchased from Fisher Scientific. 0.1M HCl solution used for pH adjustment was prepared by dissolving the appropriate amount of concentrated HCL in ultrapure water.

NaOH

Analytical reagent grade sodium hydroxide pellets (99.35 % pure) were purchased from Fisher Scientific. 0.1 M NaOH solution used for pH adjustment was prepared by dissolving the appropriate amount of NaOH pellets in ultrapure water.

HNO_3

Trace SELECT® 65% nitric acid for trace analysis was purchased from Sigma Aldrich and diluted as required (to obtain 1 or 0.1 M solution).

Sodium chloride solution

Analytical reagent grade sodium chloride was purchased from Fisher Scientific. Stock solutions of either 26 or 1300 ppm Na^+ were prepared by dissolving the appropriate amount of NaCl solid in ultrapure water. These concentrations were chosen to easily obtain the final sample concentration of 13 ppm, which is the same as in the natural lake water used in the experiments. The solution was stored refrigerated at 4° C and used within a week.

Calcium chloride solution

Analytical reagent grade calcium chloride dehydrate was purchased from Fisher Scientific. Stock solutions of either 90 or 4500 ppm Ca^{2+} was prepared by dissolving the appropriate amount of $CaCl_2 \cdot 2\ H_2O$ solid in ultrapure water. These concentrations were chosen to easily obtain the final sample concentration of 45 ppm, which is the same as in the natural lake water used in the experiments. The solution was stored refrigerated at 4° C and used within a week.

Sodium nitrate solution

Analytical reagent grade sodium nitrate was purchased from Fisher Scientific. 1M solution was prepared by dissolving the appropriate amount of $NaNO_3$ solid in ultrapure water. The solution was stored refrigerated at 4° C and used within a week.

Metal standard solutions

1000 ppm copper, cadmium and chromium standard solutions were purchased from Fisher Scientific.

Chelex® 100 sodium form

50-100 dry mesh Chelex® 100 sodium form with 0.6 meq g^{-1} binding capacity towards heavy metal ions was purchased from Sigma Aldrich. It was used to bind traces of metals in sodium nitrate solutions (in DGT experiments).

Ultrapure water

Ultra High Purity (UHP) water with a maximum resistivity of 18 MΩ cm^{-1} was used throughout the experiments. Since the experiments were conducted in 2 different laboratories different ultrapure water systems were used: Barnstead Reverse Osmosis System and Diamond TM.

This chapter details the sample preparation protocols common for all parts of the laboratory experiments. Chapter specific information (i.e. further sample handling and protocol) is detailed in later chapters according to its relevance.

3.2   **Methods**

3.2.1   **Atomic force microscopy**

With resolution over 1000 times better than the optical diffraction limit (determined by apical probe geometry and sample geometry), AFM enables 3-dimensional imaging of nanostructures up to a fraction of nanometre in size (ca. 0.1 nm) [Giessibl, 2005]. Invented in 1986, AFM belongs to the scanning probe microscopy family [Binnig et al., 1987; Morita et al., 2002; Sugimoto et al., 2007]. The term 'microscopy' is often seen as a misnomer, since it suggests seeing sample features, whereas in reality the sample is examined by 'feeling' its surface with a specially constructed probe.

AFM has been successfully and broadly used in academic and industrial research as a tool for imaging, measuring, characterisation and manipulation of matter at the nanoscale. Its applications encompass physics and physical chemistry [Cui et al., 1999; Jandt et al., 2000], polymer science [Godehardt et al., 2004; Chen et al., 2008], biological science [Wu et al., 2002; Fotiadis et al., 2002; Lyubchenko and Shlyakhtenko, 2009], environmental sciences [Balnois et al., 1999; Ramirez-Aguilar et al., 1999] and nanoscience [Deng et al., 2007; Checco et al., 2006].

The scanning probe is equipped with an atomically sharp tip. Most commonly it is made of antimony or phosphorus doped silicone or silicon nitride with heights of the order of a few μm [Veeco Catalogue, 2008]. More important, however, is the sharpness of the tip measured as a radius of curvature of the tip's apex, usually within the range of 5-20 nm. This parameter determines the lateral resolution of the microscope by determining so-called tip convolution (Fig. 3.1) [Wang and Chen, 2007]. Only an infinitely sharp tip can project the surface with no distortions. Any realistic tip geometry

will result in artifactual topography, the "blunter" the tip, the more distortions are experienced.
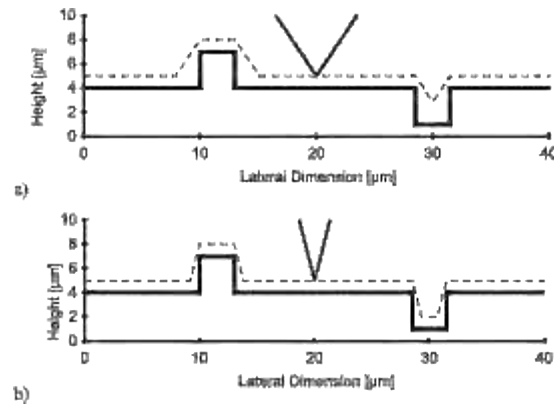
Figure 3.1. Tip sharpness v AFM resolution a) tip angle of 70 b) tip angle of 30
[source: http://wwwex.physik.uni-ulm.de]
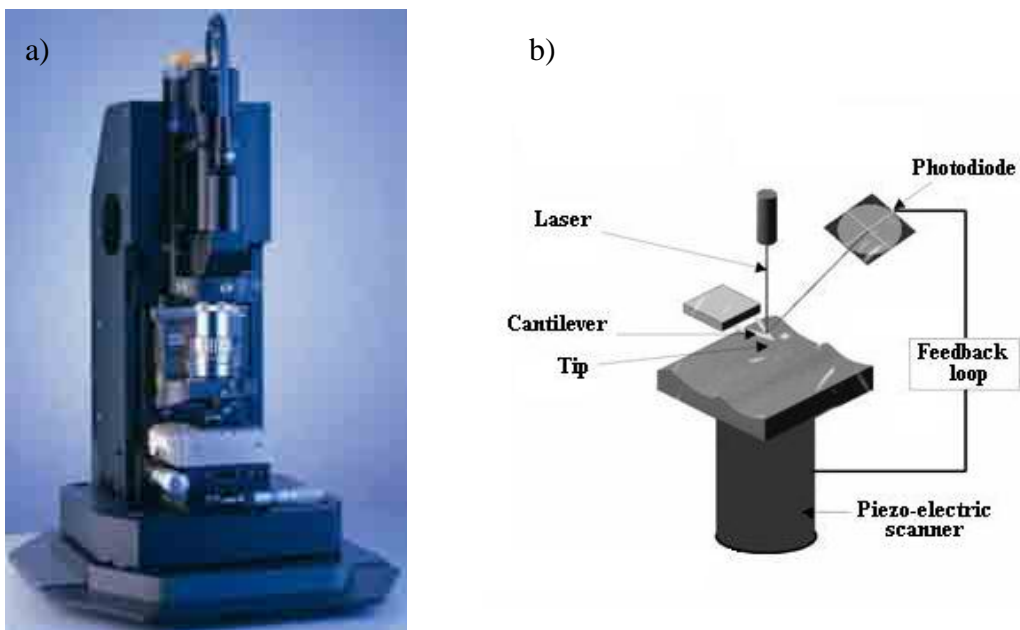
Figure 3.2. a) XE-100 AFM by Park Systems b) schematic principle of operation of an atomic force microscope (Balnois et al., 2007).

3-D image of the studied specimen is built by scanning its surface line by line and measuring the repulsive and attractive atomic forces between the sample and the tip

(Figure 3.2 b). Since the tip is attached to a flexible cantilever these forces can be measured as the deflection of the cantilever according to the Hooke's low of elasticity:

$$F = -k \, x \qquad\qquad (3.1)$$

where F is the force, k is the spring constant of the cantilever and x is distance that the cantilever has been stretched or compressed away from the equilibrium position. The interaction mechanism between the tip and the scanned surface can be provided by different kinds of forces including Van der Waals forces, mechanical contact force, capillary forces, chemical bonding, electrostatic and magnetic forces, etc. Figure 3.3 shows a typical force-distance curve (Van de Waals curve). According to Pauli principle, at small distances repulsive forces dominate since the atoms are close enough for their electronic clouds to overlap and repel each other with quantum mechanical forces. At larger distances the atoms of the tip and the surface of the sample attract each other due to Van der Waals dispersion forces [Balnois et al., 2007].
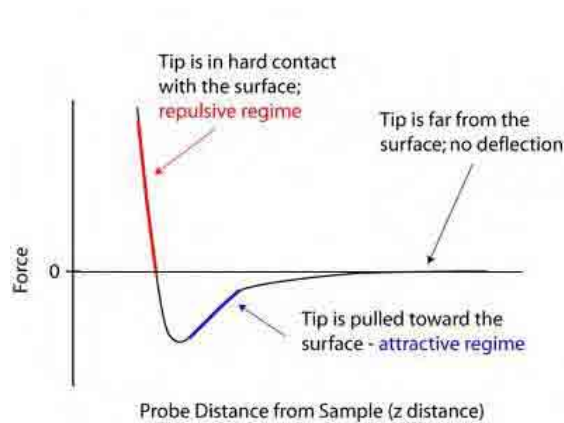
Figure 3.3. Inter-atomic total (repulsive and attractive) force v distance in AFM.
(source: http://www.nanoscience.com)

Although the interaction force between the tip and the surface of the sample is very small (usually ranging from 10^{-6} to 10^{-11} N [Rugar and Hansma, 1990]) it can be

indirectly but precisely measured by the deflection of the laser beam reflected on the cantilever. The laser beam deflection is expressed as a light intensity on an array of position-sensitive detector (Fig. 3.4) and translated into voltage. The detector consists of 2 adjacent photodiodes. A correctly aligned laser beam hits the exact centre of the detector. When the tip touches the sample surface cantilever deflects resulting in the laser beam illuminating one photodiode more than the other [Butt et al., 2005].
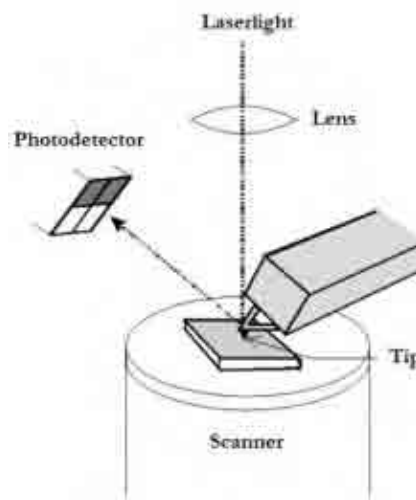
Figure 3.4. Deflection of the cantilever translated into the laser beam deflection detected on a position-sensitive photodiode and converted into voltage [Butt et al., 2005].

The output signal is produced as a difference between the signals received by the photodiodes normalized by their sum and is collected by a differential amplifier. The signal proportional to the deflection of the cantilever can detect its movements smaller than 10 Å [Alonso and Goldmann, 2003]. This data is used in a feedback mechanism to maintain the same distance between the sample and the tip (constant height mode) or the same force between the sample and the tip (constant force mode), which is crucial to avoid damage to the fragile scanning probe (Fig. 3.2 b) [Gan, 2009]. The core of this mechanism is usually a sample stage or a scanner made of piezoelectric ceramics (which is a class of materials that expand or contract as a function of the applied

voltage) that facilitates small but extremely precise three-dimensional positioning (with a sub-nanometre resolution) [Kwon et al., 2005].

Figure 3.5. Different tip scanning modes of AFM (adapted from Park Systems).

Imaging modes

AFM imaging can be operated in two main scanning modes: static (contact) and dynamic (tapping and non-contact), principles of which are shown in Fig. 3.5.

- In the contact mode the tip is in perpetual contact with the sample surface [Quate, 1994]. It is also known as a repulsive mode since in this mode the repulsive forces dominate the tip-surface interactions (Fig. 3.3). In other words pushing the cantilever against the sample results in the cantilever deflection and the z-dimension feedback loop is used to maintain a constant cantilever deflection. For this mode stiff cantilevers with low spring constant are used. Apart from the repulsive Van der Waals force described above, two other forces are usually present in the contact mode: capillary forces (due to thin water layer often present in the ambient environment, if dry) and the force exerted by the cantilever itself. The dragging motion of the tip results in significant lateral forces. This is the main limitation of the contact mode since soft fragile samples can be easily damaged, deformed or poorly attached particles displaced or removed.

- In the tapping mode (also called intermittent-contact, dynamic contact or dynamic force mode) the cantilever is oscillating at its resonant frequency with a certain amplitude (typically in the range of 10-100 nm) as shown in Fig. 3.5 [El Feninat et al., 2001]. The tip strikes against the surface on each oscillation cycle and detaches from the sample surface by using a large vibration amplitude. The tip remains in contact with the sample for a very short time (in the repulsive regime of the force curve) and the amplitude of oscillation changes. Thanks to this brief interaction between the sample and the tip, problems associated with lateral forces, friction, adhesion, electrostatic forces, etc. are overcome. This allows studying topographies of soft, deformable and weakly immobilised materials.

- In a non-contact mode the tip is kept oscillating at a constant distance from the sample surface (usually a few nm) and does not come into contact with the sample surface (i.e. operates in the attractive regime of the intermolecular force curve, Fig. 3.3) [Martin et al., 1987; Morita et al., 2002]. Since the attractive forces are much weaker then the repulsive ones, the amplitude of oscillation has to be lower than in the tapping mode to keep the tip within the range of the sample-tip interaction. This mode is non-invasive making it most suitable for fragile and soft samples. However, the relatively large distance between the tip and the sample may lead to poorer resolution than obtained with contact and tapping modes. Additionally, weaker attractive signal makes it more difficult to operate in the non-contact mode.

Tapping v non-contact mode

In general, dynamic modes (tapping and non-contact) are believed to be less perturbing and their use for studying aquatic colloids has been well documented [Balnois et al., 1999; Hannah et al., 2003; Lead et al., 2005]. In both modes the tip is kept vibrating in free-space by a piezoelectric modulator in the vicinity of the resonant frequency f_0 (Fig. 3.6). The tapping mode uses a frequency $f_{tapping}$ lower than f_0 whereas non-contact mode uses frequency $f_{non-contact}$ higher than resonant frequency (Fig. 3.6). As the tip gets closer to the sample the attractive van der Waals force appears between the probe and the sample and the spring constant of the cantilever is reduced by this interaction. Lower spring constant causes a shift in the resonance frequency ($f_{tapping}$ is now very
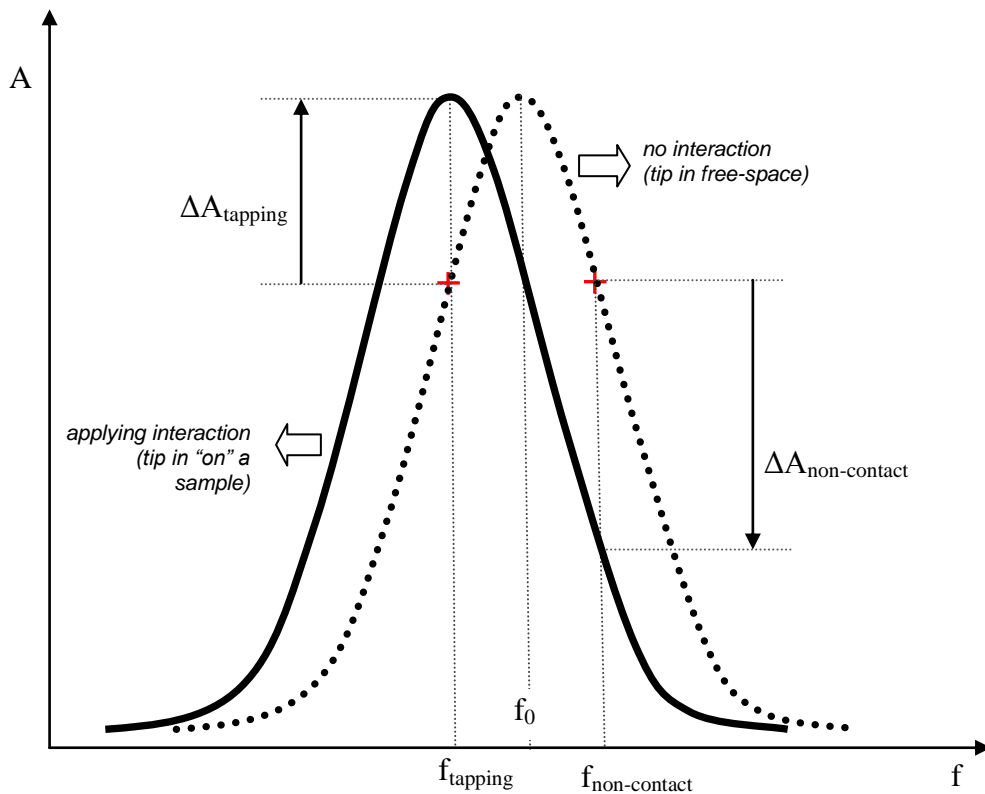
Figure 3.6. Shift of resonant frequency in tapping and non-contact AFM modes.

close to it, $f_{non\text{-}contact}$ is further from it). In the tapping mode the amplitude of oscillation at the changed frequency is increased by $\Delta A_{tapping}$ (it reaches about 100 nm) and the tip comes into a short intermittent contact with the sample. When the amplitude increases the feedback loop decreases the distance between the tip and the sample surface, when the amplitude is smaller the distance is increased so that the probe is in the "tapping" contact with the sample. In case of the non-contact mode, the shift in the resonant frequency occurring when the interaction is applied causes the change in the amplitude $\Delta A_{non\text{-}contact}$. The scanning amplitude for the non-contact mode is low (a few nm) so that the tip is constantly kept within the distance of the weak attractive force but does not physically touch the sample. Due to this weak interaction forces, non-contact mode requires extremely sensitive feedback loop mechanism and thus was developed later.

Tapping mode has been widely used for aquatic colloids characterisation in the past [Balnois et al., 1999; Plaschke et al. 1999; Wilkinson et al., 1999; Lead et al., 2005]. Being less perturbing than the contact mode, it is regarded as particularly suitable for imaging soft and fragile samples such as natural aquatic micro- and nanoparticles. In the tapping mode, frictional and lateral forces present in the contact mode are eliminated. Nevertheless, the striking force, with which the probe "taps" the sample is still relatively high and can results in damage to the tip or soft samples. True non-contact mode is expected to be even less perturbing and thus possibly even more suitable to study environmental samples [Jalili and Laxminarayana, 2004].

Phase imaging

The primary use of AFM is to provide 3-dimentional information about topography of the sample. In the dynamic modes, atomic tip-to-sample forces influence

the oscillation amplitude, phase and resonant frequency. Measuring these changes provides information about the sample's characteristics beyond topographical mapping. Phase imaging can produce information about variations in composition, hardness, adhesion, friction, viscoelasticity, electrical and magnetic properties of the studied sample [Schmitz et al., 1997]. Phase imaging builds a picture of the sample surface by mapping the phase lag between the periodic signal that drives the cantilever (and at which the cantilever oscillates when there is no interaction, i.e. cantilever oscillating in the free space) and the cantilever oscillation output signal (i.e. when there is tip-sample interaction) as shown in Fig. 3.7. This technique is very useful for contaminant identification, studying components distribution in composite materials, differentiating regions of high/low hardness or adhesion, etc.
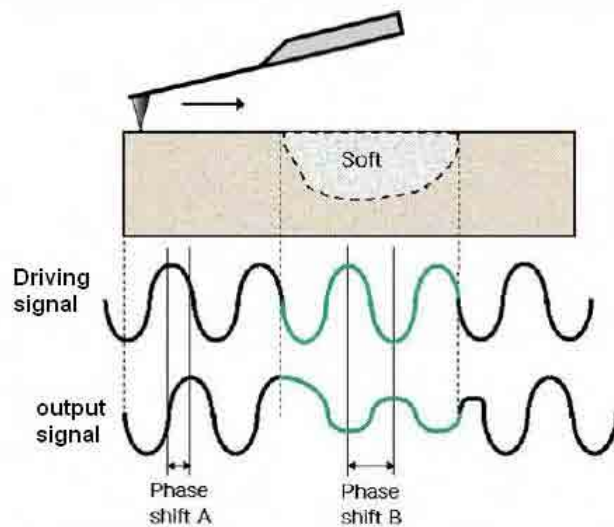
Figure 3.7. The principle of phase imaging – the phase lag varies depending on sample properties (Park Systems).

Advantages and disadvantages of AFM

Atomic force microscopy is a powerful imaging technique for the study of materials at the micro- and nanoscale in great detail. Additionally, it provides a three-

71

dimensional surface profile as well as other than morphological sample characteristics such as surface hardness. AFM is suitable for non-conductive surfaces and does not require special sample preparation (like metal coating), which is especially important in natural and biological sciences. Unlike electron microscopy, AFM operates well in ambient air so there is no need for expensive vacuum conditions, which may be damaging for fragile and wet samples. Equipped with a specially designed liquid cell, AFM can scan surfaces in aqueous environments, too.

Nevertheless, since no AFM tip can be ideally sharp, there is a range of possible artefacts. To account for the radius of curvature of the tip resulting in overestimation of lateral dimensions, AFM heights (rather than widths) are used as estimates of particles diameters. Another disadvantage of AFM is relatively small image size and slow rate of scanning, which make the technique very time consuming and unsuitable for samples unevenly distributed on microscopy specimen. Sample preparation involves fixing on a surface, which brings issues in particle shape deformation.

3.2.2   Transmission electron microscopy

If a focused beam of light (produced through a condenser lens) is transmitted through a very thin specimen and then focused and magnified with objective and ocular lenses, it can produce an image magnified by up to 1000 times [Slayter and Slayter, 1992]. Instruments used for this purpose, usually in biosciences, belong to the optical microscope family and are called light transmission microscopes [Shmaevsky, 2006]. The TEM operates on the same basic principle but uses a beam of electrons instead of light. The much lower wavelength of electrons (sub nanometre) in comparison to light (ca. 500 nm) enables the TEM to achieve very high (angstrom) resolution using the most advanced systems [Bendersky and Gayle, 2001; Williams and Carter, 2009]. Due to this powerful magnifying ability, TEM has been widely used in the broadly defined nanosciences and is now the key characterization technique to study structure, morphology and properties of all types of NMs [Spence, 2002; Murr 2009; Kumar et al., 2009; Suh et al., 2009]. TEM is also commonly utilised to study individual entities and aggregate structures of natural micro- and nanoparticles, such as atmospheric ultrafine particles and natural aquatic colloids [Perret, 1991; Sobanska, 2000; Casuccio 2004]. Throughout the experimental work in this thesis the Philips Tecnai F20 TEM operating

Figure 3.8. Tecnai TEM microscope (source: http://www.fei.com).

at 200 kV was used (Fig 3.8). A schematic view of a typical TEM microscope column is shown in Fig. 3.9. The source of electrons (which in case of the Tecnai microscope is a field emission gun) produces a beam of monochromatic electrons.
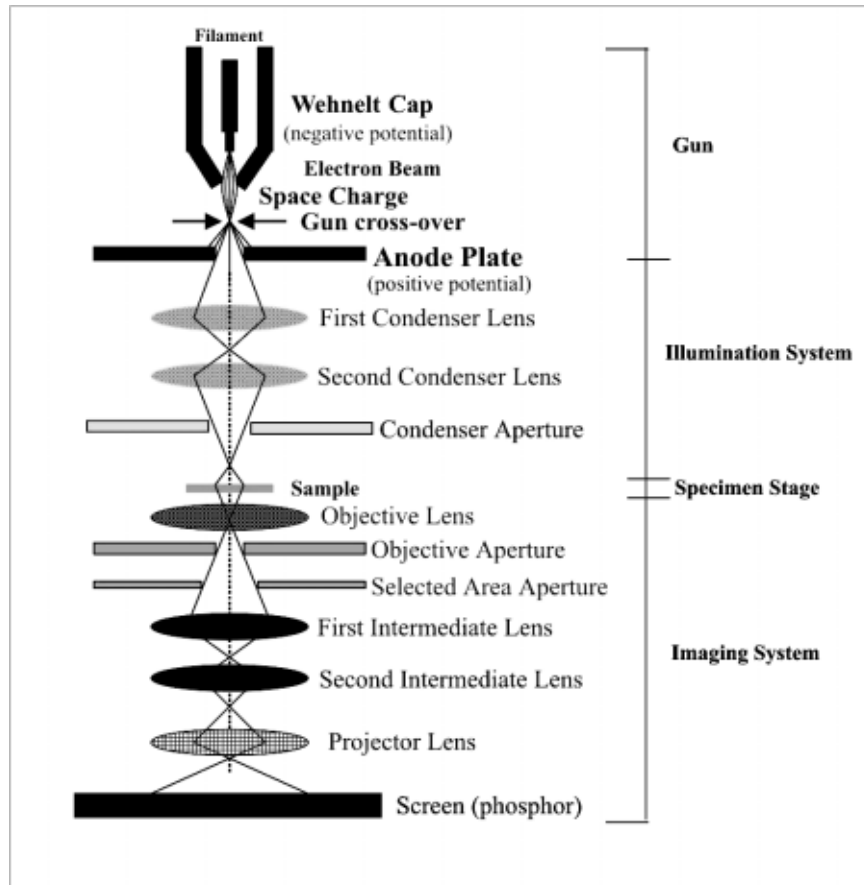
Figure 3.9. Schematic view of a TEM column (source: http://bsatpati.googlepages.com/tem).

Two electromagnetic condenser lenses are used to concentrate and focus the electrons into a very thin beam to uniformly illuminate the sample. By modification of the strength of the condenser lenses the required size of the spot striking the specimen is achieved. Before hitting the sample, the beam is finally 'filtered' through the condenser aperture to remove high angle electrons and optimise the intensity of illumination. Such optimally formed electron beam travels through an ultra thin (~ 0.1 μm) specimen

[Williams and Carter, 2009]. Interactions between the studied sample and the electrons are the source of information about the morphology and properties of the studied material (Fig. 3.10). Various electron microscopy techniques (and their modes of operation) use different electron signals [Williams and Carter, 2009]. Backscattered and secondary electrons are a source of topographical data in scanning electron microscopy (SEM) [Egerton, 2005]. In TEM imaging unscattered electrons that go through the sample are utilised.
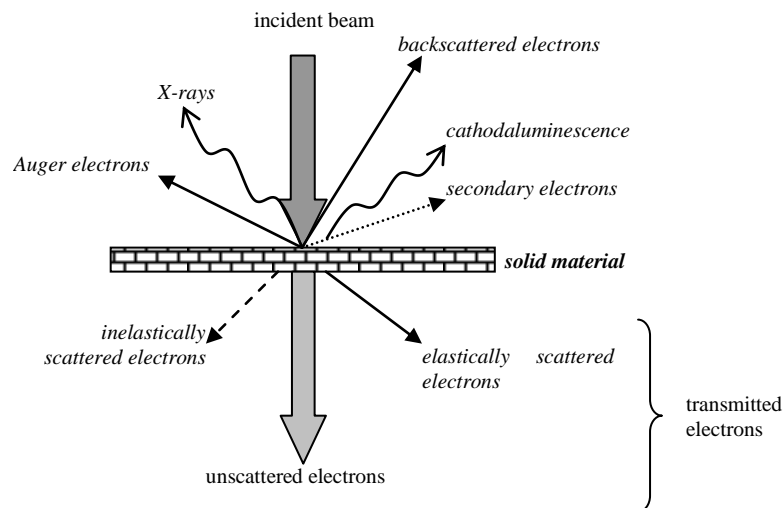
Figure 3.10. Possible interactions between high energy electrons and a solid sample
(adapted from http://www.unl.edu/CMRAcfem/temoptic.htm).

Unscattered electrons go through an objective lens, which together with the sample stage is the heart of the microscope (Fig. 3.9). The objective lens forms an inverted enlarged initial image, which is then further magnified by intermediate and projector lenses. Objective aperture is placed after the objective lens to remove elastically and inelastically scattered electrons from the transmitted beam to improve contrast of the final image. Magnification (from hundreds to a million times) is achieved by varying the strength of intermediate and projector lenses (strength of electromagnetic lenses is

tuned by changing the current in the coil) [Shmaefsky, 2006]. Finally, the processed beam of unscattered electrons produces a 2-D image on the fluorescent screen at the bottom of the microscope. Electron dense areas of the specimen let through few or no unscattered electrons and thus they appear as dark or completely black spots on the screen. Morphology of the specimen is shown as areas of varied darkness. TEM images can be compared to a photo slide or transparency image obtained when light is used instead of electrons. A CCD camera can be used to take digital images and then analyse them with appropriate software.

As has been mentioned before, the significant resolution of the TEM microscope results from the small wavelength of the electron beam. This in turn depends on the acceleration voltage of the microscope (usually in the range of 80-400 kV) [Reyes-Gasga and Garcia-Garcia, 2002; Freitag et al., 2008]. Thus higher magnifications can be obtained with microscopes operating at higher acceleration voltages. However, the achievable resolution of the TEM microscope is limited by aberration (especially spherical) of the objective lens, i.e. its failure to project the exact correspondence between an object and its image [Haider et al., 1998; Batson et al., 2002]. Images distorted by aberration appear smeared and blurred. Modern microscopes are equipped with a range of aberration correctors to compensate defocus caused by aberration and with such improved performances they can achieve resolution of 0.1 nm [Hetherington, 2004].

Since negatively charged electrons would strongly interact with charged molecules of air (they would be absorbed or deflected), high vacuum (10^{-3} - 10^{-7} Torr) conditions must be strictly kept in the microscope column to ensure uninterrupted passage of the beam through its desired path [Williams and Carter, 2009]. Vacuum is

also essential to avoid generating an arc (discharging) between the cathode and the anode, i.e. destroying the field emission gun.

The primary use of a TEM microscope is visualisation of material morphologies at a nanoscale by utilising the beam of unscattered electrons. Recent advances in TEM allow real-time observations to be made of sample changing under certain conditions, i.e. dynamic TEM [Stach, 2008]. ETEM (environmental transmission electron microscopy) technique has been used to visualise catalyst behaviour during a chemical reaction [Giorgio et al., 2006]. However, alternate modes of operation together with electron spectrometers, energy filters, and X-ray fluorescence systems allow the observation of other, non-morphological properties of the sample. These techniques can be grouped together as analytical TEM [Schneider, 2002]. Valuable information on the molecular arrangements of crystalline materials can be produced in the diffraction mode [Williams and Carter, 2009]. With the use of additional detectors elemental composition of the sample can be studied. In this case the X-ray spectrum of electrons is analysed by the Energy Dispersive X-ray Spectrometer (EDX) or inelastically scattered electrons are analysed by the Electron Energy Loss Spectroscopy (EELS) (Fig. 3.10) [Chen et al., 2004A].

Advantages and disadvantages of TEM

The primary advantage of TEM is its exceptional resolving power down to a sub-nanometre scale. Samples can be studied in great detail to analyse their morphology, internal structure and chemical composition. Nevertheless, there are certain limitations to the TEM technique. The main disadvantage of the TEM is that a specimen suitable for analysis has to meet a list of criteria. The primary criterion is that

the sample lacks volatile components, especially water, due to high vacuum conditions in the microscope column, which makes it impossible to study aquatic or biological materials in their unperturbed state. Samples should remain unchanged under high vacuum as well as resist thermal and physical stress (specifically exposure to high energy electron bombardment). Additionally, the thickness of the sample is crucial since the specimen has to be transparent to the beam. All these factors make the TEM analysis expensive, time consuming and involving skilled, experienced staff.

3.2.2.1 Overview of TEM specimen preparation methods for natural aquatic colloids

Natural aquatic systems contain living entities such as bacteria, algae, fungi, etc. and non-living particles such as cellular debris, viruses, polysaccharides, proteins, humics, metal oxides and sulphides, clays, etc. in numbers of $10^8 - 10^{13}$ L^{-1}, with size range of $1 - 10^5$ nm and varied morphotypes such as fibrillar, compact, amorphous, crystalline, etc. [Wilkinson and Lead, 2007]. To ensure good representation of suspended colloidal matter for TEM investigation, appropriate specimen preparation protocol has to be applied. The aim is to image nano- and micro-particles with a minimum of artefacts introduced by either sample preparation or by the imaging itself, possibly unperturbed and representative to their aqueous colloidal form. At the same time TEM specimen is exposed to a high energy electron beam and operation under ultra high vacuum, i.e. in the absence of water, which is essential in TEM analysis. Thus, quality and accuracy of TEM investigation critically depend on how this challenge is overcome and taken into account when interpreting the TEM data.

TEM specimens are prepared by dispersing a small volume of the studied suspension on a supporting grid of ca. 3 mm in diameter. These grids are covered with electron-transparent supporting film usually made of carbon, pioloform or formvar laid on a metal (copper, nickel, gilded, etc.) square or hexagonal mesh [Agar Scientific, Pacific Grid-Tech product catalogues].

There are a number of TEM specimen preparation techniques depending on how the aquatic suspension is dispersed on the grid:

- **Whole mounts technique** – direct deposition followed by air drying (Fig. 3.11) [Baalousha et al., 2005 B; Diegoli et al., 2008; Park et al., 2009]. Approximately 10 µL of the sample is pipetted onto the grid, the excess liquid is removed with filter paper and the grid is left to evaporate in ambient conditions sheltered from vertical atmospheric deposition. This approach is the most rapid and straightforward. Nevertheless, there are a few possible artefacts induced by this method [Wilkinson and Lead, 2007]:

  - major aggregation during drying is usually unavoidable. Flexible aggregated organic materials might shrink and smaller particles might coagulate;

  - within the droplet of the water particles are held by surface tension and deposit unevenly on the grid, usually the sample covers a small area on the supporting film;

  - crystallisation of undesired electrolytes, especially in case of marine samples or samples whose pH or ionic strength was changed with electrolyte solutions during experiments. This effect can be minimised by washing the specimen in ultra pure water.

Figure 3.11. A droplet of the sample drying on the TEM grid as a way of TEM specimen preparation (whole mounts technique).

- **Ultramicrotomy** – cutting the specimen into transparent thin sections [Wilkinson and Lead, 2007]. Firstly, the suspension is embedded in a hydrophobic or hydrophilic resin to preserve the structure of colloidal entities. For abiotic NAC usually hydrophobic resins are used together with sequential dehydration in organic solvents [He et al., 1996; Robert et al., 2004]. For bacteria, algae, polymers, organic flocs, etc. hydrophilic resin (Nanoplast) can be used [Perret et al., 1991; Swartz et al., 1997; Lienemann et al., 1998]. Hydrophilic resins are more suitable since dehydration in organic solvents (required in case of hydrophobic ones) introduces additional artefacts such as dissolution of organic components [Leppart et al., 1990]. The resin protects colloids from changes during drying and beam exposure and serves as a matrix fixing colloids in the dehydrated sample. The resin embedded sample is then cut into thin slices (about 50-100 nm) with a diamond knife, which has sufficient hardness for mineral particles.

An additional step of staining prior to resin embedding might be required to improve contrast of the TEM images. Staining chemicals used for microbiota usually contain salts of osmium, uranium and/or lead [Wilkinson et al., 1995; Lienemann et al., 1998; Koukal et al., 2007]. However, this technique is well

developed for hydrophobic rather than hydrophilic resins [Wilkinson and Lead, 2007].

Ultramicrotomy is an advanced technique allowing a good representation of minimally perturbed aquatic colloids and their interactions. Nevertheless, taking thin sections is demanding and time consuming; it requires practice and skill. In the case of hydrophobic resins possible artefacts may result from dehydration of the sample in organic solvents. The cutting process itself is precise and painstaking and may produce sectioning–induced artefacts such as knife marks, curling, rumpling, pullout, etc [Wilkinson and Lead, 2007].

- **Ultracentrifugation** (quantitative mounts) – direct centrifugation of the suspension onto the TEM grid at high speeds [Perret et al., 1991; Lienemann et al., 1997; Benedetti et al., 2003; Koukal et al., 2008; Chanudet and Filella, 2008]. By varying the volume and/or particle concentration in the sample the optimum film coverage can be obtained: longer time and higher cost of analysis result from too dilute samples whereas a too concentrated sample may lead to erroneous conclusions about particle aggregation or a sample too thick for the electron beam [Lienemann et al., 1998]. Swing-out buckets are usually used allowing even deposition of particles. As the deposition of particles can be controlled (with rotor speed, run time, sample volume, etc) ultracentrifugation is suitable for quantitative analysis (e.g. particle size distribution). Stoke's law is used to calculate the time t required for a hard, spherical particle with a diameter d to settle from the surface of the sample r_{min} to the grid r_{max} (measured as a distance from the rotor's axis of revolution) [Wilkinson and Lead, 2007]:

$$t = \frac{18 \, \eta \, \ln(r_{max}/r_{min})}{d^2 \, (\rho - \rho_0) \, \omega^2} \qquad (3.2)$$

where η is viscosity of the suspension, ρ density of the colloid, ρ_0 density of the suspension and ω angular rotation speed.

A thin layer of Nanoplast resin may be spun onto the surface of the grid after centrifugation to protect fragile colloids (e.g. flexible fibrils) from shrinkage or damage during dehydration prior to TEM analysis [Perret et al., 1991; Lienemann et al., 1997; Swartz et al., 1997; Benedetti et al., 2003].

- **Cryotechniques** – preserving the three-dimensional colloidal relationships by fixing them in a frozen form. Vitrification is an ultra-fast freezing method usually used for aqueous samples since is allows freezing water without forming ice crystals i.e. damaging labile biological entities [Dubochet and Lepault, 1984; Ruiz et al., 1994]. In freeze-etching, which is another cryotechnique for TEM specimen preparation, vitrified sample is fractured along a natural plane of weakness to make a metallic replica of the surface revealing the internal structure of the sample [Mondain-Monval, 2005]. It should be noted, however, that significant differences of thermal conductivity between particles and surrounding water lead to ice formation, especially in case of colloids larger than several nanometres.

Cryotechniques in general are thought to faithfully preserve the original three-dimensional structures. However, although these techniques have been used in

biological sciences and have potential for aqueous samples, they have not been utilised for aquatic colloids due to their technical complexity and high costs [Wilkinson and Lead, 2007].

- **Focused ion beam milling** – a relatively new technique for cutting thin sections by using a finely focused beam of charged ions [Obst et al., 2005]. The sectioning takes place in a scanning electron microscope where the operator examines the sample in real-time and precisely selects the area of the sample which is to be sectioned and subsequently analysed with TEM. Depending on the type of ions in the cutting beam irradiation damage to the sample can occur, usually about 20 nm deep [Labar & Egerton, 1999; Giannuzzi & Stevie, 1999]. Newer low-energy ion beams (Si/0.25 keV, GaAs/0.25 keV, Si/0.12 keV) combined with controlled angle of incidence can reduce this effect to below 1 nm [Barna et al., 1998].

3.2.3 Diffusive Gradients in Thin films technique

According to IUPAC recommendations, chemical speciation defines which types of different chemical forms (species) containing an element are present and what is the distribution of the element between these forms [Templeton et al., 2000]. Metal speciation is crucial to determine metal bioavailability and thus toxicity in aquatic systems. It has been accepted that free ionic activity of metal rather than total metal concentration represents much more accurately the amount of metal that can be taken up by aquatic biota [Campbell, 1995]. Natural waters rarely stay in equilibrium [Worms et al., 2006]. Processes of metal complexation and complex dissociation bind or release metal ions continuously (Fig. 3.12). Consequently, potentially bioavailable metal fraction contains free metal ions produced by kinetically unstable (i.e. labile) metal species [Van Leeuwen et al., 2005].

Diffusive Gradients in Thin-films (DGT) is a technique for in-situ determination of labile metal concentrations in water and soil samples [Zhang et al., 1995].
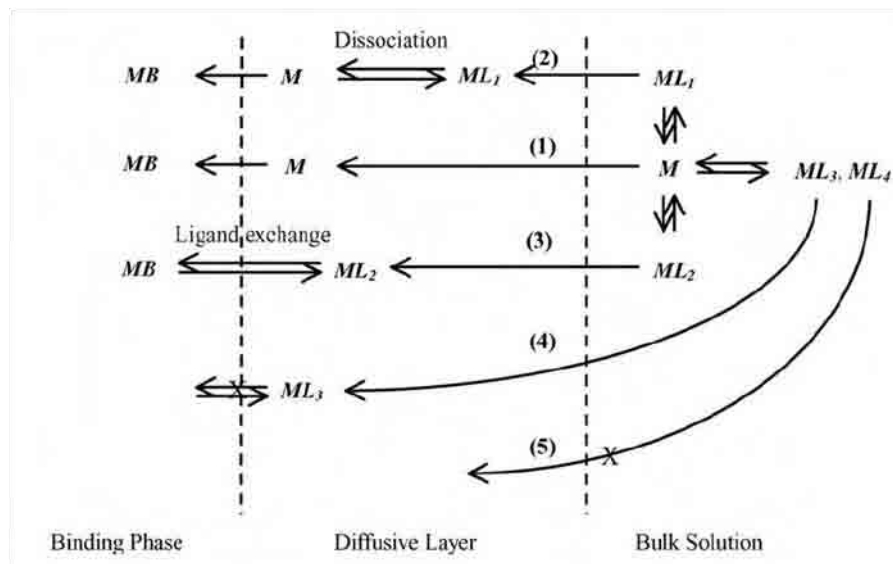
Figure 3.12. Schematic model of binding free metal ions from the bulk solution in the DGT binding phase [Li et al., 2005].

Consequently, DGT measured concentrations of metal can be treated as surrogates for bioavailable metal. Fig. 3.12 schematically explains metal speciation in a solution and metal species available for the DGT binding phase (i.e. metal species detected by the technique). DGT available metal forms include free metal ions (M), metal ions produced by the dissociation of complexes ML_1 which dissociate within the time required to pass through the diffusive gel layer, and metal ions exchanged between complexes ML_2 and the binding phase functional groups (Fig. 3.12). The amount of metal bound in inert complexes ML_3, which do not dissociate and in complexes ML_4, which are too big to pass through the diffusive gel pores (colloidal and particulate matter) are not accumulated by the binding phase and thus are not measured by DGT [Li et al., 2005].

Labile metal species from the analysed solution are bound on a resin-impregnated layer after they diffusively pass the hydrogel layer (Fig. 3.13).Shortly after deployment into water, a steady-state linear concentration gradient between bulk water and the resin layer is established. Then the flux of ions through the gel, J, can be described by the Fick's first law of diffusion:

$$J = D \cdot \frac{dC}{dx} \qquad (3.3)$$

where D is the diffusion coefficient and dC/dx is the concentration gradient.

If the following conditions are met:

- D is the same in the diffusive layer as in the diffusive boundary layer (DBL), where transport of ions is solely governed by molecular diffusion;

- free metal ions are in rapid equilibrium with the binding agent of a large binding constant (concentration of metal ions effectively equals 0 on the resin layer);

- bulk solution is well-stirred (δ is negligibly small)

concentration gradient can be expressed as:

$$\frac{dC}{dx} = \frac{C}{\Delta g} \qquad (3.4)$$

where C is the concentration of metal in the bulk solution and Δg the thickness of the diffusive gel. And thus combining equations 3.3 and 3.4:

$$J = \frac{D \cdot C}{\Delta g} \qquad (3.5)$$
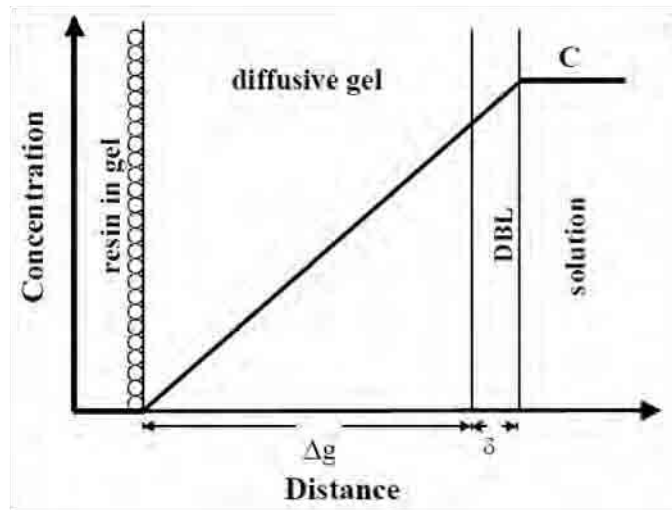
Figure 3.13. Schematic view of steady-state concentration gradient in a cross-section of a DGT device [Zhang et al., 1995].

Flux of ions, J, can be calculated from the mass of metal accumulated on the binding gel layer (measured with AAS, ICP-MS or other techniques). The diffusion coefficient is a known parameter for each gel layer depending on target ion and temperature. Consequently, the concentration of an analysed metal species in bulk water can be calculated as:

$$C = \frac{J \cdot \Delta g}{D} \qquad (3.6)$$

To minimise the volume of sample needed for the measurement to 500 ml, µ-DGT devices were used [Alexa et al., 2009]. µ-DGT device and its design are shown in Fig. 3.14.
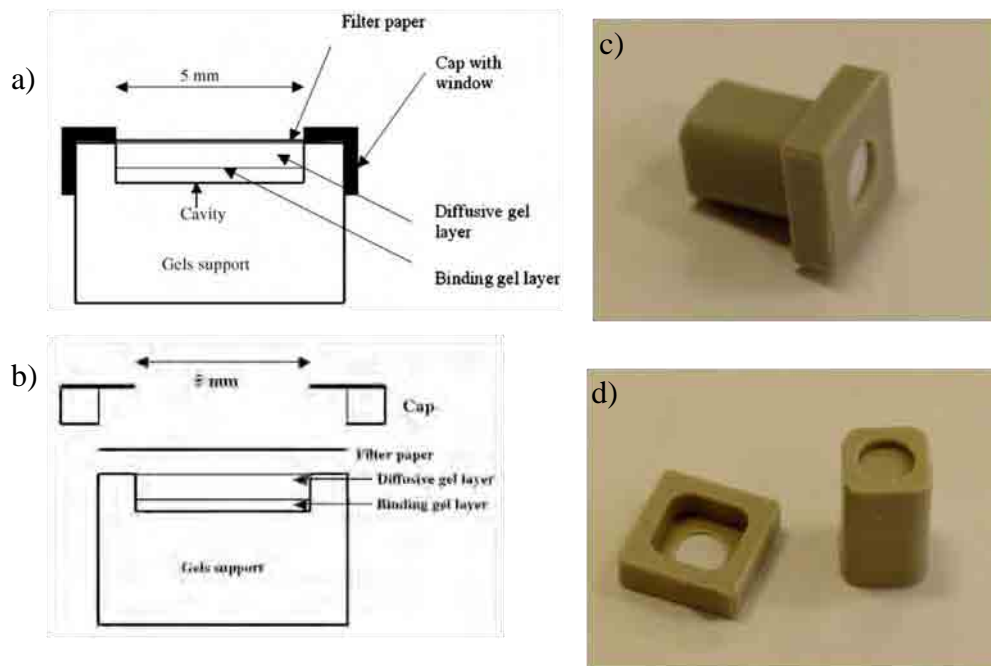
Figure 3.14. Schematic design representation of µ-DGT device (a) including exploded view (b) [Alexa et al., 2009]. Photos of assembled (c) and unassembled (d) µ-DGT device.

3.2.4 Inductively coupled plasma mass spectrometry

ICP-MS is an analytical technique for trace metal (and several non-metals) detection and concentration measurements with a detection limit in the range of parts per trillion (ng L^{-1} for aqueous solutions). Mass spectrometry detects and measures concentration of elements using charge to mass ratio. Ionised (positively charged) atoms are accelerated into a finely focused beam and travel in vacuum through a mass separation device where external magnetic field bends their trajectory: the lighter the ions, the most deflected they are (Fig. 3.15 a). The ions are sorted and separated
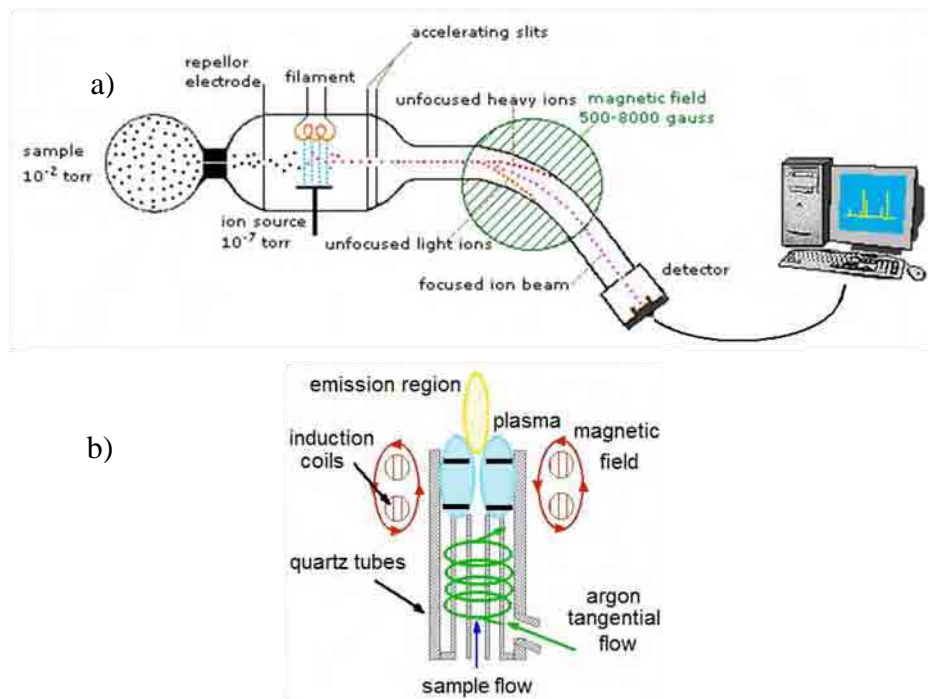
Figure 3.15. a) Schematic of a mass spectrometer (source: www.cem.msu.edu); b) schematic of an ICP torch (source www.chemistry.adelaide.edu.au).

according to their mass and charge, which ratio is characteristic for every element (or to be more precise for every isotope). The electronic detector device tallies the type of ions and their relative abundance.

In case of ICP-MS technique, the sample is ionised by an inductively coupled plasma torch (Fig. 3.15 b). The liquid sample is introduced through a nebuliser in high velocity argon to spray chamber where the smallest droplets are selected. Argon plasma flame is produced by heating the gas to ca. 6000 °C and exciting it in an oscillating magnetic field. As the atoms travel through the plasma they release electrons and become positively charged.

ICP-MS measurements were performed on the Agilent 7500ce instrument by Steve Baker, School of Geography, Earth and Environmental Sciences (University of Birmingham).

4 RESULTS: Characterisation of atmospheric nanoparticles with atomic force microscopy

4.1 Summary

In this chapter the application of AFM for characterisation of atmospheric particles is discussed.

In the next section (4.2) sampling and microscopy specimen preparation protocols are presented. The mechanism of inertial impaction utilised by MOUDI cascade impactor used in this study is explained. This section contains also sampling parameters and sample handling procedures prior to analysis.

Section 4.3 begins with a short summary of visualisation of atmospheric NPs with AFM available in the literature. It is followed by a selection of representative AFM micrographs obtained in this study for the two examined stages of the impactor, which are designed to collect particles at the nanoscale. Sizes and morphologies of imaged particles are discussed. An additional section is focused on phase imaging and how it can be used to examine particle properties beyond topography.

Collected images were used to calculate size distribution histograms for both stages, which are presented in section 4.4. The results are compared to expected theoretical aerodynamic diameters and possible causes for significant discrepancies are discussed.

4.2   Sampling and specimen preparation

Atmospheric samples in this study were collected with a 10-stage MOUDI[TM] (Micro-Orifice Uniform Deposit Impactor) cascade impactor (Fig. 4.1 a). As all inertial impactors, MOUDI fractionates atmospheric particulate matter on the basis of its inertial properties, which depend on the shape, size and density of the particles [Marple et al., 1991]. Particles with the same inertia can be represented by the same aerodynamic diameter, d_{ae}, which is the diameter of an ideal sphere with unit density (1 g cm^{-3}) and the same aerodynamic properties (such as sedimentation velocity, terminal velocity, drag coefficient, etc.) as the particle in question.

In an inertial cascade impactor particle laden air is directed through a number of impaction stages with multiple nozzles above them (Fig. 4.1 b) [Hering and Marple, 1986; Marple et al., 1992; Papastefanou, 2007; MSP Corporation, MOUDI Product Brochure]. As the sampled air flows through the impactor, particles follow air streamlines perpendicularly directed onto the impaction stages (Fig. 4.2). An impaction stage deflects the air flow to form a 90 degree bend in the streamlines. Only the particles with certain inertia (lower than the cut-off value for the stage) are able to follow the streamlines to the next impaction stage. Particles with enough inertia hit the stage and are deposited onto the impaction plate. With each subsequent stage, air nozzles are smaller and thus particle velocity increases so smaller and smaller particles are deposited on consequent impaction stages. To ensure more even plate coverage, the impactor is equipped with a rotator so the particles are collected in circular pattern rather than in spots corresponding to the nozzles.

Microscopic specimens for AFM was prepared by attaching thin, freshly-cleaved mica sheets to the impaction stages so that particles carried by air could deposit directly onto mica.
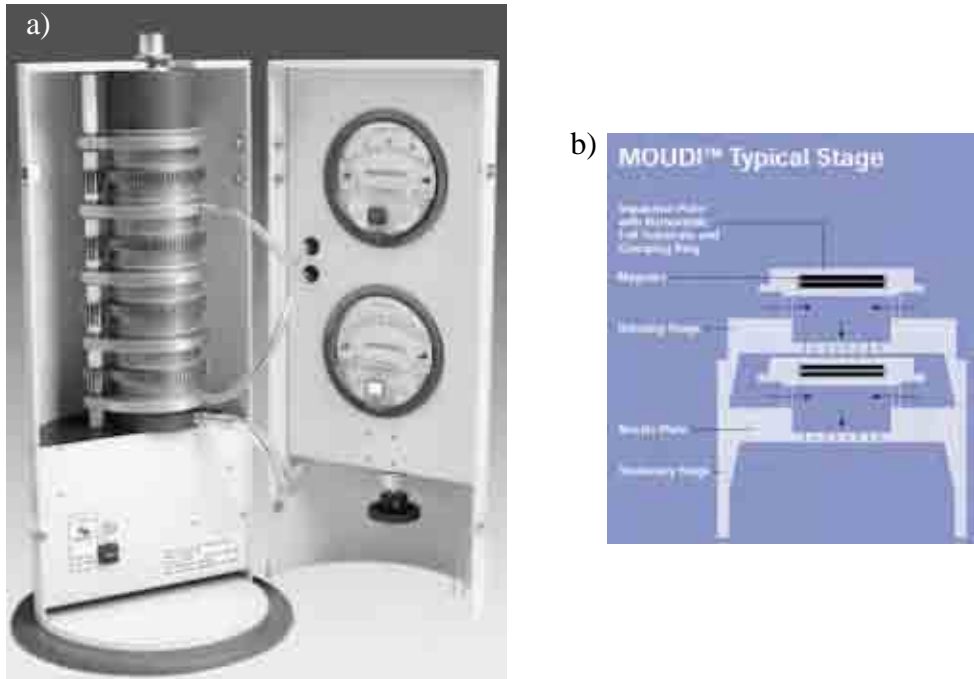
Figure 4.1. a) MOUDI^{TM} b) a schematic view of a typical stage in MOUDI^{TM} (source: www.appliedphysicsusa.com).
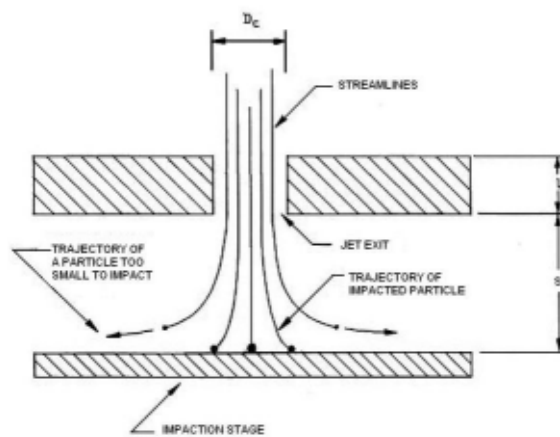
Figure 4.2. Principle of operation of a typical inertial cascade impactor (source: www.scientificfilters.com).

92

Samples were collected in a suburban background. Mica sheets were placed on the two last stages of the impactor (9th and 10th) to collect particles within the nanoscale size range. Nominal aerodynamic diameters on these stages are as follows:

-   stage 9: 100 - 180 nm

-   stage 10: 56 - 100 nm.

Sampling parameters:

-   sampling time: 36 min

-   air flow rate: 20 L min^{-1}.

Collected samples were kept refrigerated for 5 days prior to the AFM analysis. A blank mica sheet was prepared by exactly the same protocol apart from mounting the mica on an impaction stage. This blank sample was analysed with AFM to exclude contamination from specimen preparation and transport.

A XE-100 atomic force microscope by Park Systems was used in all the experimental work. The image of the device and its principle of operation are shown in Fig. 3.2.

4.3   AFM imaging of atmospheric nanoparticles

Electron microscopy was the first technique to visualise airborne particles too small to see with an optical microscope [Friess and Muller, 1939]. However, high vacuum conditions and high-energy probe inherent in these techniques might result in altering the particles morphologically and chemically [Posfai et al., 1998]. Therefore, AFM as a less perturbing technique provides a more suitable alternative for environmental particles. The use of AFM for imaging of atmospheric particles has been well documented in the literature. Rural aerosol with mean particle aerodynamic diameter of 21 nm and 170 nm collected on polyester and aluminium substrates was scanned with contact mode AFM (Fig. 4.3 a) [Friedbacher et al., 1995]. The same study analysed some of these particles, probably ammonium sulphate, with an atomic resolution (Fig. 4.3 b). Bigger particles were imaged with light and scanning electron microscopy to compare observed morphologies, which proved to be in a good agreement. AFM imaging of micro-scale fly-ash particles was performed in contact mode and their surfaces scanned with much higher resolution in tapping modes revealing smaller particles attached and crater-like features [Demanet, 1995]. Airborne ammonium sulphate particles analysed in ambient conditions by AFM were found to be about 4 times bigger than when analysed by TEM, which was attributed to the volatile species (presumably water) - an example is shown in Fig. 4.3 c [Posfai et al., 1998]. Ramirez-Aguilar et al. (1999) found AFM an excellent technique for environmental particles characterisation with a promising potential for not only topographical mapping but also chemical analysis of particles (by phase imaging or use of reactive gas) (an example of AFM image shown in Fig 4.3 d). More recently, atmospheric aerosols form

Amazonian ecosystem collected with an inertial impactor were analysed with AFM and

TEM (Fig. 4.3 e and f) [Gwaze et al., 2007].
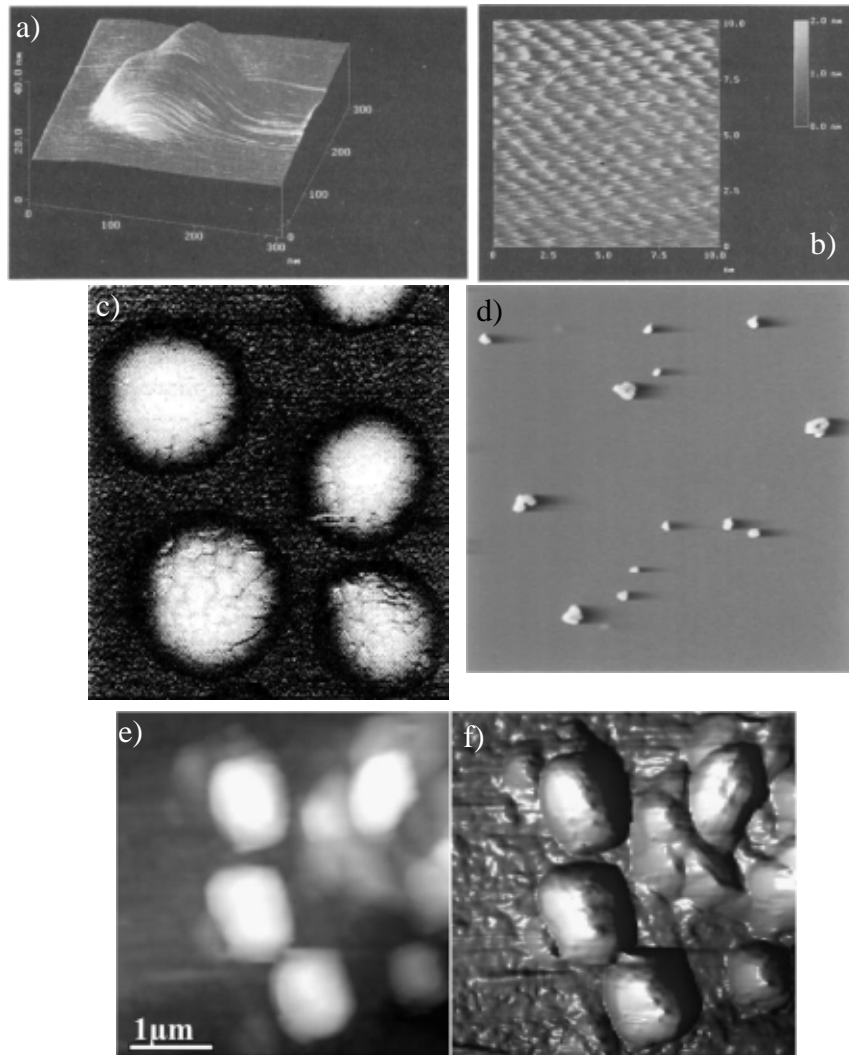
Figure 4.3. Atmospheric PM studied with AFM a) crystalline particle with diam. 150 nm and height 17 nm and b) its crystalline structure [Friedbacher et al., 1995]; c) ammonium sulphate particles with diam. ~1.6 µm and heights ~320 nm [Posfai et al., 1998]; d) atmospheric particles collected during a bush fire [Ramirez-Aguilar et al., 1999]; e) aerosol particles, a colour depth scale of 280 nm d) 3D shaded relief version of the image e [Gwaze et al., 2007].

In this study atmospheric particles collected on the mica sheets from the last two

stages of the impactor were scanned with AFM in ambient conditions. Commercially

available aluminium coated tips made of doped silicone with a radius of curvature < 10 nm were used in the tapping (dynamic contact) mode. X-Y scan sizes were varied up to 10 x 10 μm with resolution of 256 pixels per line. Scanning rates were optimised to acquire a stable and clear image without damaging the tip or detaching particles during scanning, usually 0.5, 1 or 2 Hz. Both samples were scanned at random to obtain 20-30 images. It is also important to note that the scanning areas were selected with the high resolution digital CCD camera to avoid the most densely covered regions, i.e. those where the most impaction takes place. This procedure was necessary to avoid damaging the tip by relatively huge and loosely packed particle 'heaps'. Consequently, the AFM analysis was focused on the low mass fraction.

Representative images are shown in Fig. 4.4 (for stage 10) and 4.5 (for stage 9). In both samples numerous roughly spherical NPs were found with the average height of 10 nm or less. Bigger particles tend to have more irregular shapes possibly due to aggregation. The morphology of the big aggregates in Fig. 4.4 suggests that they are probably soot particles [Mavrocordatos et al., 2002]. Since no additional analysis was performed it is impossible to establish the chemical classification or moisture content of observed particles.
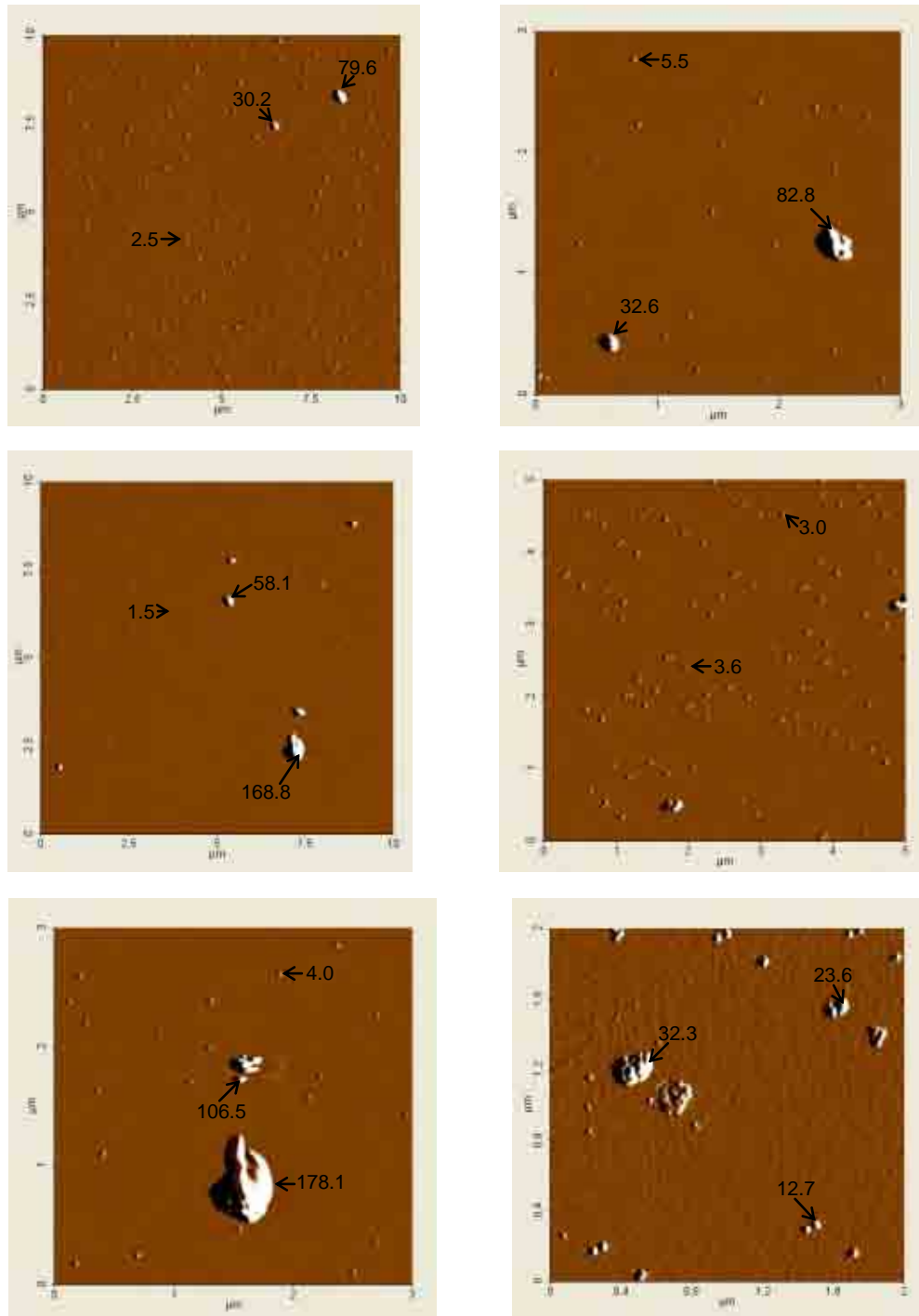
Figure 4.4. AFM images for the 10th stage of MOUDI (theoretical aerodynamic diameter range 56-100 nm). Numbers in black font show maximum height in nm of indicated particles.
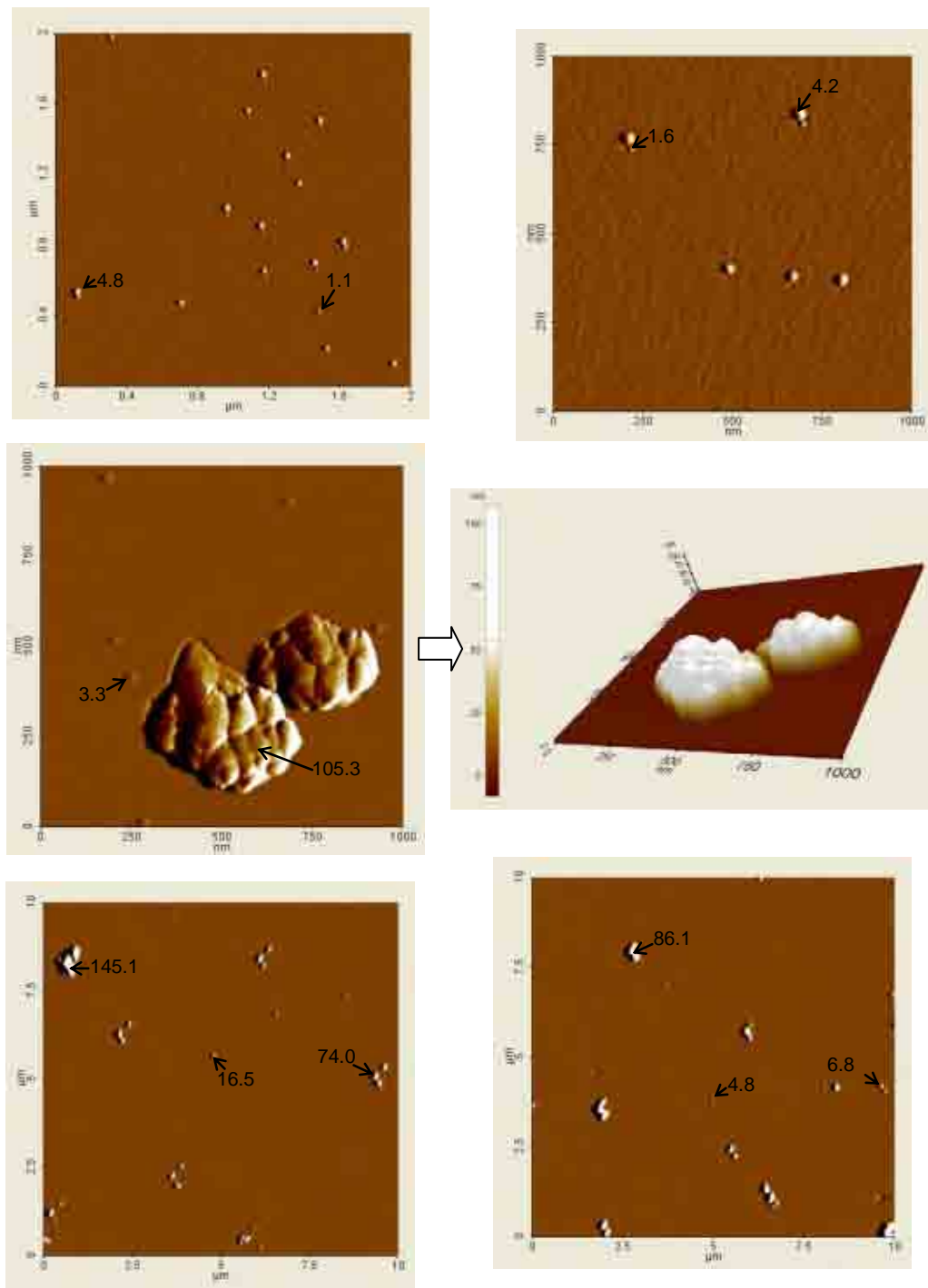
Figure 4.5. AFM images for the 9th stage of MOUDI (theoretical aerodynamic diameter range 100-180 nm). Numbers in black font show maximum height in nm of indicated particles.

As mentioned in the previous chapter (3.2.1), AFM can be used to obtain information beyond morphology. In this study phase imaging was used along with topographical mapping. Phase lag is a source of data on the properties of the scanned surface, i.e. hardness, moisture content, elasticity, hygroscopy, etc. Fig. 4.6 shows topography and phase images of the same particles found on stage 9 of the impactor.
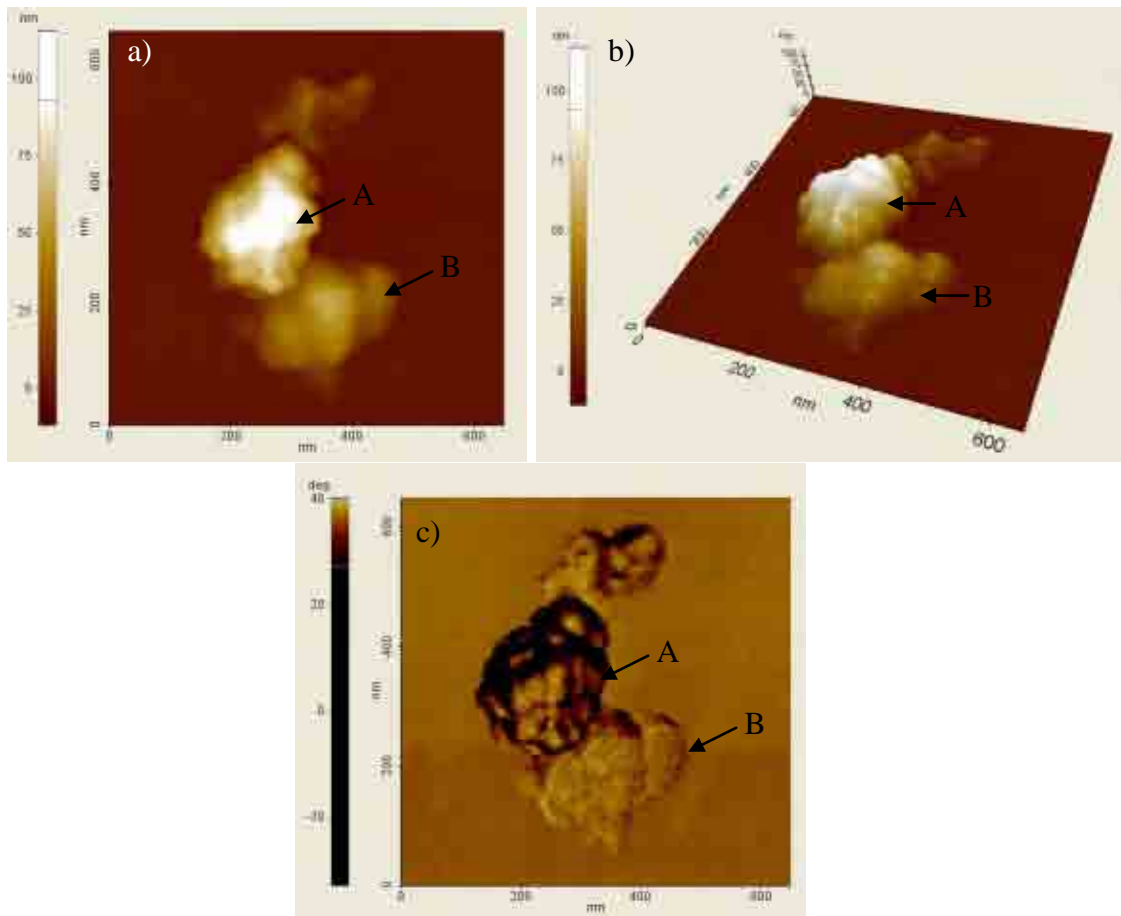
Figure 4.6. Topographic (a & b) and phase (c) image of atmospheric particles from stage 9. Max. height of particle *A* – 115.5 nm, max. height of particle *B* – 55.0 nm.

Particles *A* and *B* have similar topographies suggesting that they were formed by aggregation of smaller particles, particle *A* being about twice as high as *B*. The surface of particle *A* is more uneven and 'bumpy'. However, phase imaging of the same area

(Fig. 4.6 c) gives a very different phase contrast of these aggregates. Particle *A* shows strong (dark) phase contrast indicating stronger interaction between the tip and the particle (i.e. higher phase lag) and thus higher local adhesive forces. Such observation can be explained by either particle *A* being softer than *B* or containing more moisture. By absorbing vibrational energy of the tip, soft surfaces tend to hinder the oscillation resulting in higher phase lags [Schmitz et al., 1997]. Wet surfaces cause considerable capillary forces, which lead to the delay in the oscillating tip escaping out of water layer [Schmitz et al., 1997]. The dark frames of particles in the phase image are a result of sudden change in tip-sample interactions when the tip encounters a relatively big particle. Such areas are characterised by a different contact angle and larger contact area probably leading to increased capillary condensation [Köllensperger et al., 1999]. Phase imaging is a useful tool for differentiating between regions of varied hardness or water content. It should be noted, however, that phase lag is also a function of operating parameters (such as scan speed) as well as ambient atmosphere conditions (temperature, humidity) so accurate quantitative analysis is difficult or impossible. Nevertheless, comparative analysis can be a source of valuable information on the surface characteristics.

4.4   Size distribution of collected particulate matter

There are a number of publications which report having used inertial impactors effectively to separate atmospheric particles in the sub-100nm range and analyse them with AFM of EM. A study on rural aerosol did not find particles smaller than 10 nm, which was with a good agreement with the impactor working parameters, i.e. cut-off point of d_{ae} = 15 nm [Friedbacher et al., 1995]. In another study urban aerosol was collected on polyester foil on four last stages of the 11-stage low pressure impactor with d_{ae} ranging 21-170 nm and analysed with AFM [Kollensperger et al., 1999]. The authors used a computational algorithm for particle detection and volume calculations to estimate particles aerodynamic diameter equivalents from AFM-measured heights. The presented size distributions for the last three impactor stages were in good agreement with the predicted performance of the impactor, with maximum number of particles roughly in the region of the mean d_{ae} for the analysed impactor stage. For the stage with the biggest particles (d_{ae}=170 nm), however, considerable number of small particles were found with a peak of about 20-30 nm, which was explained by unstable conditions of scanning, considerable water content and destroying liquid droplets during scanning.

In this study, size distribution histograms were calculated for both analysed stages of the impactor. Heights of about 150 randomly picked particles were used for calculations. The results for stage 10 and 9 are shown in Fig. 4.7 and 4.8 respectively. Although clearly bigger particles were found on stage 9 than on stage 10, in both samples most measured particles have maximum AFM heights of 10 nm or less (78% for stage 10 and 62 % for stage 9), much below the theoretical cut-off aerodynamic diameter of the stage.
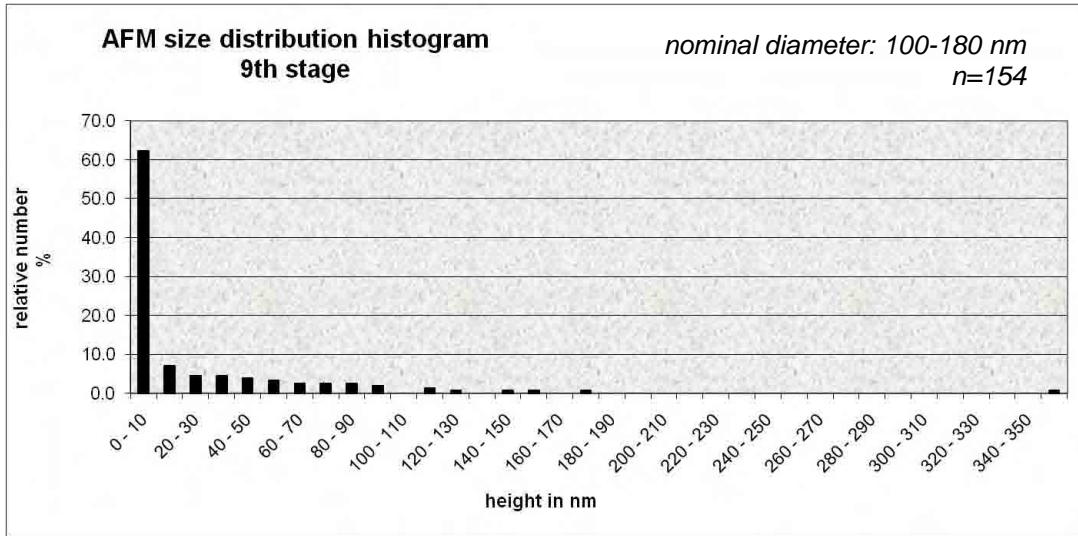
Figure 4.7. AFM size distribution histogram for the 9th stage of MOUDI (n- number of particles measured).
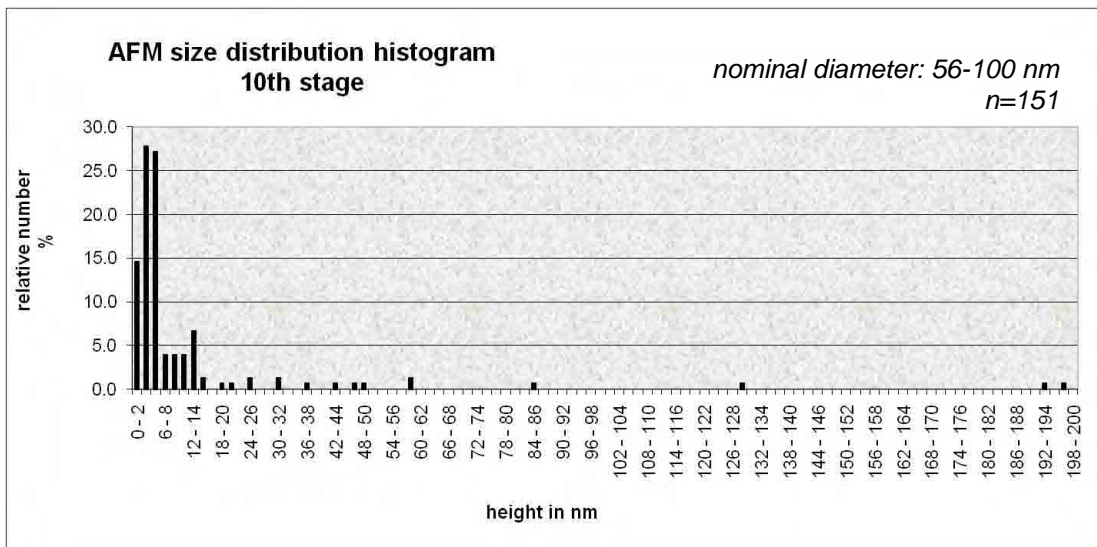
Figure 4.8. AFM size distribution histogram for the 10th stage of MOUDI (n- number of particles measured).

According to the impactor specifications, particles with aerodynamic diameters < 56 nm are too small to be deposited even on the last stage. Median height on stage 9 is 4.15 nm, whereas on stage 10 it is 4.4 nm. Measured AFM heights are within the theoretical

range only for 2% (in case of stage 10) and 4 % (in case of stage 9) of the analysed particles. However, keeping in mind that the AFM analysis concentrated on substrate areas away from the dark deposits, one can expect significant contribution of diffusive mechanism of deposition, for which theoretical cut-off dimensions do not apply. It has been proven that inter-stage diffusive mass losses attributed to particles smaller than 100 nm can account for 5-10 % [Marple et al., 1991]. In a recent study [Gwaze et al., 2007] volume equivalent diameters of particles measured with AFM were compared to equivalent Stokes diameters for the 10-stage MOUDI impactor they were collected with. The AFM measurements did not accurately reproduce expected theoretical size distributions. AFM-derived volume diameters were smaller than predicted Stoke diameters for the analysed stages by factors of up to 3.6. This poor concurrence between physical sizes observed by AFM and theoretical aerodynamic diameters were explained by mass losses, presumably water adsorbed on particles.

As has been said before, the biggest influence on the discrepancy of the results and impactor specifications is probably connected with the selection of the areas for scanning, i.e. avoidance of the 'dirtiest' regions, which possibly had the majority of particles on them (by mass). No further investigation was undertaken to support this hypothesis and it is unknown what was the particle mass and number partitioning between 'clean' and 'dirty' areas. However, there are also a number of other factors that could mitigate the disagreement of expected and obtained particle size distribution presented in Fig. 4.7 and 4.8. To some extent, such results can be explained by the difference between physical sizes of particles measured by AFM and nominal aerodynamic diameter used by the impactor. Maximum particle height does not account for aerodynamic properties of particles, nor their shapes or densities. Secondly, there is

no information on the humidity of collected and analysed particles so smaller particles found on mica might possibly be a result of mass losses caused by drying.

Obtained results would generally suggest that there is contamination of the expected size range by smaller particles. A similar phenomenon was reported for the fractionation of aquatic colloids [De Momi and Lead, 2008]. Split-flow thin-cell fractionation technique was employed to separate two size fractions in the lake water: < 1 µm and > 1µm and to assess contamination of the bigger fraction with nanocolloids (particles with dimensions < 100 nm). Although significantly more smaller particles were found in the < 1µm fraction (6-9 times), the > 1 µm fraction was heavily contaminated with NPs: about 90% of the particles were smaller than 10 nm. This contamination was attributed to the diffusive transport of NPs in the cell.

In this study the AFM analysis concentrated on substrate areas with visibly smaller particle density further away from the streamlines directly hitting mica surface. Consequently, it is possible that the particles observed with AFM are mainly contaminants deposited diffusively. Further analysis is required to validate this hypothesis. Contamination of size fractionated water or atmospheric particles with nanosize particles, even if not substantial in terms of mass distribution, may be significant when studying trace components. With considerably higher specific surface area, small particles bind more pollutants per unit mass than larger particles [Lyven et al., 2003].

5   RESULTS: CHARACTERISATION OF SINGLE-WALLED CARBON NANOTUBES WITH TRANSMISSION ELECTRON MICROSCOPY

5.1   Summary

This chapter discusses the application of transmission electron microscopy (TEM) to characterise certain engineered NMs, specifically carboxylate functionalised SWCNTs, in aquatic systems.

Section 5.2 gives a list of samples used in the experiments, their composition and concentrations. Section 5.3 contains a discussion of visual observation of the samples with a view to describe and explain possible interactions between engineered and natural NPs in the suspensions.

Next, section 5.4 presents numerous TEM micrographs of SWCNTs in the absence/presence of natural aquatic colloids and cations (SRHA, PHA, succinoglycan, natural lake water, Ca^{2+} and Na^+) at three different pH values: 3, 6.5 and 10. Observed morphologies are shown and discussed with the emphasis on the interactions between engineered and natural NPs in natural waters.

In addition to qualitative comparison of the observed interactions, samples are compared quantitatively on the basis of the average nanotube bundle thicknesses to better understand the interaction mechanism (section 5.5).

5.2   <u>**Sample preparation and analysis**</u>

Test samples were prepared by mixing the appropriate amounts of stock solutions (as discussed in chapter 3.1) to obtain the following suspensions:

1. SWCNT (10 mg L^{-1})

2. SWCNT (10 mg L^{-1}) & SRHA (10 mg L^{-1})

3. SWCNT (10 mg L^{-1}) & PHA (10 mg L^{-1})

4. SWCNT (10 mg L^{-1}) & SG (10 mg L^{-1}, nominal concentration before filtration)

5. SWCNT (10 mg L^{-1}) & natural lake water (NW) (twice diluted after filtration)

6. SWCNT (10 mg L^{-1}) & Ca^{2+} (45 mg L^{-1}, the same as in NW used)

7. SWCNT (10 mg L^{-1}) & Na^{+} (13 mg L^{-1}, the same as in NW used)

8. SWCNT (10 mg L^{-1}) & SRHA (10 mg L^{-1}) & Ca^{2+} (45 mg L^{-1})

9. SWCNT (10 mg L^{-1}) & SRHA (10 mg L^{-1}) & Na^{+} (13 mg L^{-1})

All samples were prepared at 3 different pH values: 3, 6.5 and 10. PH of each sample was adjusted with 0.1 M HCl or 0.1 M NaOH. Before preparing microscopic specimens all the samples were gently shaken for about 15 hours and their pH measured and readjusted if needed.

SWCNT concentration at 10 mg L^{-1} was chosen to ensure good quality of TEM specimen (grids with sufficient amount of NPs on them but not overloaded). This concentration is highly unlikely to be seen in environmentally relevant conditions. Predicted environmental concentration for CNTs was estimated in the range of 0.005 – 0.008 µg L^{-1} [Mueller and Nowack, 2008]. This estimation was calculated for current production output of nanotubes in Switzerland without accounting for localised effects. However, an elevated concentration in laboratory conditions enabled visual examination of observed behaviour. Concentrations of humic acids are environmentally relevant and

comparable for reported concentrations in natural water samples [Buffle et al., 1998; Michalowski et al., 2001]. Na^+ and Ca^{2+} concentrations are the same as measured in the lake water (NW).

The selected pH range encompasses acidic, neutral and alkaline conditions. Very low and very high pH values (3 and 10) are rare in natural waters but were chosen to intensify any possible effects. Such a selection was supposed to depict the change in behaviour and at the same time minimise the number of samples keeping in mind the availability of the TEM and the costs of using the instrument.

TEM specimens were prepared on a holey carbon film supported on a 300 mesh copper grids (purchased from Agar Scientific, UK). Microscopic specimens were prepared by slow evaporation of one drop of the nanoparticle suspension directly placed onto the carbon film (whole mounts technique). Excess liquid was removed with filter paper before air drying to ensure more even grid coverage and minimise possible salt crystal formation while drying. All samples were imaged on a FEI Philips TECNAI F20 TEM operating at 200 kV (Fig. 3.8). At least 10 different TEM images at different magnifications (from 2000x to 250kx) were taken for each suspension and analysed with Digital Micrograph software.

5.3   SWCNT suspensions by visual examination

Methods for dispersing carbon nanotubes in water

Although pristine carbon nanotubes are inherently insoluble in aqueous media (due to strong Van der Waals attraction along the tubes [Jiang et al., 2003]), many efforts have been made to disperse them in water to exploit their unique properties in biology, medicine and material science by polymer wrapping, sidewall functionalization and surface modification [Paloniemi et al., 2005; Hu et al., 2007; Xue et al., 2008]. MWCNTs have been found to form very stable water suspensions [Hyung et al., 2007; Schierz and Zaenker, 2009]. Carboxyl, carbonyl and hydroxyl group functionalization has been reported as a way of dissolving SWCNTs in water resulting in significant stability [Li et al., 2008B; Zhang et al., 2009]. Table 5.1 presents a short summary of available methods to prepare aqueous suspensions of CNTs reported in the literature.

High stability of oxidised nanotubes in water can be explained by strong electrostatic repulsion between SWCNTs, since their surface is functionalised by carboxylic groups (i.e. negatively charged). This behaviour has been reported for MWCNTs treated by surface oxidation and Zeta potential of about -35 mV was measured for samples at pH 4-11 (Table 5.1) [Schierz, 2009]. The stronger oxidation, the higher the negative surface charge: at pH 7 a zeta potential of -34.8 mV was measured for nanotubes functionalised with carboxyl groups –COOH and an even stronger charge of -53.2 mV was recorded in case of carboxyl anion groups –COO$^-$ [Lee et al., 2007].

kind of CNT	concentration	method of solubilisation	surface charge	ref.
structure not specified, purified with acid	0.5 wt%	dispersing agent (sodium dodecyl sulphate, 2.0 wt %)	zeta potential: -10 - -40 mV at a pH range 3-11	Jiang et al., 2003
SWCNT	not specified	1) acid treatment 2) non-ionic surfactant and sonication 3) acid treatment and non-ionic surfactant	not measured	Chen et al., 2004B
MWCNT	not specified	surface oxidation, sonication	not measured	Cho et al., 2008
MWCNT	0.01 wt%	surface oxidation (carboxylation)	zeta potential at pH 7: -34.8 mV (-COOH groups), -53.2 mV (-COO$^-$ groups)	Lee et al., 2007
MWCNT	0.6 - 6.9 mg/L	1) presence of NOM (up to 100 mg/L) 2) surfactant (sodium dodecyl sulphate, 1 %)	not measured	Hyung et al., 2007
SWCNT	20 mg/mL	surfactant (sodium dodecylbenzene sulfonate)	not measured	Islam et al., 2003
SWCNT	50 µg/ml	noncovalent functionalization with proteins and ultrasonication	not measured	Karajanagi et al., 2006
MWCNT	ca. 3.2 mg/mL	solubilising agent (alginic acid)	not measured	Liu et al., 2006
SWCNT	3 g/L	surface modification by starch wrapping	not measured	Star et al., 2002
MWCNT	100 mg/L	surface oxidation	zeta potential: -10 - -35 mV at a pH range 2-11	Schierz and Zaenker, 2009

Table 5.1. Methods used to disperse carbon nanotubes in water.

NOM shows a strong stabilising effect towards aqueous CNTs. In fact it has been used as a dispersing agent at concentrations of 10-100 ppm with better results than commonly used 1 % sodium dodecyl sulphate [Hyung et al., 2007]. The stabilising mechanism was attributed to surface shielding, which leads to electrostatic and steric stabilisation. A more recent study confirms the surfactive properties of humic substances towards MWCNTs [Chappel et al. 2009].

Visual examination of SWCNT behaviour

In this study sonicated carboxylic acid functionalised SWCNTs were used (more details are provided in chapter 3.1.2). The results obtained confirm that once suspended in water, surface functionalized SWCNT remain essentially unaltered for weeks. Fig. 5.1 shows a sample at the start of the experiment and after 5 days of undisturbed sedimentation. Although after this time there is some material precipitated at the bottom of the vial, the reduction in concentration in the water column cannot be confirmed without additional measurements. Similarly, the presence of SRHA, PHA and SG does
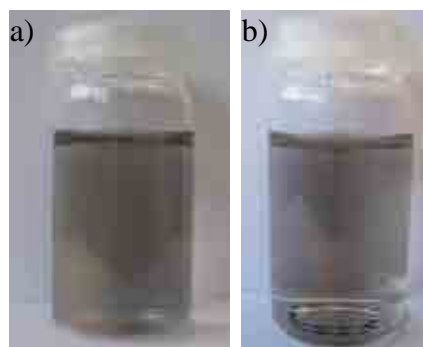
Figure 5.1. Visual stability of aqueous suspensions of SWCNTs (concentration of 10 ppm) a) settling time of 0 b) settling time of 5 days.

not cause any significant change in SWCNTs stability that could be verified without further laboratory analysis (samples not shown).
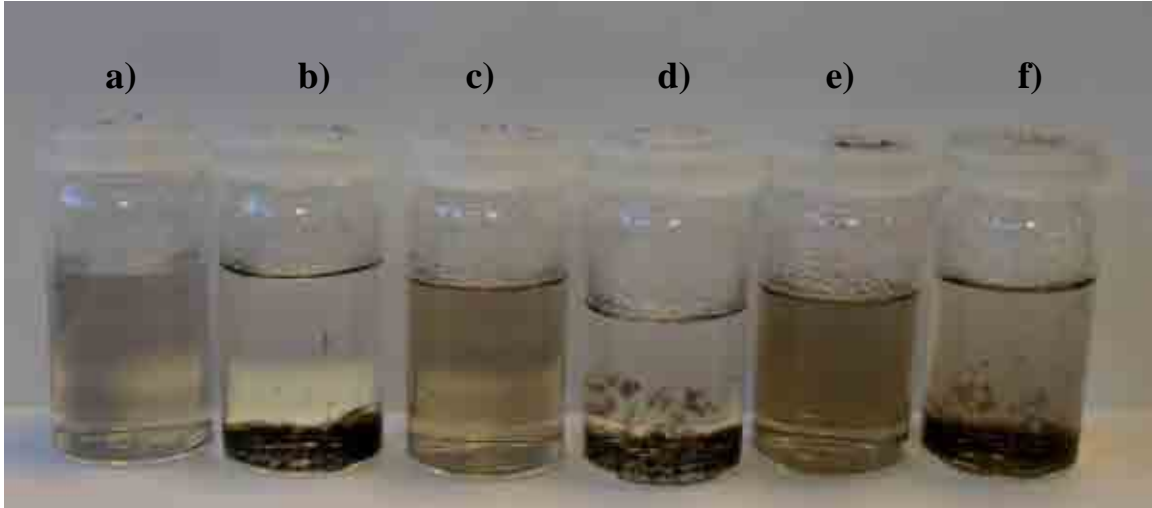
Figure 5.2. The influence of cations present in natural water on SWCNT suspensions stability. Photos taken after 3-day settling time a) alone; b) with NW, c) with Na^+, d) with Ca^{2+}, e) with Na^+ and SRHA, f) with Ca^{2+} and SRHA.

Distinctively different behaviour is observed in case of the presence of natural water (Fig. 5.2 a and b). Although immediately after mixing all of the samples look similar, in the presence of lake water SWCNTs flocculate and sediment within not more than an hour (even though NW itself remains stable over significant periods of time). To explain this observation, a hypothesis was formed that cations present in the lake water are responsible for the instant precipitation caused by surface charge neutralisation (also previously reported elsewhere [Liu et al., 2006]). Additional set of experiments was conducted with Na^+ and Ca^{2+} cations at the same concentrations as in the lake water (13 mg L^{-1} for sodium and 45 mg L^{-1} for calcium). Sodium and calcium were chosen as the most ubiquitous in natural waters. Visual observation confirms that the presence of divalent cations (Ca^{2+} in this experiment) in the solution may hugely contribute to the instantaneous destabilisation of SWCNTs in natural waters (Fig. 5.2 b and d). Na^+ does

not cause visible aggregation of SWCNTs (Fig. 5.2 c and e). Divalent cation destabilisation of nanotube suspensions is consistent with the DLVO theory, which explains how electronegative colloids can be flocculated using cationic solutions [Derjaguin & Landau, 1941; Verwey & Overbeek, 1948].

As far as humic acid is concerned, a slight stabilising effect can be observed. It is more profound in the case of simultaneous presence of Ca^{2+}: the sample with SRHA has visibly higher concentration of suspended nanotubes than the sample without humic acid (Fig. 5.2 d and f).

5.4   TEM imaging of SWCNTs

For theoretical background on the TEM technique please refer to chapter 3.2.2. TEM was used to analyse 27 samples in total which encompasses SWCNTs without and with natural aquatic colloids (SRHA, PHA, SG, NW, Ca^{2+}, Na^+, Ca^{2+} & SRHA and Na^+ & SRHA) at three pH values: 3, 6.5 and 10. TEM images for all samples revealed typical morphologies for SWCNTs: long randomly entangled nanotubes. Since the SWCNT powder used in the experiments is produced by the electric-arc technique (which leads to formation of self-organised filamentous crystallites consisting of up to about 20 single nanotubes cleaved to each other [Journet, 1997]), no single nanotubes were observed. Instead they were organised in bundles. These bundles are roughly circular in a cross-section with diameters ranging from 5-20 nm. Figure 5.3 shows a TEM image of a SWCNT bundle with individual nanotubes clearly visible.
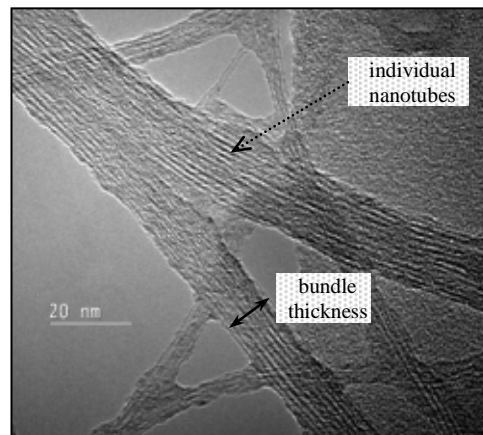
Figure 5.3. Individual SWCNTs in bundles and bundle thickness.

Figures 5.4, 5.5 and 5.6 show examples of SWCNTs alone at pH 3, 6.5 & 10. As samples were prepared by air drying, nanotubes are unevenly distributed on the carbon films but they tend to form randomly entangled networks. Irregularly or roughly spherically shaped dense particles present in the samples are carbonaceous and/or metal

impurities. In all 3 samples small amounts of thin film suspended between nanotube bundles can be observed on the holey area of the carbon film, especially at pH 6.5 (Fig. 5.5 a). The cleanest sample (with little visible impurities) was observed at pH 10.
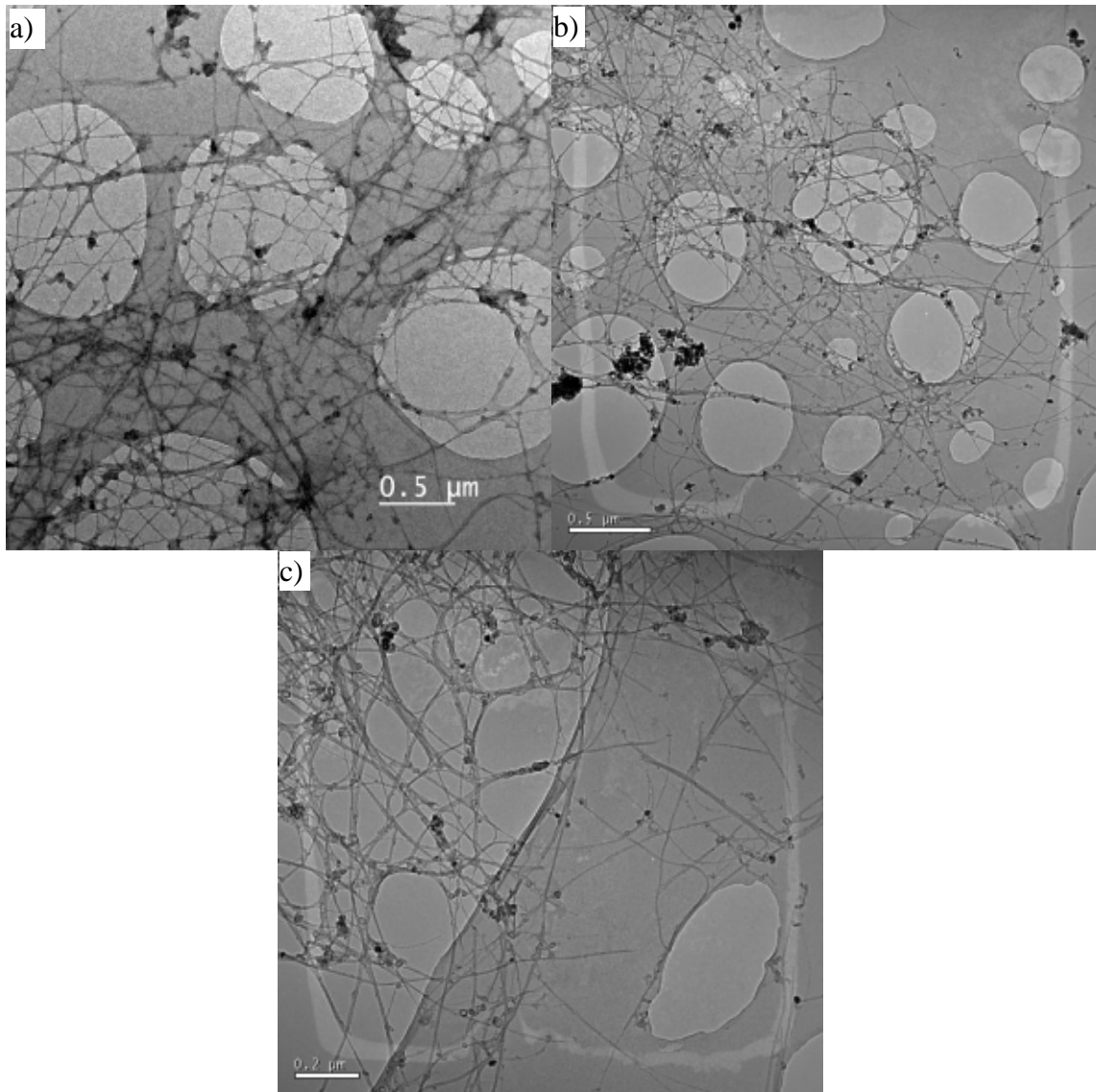
Figure 5.4. TEM micrographs of aqueous SWCNTs alone at pH 3.
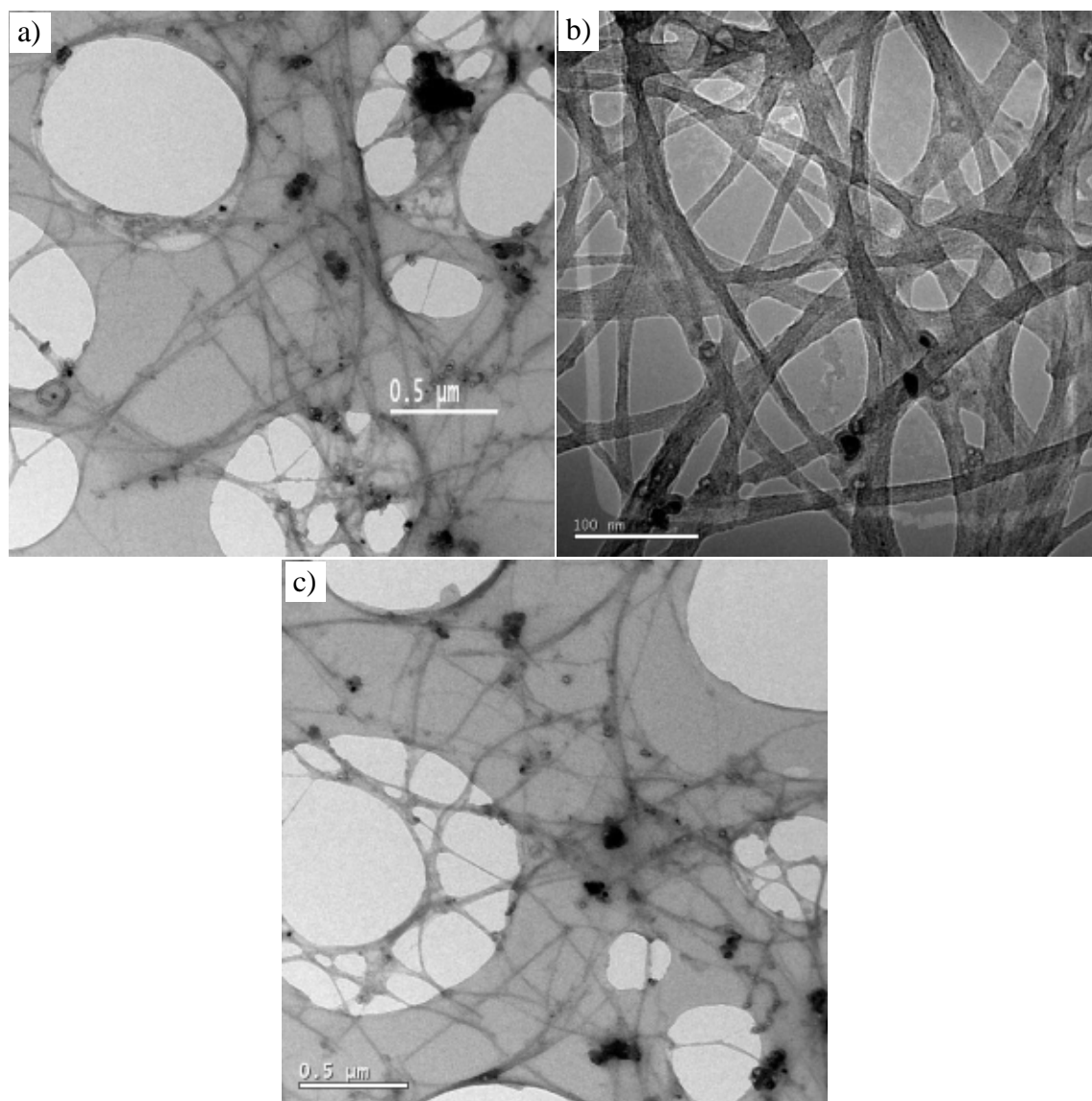
Figure 5.5. TEM micrographs of aqueous SWCNTs alone at 6.5.
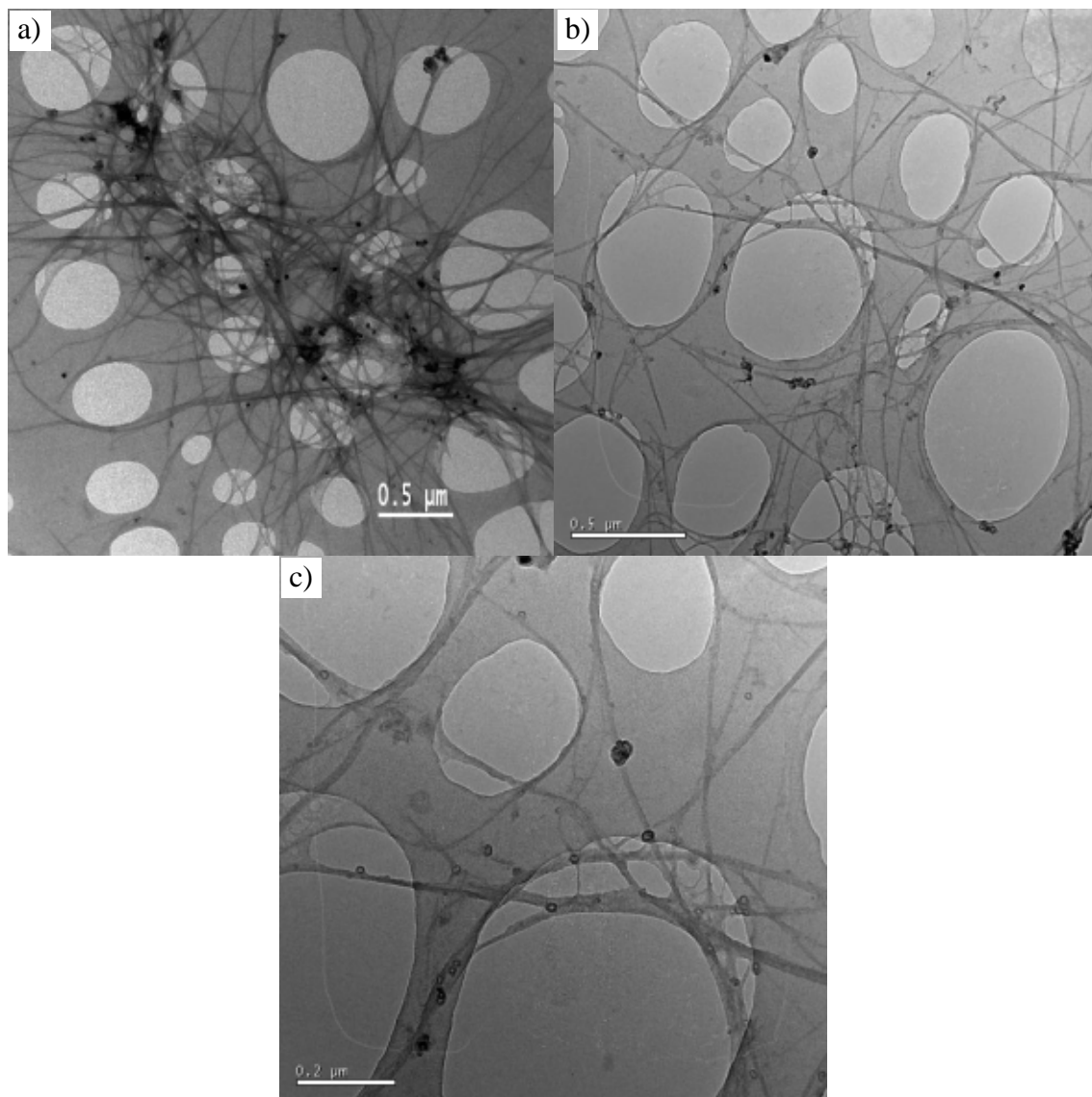
Figure 5.6. TEM micrographs of aqueous SWCNTs alone at pH 10.

The presence of natural colloids significantly changes the morphology of the analysed samples. Images 5.7, 5.8 and 5.9 show CNTs in solution of SRHA at three different analysed pH values. Interaction between them is evident especially at pH 3 and 6.5 (Fig. 5.7 and 5.8). At pH 3 nanotubes are homogenously coated with circular particles of humic acid. At pH 6.5 significant amounts of roughly homogenous material bridging between nanotubes can be seen. Some coating and bridging with humic material can be observed at pH 10 too. However, at pH 10 nanotubes look 'clean' and do not show such a significant difference to those without humic acid. This effect can be explained by stronger repulsion between more negatively charged SWCNT and SRHA molecules in higher pH values. These observations go in line with TEM analysis of SRHA blank samples (i.e. without SWCNTs). Similar granular branch-network morphology was imaged for SRHA at pH 3 (Fig. 5.10). Less characteristic roughly spherical particles of humic acid were spotted at higher pH (not shown here). At pH 10, similarly to SWCNTs with SRHA, very few spherical particles of humic acid were found.

Additionally, significant amounts of thin film suspended between nanotube bundles can be observed on the holey area of the carbon film, especially at pH 3 (Fig. 5.7) and 6.5 (Fig. 5.8). In some images about 60 % of the total holey area in the image is covered by this webbing structure. Although these films were observed in the samples without humic acid, analysis of SRHA alone (Fig. 5.10) suggests that its presence may hugely contribute to this effect. These webbing structures were found in abundance and despite being difficult to quantify, they were clearly present. In some samples (Fig. 5.7 b and c, Fig. 5.10 c) the film occurring in the holey areas was cracked and upturned

indicating shrinkage caused by drying. This suggests that the webbing effect could be more profound if imaged without UHV conditions.
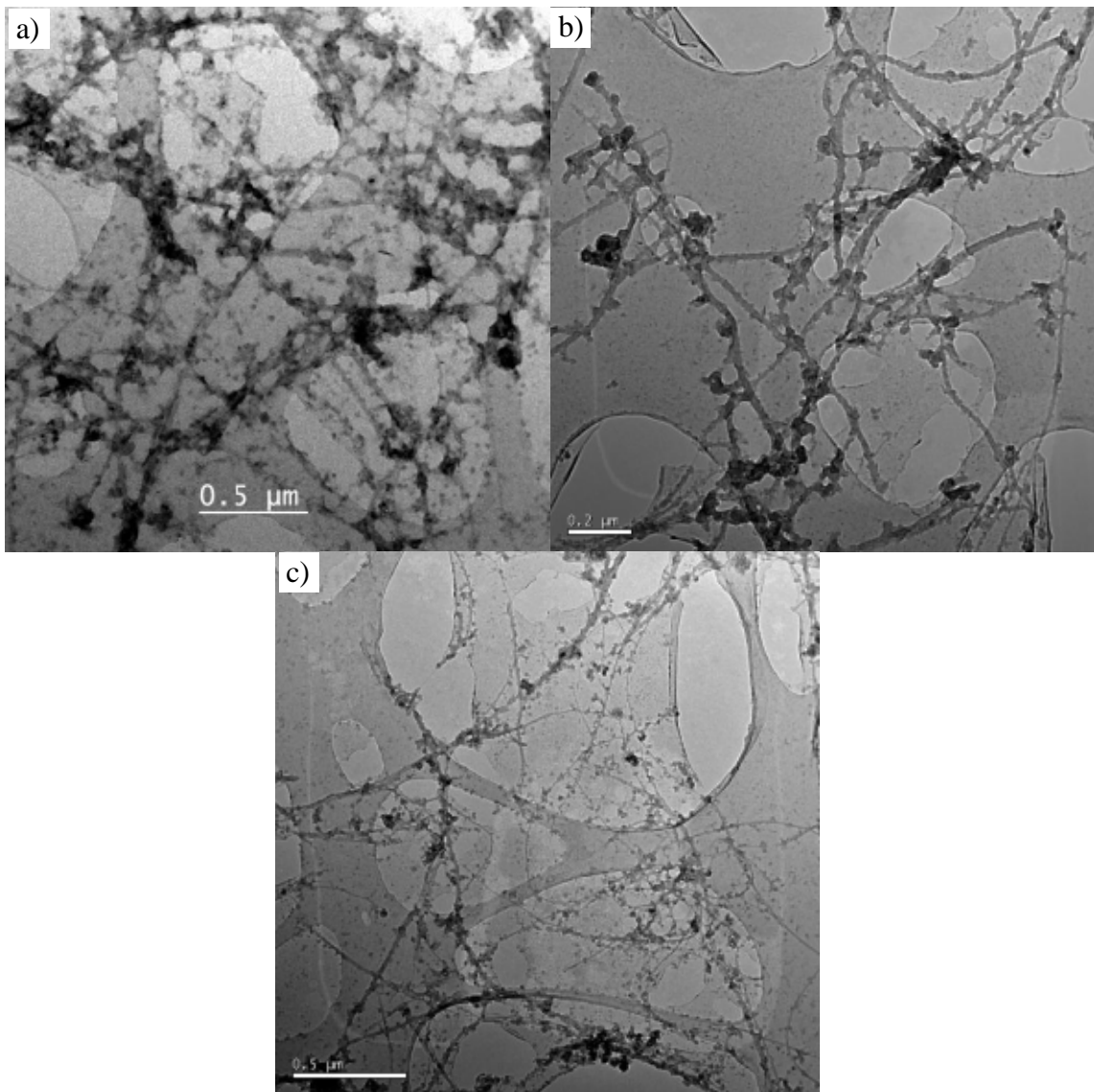
Figure 5.7. TEM micrographs of aqueous SWCNTs in the presence of SRHA at pH 3.
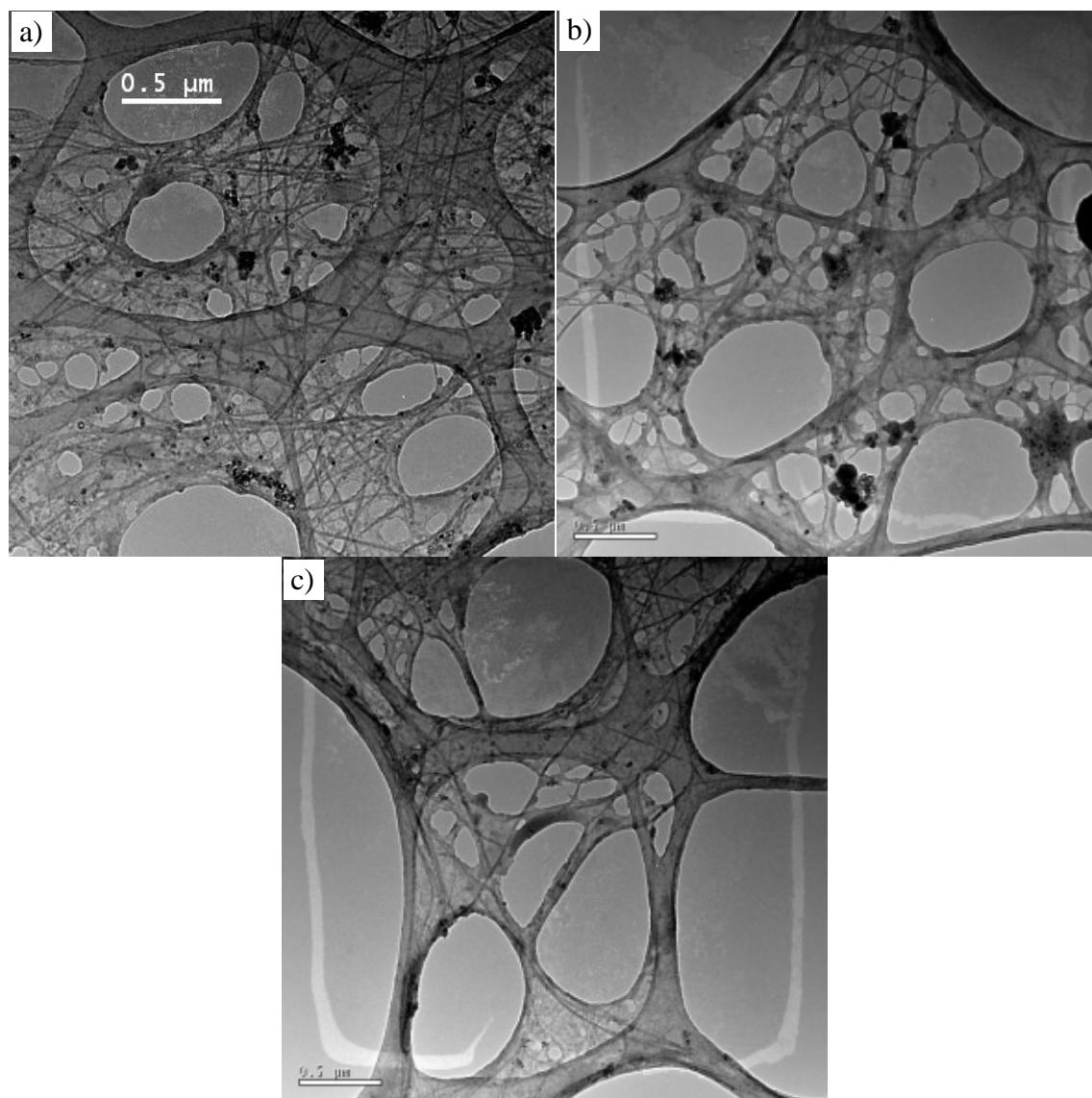
Figure 5.8. TEM micrographs of aqueous SWCNTs in the presence of SRHA at pH 6.5.
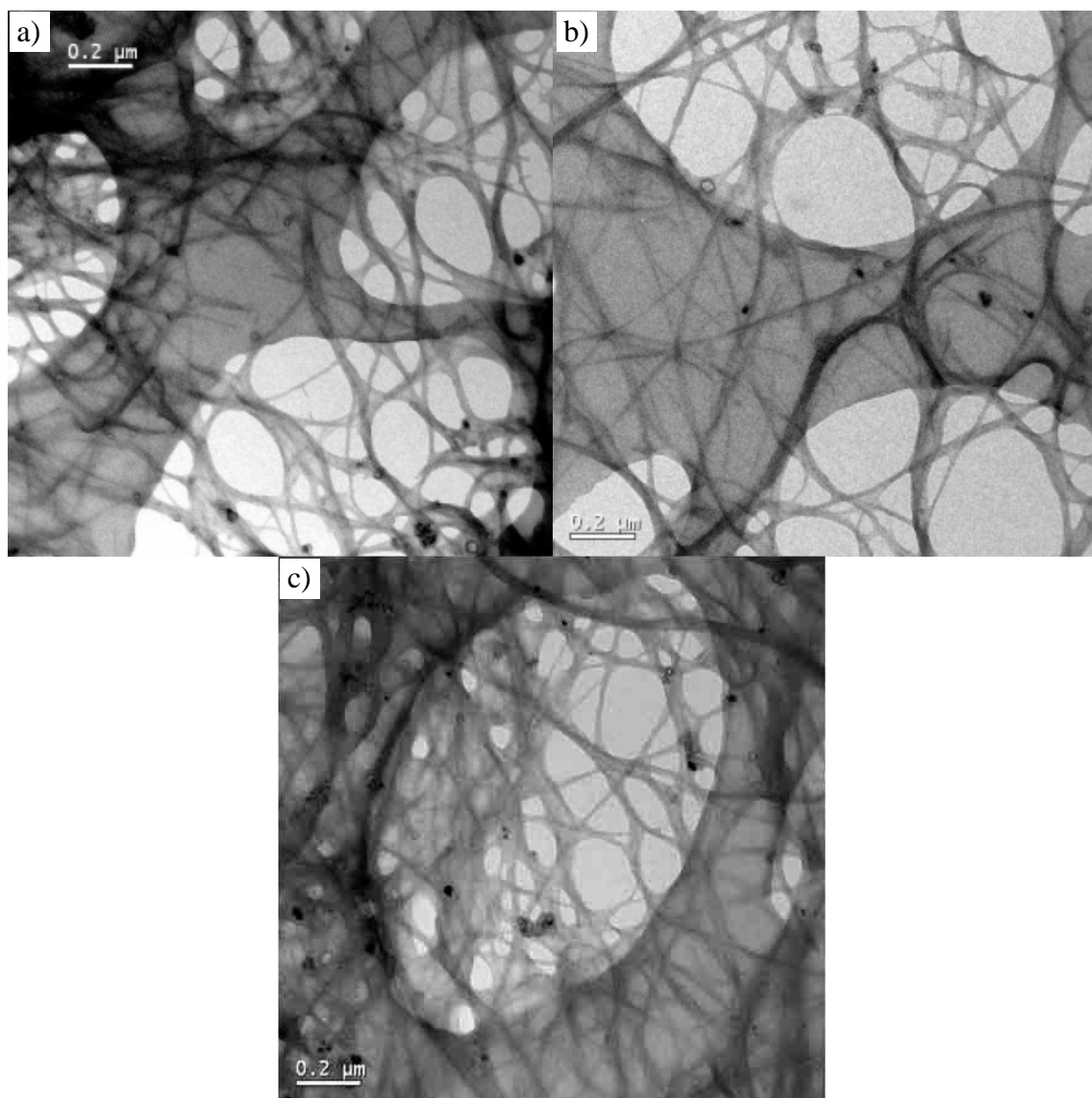
Figure 5.9. TEM micrographs of aqueous SWCNTs in the presence of SRHA at pH 10.
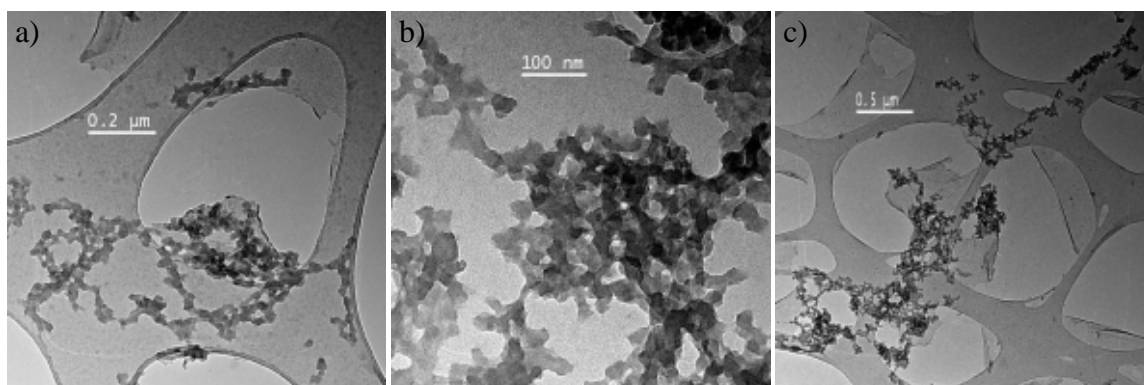
Figure 5.10. TEM micrographs of SRHA at pH 3.

Images of SRHA (Fig. 5.10) compare well with the literature data [Bufle et al., 1998; Leppard et al., 1999; Wilkinson et al., 1999; Baalousha et al., 2005 A; Baalousha et al., 2006].

Very similar pattern of interaction (although less profound) is observed for Pahokee peat humic acid (Fig. 5.11, 5.12 and 5.13). At low pH spherical particles of HA can be seen in abundance along the nanotubes and as bridging structures between nanotube bundles (Fig. 5.11). Significant amounts of filming structures were present at pH 6.5 (Fig. 5.12). At high pH, however, hardly any humic acid can be observed (Fig. 5.13). TEM analysis of PHA alone showed very similar morphologies as in the case of SRHA, i.e. granular branched networks of humic acid at pH 3 and few particles in higher pH values (not shown).

The observed interactions between SWCNTs and humic acids compare well to the literature data. The formation of humic surface films of natural organic nanoscale material has been well documented in the literature [Hunter and Liss, 1982]. More recently humic coating was directly observed and measured on macroscopic surfaces [Lead et al., 2005].
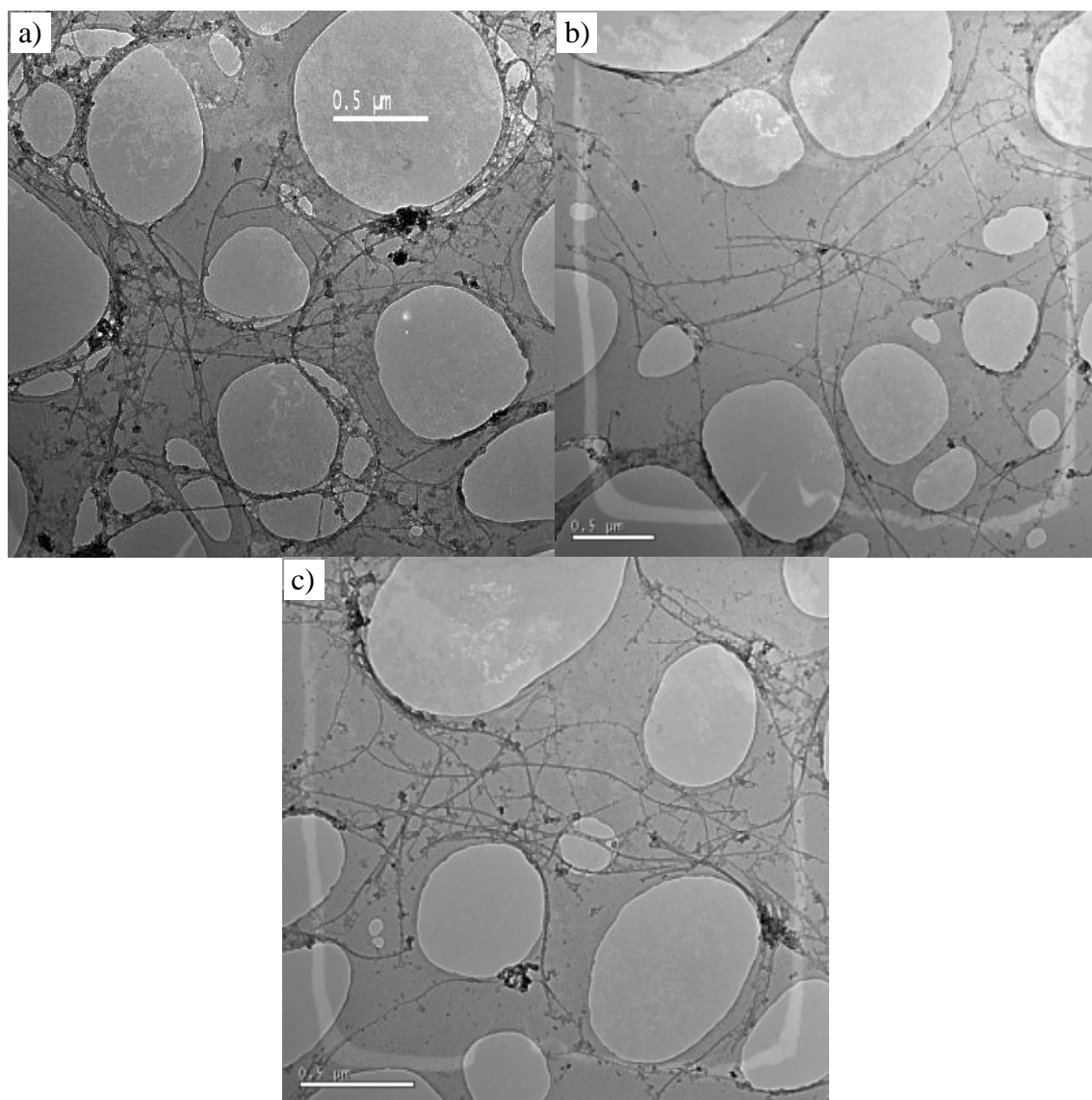
Figure 5.11. TEM micrographs of aqueous SWCNTs in the presence of PHA at pH 3.
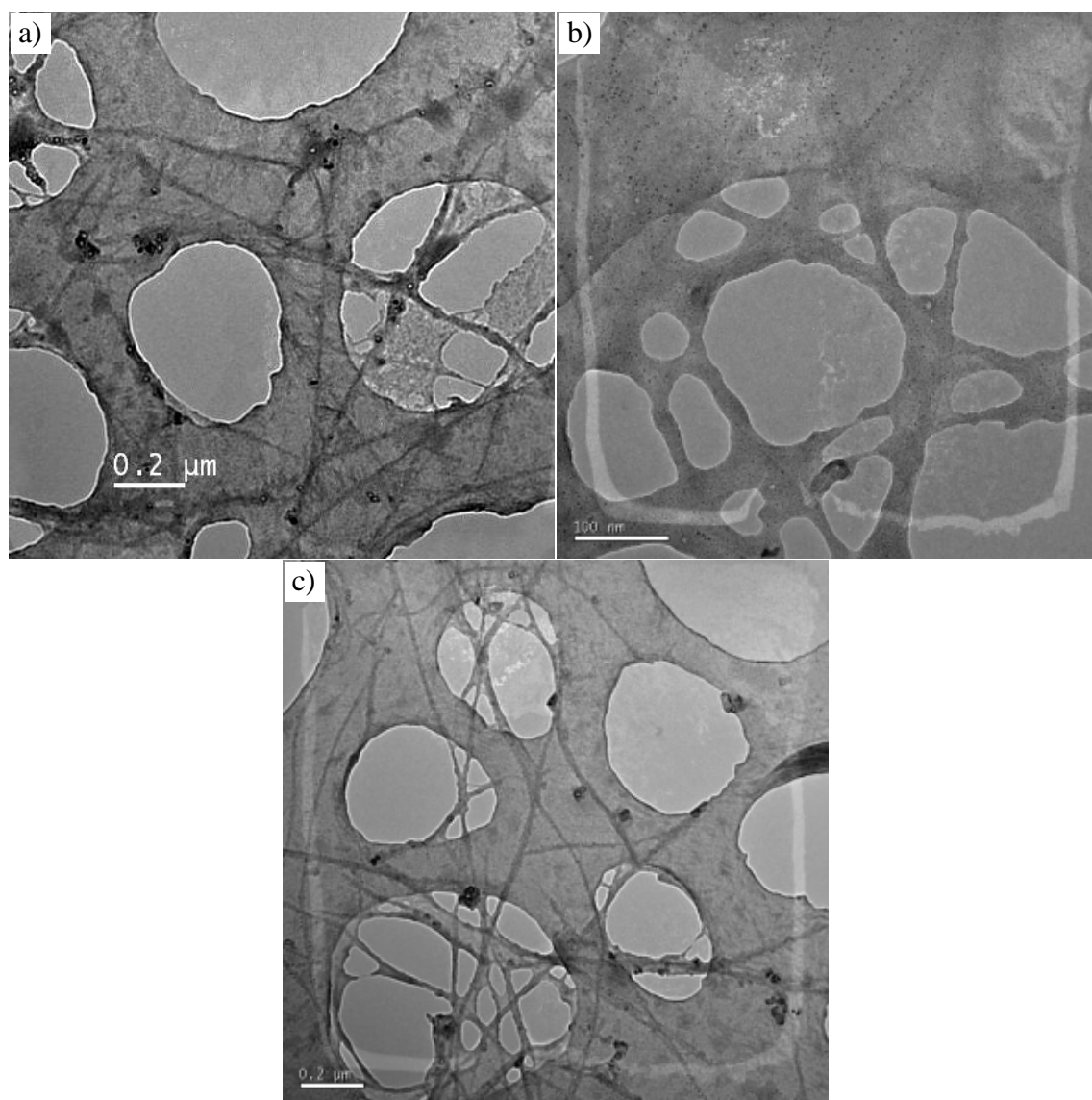
Figure 5.12. TEM micrographs of aqueous SWCNTs in the presence of PHA at pH 6.5.
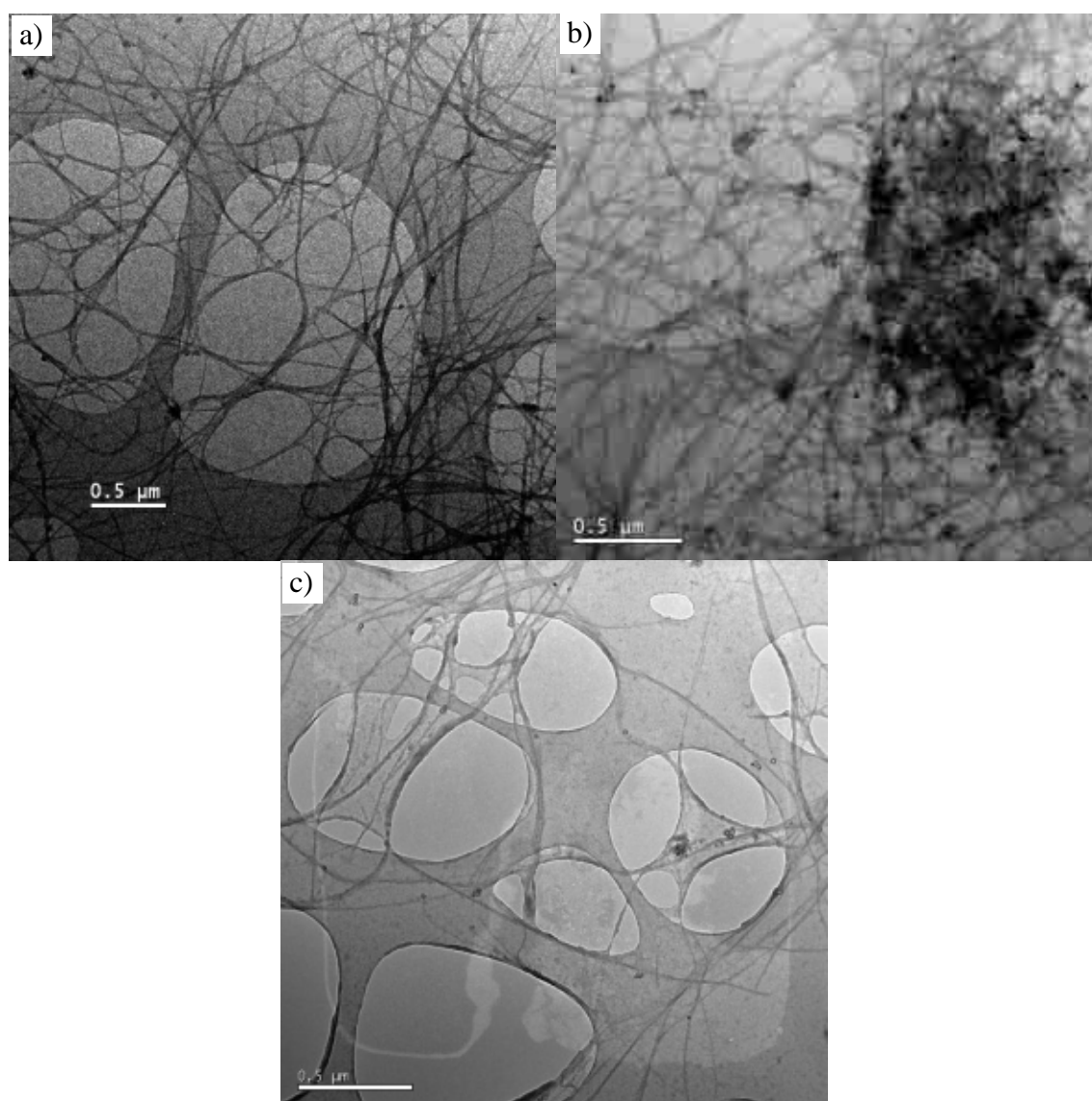
Figure 5.13. TEM micrographs of aqueous SWCNTs in the presence of PHA at pH 10.
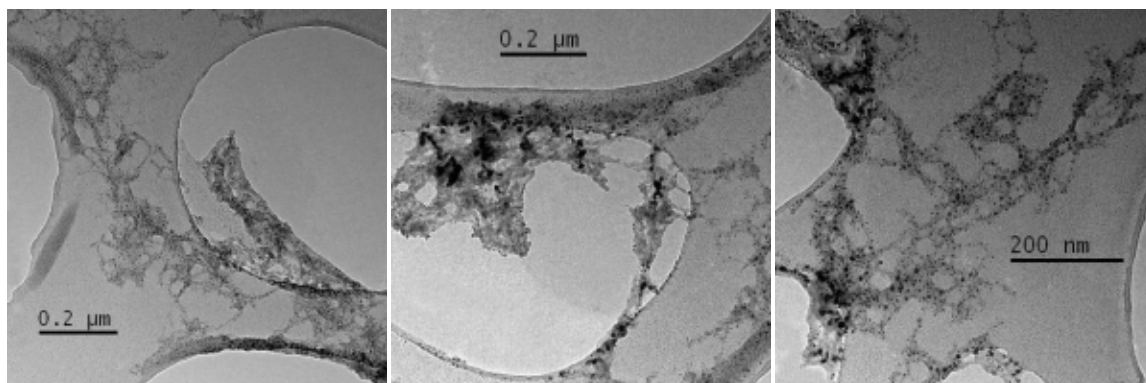
Figure 5.14. TEM micrographs of succinoglycan at pH 3.

Succinoglycan has also been proven to interact with SWCNTs in aqueous solutions. Figure 5.14 shows characteristic fine-grainy fibrillar patches of succinoglycan alone found at pH 3. The same structures evenly coating nanotube bundles were photographed for the sample at pH 10 (Fig. 5.17 a and c). In this sample succinoglycan occurred in irregularly shaped patches of about 100 nm in width filling the area in the nanotubes network. Apart from forming webbing structures between nanotubes in the holey area, it also stained the carbon film. For the lower two pH values (Fig. 5. 15 and Fig. 5. 16) morphology of samples did not show any immediate difference from SWCNTs alone. Such observation cannot be regarded as a proof of the lack of interaction between nanotubes and succinoglycan. Due to the microscopy specimen preparation method, analysed samples are highly heterogeneous, i.e. on the same support grid there are areas covered with nanotubes with different morphologies. Firstly, this can be caused by air-drying resulting in shrinking of the solid material. Secondly, a drop of the sample used for the TEM grid preparation might not be fully representative to the whole sample.
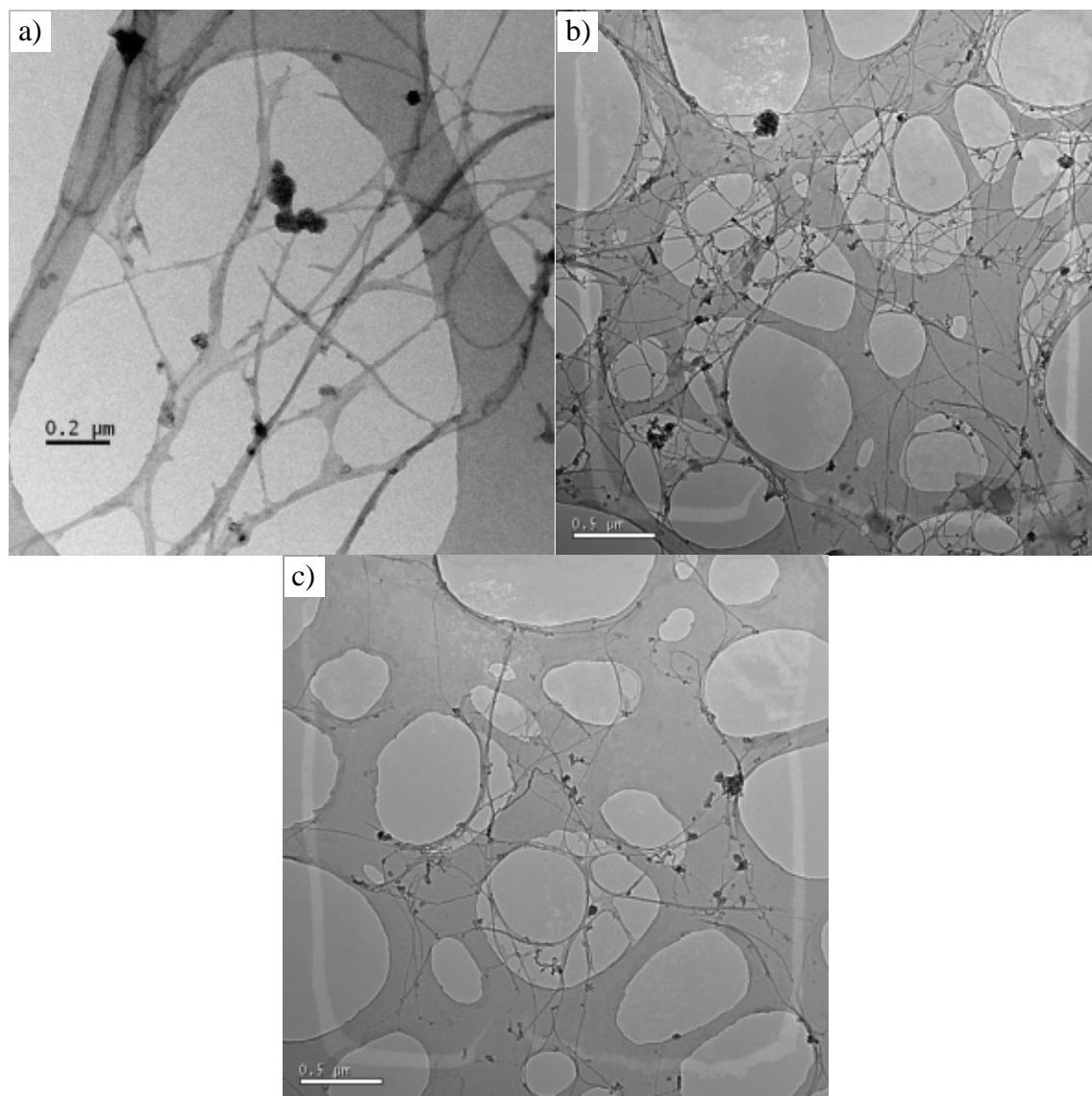
Figure 5.15. TEM micrographs of aqueous SWCNTs in the presence of SG at pH 3.
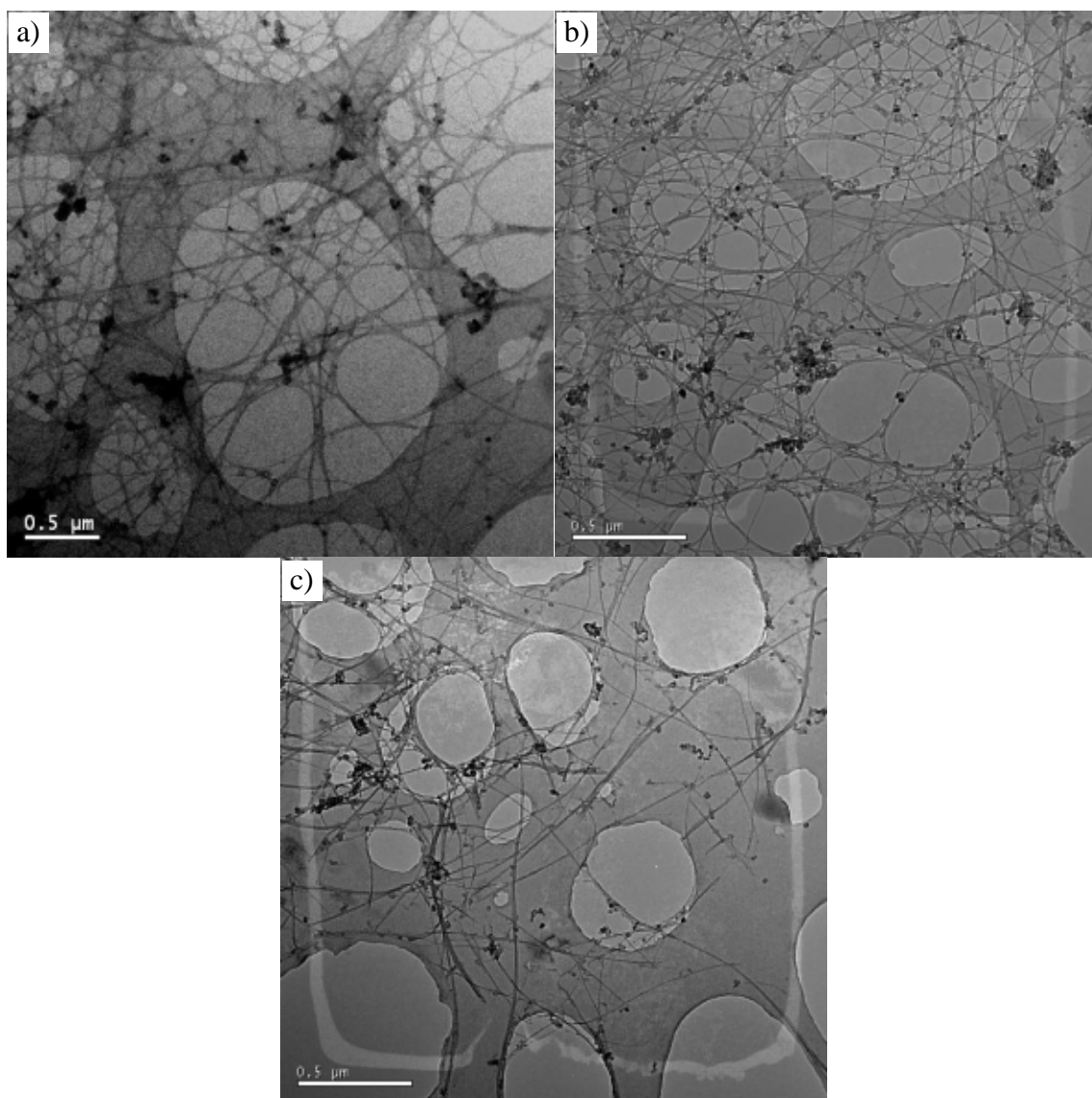
Figure 5.16. TEM micrographs of aqueous SWCNTs in the presence of SG at pH 6.5.
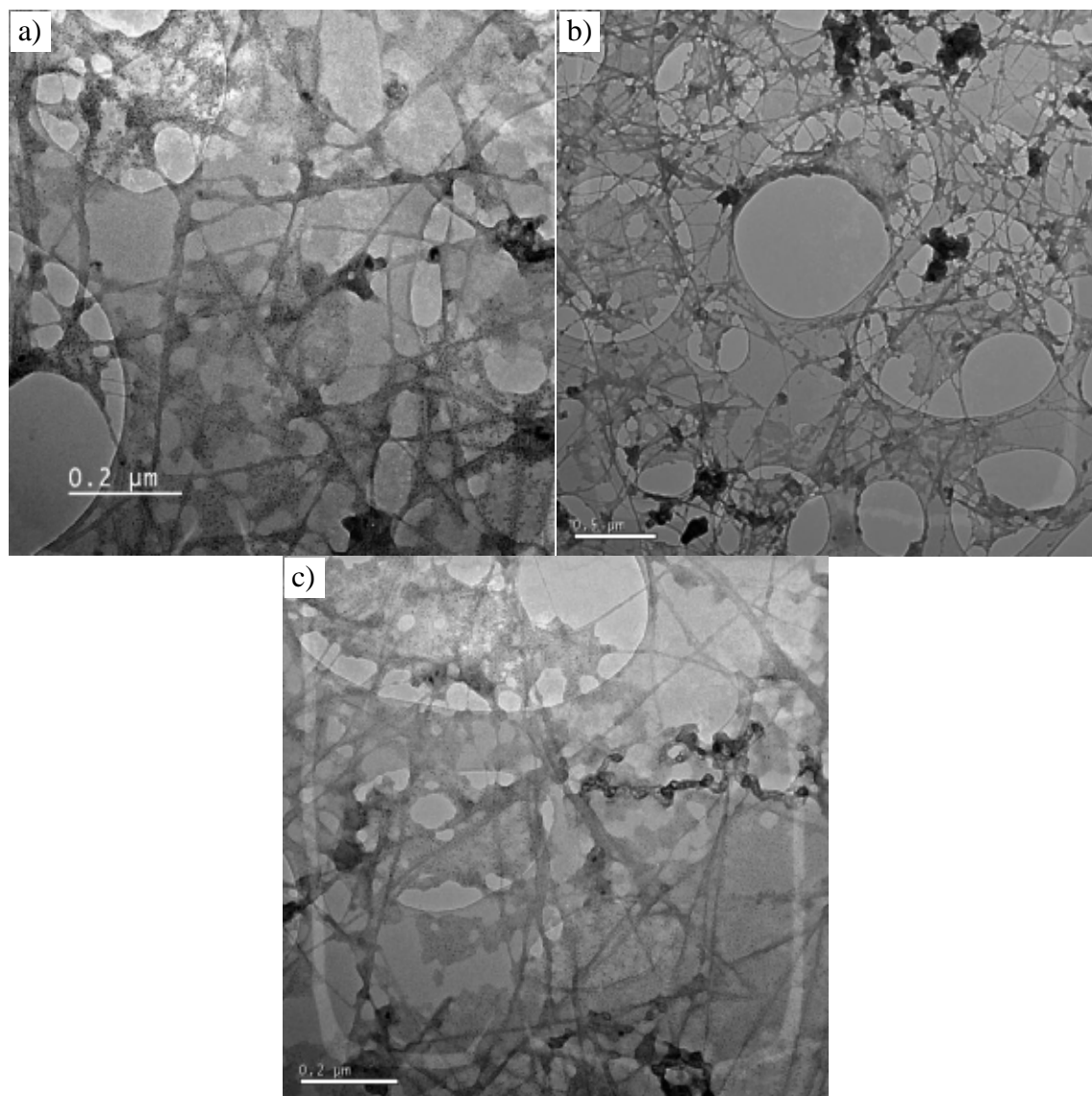
Figure 5.17. TEM micrographs of aqueous SWCNTs in the presence of SG at pH 10.

As expected the widest range of colloidal material, however, was found in samples with SWCNTs and natural water (Fig. 5.18, 5. 19 and 5.20). In these samples CNTs formed a diverse net of entangled nanotube bundles interlacing with natural colloids. In many places these structures filled holey areas of the film, especially at pH 10 (Fig. 5.20 a and b). Owing to the great diversity of natural colloids and the fact that the information from the images is limited to morphology only, it is impossible to say
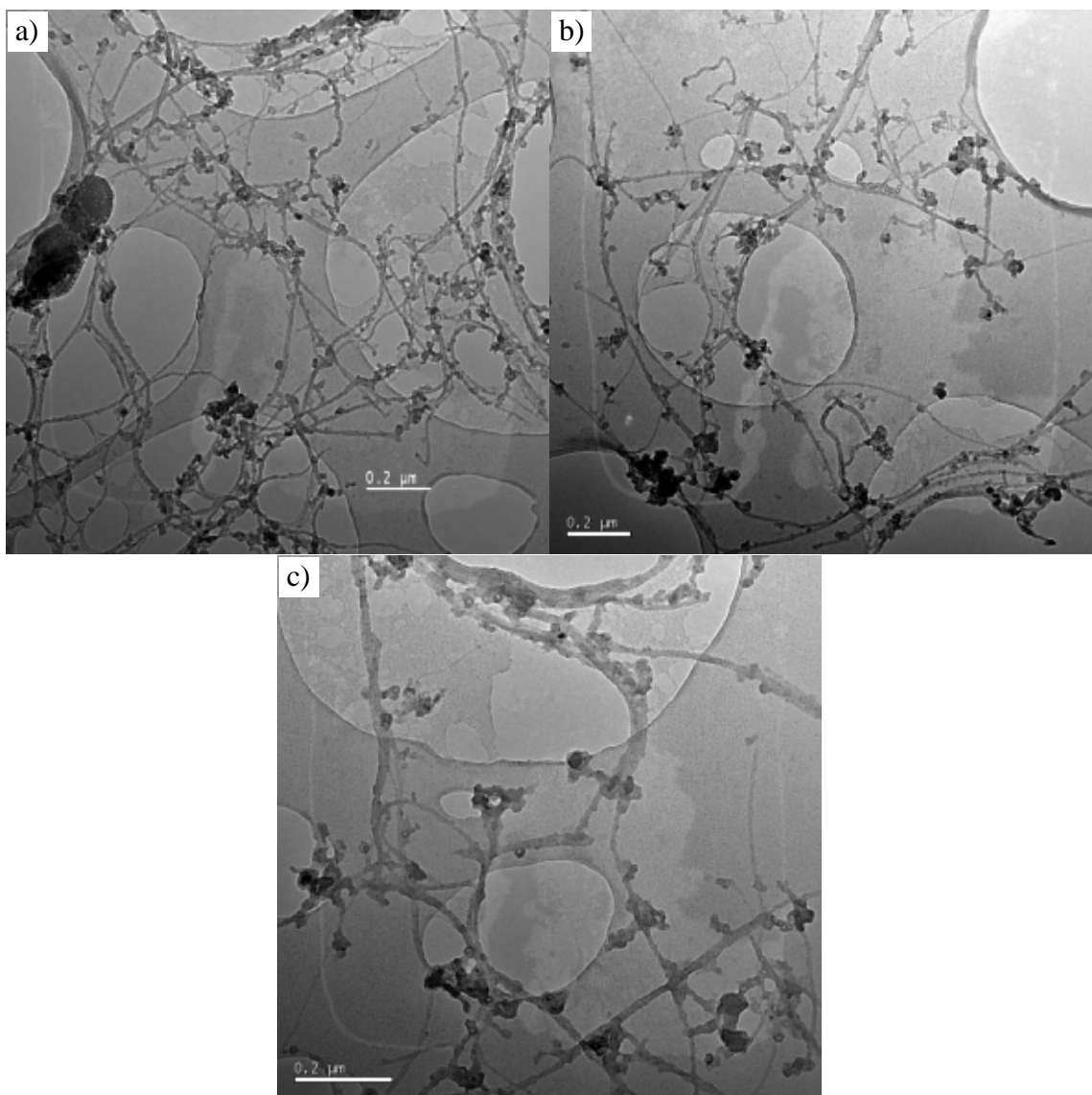
Figure 5.18. TEM micrographs of aqueous SWCNTs in the presence of NW at pH 3.

exactly what these natural colloids are. Possibilities include humic and fulvic substances, polysaccharides, proteins, cellular debris, viruses, clay particles, metal oxides etc.
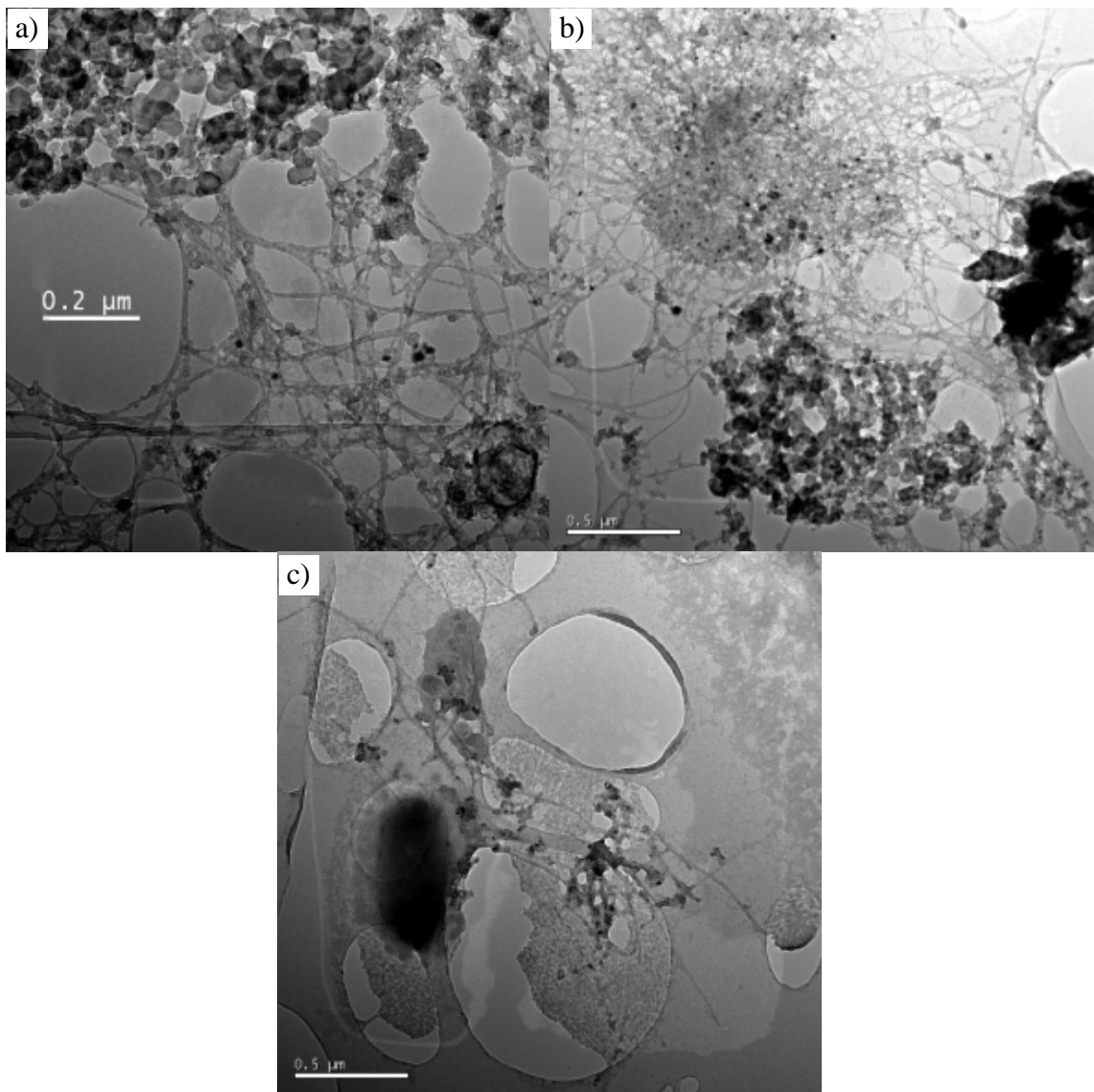
Figure 5.19. TEM micrographs of aqueous SWCNTs in the presence of NW at pH 6.5.
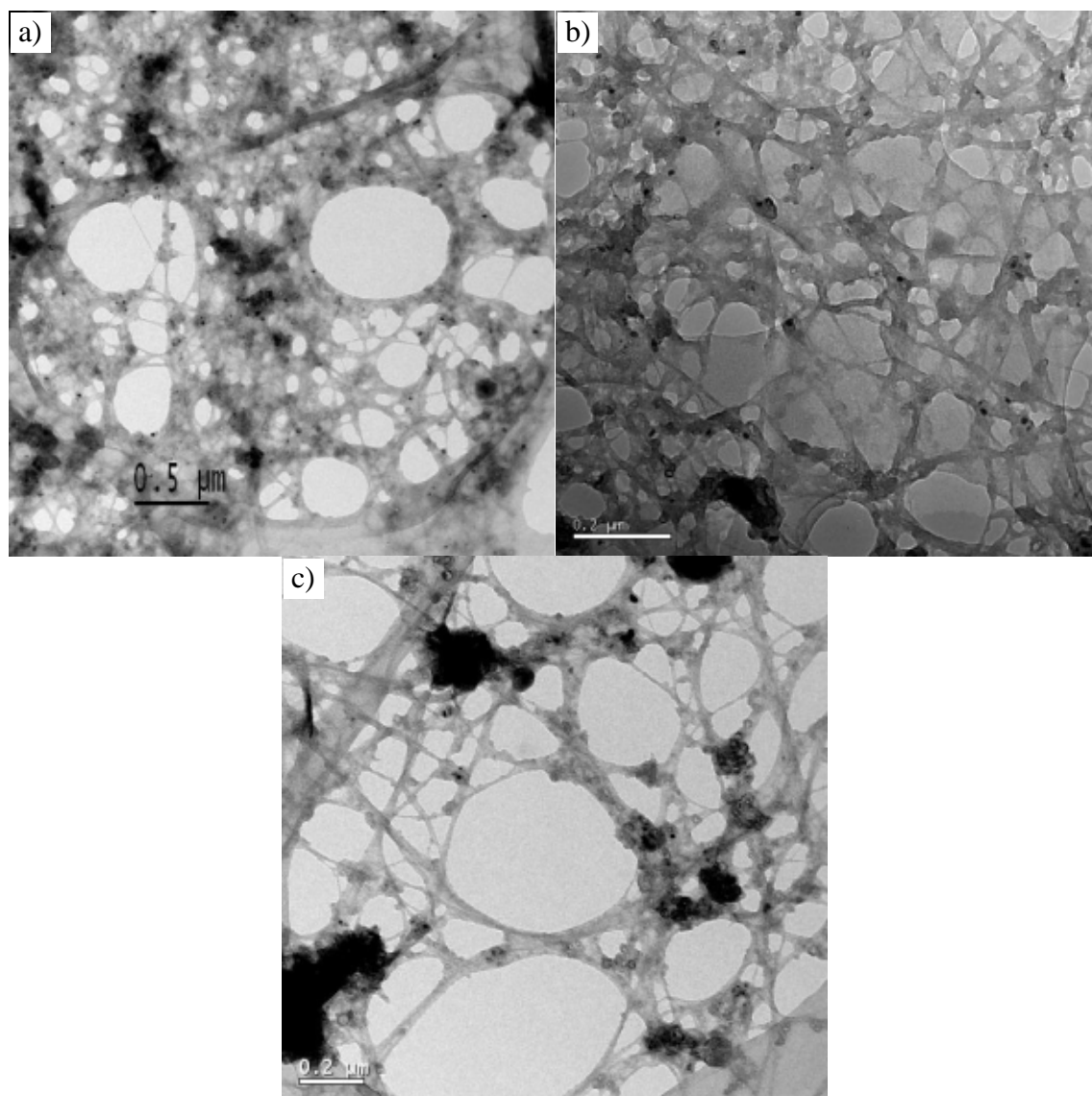
Figure 5.20. TEM micrographs of aqueous SWCNTs in the presence of NW at pH 10.

In good correlation with macroscopic observations (please refer to chapter 5.3 and Fig. 5.2), SWCNTs in the presence of Ca^{2+} cations form huge (in tens of μm across) and dense fluffy aggregates (Fig. 5.21).
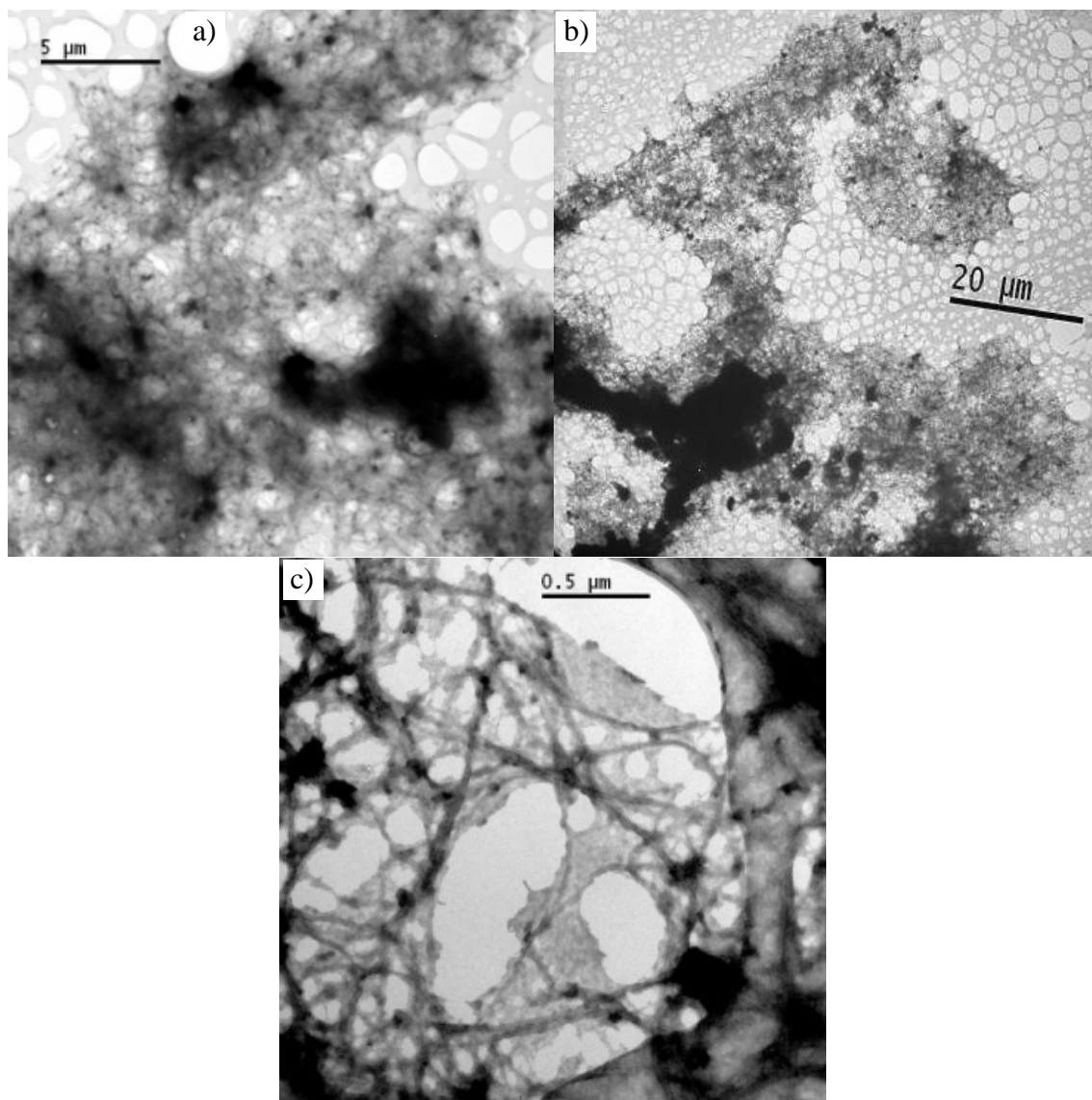
Figure 5.21. TEM micrographs of aqueous SWCNTs in the presence of Ca^{2+} at pH 10.

5.5   <u>Average bundle thickness measurements and statistical calculations</u>

From the TEM micrographs discussed previously (section 5.4), average bundle thickness (as shown in Fig. 5.3) was quantified for all samples. Table 5.2 summarises the results. At least 60 bundles (up to 164) per sample were measured with the Digital Micrograph software, depending on CNTs availability on the TEM grids. All results have been analysed with SPSS software with one sample Kolmogorov-Smirnov test (with $\alpha=0.05$) to assess the normality of the data distributions. One out of 27 samples (SWCNTs in the presence of natural water at pH 6.5) did not show the normal distribution. The statistical analysis (Mann-Whitney U test at $\alpha=0.05$ with SPSS software) was performed to check which samples were significantly different from the reference sample (i.e. SWCNTs alone at the same pH) and between samples at the same pH.

Average bundle thickness for nanotubes alone is slightly higher but in good agreement with the manufacturer's specification. Relatively high standard deviations derive from the production process itself and the thickness of observed fibrils depends on the number of single nanotubes in a bundle. Consistent with other reports [Journet et al., 1997], the thickness of the SWCNT bundles is in the range from 4-20 nm.

In the majority of samples, bundle thickness in the presence of natural colloids is statistically significantly different than in the absence of NAC (results in bold in Table 5. 2). The only sample not showing any significant difference to the reference samples at two pH values (3 and 10), is the sample with succinoglycan. Most of other samples (with one exception for SWCNTs with NW at pH 10) have average bundle thickness significantly higher than nanotubes alone. This effect can be explained by surface coating with humic material or bundles clinging to each other in solutions with cations.

		pH 3	pH 6.5	pH 10
SWCNT alone	average thickness in nm	7.2	7.2	8.1
	standard deviation in nm	*2.5*	*2.8*	*4.0*
	count	*80*	*107*	*131*
SWCNT + SRHA	average thickness in nm	**13.5**	**11.0**	**10.3**
	standard deviation in nm	*4.5*	*3.4*	*2.9*
	count	*108*	*75*	*64*
SWCNT + PHA	average thickness in nm	**7.9**	**12.5**	**10.5**
	standard deviation in nm	*2.4*	*2.8*	*4.7*
	count	*100*	*61*	*83*
SWCNT + succinoglycan	average thickness in nm	7.0	**6.0**	8.1
	standard deviation in nm	*2.1*	*2.1*	*2.5*
	count	*112*	*85*	*71*
SWCNT + NW	average thickness in nm	**10.5**	**9.0**	8.2
	standard deviation in nm	*3.5*	*3.5*	*3.3*
	count	*142*	*96*	*91*
SWCNT + Ca^{2+}	average thickness in nm	**15.0**	**9.7**	**14.7**
	standard deviation in nm	*5.2*	*3.1*	*4.8*
	count	*124*	*152*	*130*
SWCNT + Na$^+$	average thickness in nm	**15.6**	**9.9**	**16.7**
	standard deviation in nm	*4.1*	*4.6*	*4.5*
	count	*132.0*	*125.0*	*80.0*
SWCNT + Ca^{2+} & SRHA	average thickness in nm	**16.0**	**14.3**	**15.4**
	standard deviation in nm	*4.1*	*4.3*	*5.0*
	count	*153*	*101*	*113*
SWCNT + Na$^+$ & SRHA	average thickness in nm	**16.1**	**13.1**	**21.1**
	standard deviation in nm	*4.7*	*5.7*	*6.0*
	count	*123*	*164*	*90*

Table 5.2. Average thicknesses of bundles of SWCNTs alone and in the presence of natural organic matter measured from TEM micrographs (results for samples statistically different from the reference sample, i.e. SWCNTs alone at the same pH, are in bold).

Generally speaking, differences between morphologies of studied suspensions could not always be represented by a different average bundle thickness. This is

especially so in cases where the webbing effect was profound, which is difficult to quantify and compare.

The influence of pH did not show any consistent pattern on SWCNTs bundle thickness. In the case of SWCNTs with SRHA, a maximum bundle thickness was observed at pH 3, whereas in cases of SWCNTs with PHA at pH 6.5 and at pH 10 for SWCNTs with SG. Only in the cases of SWCNTs with PHA, SWCNTs with succinoglycan and SWCNTs with SRHA and Na^+ did all three pH values show statistically different bundle thicknesses. In the former case the highest thickness was found at pH 6.5, whereas in the latter case the maximum bundle thickness occurred at pH 10.

Understanding the interactions of CNTs with natural aquatic colloids is fundamental to defining their toxicity and fate & behaviour in natural waters. Aggregation behaviour is a key factor in the assessment of persistence and bioavailability of nanotubes. Significantly higher bundle thickness in the presence of humic acids (Table 5.2) is evidence of surfactant properties of natural organic matter towards SWCNTs. Coating nanotubes by forming a nanoscale layer of HA on the surface (also in the presence of major cations), decreases strong Van der Waals attraction between SWCNTs particles and maintains them in suspension. Thus in waters rich in humic substances (e.g. dystrophic lakes) exposure of aquatic biota to CNTs may occur to unexpected extent.

The stability of aqueous oxidised CNTs is a result of a strong negative surface charge (Table 5.1), which keeps the particles apart (i.e. counteracts aggregation). The presence of major cations may interfere with this stabilising mechanism by charge neutralisation. In this study the influence of Na^+ and Ca^{2+} was examined. No effect of

Na^+ was observed at the tested concentration (which matched the concentration in the lake water used in the experiments). However, the presence of Ca^{2+} (again, at the same concentration as in the natural lake water) showed a strong destabilising effect on aqueous SWCNTs. The water column was cleared of the majority of visibly suspended SWCNTs within 24 h. Consequently, in hard waters (with higher concentrations of divalent cations) or waters with high ionic strength (i.e. marine environments), SWCNTs could be efficiently removed from the bulk water and transferred to sediments.

6   RESULTS: ULTRACENTRIFUGATION ONTO SUPPORTING GRIDS AS A TRANSMISSION ELECTRON MICROSCOPY SPECIMEN PREPARATION METHOD FOR AQUATIC SUSPENSIONS OF CARBONACEOUS NANOPARTICLES

6.1   Summary

In the previous chapter TEM was employed to study CNTs in the aquatic environment. This chapter builds on this work and discusses optimisation of the TEM specimen preparation protocol. Ultracentrifugation has been used successfully as a way of preparing native colloidal material from natural waters for examination using TEM (which was discussed in section 3.2.2.1) [Lienemann et al., 1998; Wilkinson & Lead, 2007]. This chapter addresses the application of a similar approach to water-suspended carbonaceous NPs: SWCNTs and fullerenes C_{60}.

Section 6.2 describes the protocol applied to prepare SWCNTs and nC_{60} aqueous suspensions with and without natural aquatic colloids (Suwannee River Humic Acid, Suwannee River Fulvic Acid, succinoglycan and natural lake water) as well as centrifugation parameters.

Sections 6.3 and 6.4 contain representative images for each sample and discuss observed morphologies.

The chapter concludes with a comparison of ultracentrifugation versus the "drop-drying" method for carbonaceous NPs (as used in chapter 5).

6.2 Sample preparation and ultracentrifugation parameters

Single-walled carbon nanotubes

Test samples were prepared by mixing the appropriate amounts of stock solutions (as discussed in chapter 3.1) to obtain the following suspensions:

1. SWCNT (10 mg L^{-1}), pH 5.7

2. SWCNT (10 mg L^{-1}) & SRHA (10 mg L^{-1}), pH 4.1

3. SWCNT (10 mg L^{-1}) & SG (10 mg L^{-1}, nominal conc. before filtration), pH 4.8

4. SWCNT (10 mg L^{-1}) & NW (twice diluted after filtration), pH 7.6

To compare ultracentrifugation and whole mounts (used in a previous chapter) as a TEM specimen preparation method, test samples were prepared according to the same protocol. In this experiment, however, the pH of the samples was only measured (not adjusted). To ensure optimal grid coverage for centrifuged specimens the listed samples were diluted 10 times. The correct dilution was found via a process of trial and error. For more routine experiments it is advisable to prepare a calibration curve (concentration v optical properties of a sample e.g. UV-Vis absorbance) [Lienemann et al., 1998]. From this work a rule of thumb can be formulated; the optimal concentration corresponds quite well to a concentration at which the sample loses its visually detectable light absorbance (i.e. coloration).

Fullerenes C_{60}

Test samples were prepared by mixing the appropriate amounts of stock solutions (as discussed in chapter 3.1) to obtain the following suspensions:

1. nC_{60} (2 x diluted from the stock), pH 6.5

2. nC_{60} (2 x diluted from the stock) & SRFA (10 mg L^{-1}), pH 4.8

3. nC_{60} (2 x diluted from the stock) & SG (10 mg L^{-1}, nominal conc. before filtration), pH 5.3

4. nC_{60} (2 x diluted from the stock) & NW (twice diluted after filtration), pH 7.7

To ensure the optimal grid coverage for centrifuged specimens the listed samples were diluted 10 times. Similarly to SWCNT samples, the optimal concentration was determined by a trial and error method.

Centrifugation

10 ml samples with an optimal dilution were ultracentrifuged onto holey carbon films (2 per sample) on 400 copper mesh. Beckman L7-65 Ultracentrifuge with SW40 swinging bucket rotor (Fig. 6.1) was used in the experiments. To provide a flat support for grids Teflon caps were placed at the bottom of the tubes. A threaded slot to facilitate removal from centrifuge tubes was drilled.

Ultracentrifugation parameters are as follows:

- speed: 30.000 rpm

- relative centrifugal field at r_{max}: 160.000 g, r_{av}: 114.000 g and r_{min}: 67.200 g

- temperature: 15° C

- run time: 60 min.

The ultracentrifugation parameters are similar to those reported by Lienemann et al. (1998). They were used as a starting point in the experiments presented here. Ultracentrifugation at these parameters proved satisfactory so no further modifications were tested. After centrifugation the tubes were carefully emptied, the bottom cups removed and TEM grids dried in ambient conditions prior to the microscopy analysis.

Figure 6.1. Beckman SW40 swinging bucket rotor with a centrifugation tube and TEM grids.

Transmission Electron Microscopy

All samples were imaged on a FEI Philips TECNAI F20 TEM operating at 200 kV (shown in Fig. 3.8). At least 10 different TEM images at different magnifications (from 2000x to 250kx) were taken for each suspension and analysed with Digital Micrograph software.

6.3   TEM imaging of ultracentrifuged SWCNTs

Representative images from ultracentrifuged specimen are shown in Fig. 6.2. The observed morphologies do not differ significantly from the samples prepared by the whole mounts (air drying) method (presented and discussed in chapter 5). The SWCNT bundle thickness ranges from 2-30 nm with most nanotube bundles about 5-10 nm thick.
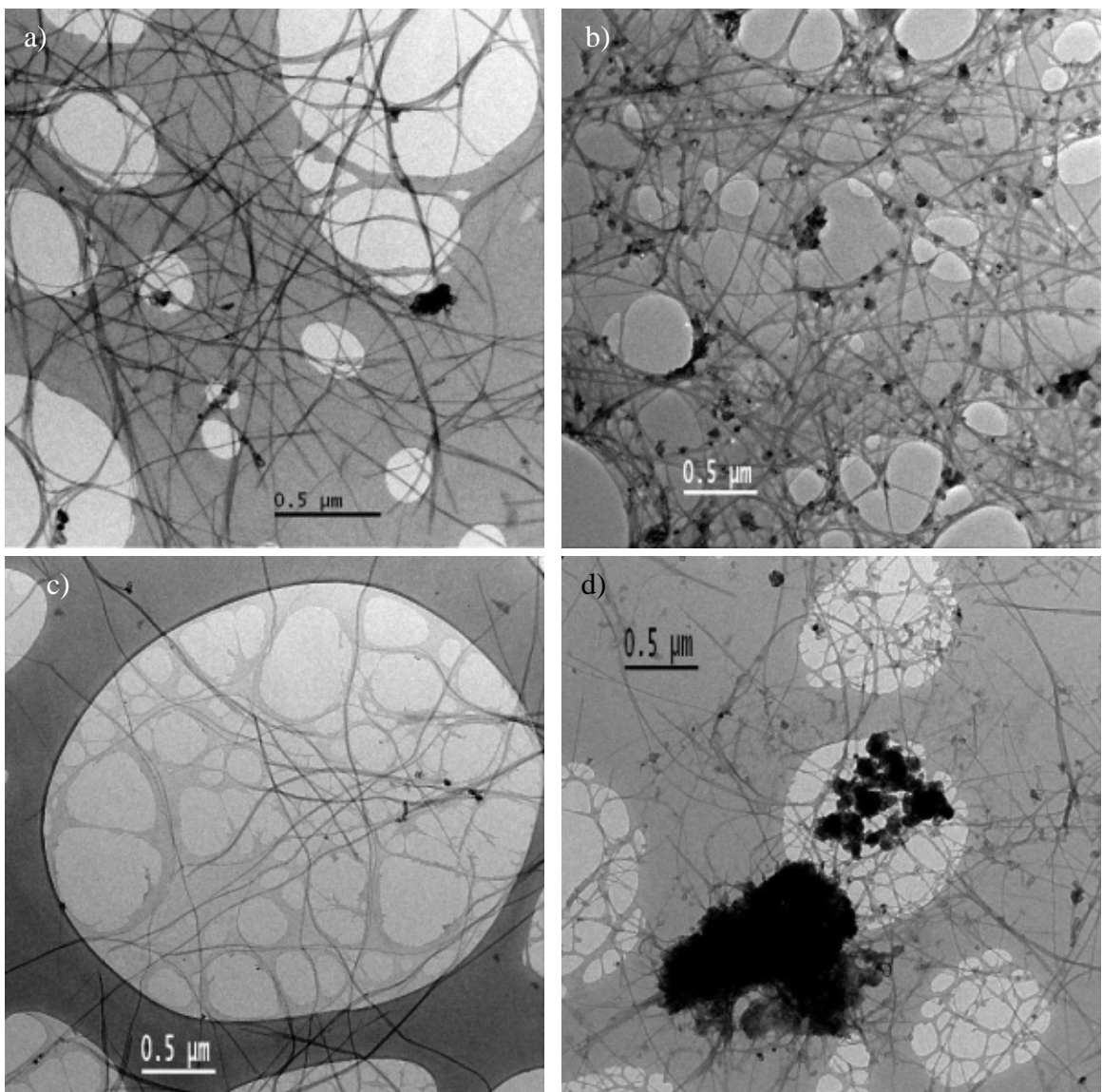
Figure 6.2. TEM micrographs of ultracentrifuged SWCNTs alone (a) and in the presence of SRHA (b), succinoglycan (c) and natural water (d).

Nanotubes alone show different morphologies than when mixed with aquatic colloids: humic acid particles are trapped in entangled networks of nanotubes (Fig. 6.2 b), thin filming structures are abundant in the presence of succinoglycan (Fig. 6.2 c), and various nano and microscale particles present in the lake water are incorporated in SWCNT networks.

More TEM images (obtained with a different specimen preparation protocol, i.e. drop-drying), detailed discussion of observed morphologies and their environmental implications can be found in sections 5.3 – 5.5.

6.4   TEM imaging of ultracentrifuged nC$_{60}$

Fig. 6.3-6 show representative images of ultracentrifuged water-stirred fullerenes C$_{60}$ alone and in the presence of aquatic colloids: Suwannee River fulvic acid, succinoglycan and natural lake water.

The extended-mixing method of preparing aqueous suspensions of fullerenes produces stable colloidal aggregates nC$_{60}$ with reported sizes in the range of 50-2000 nm with average dimensions of ca. 250 - 500 nm [Brant et al., 2006; Spohn, 2009]. In this study too, a broad range of aggregate sizes was found with average dimensions of a few hundred nm. The smallest clusters have dimensions ca. 30 nm whereas the biggest are up to 3 µm. Similar particles were found in abundance in all studied samples. Some aggregates show more compact morphologies (Fig. 6.3 c) and others are loosely grouped together (6.3 a). The biggest particles exhibit angular faceted shapes (Fig. 6.6 a, b and c). Particles with sizes below 1 µm are more oval with smoother edges (Fig. 6.3 d). More information on nC$_{50}$ characterisation with TEM and other techniques can be found in chapter 9.

Interactions of fullerenes with aquatic colloids are less apparent than in the case of CNTs. At low resolution, morphologies of collected particles show little difference from the sample with nC$_{60}$ alone.

In the presence of fulvic acid most particles exhibit the same morphologies as nC$_{60}$ alone (Fig. 6.4 c and d). In some images humic acid and fullerenes are depicted together with little evidence of mutual interaction (Fig. 6.4 b). However, Fig. 6.4 a gives an example of fullerene-colloid interactions: nC$_{60}$ cluster surrounded (possibly coated) by smaller particles of fulvic acid.

In the presence of succinoglycan, suspended thin film structures can be observed (Fig. 6.5 a) linking both C_{60} and SG. This thin layer of material provides a clearly visible coating for fullerene aggregates and smoothes their edges (Fig. 6.5 a and d). Fig. 6.5 b illustrates a situation where both kind of particles are present (nC_{60} and SG) but no interaction takes place. Many aggregates do not exhibit any difference from fullerenes alone (Fig. 6 5.c).
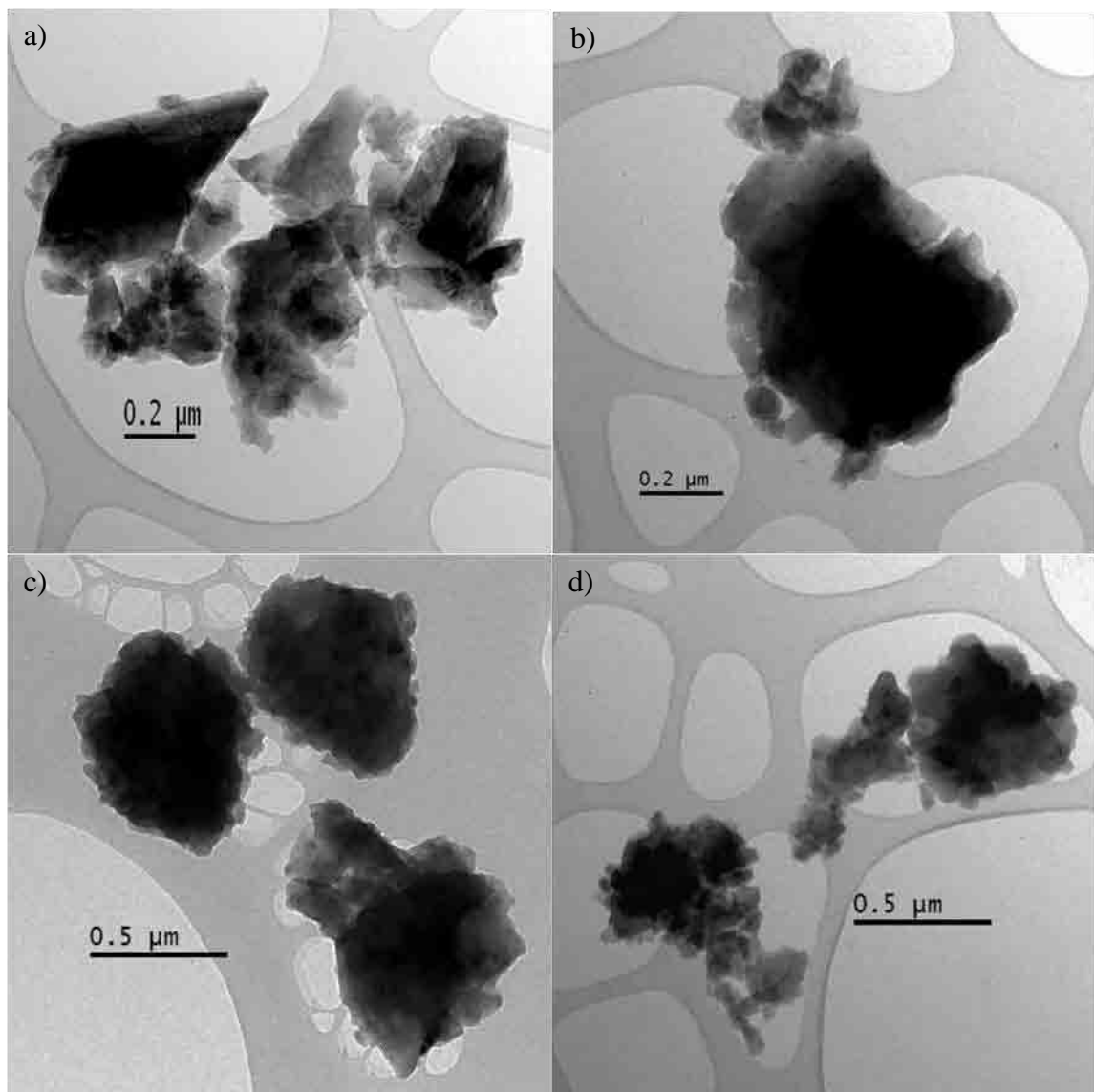
Figure 6.3. TEM micrographs of ultracentrifuged nC_{60}.

In the presence of natural water (Fig. 6.6) more diverse material can be seen; large (over 1 μm) angular particles with even surfaces as well as smaller heterogeneous ones with ragged edges. In some cases, smaller material (morphologically similar to humics) fills in the spaces between nC_{60}. Fig. 6.6 d presents an example of strong interaction; a fullerene cluster evenly coated with colloidal particles (presumably humics).
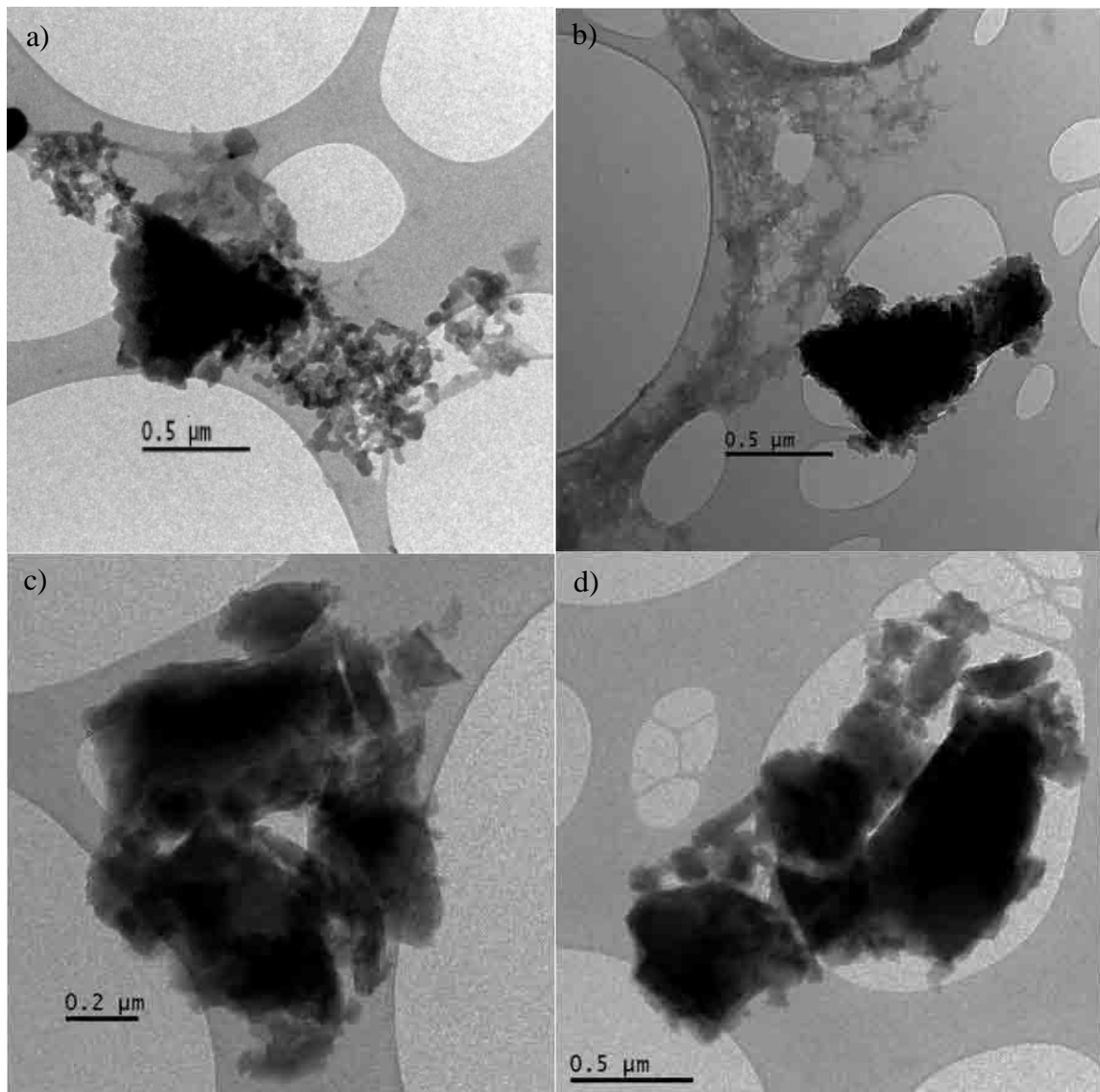
Figure 6.4. TEM micrographs of ultracentrifuged nC_{60} in the presence of SRFA
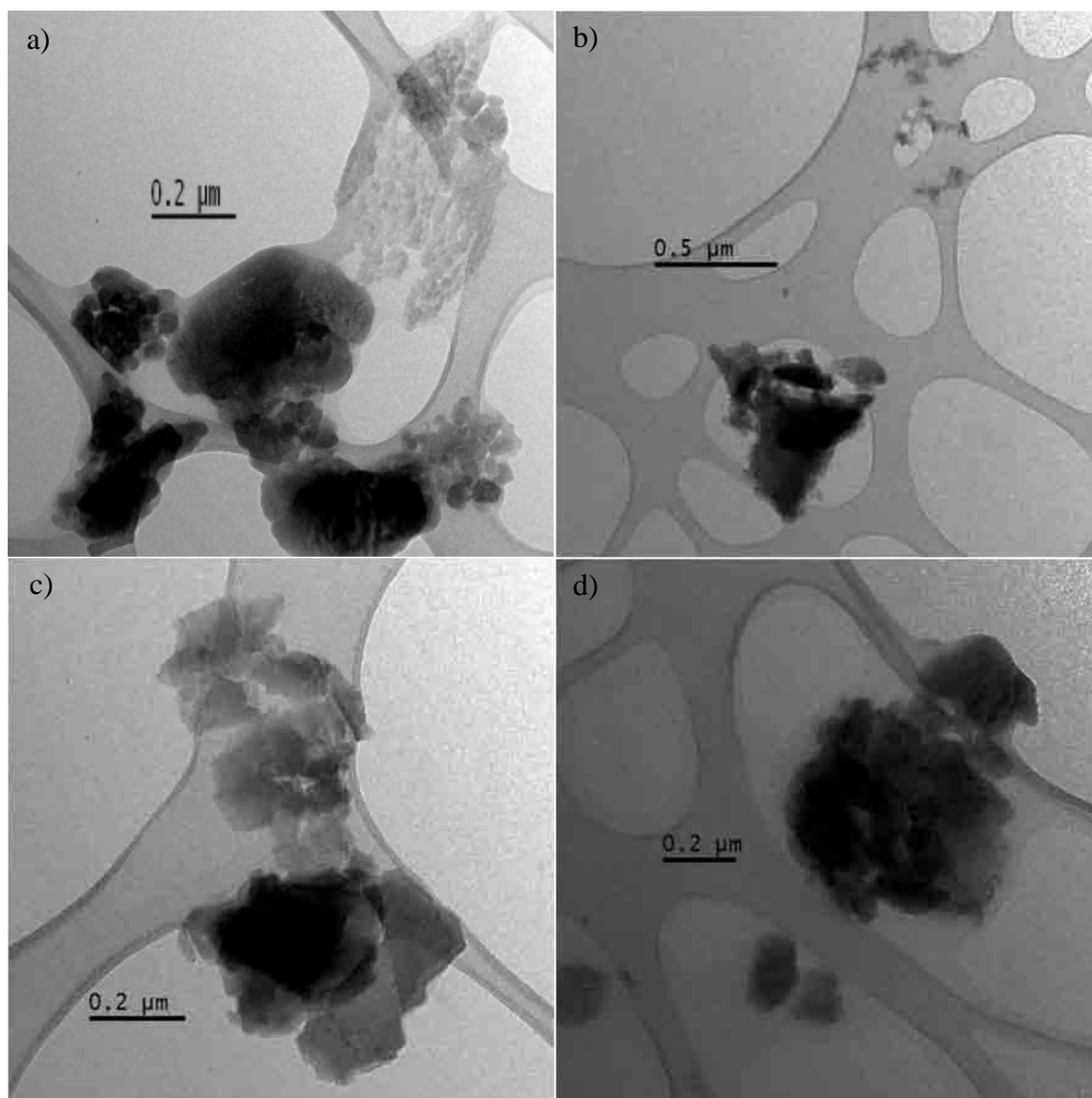
Figure 6.5. TEM micrographs of ultracentrifuged nC_{60} in the presence of succinoglycan.
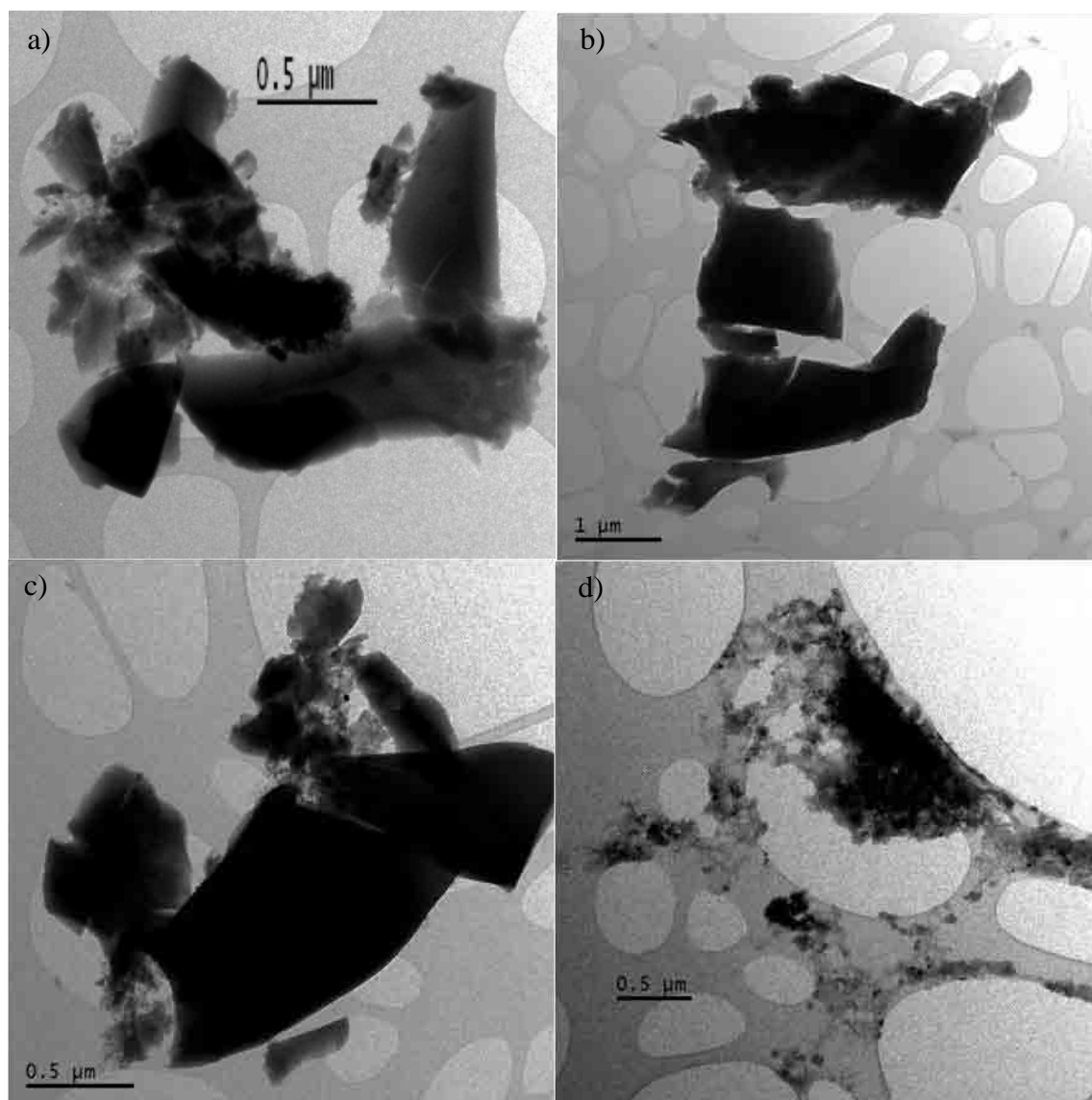
Figure 6.6. TEM micrographs of ultracentrifuged nC_{60} in the presence of natural water.

6.5   Ultracentrifugation v the whole mounts technique for carbonaceous nanoparticles

Ultracentrifugation has been used successfully as a way of examining native colloidal material in natural waters with TEM [Perret et al., 1991; Lienemann et al., 1997; Lienemann et al., 1998; Benedetti et al., 2003; Koukal et al., 2008; Chanudet and Filella, 2008]. In this study it was applied to examine SWCNTs and fullerenes C_{60} in aqueous suspensions in the absence and presence of natural aquatic colloids. The presented preparatory methodology proved to be superior to traditional 'drop drying' technique due to optimal grid coverage and substantially higher homogeneity of the microscopy specimen.

The previous chapter (5.4) presents an extensive body of work on SWCNTs in aqueous samples where all TEM specimens were prepared by the whole mounts technique. In this chapter the same samples were imaged from the ultracentrifuged samples. Although the observed morphologies do not show differences (and thus cannot be represented by TEM images), the time needed for the TEM analysis has been shortened considerably. In drop-dried specimens large parts of the grid have no sample at all - particles from the samples are often confined to a few (out of 300-400) squares on the grid. Locating such areas on the carbon film takes a considerable amount of time. In the case of C_{60} only two samples were prepared with the drop-drying method and both were empty on the majority of the grid with only 1-2 squares displaying densely packed nC_{60} clusters (about 6400 μm^2, which constitutes about 0.25 % of the grid surface).

Figure 6.7 illustrates the difference in grid coverage for both techniques. In case of the whole mounts technique, locating the studied NPs on the grid tends to be a time

consuming and tedious procedure. The homogeneous and optimal grid coverage which is easily obtainable with ultracentrifugation method, allows much easier and faster TEM analysis of the specimen. Aggregation caused by drying is minimised thus the sample is less perturbed by the preparatory procedure. Additionally, by controlling conditions of deposition during ultracentrifugation, valuable quantitative information about the sample can be obtained (such as particle size distribution, number concentration).

For more information on TEM analysis of nC_{60} (also involving ultracentrifugation) please refer to chapter 9.5.

whole mounts   *ultracentrifugation*
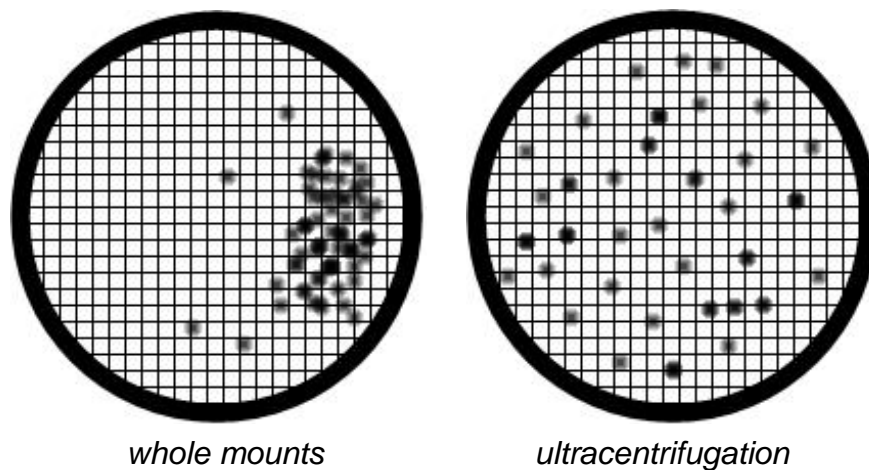
Figure 6.7. Schematic representation of the grid coverage for whole mounts v ultracentrifugation techniques (note: dots represent areas with the particles on them, not the particles themselves).

7 RESULTS: CHARACTERISATION OF SINGLE-WALLED CARBON NANOTUBES WITH ATOMIC FORCE MICROSCOPY

7.1 <u>Summary</u>

In this chapter the application of AFM to characterise engineered NPs (SWCNTs) in aquatic systems is discussed.

Seven representative samples are analysed in the presence/absence of humic acid, sodium and calcium cations and natural water at pH 3, 6.5 or 10. Sample concentrations are listed in chapter 7.2. The microscopy specimen preparation protocol is also included in this section.

The results of AFM imaging of these samples are presented in chapter 7.3. Observed morphologies are discussed in detail and compared with TEM images obtained for the same samples (to which chapter 5 was devoted).

For more quantitative analysis average nanotube bundle heights are calculated for each sample. The results with their statistical significance are presented and discussed in chapter 7.4. Average SWCNT bundle heights measured with AFM are compared to average SWCNT bundle thicknesses determined with TEM in section 7.5.

The last section in this chapter (7.6) contains discussion on non-contact and tapping modes used during the study. Presented results suggest that the tapping mode exerts stronger forces on a sample, which results in sample surface modification (height reduction).

7.2 Sample and microscopy specimen preparation

The aim of this chapter is to build on the work presented in sections 5.4 and 5.5, where 27 samples of SWCNTs with and without aquatic colloids at three pH values were analysed (see also Table 5.2). To minimise the workload a selection of seven aqueous suspensions of SWCNTs was made with a view to representing different conditions and compositions of samples analysed with TEM. Test samples were prepared by mixing the appropriate amounts of stock solutions (as discussed in chapter 3.1) to obtain the following suspensions:

1. SWCNT (10 mg L^{-1}) & NW (twice diluted after filtration), pH 6.5

2. SWCNT (10 mg L^{-1}) & Ca^{2+} (45 mg L^{-1}, the same as in NW used), pH 6.5

3. SWCNT (10 mg L^{-1}) & Na$^+$ (13 mg L^{-1}, the same as in NW used), pH 6.5

4. SWCNT (10 mg L^{-1}) & SRHA (10 mg L^{-1}) & Ca^{2+} (45 mg L^{-1}), pH 6.5

5. SWCNT (10 mg L^{-1}) & SRHA (10 mg L^{-1}) & Na$^+$ (13 mg L^{-1}), pH 3

6. SWCNT (10 mg L^{-1}) & SRHA (10 mg L^{-1}) & Na$^+$ (13 mg L^{-1}), pH 6.5

7. SWCNT (10 mg L^{-1}) & SRHA (10 mg L^{-1}) & Na$^+$ (13 mg L^{-1}), pH 10

pH of each sample was adjusted with 0.1 M HCl or 0.1 M NaOH. Before preparing microscopic specimens all the samples were gently shaken for about 15 hours and their pH measured and readjusted if needed.

The standard AFM specimen preparation protocol widely used for aquatic colloids involves inserting a freshly cleaved and rinsed with ultra pure water sheet of mica to the solution and keeping it in the vertical position for 30 min (spontaneous adsorption of colloidal matter to the surface of mica takes place), after which time the mica is rinsed again and left to air-dry sheltered form atmospheric contamination

[Balnois et al., 1999; Lead et al., 2005; Guo and Ma, 2006]. This method was tested for the suspensions of SWCNTs but adsorption proved insufficient for NPs to be imaged with AFM. Mica surface remained clean and identical to the blank sample and no nanotubes were detected after imaging. This observation may be explained by electrostatic repulsion between negatively charged mica surface [Plaschke et al., 1999; Jiang et al., 2003; Lee et al., 2007; Schierz and Zaenker, 2009] and negatively charged SWCNTs (due to functionalization with carboxylic groups). It is also conceivable that nanotubes are too large to effectively adsorb. Their extremely long shapes (aspect ratio of 100-400) may additionally hinder vertical deposition, which would require approximately even adsorption along a nanotube. To ensure the presence of particles a different protocol was applied. Freshly cleaved mica placed horizontally was used as a substrate, onto which 10-15 µL of the test solution was pipetted and left to dry in ambient conditions. To remove the weakly attached fraction, which might interfere with the AFM scanning process, the mica surface was rinsed with ultra pure water and dried again. Apart from the different substrates used, specimen preparation protocol was essentially the same for AFM and TEM (chapter 5.2).

All samples were imaged on a XE-100 AFM by Park Systems in non-contact and tapping modes (Fig. 3.2 a). Commercially available aluminium coated tips made of doped silicone with a radius of curvature < 10nm were used. X-Y scan sizes were varied up to 10 x 10 µm with resolution of 256 pixels per line. Scanning rates were optimised to acquire a stable and clear image without damaging the tip or detaching particles during scanning, usually 0.5, 1 or 2 Hz.

7.3 AFM imaging of SWCNTs. Comparison with TEM results

The theoretical background to AFM is given in chapter 3.2.1, where its principle of operation is explained, advantages and disadvantages as well as the most popular scanning modes are discussed.

The morphologies of SWCNTs in the presence of natural aquatic colloids observed with AFM are similar to those imaged with TEM (chapter 5.4). Single nanotube bundles or their randomly entangled clumps were found in all studied samples. Fig. 7.1 b - e shows four selected AFM micrographs of SWCNTs in the presence of sodium cations (pH 6.5). Nanotube bundles in these images are 2-15 nm high and up to 2 µm long. Roughly spherical particles visible in the micrographs are
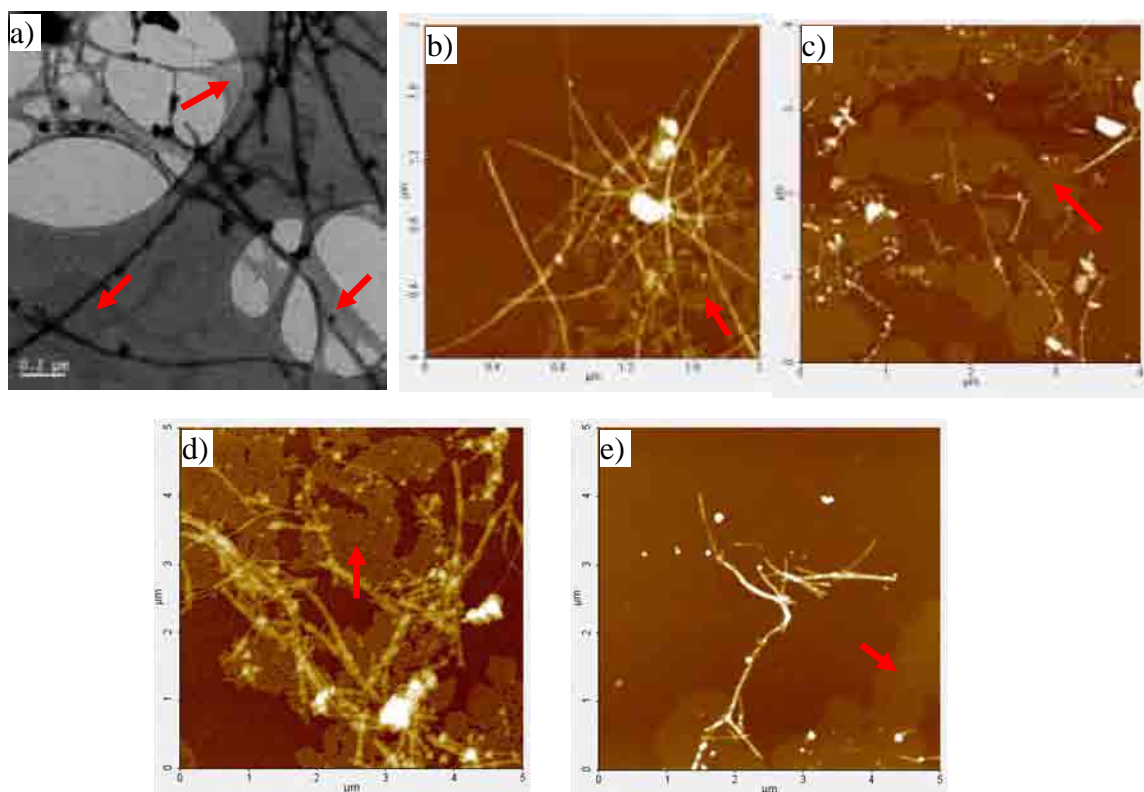
Figure 7.1. SWCNTs in the presence of Na^+ at pH 6.5 imaged with TEM (a) and AFM in non-contact mode (b, c, d, e).

carbonaceous and/or metal impurities from the nanotube powder, which were also present in the TEM images. Another structure found in AFM images of this sample is patchy films easily visible on the mica surface (indicated by red arrows). This coating is about 1-1.5 nm thick and corresponds well with thin film suspended in the holy areas of TEM grid (Fig. 7.1 a). Different, more angular shapes of the coating probably result from the damage caused by drying in the areas with no substrate (carbon film) and thus no support. Indeed, on the carbon film the patchy coating takes more oval shapes although it is less clearly visible with considerably reduced contrast, which suggests that the coating is very thin.
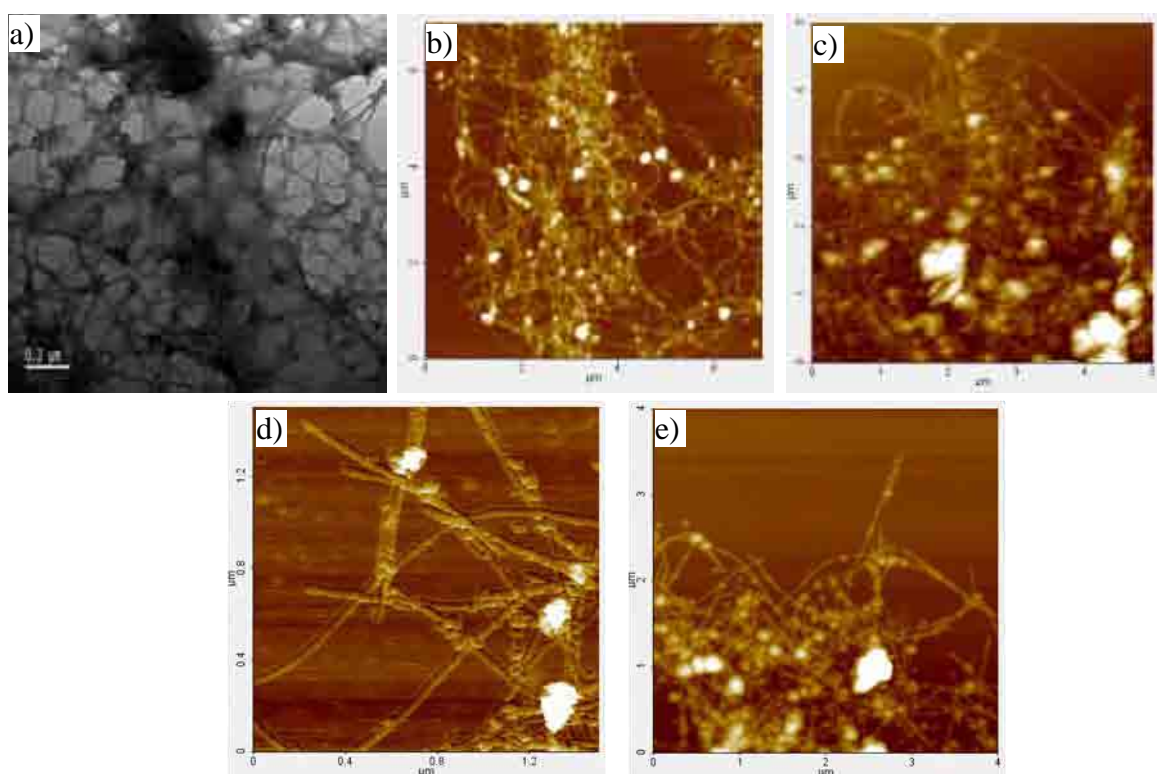
Figure 7.2. SWCNTs in the presence of Ca^{2+} at pH 6.5 imaged with TEM (a) and AFM in non-contact mode (b, c, d, e).

Remarkably good agreement between the AFM and TEM images was found for the sample with calcium cations at pH 6.5 (Fig. 7.2). Both techniques showed thick and

dense clumps of nanotube bundles, which is consistent with visual examination of the samples (Fig. 5.2).

To examine pH effect on the suspensions, one set of samples, i.e. SWCNTs in the presence of SRHA and Na$^+$ was imaged in all three pHs analysed with TEM: 3, 6.5 and 10 (Fig. 7.3). It was hard to see any consistent difference in the morphologies of nanotubes between high and low pH. It should be noted, however, that at pH values if 6.5 and 10 mica surface was significantly cleaner, and at the highest pH in particular, finding nanotubes on the substrate was troublesome (Fig. 7.3 e & f and h & i). At low pH (lower than 4) oxidised nanotubes show less negative surface charge in aqueous suspensions [Schierz and Zaenker, 2009], which may facilitate adsorption onto the mica.

For humic acid at different pH values, similar observations as in case of TEM were made: numerous particles at low pH (i.e. 3) and few in higher pH (i.e. 6.5 and 10). In the images obtained for the sample at pH 3 (Fig. 7.3. b & c) evenly spread homogenous aggregates of spherical SRHA particles can be identified with the coating thickness of about 3 nm, which is in good agreement with previous findings [Plaschke et al., 1999; Liu et al., 2000; Chen et al., 2007B]. Significantly less evident presence of humic acid at high pH has been reported elsewhere (at lower pH the surface coating formed by humic acid is considerably more profound) [Plaschke et al., 1999]. Similarly as in the case of nanotubes, this effect can be attributed to the less negative surface charge at lower pH values.

Considerably thicker (up to 15 nm) coating of humic acid was found in the presence of calcium cations (Fig. 7.4 b, c, d and e). Humic acid aggregates and nanotube bundles form dense and compact patches, which were observed with both microscopy techniques (Fig. 7.4).
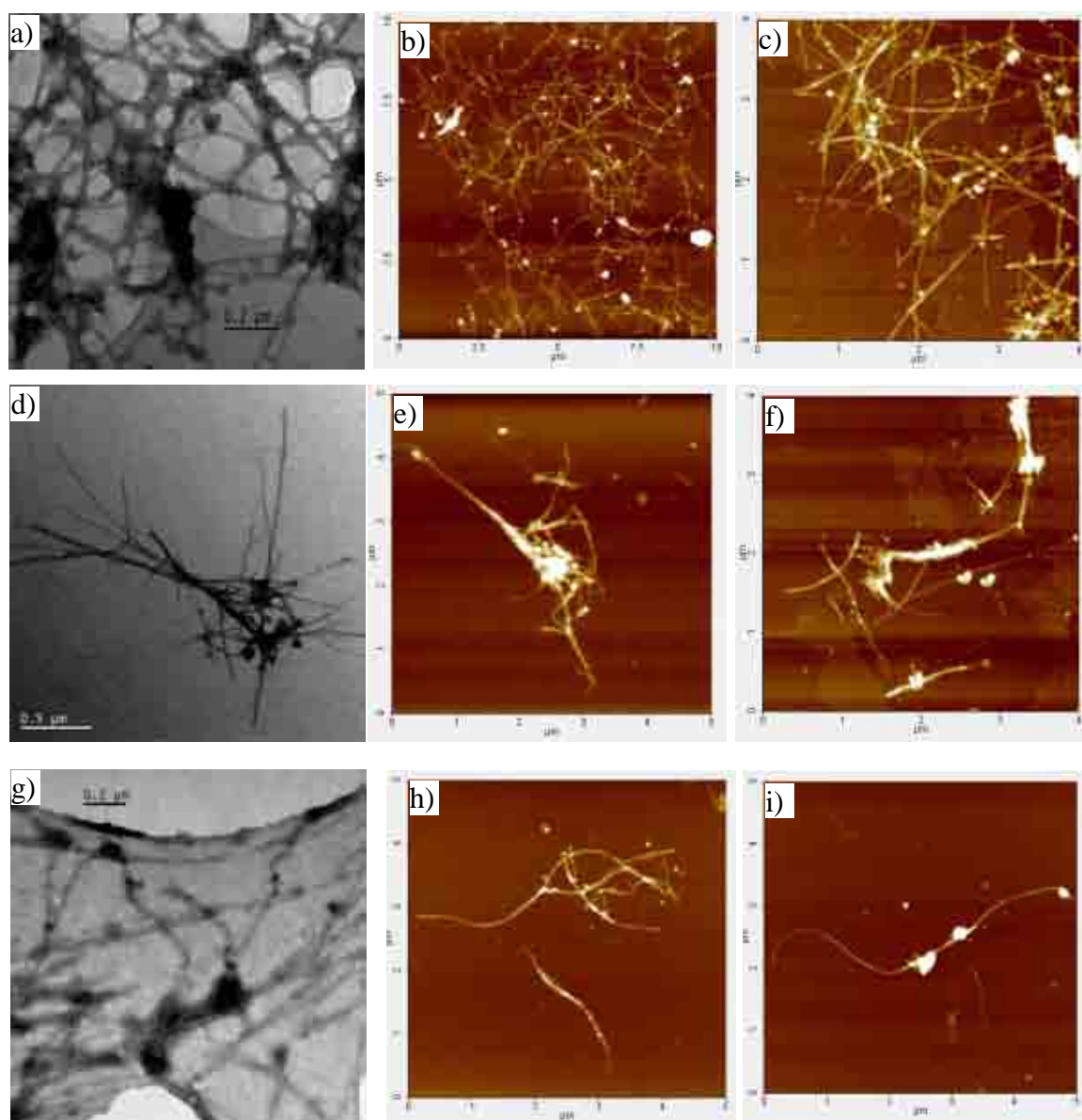
Figure 7.3. SWCNTs in the presence of SRHA and Na$^+$ at pH 3 (a, b, c), pH 6.5 (d, e, f) and pH 10 (g, h, i) imaged with TEM (a, d, g) and AFM in tapping mode (b, c, e, f, h, i).

156
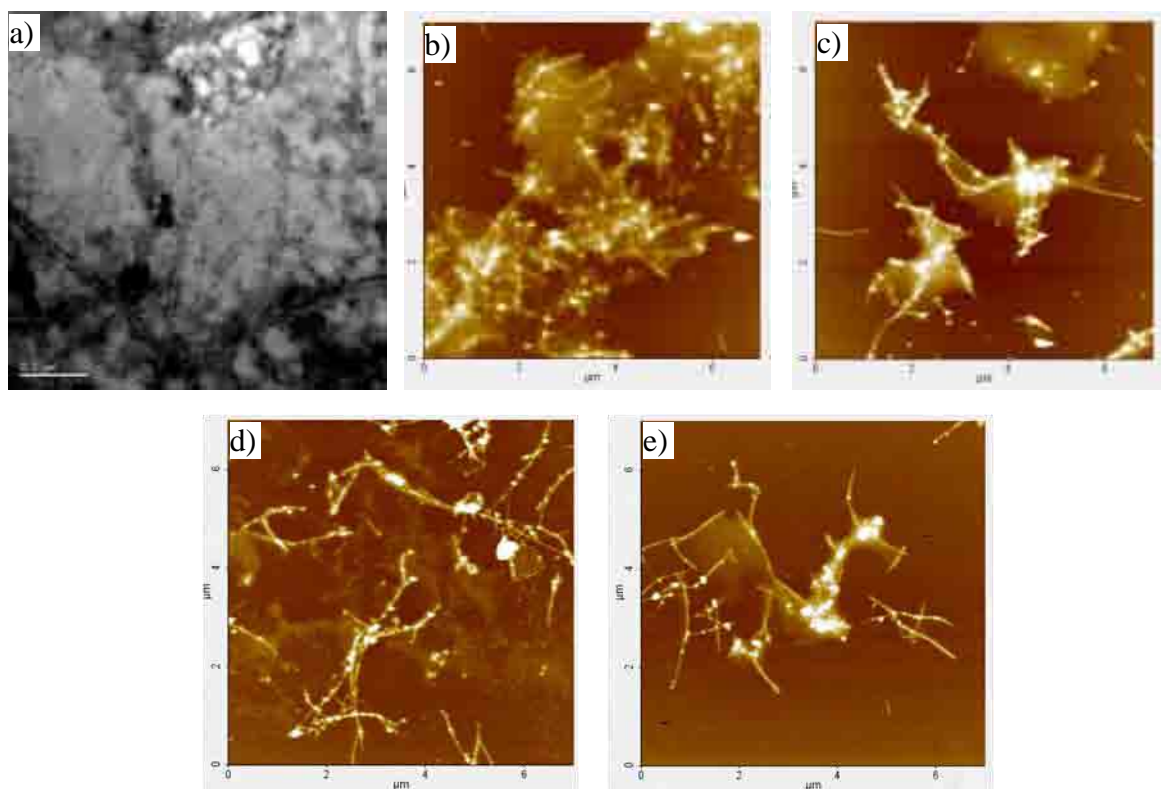
Figure 7.4. SWCNTs in the presence of SRHA and Ca^{2+} at pH 6.5 imaged with TEM (a) and AFM in non-contact mode (b, c).

The morphology of the sample with lake water encompasses structures reported for the previous samples: nanotube bundles networks, mica coating, and larger spherical particles (Fig. 7.5). Due to the unknown composition of the natural water is it impossible to identify entities incorporated in the entangled nanotube clumps.

AFM proved to be a powerful tool for the examination of SWCNTs in aqueous solutions and their interactions with natural aquatic colloids. Observed morphologies are in a good agreement with the TEM results for all analysed samples. For both techniques, samples represented by microscopy specimens were very heterogeneous, with some areas tightly packed with particles as well as huge regions with no sample on the substrate. Additionally, within the same sample imaged morphologies varied. For

example, in the presence of humic acid some areas showed SRHA aggregates incorporated in the nanotube bundles networks and elsewhere SWCNTs with no distinguishable humic material (e.g. Fig. 7.3 e and f). Such inconsistency can be partly attributed to the specimen preparation method since air-drying causes major aggregation and uneven distribution of the sample on substrate. In the case of TEM, ultracentrifugation onto the grid proved to successfully reduce such undesired effects (which was discussed in chapter 6). It is thus recommended that the AFM specimen preparation protocol should follow a similar approach, i.e. ultracentrifugation of samples onto mica.
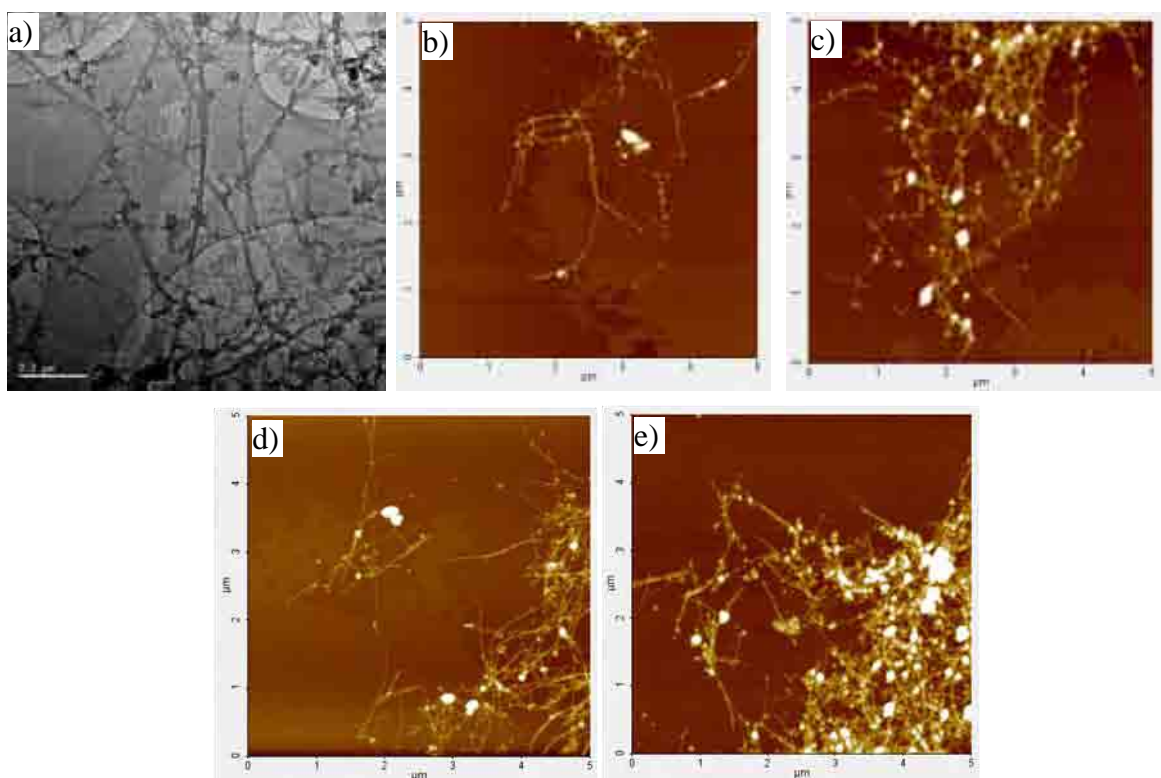
Figure 7.5. SWCNTs in the presence of natural lake water at pH 6.5 imaged with TEM (a) and AFM in non-contact mode (b, c, d and e).

7.4   <u>Average bundle height measurements</u>

The lateral resolution of AFM is limited by the radius of curvature of the scanning tip [Keller, 1991]. Due to nonideal shape (finite sharpness) lateral dimensions measured with AFM might be largely overestimated (see also Fig. 3.1). Secondly, during adsorption onto mica spherical natural aquatic colloid particles may undergo flattening, which might be further enhanced by drying (although not as severe as with TEM). Consequently, the lateral dimension of such particles can be more than an order of magnitude bigger than the diameter of the spherical particle in its native aqueous state [Balnois et al., 1999; Lead et al., 2005]. For these reasons, AFM uses height rather than width measurements for aquatic colloid characterisation [Doucet et al., 2004; Baalousha and Lead, 2007; Chen et al., 2007B; De Momi and Lead, 2008].

The same approach was applied in this study to quantify the morphology of SWCNTs in the presence of aquatic colloids with AFM. Figure 7.6 illustrates AFM height measurements with XEI software by Park Systems. The thicker bundle on the left is 5.5 nm high, the thin one on the right – 0.8 nm, the spherical particle is 47.2 nm high and the measured thickness of the surface coating is 1.2 nm. Depending on the availability of nanotubes on the mica, between 28-83 such bundle heights measurements were taken for each sample scanned with AFM in the non-contact mode to arrive at an average dimension representing bundle diameter.
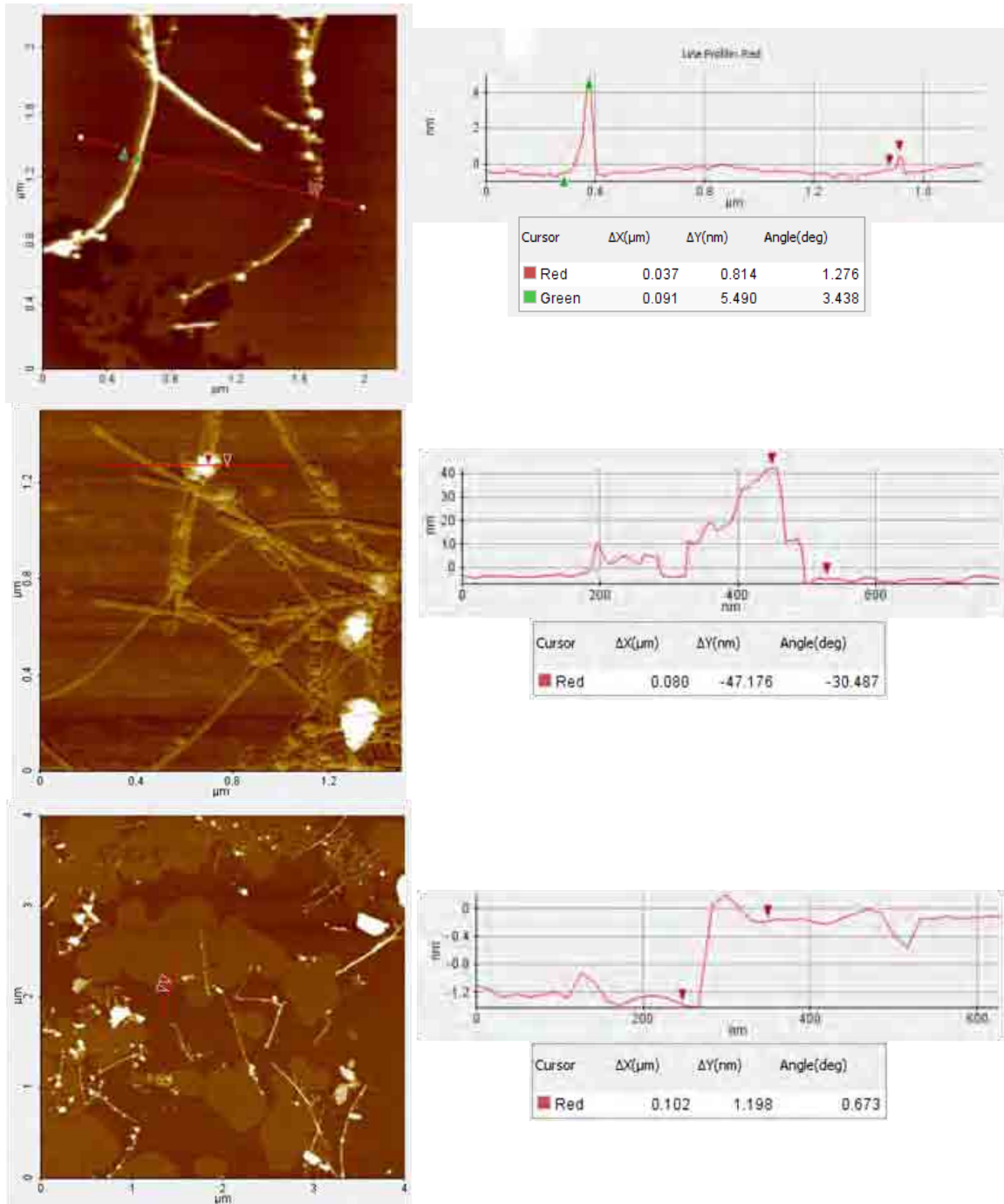
Figure 7.6. AFM height measurements with XEI software for bundle height, particle height and thickness of surface coating.

The results including standard deviation and count number are presented in Table 7.1.

		average height in nm	*standard deviation in nm*	*count*
1	**SWCNT + Na⁺, pH 6.5**	6.8	3.4	80.0
2	**SWCNT + Ca²⁺, pH 6.5**	9.0	4.0	83.0
3	**SWCNT + SRHA + Na⁺, pH 3**	6.2	2.7	83.0
4	**SWCNT + SRHA + Na⁺, pH 6.5**	7.9	6.9	36.0
5	**SWCNT + SRHA + Na⁺, pH 10**	5.6	2.6	28.0
6	**SWCNT + SRHA + Ca²⁺, pH 6.5**	10.1	4.2	70.0
7	**SWCNT + NW, pH 6.5**	6.9	3.6	81.0

Table 7.1. Average nanotube bundle AFM heights (non-contact mode).

Statistical calculations

Results presented in table 7.1 were also further analysed with SPSS software with one sample Kolmogorov-Smirnov test (with α=0.05) to assess the normality of the data distributions. Two samples did not show a normal distribution (SWCNT + SRHA + Na⁺ at pH 3 and 6.5). To determine which samples show statistical difference a Mann-Whitney U test at α=0.05 has been performed with SPSS software (Table 7.2).

column no	1	2	3	4	5	6	7
1		✓	✗	✗	✗	✓	✗
2	✓		✓	✓	✓	✗	✓
3	✗	✓		✗	✗	✓	✗
4	✗	✓	✗		✗	✓	✗
5	✗	✓	✗	✗		✓	✗
6	✓	✗	✓	✓	✓		✓
7	✗	✓	✗	✗	✗	✓	

Table 7.2. Statistical calculations for average bundle AFM height (α=0.05): ✓ - difference, ✗ - no difference, column numbers correspond with Table 7.1.

Additionally, since the availability of nanotubes on the mica was limited (especially for two samples: SWCNT + SRHA + Na⁺, pH 6.5 (36 measurements) and SWCNT + SRHA + Na⁺, pH 10 (28 measurements)), the minimum sample size, n_{min}, was determined with the equation [Zar, 1999]:

$$n_{min} = \frac{s^2 \cdot t^2_{\alpha(2),(n-1)}}{d_\pm^2} \qquad (7.1)$$

where:

s^2 – estimate of the population variance (calculated as a variance of the available height measurements)

$t_{\alpha(2),(n-1)}$ - two-tailed critical value of Student's t with n-1 degrees of freedom

$d_\pm$ - half-width of the confidence interval i.e. the mean bundle thickness is to be estimated to within ± d ($d_\pm$ was assumed at 1 nm, i.e. the confidence interval of 2 nm).

Results for a confidence level of 95 % are summarised in Table 7.3.

sample	n_{min}	count
SWCNT + Na$^+$, pH 6.5	47	80
SWCNT + Ca^{2+}, pH 6.5	63	83
SWCNT + SRHA + Na$^+$, pH 3	29	83
SWCNT + SRHA + Na$^+$, pH 6.5	*181*	*36*
SWCNT + SRHA + Na$^+$, pH 10	*29*	*28*
SWCNT + SRHA + Ca^{2+}, pH 6.5	69	70
SWCNT + NW, pH 6.5	53	81

Table 7.3. Minimum sample size v number of AFM height measurements for nanotube bundle AFM heights (α = 0.05)

For two samples, in the presence of Na$^+$ and SRHA at pH 6.5 and 10, the calculated average bundle height is not statistically reliable due to the minimum sample size being larger than the number of measurements taken. Especially, the sample with Na$^+$ and SRHA at pH 6.5 has a n_{min} five times higher than the obtained number of AFM heights (count), which is a result of a high variance for this sample (standard deviation is 87 % of the result; see Table 7.1).

The lowest average bundle height of 5.6 nm was found in the sample with Na$^+$ and SRHA at pH 10, surprisingly even lower compared to the sample without humic

acid (6.8 nm). As has been mentioned above, however, finding nanotubes on mica for the latter sample was troublesome, which is shown by the lowest number of measurements taken and statistical calculations of n_{min}, which suggest that the average bundle height for this sample is not statistically representative.

Consistent with visual observations (Fig. 5.2) the biggest bundle diameters were calculated for the sample with Ca^{2+} (9 nm), especially in the presence of SRHA (10.1 nm), although there is no statistical difference between the average bundle heights for these two samples (Table 7.2). Similarly in case of the samples with Na^+ at pH 6.5, the average bundle height in the presence of SRHA is higher (6.7 nm v 7.9 nm) but the difference cannot be confirmed with statistical calculations (Table 7.2). The average bundle height (and its standard deviation) in the presence of the lake water is very similar to the average bundle height in the presence of Na^+ (6.9 nm v 6.8 nm) (Table 7.1).

The only sample not showing any statistical difference in the majority of cases (with the exception of when compared to SWCNT in the presence of Ca^{2+} at pH 6.5) is SWCNT with Na^+ and SRHA at pH 6.5 (Table 7.2). It should be noted, however, that with a very high standard deviation (and sample variance) the measurements taken for this sample are not sufficient to represent it with a reasonable confidence level (Table 7.3). Even if the n_{min} slightly higher than count for the sample with humic acid and Na^+ at pH 10 is neglected, the influence of pH with two extreme values (3 and 10) cannot be confirmed. Although at lower pH the average bundle height is higher, there is no statistical difference between low and high pH values.

For all samples the standard deviation was high, even up to 87% of the average bundle height. Apart from different morphologies in different samples (e.g. coating with

humic acid), such a big range in measurements can be attributed to a different number of single nanotubes in a bundle, which results from the production method [Journet et al., 1997].

7.5   Comparison of TEM average bundle thickness and AFM average bundle height measurements

As has been discussed in one of the previous sections (7.3)**,** AFM and TEM are two complementary techniques to image SWCNTs in the aqueous suspensions. The observed morphologies were remarkably consistent although the imaging mechanisms for both microscopy techniques are essentially different.

For both techniques samples have been characterised quantitatively by bundle diameters represented by the average bundle thickness in the case of TEM (table 5.2) and average bundle height in the case of AFM (table 7.1). All the results are gathered in one table for convenience and can be compared in Table 7.4.

		AFM	TEM
SWCNT + Na+, pH 6.5	**average height/thickness in nm**	**6.8**	**9.9**
	standard deviation in nm	3.4	4.6
	count	*80.0*	*125*
SWCNT + Ca2+, pH 6.5	**average height/thickness in nm**	**9.0**	**9.7**
	standard deviation in nm	4.0	3.1
	count	*83.0*	*152*
SWCNT + SRHA + Na+, pH 3	**average height/thickness in nm**	**6.2**	**16.1**
	standard deviation in nm	2.7	4.7
	count	*83.0*	*123*
SWCNT + SRHA + Na+, pH 6.5	**average height/thickness in nm**	**7.9**	**13.1**
	standard deviation in nm	6.9	5.7
	count	*36.0*	*164*
SWCNT + SRHA + Na+, pH 10	**average height/thickness in nm**	**5.6**	**21.1**
	standard deviation in nm	2.6	6
	count	*28.0*	*90*
SWCNT + SRHA + Ca2+, pH 6.5	**average height/thickness in nm**	**10.1**	**14.3**
	standard deviation in nm	4.2	4.3
	count	*70.0*	*101*
SWCNT + NW, pH 6.5	**average height/thickness in nm**	**6.9**	**9**
	standard deviation in nm	3.6	3.5
	count	*81.0*	*96*

Table 7.4. Comparison of the average SWCNT bundle thicknesses measured with TEM and average SWCNT bundle heights measured with AFM.

In general, there is good agreement (within a few nm) between TEM and AFM measurements. In all cases TEM thicknesses exceed AFM heights. The most remarkable discrepancy was found for the sample with Na^+ and humic acid at pH 10 (by a factor of 3.8). The best agreement between techniques was recorded for SWCNT in the presence of Ca^{2+} at pH 6.5. TEM thickness is a lateral dimension and can be overestimated due to flattening of particles, which takes place during adsorption to the TEM grid and air-drying and was reported for humic acid aggregates [Balnois et al., 1999; Lead et al., 2005]. This phenomenon was discussed at the beginning of the previous section (7.4).

On the other hand, searching unevenly covered sample is much easier and quicker in case of TEM and consequently in all samples considerably more nanotubes were found in the TEM microscopy specimens. Fewer measurements in case of AFM produce results less reliable statistically, i.e. less credible and representative.

Generally speaking, qualitative results obtained with TEM and AFM are in good agreement and complementary. Qualitative results, however, show remarkable discrepancies between different samples in average nanotube dimensions as well as general trends of them.

7.6   **Tapping v non-contact mode**

In this study, all samples listed in chapter 7.2 were scanned in both tapping and non-contact modes. Theoretical differences between the two modes are discussed in section 3.2.1. The obtained morphologies showed no apparent differences. To quantify the comparison, heights of the same nanotubes were measured in both modes. Figure 7.7 illustrates the comparison procedure.
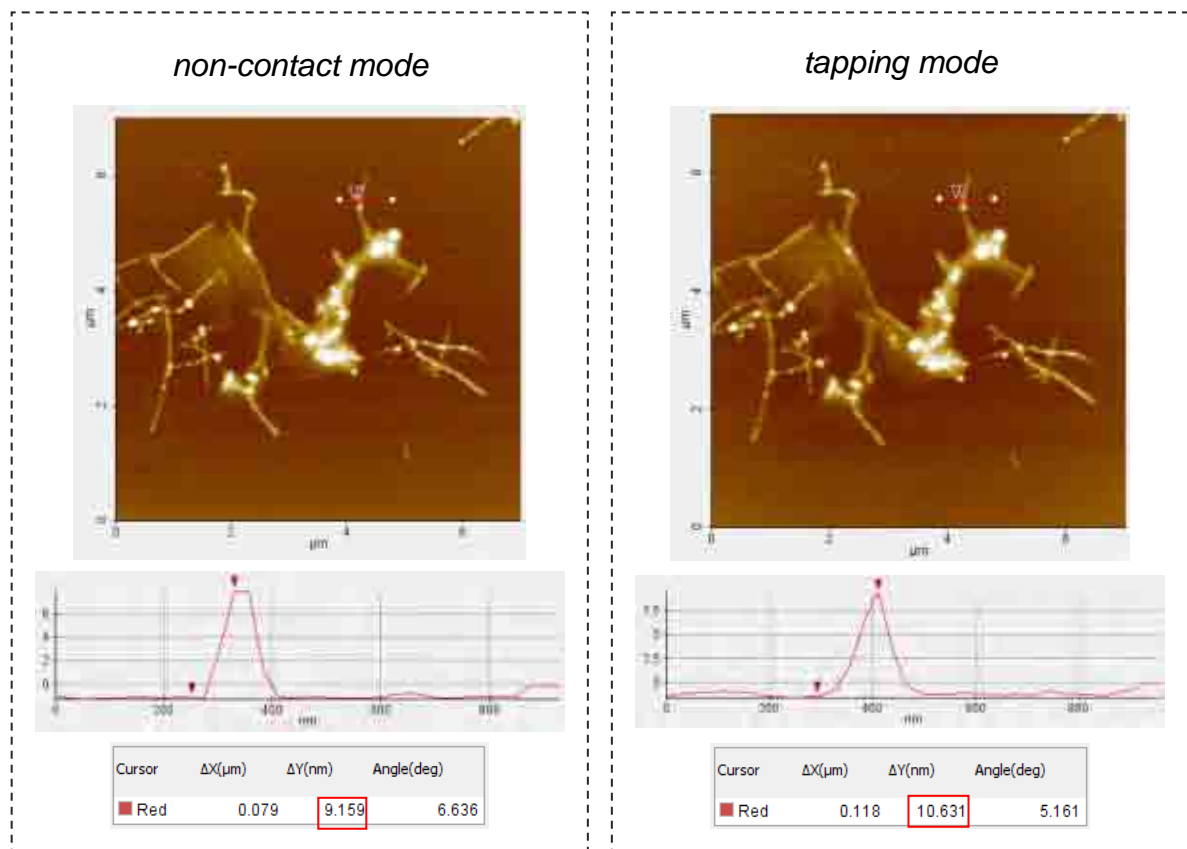
Figure 7.7. AFM height measurements in non-contact and tapping modes.

A selected nanotube was measured in the same place in the non-contact and the tapping modes. In the former case it was 9.2 nm high, in the latter 10.6 nm high – in the non-contact mode the height was 8.2% smaller. The same procedure was repeated 100 times for different randomly selected nanotube bundles in different samples. It is conceivable

that the tapping contact between the sample and the tip in the dynamic force mode could modify the sample surface so 100 comparison measurements were taken under two scenarios: (a) when the sample was scanned in the tapping mode first and (b) when the sample was scanned in the non-contact mode first (Table 7.5). The statistical test did not show a difference between the measurements in both cases. (since one out of four datasets did not show a normal distribution as tested with the one sample Kolmogorov-Smirnov method, Mann-Whitney U test at $\alpha=0.05$ with SPSS software was used).

	tapping first (a)			non-contact first (b)	
	non-contact (a)	tapping (b)		non-contact (a)	tapping (b)
number of comparisons	100			100	
average AFM height	*8.8*	*9.6*		10.6	10.3
a v b statistically	no difference			no difference	
a v b on average	+ 7.2 %			- 1.0 %	

Table 7.5. Comparison of non-contact v tapping mode measurements (when sample scanned in the tapping mode first or non-contact mode first).

Nevertheless, when the sample was first analysed in the tapping mode, the tapping mode bundle height was on average 7.2 % bigger than in the non-contact mode (Table 7.2). When the non-contact mode was applied first, the tapping bundle height was on average 1 % smaller than in the non-contact one. This result suggests that the tapping interaction between the tip and the sample modifies slightly the surface of studied NPs. A similar reduction in the particle size scanned in the tapping mode was reported for antibody molecules [San Paulo and Garcia, 2000]. Particles were measured in the attractive regime (non-contact mode), scanned in the repulsive regime (tapping mode) and then re-measured in the attractive regime. The average size reduction by a factor of

1.8 was calculated implying some sort of sample damage. It has been reported previously that the forces exerted on a sample in the tapping mode are comparable to those in the contact mode [Spatz et al., 1995] with the main advantage of the tapping mode being the elimination of shear forces.

8 RESULTS: METAL SPECIATION IN AQUEOUS SUSPENSIONS OF SINGLE-WALLED CARBON NANOTUBES

8.1 Summary

This chapter presents metal speciation results for aqueous suspensions of SWCNTs. The experiments involved analysing three sets of SWCNTs samples at a pH range ~ 4-9: in the presence of Na$^+$, in the presence of Na$^+$ and SRHA and in the presence of Ca^{2+}.

Experimental techniques used in this chapter (DGT and ICP-MS) have been introduced previously (chapter 3.2.3 and 3.2.4). Chapter 8.2 explains the experimental design, which included total metal concentrations, metal concentrations in filtrates and ultrafiltrates and Diffusive Gradients in Thin-films (DGT) measurements. The aim of this work was to determine which fractions of the total amount of metal are bound to aggregates with sizes bigger and smaller than 1.2 μm as well as dissolved and labile metal fractions and how the presence of Na$^+$, Ca^{2+} and SRHA influences this partitioning.

A selection of five metals was included in the experiments: Ni, Y, Cr, Cu and Cd. Of these, Y and Ni are inherently present in the SWCNT powder used in the experiments. Metallic catalysts are commonly used in production of commercially available carbon nanotubes, which is discussed in chapter 8.3. The remaining metals (Cr, Cu and Cd) were spiked into the suspension.

The next four sections (8.4 – 8.7) present and discuss the results.

8.2   Experimental design

Metal speciation in aqueous suspensions of SWCNTs was determined by measuring 4 different metal concentrations in the same sample (Fig. 8.1):

1. Total metal concentration in the sample

2. Metal concentration in the 1.2 μm filtrate (mixed cellulose esters membrane, Millipore, nominal pore size 1.2 μm)

3. Metal concentration in 1 kDa ultrafiltrate (regenerated cellulose membrane, Millipore, nominal pore size 1 kDa NMWL)

4. DGT metal concentration in the sample (i.e. labile metal concentration).
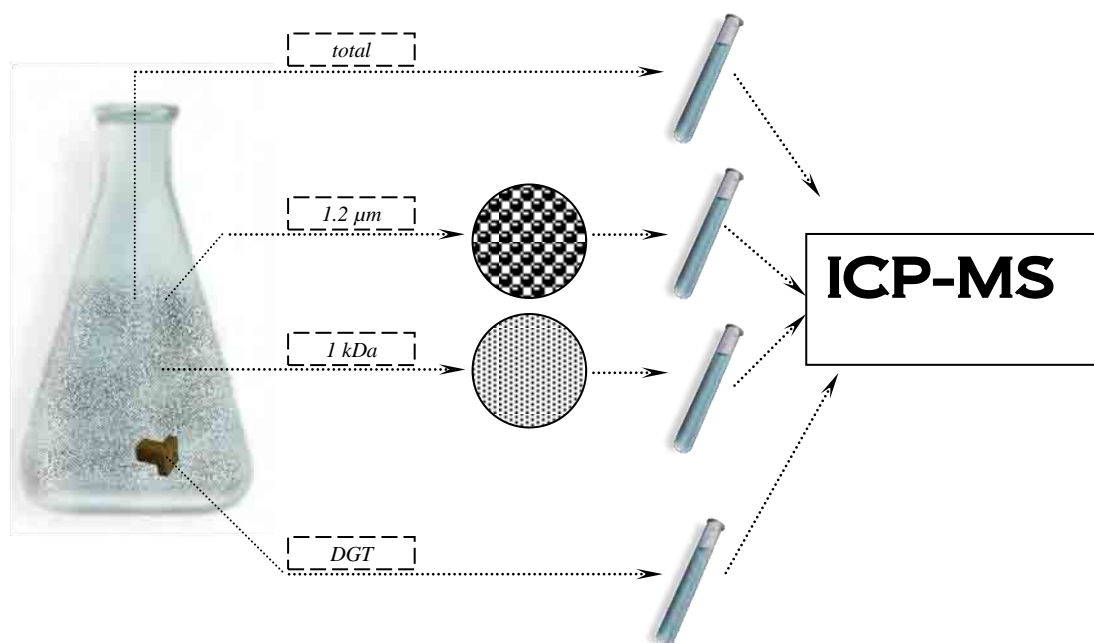
Figure 8.1. Schematic representation of the experimental design for metal speciation in aqueous suspensions of SWCNTs.

All laboratory glassware, utensils and instruments having any contact with samples were stored in an acid bath and thoroughly rinsed with ultrapure water prior to the experiments.

Due to time constraints, a selection of 3 sets of samples (out of 9 from previously analysed with TEM, chapter 5.2) were made. 500 mL test samples including:

1. SWCNT (10 ppm) with Na$^+$ (13 ppm, the same as in NW used)

2. SWCNT (10 ppm) with Na$^+$ (13 ppm) and SRHA (10 ppm)

3. SWCNT (10 ppm) with Ca^{2+} (45 ppm, the same as in NW used)

were prepared from stock solutions, for which the preparation protocol is explained in chapter 3.1. All three sets of samples were analysed in a pH range of about 4-9 (5 different pH values for each set of samples). The pH was adjusted with small amounts of 1M TraceSELECT® HNO$_3$ and 1M NaOH (stored with chelex resin granules to remove any trace metals present in sodium hydroxide pellets). The pH was monitored and readjusted for 3-4 days until reasonable stability was achieved ($\pm$ 0.3 over 24 h). Samples with stable pH were filtered and analysed according to the protocol explained in Fig. 8.1. Before ICP-MS measurements, samples were acidified with TraceSELECT® HNO$_3$ to pH ca. 2.

Binding (chelex impregnated) gel and open pore diffusive gel (to allow detection of organic and inorganic metal species) used for DGT measurements were supplied by DGT Research Ltd. As instructed by the supplier, the binding gel was refrigerated and stored in ultrapure water and diffusive gel with a thickness of 8 mm was stored at room temperature in 0.01M NaNO$_3$. A filter paper 0.14 mm thick with nominal pore size of 0.45 µm made of hydrophilic polyethersulfone (PALL, Gelman Laboratory) was cut to the right size with ceramic blade scissors (to minimise contact with metals), washed in

10% HNO$_3$ for 24 h and then repeatedly rinsed in ultrapure water prior to use. All laboratory glassware and utensils used to assemble and deploy DGT devices (plastic tweezers, trays, vials and gel cutters) were stored in an acid bath and thoroughly rinsed with ultrapure water. Before deployment the assembled DGT devices (3 per sample) were soaked for 1h in 0.01M NaNO$_3$ (the solution was purified from any trace metals present in sodium nitrate salt by adding chelex granules). The assembly of the DGT devices took place in a Class-100 laminar flow cabinet to avoid contamination.

To ensure complete immersion, the μ-DGT devices were weighed down by adding a plastic screw and 5 nuts to each device. During the deployment time of 6 hours, the samples were shaken at 140 rpm and maintained at a constant temperature of 20 °C. At the end of the experiment, the binding gel was removed from the devices and eluted in high purity nitric acid solution. Metal content accumulated on the gel discs was determined with inductively coupled plasma mass spectrometry, ICP-MS (Thermo Elemental, X7). To compensate for the amount of metal that stays on the chelex layer, an elution factor of 0.8 was used for calculations.

8.3 Choice of metals to be analysed. Metal impurities in commercially available carbon nanotubes

According to the manufacturer's specifications, SWCNTs used throughout the experimental work (acid functionalized, 80-90% pure purchased from Sigma Aldrich) are contaminated with catalyst residue of nickel and yttrium. To verify this, metal content in acid washed (in 1M HNO$_3$) aqueous suspension was measured with ICP-MS. This confirmed that in 10 ppm solution of SWCNTs, Ni and Y are present in concentrations of ~20 ppb and 10 ppb respectively (i.e. SWCNT powder is contaminated with 0.2 % of Ni and 0.1 % of Y) (Table 8.1). These two metals inherently present in SWCNT powder were to be analysed in all samples outlined in chapter 8.2. The list of metals of interest was expanded to include copper, chromium and cadmium, which were spiked into aqueous suspensions in the form of 1000 ppm standard solution (purchased form Fisher Scientific) to obtain the concentration of 50 ppb for each of added metals.

To analyse and compare metal contamination in manufactured CNTs, six other types of commercially available products were analysed for the five chosen metals (Ni, Y, Cu, Cr and Cd). The complete list of CNT powders analysed with ICP-MS includes:

A. SWCNT (Sigma Aldrich), carboxylic acid functionalized, bundle diam. × length at 4-5 nm × 0.5-1.5 µm (with the average diameter of individual nanotubes 1.4 ± 0.1 nm)

B. Short SWCNT (Sigma Aldrich), 90 % pure, diam. × length at 1-2 nm × 0.5-2 µm

C. MWCNT (Sigma Aldrich), > 95 % pure, outer diam. × internal diam. × length at 7-15 nm × 3-6 nm × 0.5-200 µm

D. SWCNT (Elicarb), high purity

E. MWCNT (Elicarb), high purity

F. SWCNT (Cheap Tubes), > 90% purity, outer diam. × length at 1-2 nm × 5-30 µm

G. MWCNT (Cheap Tubes), > 95% purity, outer diam. × length at < 8 nm × 10-30 µm

The results are summarised in table 8.1. Nickel is the most common contaminant and it was found in 4 products. Metals used for spiking the samples (Cr, Cu and Cd) were not found in any of the nanotube powders.

type of NT	CONCENTRATION (%)				
	Cr	Ni	Cu	Y	Cd
A	< LOD	0.21	< LOD	0.10	< LOD
B	< LOD	< LOD	< LOD	< LOD	< LOD
C	< LOD	0.21	< LOD	< LOD	< LOD
D	< LOD	< LOD	< LOD	< LOD	< LOD
E	< LOD	0.20	< LOD	< LOD	< LOD
F	< LOD	< LOD	< LOD	< LOD	< LOD
G	< LOD	0.22	< LOD	< LOD	< LOD

Table 8.1. Metal impurities in commercially available carbon nanotubes powders (LOD – limit of detection, i.e. 0.1 ppb for Y and Cd and 0.2 ppb for Cr, Ni and Cu).

8.4   SWCNT in the presence of Na$^+$

Fig. 8.2 presents absolute and relative (to the total concentration) nickel and yttrium concentrations in a pH range ~4-9 in 10 ppm SWCNT aqueous suspension in the presence of Na$^+$ (conc. 13 ppm, the same as in the natural lake water used in experiments described in chapters 5, 6 & 7).

The total concentration of Ni, ca. 20 ppb is reduced to 8-15 ppb (40-70%) after filtration through a 1.2 μm membrane. The largest loss occurs at pH 4.8, which means that the biggest fraction of nickel (59 %) was bound to aggregates with sizes over 1.2 μm. The possible explanation is that Ni is more labile or present as smaller complexes

Figure 8.2. Nickel and yttrium speciation in aqueous suspensions of SWCNTs in the presence of sodium cations in a pH range ~ 4-9 (in ppb and related to the total concentration) (dashed line used for contaminated samples).

(e.g. inorganic dissolved complexes). Ultrafiltration was used to remove all NPs and to represent the dissolved metal fraction by metal content in the ultrafiltrate. As expected, more nickel is dissolved in low pH, which can be explained by increased competition between Ni ions and H$^+$ on nanotube carboxylate binding sites. At pH 3.8 the concentration of nickel in the ultrafiltrate reaches 61 % of the total. At pH 4.8 the amount of Ni that passes through the ultrafilter is considerably smaller (33 %) and for the rest of the pH range it is constant at around 20%. In other words, CNTs act as an effective sorbent towards Ni, especially at neutral and alkaline pH and this property has been previously reported [Lu and Liu, 2006; Duran et al., 2009]. DGT results for this set of samples cannot be interpreted since there is strong evidence for major contamination (i.e. concentrations bigger or close to total nickel concentration). DGT measured Ni is unrealistically high (84-174 % of the total) and in all cases significantly higher than dissolved metal in the 1 kDa filtrate.

The second catalytic contaminant in CNT powder, yttrium shows distinctively different behaviour (Fig. 8.2). Total concentration of yttrium is 8-10 ppb. Ultrafiltration and DGT results imply that no yttrium is dissolved or chemically labile (concentrations of Y in these samples are below the limit of detection for the ICP-MS, which is 0.1 ppb). All yttrium mass is distributed between particles with sizes below and above 1.2 μm. At lower pH values (3.8 and 4.8) 55-56% of yttrium is bound to the < 1.2 μm size fraction, presumably either strongly associated with the CNTs or present as oxides. This proportion increases to 85% at pH 6.1 and stabilises at around 77% for the remaining pH values (8 and 9.2).

Chromium was mostly bound to the smaller size fraction, i.e. < 1.2 μm, which has higher specific surface area and thus more binding sites (Fig. 8.3). Only 0-8% is

retained by the 1.2 μm membrane. In fact, the ultrafiltration results suggest that little chromium is absorbed effectively to SWCNTs. The amount of metal that passes through the 1 kDa ultrafilter is also high with 75-99 % of the total chromium passing through the membrane. For both filters the highest concentration of chromium in the filtrate is found at pH 6.1 (no particle-bound chromium). In all analysed pH values, 32-34 % of the total amount of chromium in the samples is detected by DGT. It is considerably less than dissolved chromium in the ultrafiltrate. Possibly the deployment time of 6 h is too short for some of the dissolved metal (about 40-65 %) to diffuse through the DGT gel layer.

More efficient metal sorption to SWCNTs was recorded in case of copper. A similar trend for 1.2 μm filtration as in case of Ni and Y can be observed. 58 and 55 % of the metal is found in the 1.2 μm filtrate at pH 3.8 and 4.8 respectively. For the remaining three samples (pH 6.1, 8 and 9.2) this amount stabilises at 79-83 %. The highest dissolved copper concentration (i.e. in the 1 kDa filtrate) occurs in the lowest pH of 3.8 and equals 19 ppb (36 % of the total). At pH 4.8, 1kDa filtrate contains 9 ppb (18 % of the total) and for the remaining pH values it is 6-7 ppb (11-13 % of the total). Less efficient sorption of Cu onto SWCNTs in acidic conditions can be explained by the presence of H^+ ions, which compete with the metal ions for negatively charged sorptive sites on the surface of nanotubes. DGT measurements for this set of samples are contaminated and cannot be interpreted. Considerable amounts of seemingly DGT available Cu cannot be explained, especially since concentrations of dissolved Cu are low at the same time.

Figure 8.3. Chromium, copper and cadmium speciation in aqueous suspensions of SWCNTs in the presence of sodium cations in a pH range ~ 4-9 (in ppb and related to the total concentration) (dashed line used for contaminated samples).

Similar fractions of Cd are recorded for 1.2μm and 1 kDa filtrates at the lowest pH of 3.8 (68 and 65 % respectively). This result implies that very little Cd is bound to

179

the smaller SWCNTs fraction in acidic conditions. By calculating the mass balance, only 32 % of the total cadmium can be allocated to the particle-bound fraction, and the majority to largest CNTs aggregates. These results suggest that particle-bound cadmium is trapped inside nanotube aggregates, rather than adsorbed onto the surface of NPs. At pH 3.8 65 % of the total cadmium passes through the 1 kDa filter, which again can be explained by competition of H$^+$ with metal ions. Similarly to copper and yttrium, the higher amounts of cadmium pass through the 1.2 μm filter at higher pH values (neutral and alkaline). For the dissolved cadmium concentration, there is a similar but more profound trend as for copper and nickel: the higher pH, the higher sorption efficiency of CNTs towards cadmium (up to 89 %), which can be explained by reduced competition from H$^+$ and stronger electrostatic attraction between metal cations and a more negatively charged SWCNT surface. Considerable amounts of cadmium were measured with DGT in all analysed samples in the presence of Na$^+$. There is a consistent, approximately linear dependency: the higher the pH, the more metal is bound on the chelex resin (56-82 % of the total concentration). Higher labile (DGT) than dissolved (1 kDa filtrate) Cd concentrations suggest that some nanotubes with adsorbed cadmium diffused through the gel pores.

8.5   SWCNT in the presence of Na⁺ and SRHA

Fig. 8.4 presents nickel and yttrium speciation in aqueous suspension of SWCNTs (10 ppm) in a set of samples at a pH range of ~ 4-9 in the presence of Na⁺ (13 ppm) and SRHA (10 ppm).
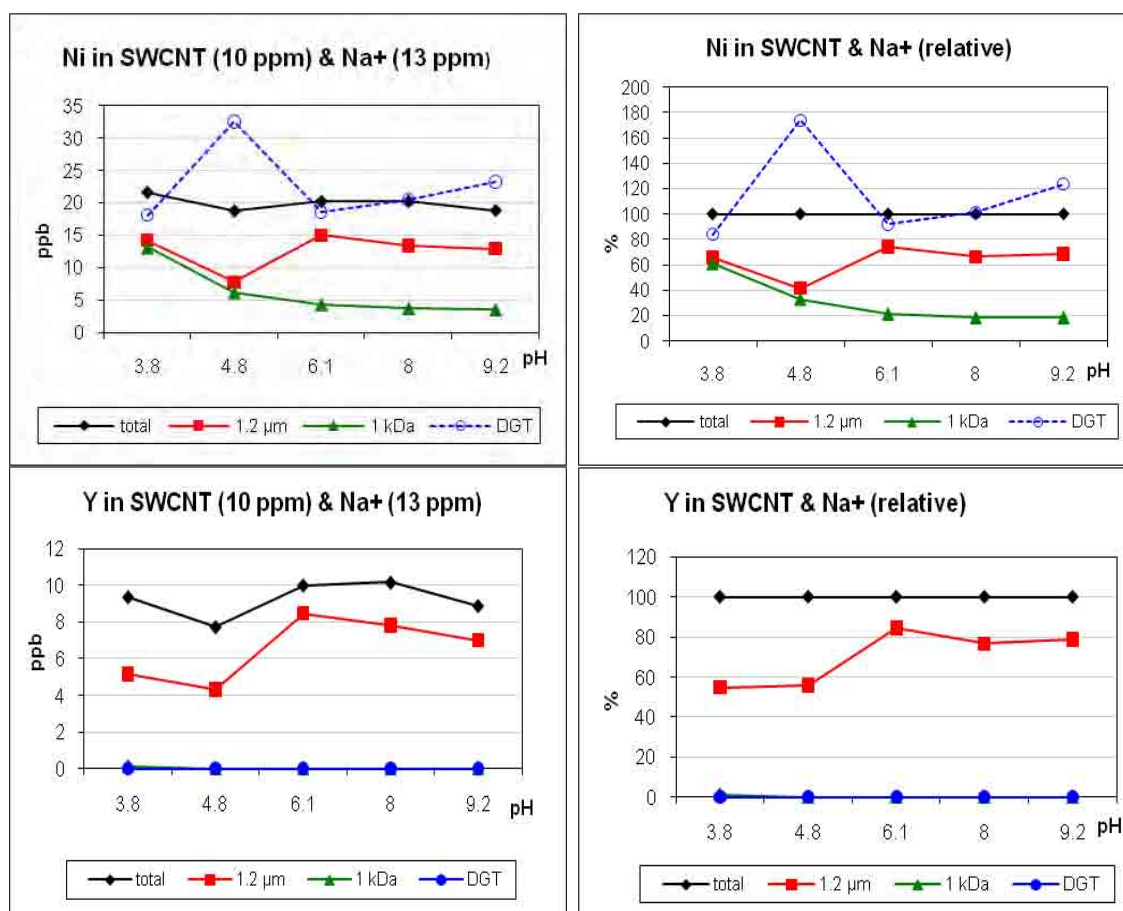

Figure 8.4. Nickel and yttrium speciation in aqueous suspensions of SWCNTs in the presence of sodium cations and humic acid in a pH range ~ 4-9 (in ppb and related to the total concentration) (dashed line used for contaminated samples).

Nickel measurements for these samples are similar to those in the absence of humic acid (Fig. 8.2). At lower pH less nickel passes through a 1.2 µm filter (64 % at pH 3.8, 48% at pH 4.9 and 57% at pH 5.9). At higher pH values, 6.8 and 8.8, this

amounts to 74 % and 78 % respectively. Ultrafiltration results suggest that $45 - 100$ % of nickel is bound to particulate matter. However, the presence of humic acid increased particle bound metal concentration. This can be explained by the sorptive properties of aquatic organic matter, which are well documented in the literature [Martin and Dai, 1995; Lead et al., 1999; Tipping et al., 2002; Koukal et al., 2003]. The amount of nickel in the 1 kDa filtrate is inversely proportional to the pH value. With figures bigger than total nickel concentrations, DGT measurements for this set of samples are contaminated and cannot be interpreted.

In the presence of humic acid, yttrium concentrations in the 1.2 μm filtrate versus pH show a roughly linear relationship: the higher the pH, the more yttrium is found in the fraction with aggregates smaller than 1.2 μm (Fig. 8.4). The proportion of yttrium found in this size fraction amounts to 44 % at the lowest pH and decreases to 88 % at the highest pH value. The presence of humic acid decreased the amount of Y bound to the < 1.2 μm fraction at low pH values and increased it in alkaline conditions. It can be explained by better sorption of metals by humic acid particles at higher pH values [Pourret et al., 2007]. Ultrafiltration and DGT results are the same as in the absence of humic acid: yttrium concentrations in all these samples are below the limit of detection, which suggests there is no dissolved or labile yttrium.

The presence of humic acid did not significantly change chromium speciation in aqueous suspensions of SWCNTs. Again, most of the metal occurs in the <1.2 μm size fraction: at lower pH less than at higher pH (79 % at pH 3.8, around 100 % in other samples). Ultrafiltration results imply that at more alkaline pH than ~ 6 almost all chromium is dissolved. In acidic conditions the 1 kDa filtrate contains considerably less chromium (51 % of the total Cr concentration at pH 4.9 and 15 % at pH 3.8). These

results are in line with the previously reported high efficiency of Cr sorption from aqueous solutions of CNTs at low pH values with no absorption taking place for pH values > 6 [Hu et al., 2009]. The sorption mechanism is metal complexation (rather than ion exchange). Dissolved chromium occurs in negatively charged ion groups (such as $HCrO_4^-$, $Cr_2O_7^{2-}$ and as CrO_4^{2-}), which are easier adsorbed to SWCNTs surface – COOH groups protonated to $C_xOH_2^+$ at acidic pH [Hu et al., 2009]. This effect is additionally intensified by the presence of HA, which also absorbs Cr much more efficiently at low pH [Li et al., 2008D]. DGT chromium concentration peaks at neutral pH (30 and 33 % of the total chromium at pH 5.9 and 6.8 respectively). The lowest DGT chromium concentration was measured at the lowest pH (8% of the total). For neutral and alkaline pH values the DGT deployment time is insufficient for the majority of dissolved metal measured in the 1 kDa filtrate to dissociate during diffusion through the gel layer.

In the presence of humic acid, more copper is found in the < 1.2 μm size fraction (Fig. 8.3 and 8.5), which can be attributed to the increase in sorption efficiency by added humic material. Similarly, in all analysed pH values, the amount of dissolved copper (which passes through a 1 kDa membrane) is lower than in the sample without humic acid. In other words, humic acid particles increase the amount of copper bound by particulate matter in the sample. The highest concentration of dissolved copper was found at the lowest pH (28 %). At all other pH values, only up to 5 % of the total copper is found in the ultrafiltrate. Very high figures for DGT measurements undermine their credibility suggesting sample contamination with external copper sources.
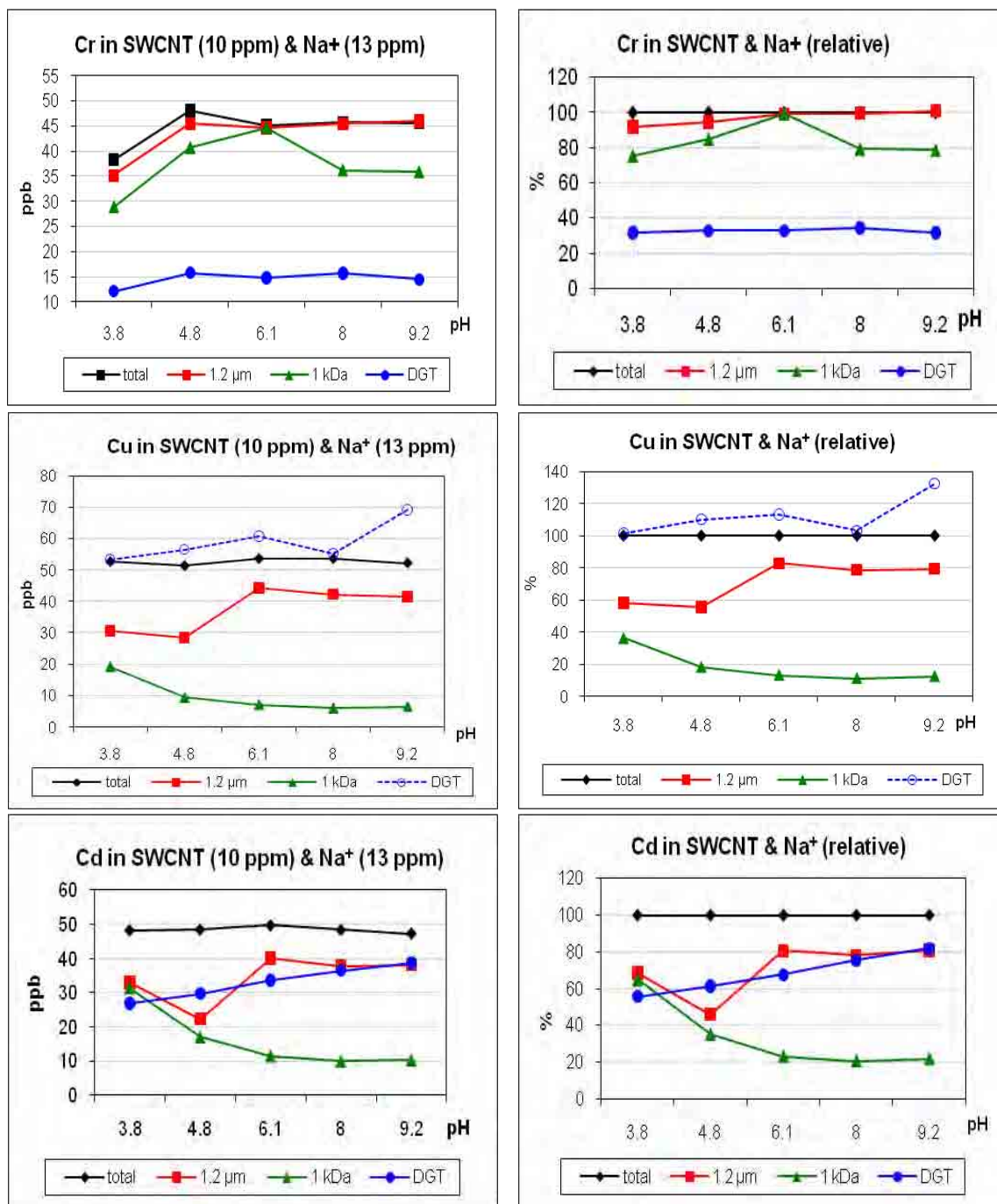
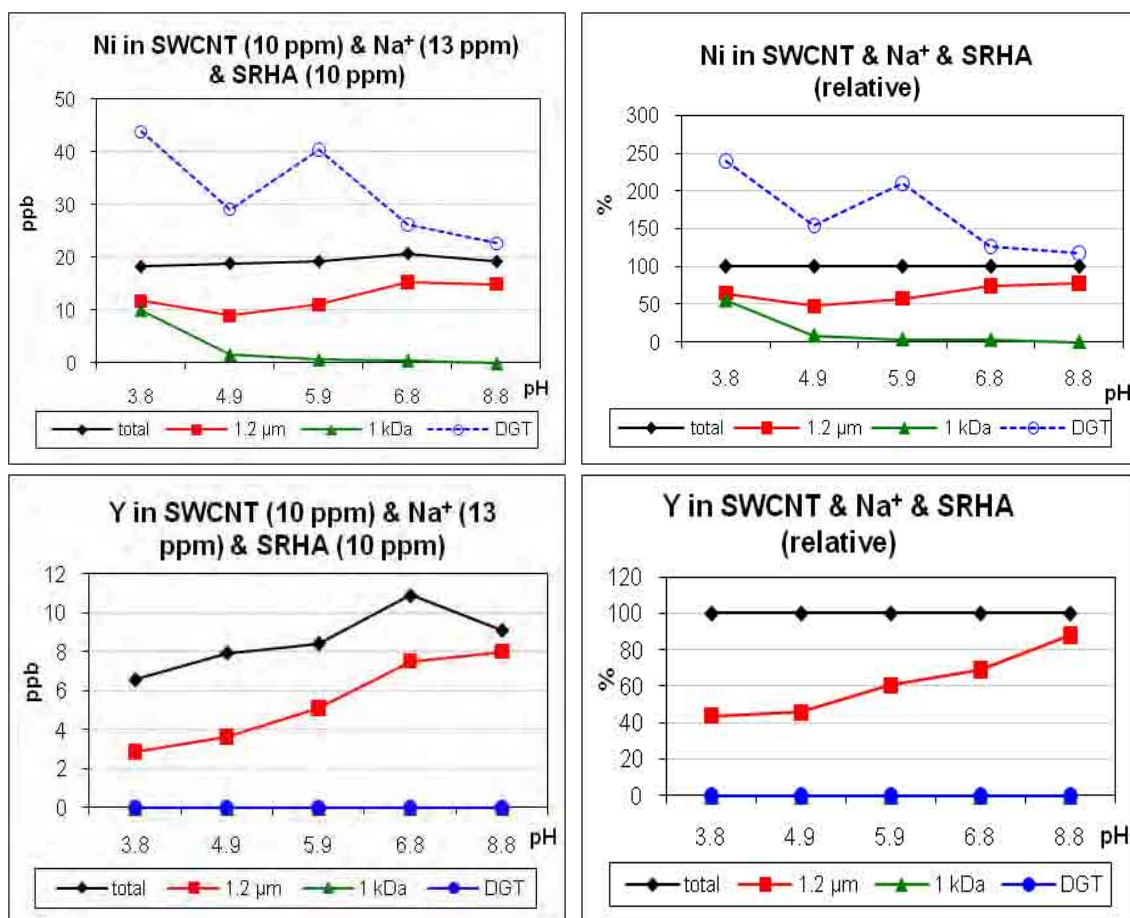Figure 8.5. Chromium, copper and cadmium speciation in aqueous suspensions of SWCNTs in the presence of sodium cations and humic acid in a pH range ~ 4-9 (in ppb and related to the total concentration) (dashed line used for contaminated samples).

Concentrations of cadmium in the 1.2 μm filtrate are similar in the presence and absence of humic acid (Fig. 8.3 and 8.5). At the lowest pH, i.e. 3.8, 66 % of the total

cadmium is found in the 1.2 µm filtrate in the sample with humic acid (68% without SRHA). Also in both sets of samples, the lowest fraction of Cd in the 1.2 µm filtrate was found at pH ~ 5 (40 % in the sample with humic acid, 46 % in the sample without HA). For the three remaining samples (pH 5.9, 6.8 and 8.8), the concentration of Cd passing through the 1.2 µm increases: 60 %, 72 % and 88 % respectively, which also compares well with the results in the absence of humic acid (around 80% for all three samples). However, in case of dissolved cadmium measured in the 1 kDa ultrafiltrate samples only at the lowest pH (~4) there is satisfactory agreement regardless of the presence or absence of humic acid (66% with SRHA, 65 % without SRHA). For all the remaining four pH values, the presence of humic acid considerably reduces the amount of dissolved cadmium (from 22-35 % in the samples with no HA to 0-8 % in the presence of SRHA). Samples analysed by the DGT technique cannot be interpreted due to unrealistic results (close to or over 100 % of the total cadmium concentration).

8.6   SWCNT in the presence of Ca^{2+}

It has been explained in previous chapters (5 and 7) that the presence of divalent cations (like Ca^{2+}) causes significant aggregation and precipitation of SWCNTs in aquatic environments. No other isolated aquatic colloid or cation studied in this thesis (SRHA, PHA, succinoglycan or sodium cations) was found to alter the behaviour of SWCNTs suspended in aqueous media to the same degree. Also speciation of the five analysed metals (Ni, Y, Cr, Cu and Cd) appears significantly different from the two previously presented sets of samples (chapters 8.4 and 8.5).

Figure 8.6. Nickel and yttrium speciation in aqueous suspensions of SWCNTs in the presence of calcium cations in a pH range ~ 4-9 (in ppb and related to the total concentration) (dashed line used for contaminated samples).

Filtration through a 1.2 μm pore size membrane produced high concentrations of nickel in all analysed pH (Fig. 8.6). At the lowest pH (3.8) the sample was contaminated and produced an unrealistic recovery of over 200 %. It is also questionable whether the very high result for the sample at pH 4.8 (16 ppb, i.e. 87 %) is reliable or whether it is also contaminated. At pH 6.4, 60% of the total nickel was measured in the 1.2 μm filtrate; at pH 7.8 and 9, 51 % and 41 % respectively, i.e. at higher pH less nickel passes through the filter. It can be explained by higher SWCNT aggregates retention on the membrane resulting from considerable flocculation of NPs in the presence of Ca^{2+} and a competitive role of Ca^{2+} towards binding sites [Wang et al., 1997]. At the same time, ultrafiltration results would suggest that the amount of particles passing through the 1.2 μm membrane is comparable (i.e. very small) with the amount of particles in the ultrafiltrate since nickel concentrations are very similar between filtrates and ultrafiltrates. The amount of dissolved Ni is significantly higher than in the previous two sets of samples, which suggest that in the presence of Ca^{2+}, absorption of Ni onto the SWCNTs is considerably decreased (possibly due to decreased surface area of aggregated CNTs and competition with calcium cations). DGT measurements found 66-72% of the total nickel in samples at pH 3.8, 4.8 and 6.4. The remaining two samples (pH 7.8 and 9) with DGT concentrations of about 100 % of the total Ni concentration seem to be contaminated, especially since all previous Ni samples analysed with DGT showed strong evidence of contamination (Fig. 8.2 and 8.4). However, the high percentage of dissolved Ni at pH < 7 can be confirmed by high labile (DGT) metal concentrations.

In case of yttrium samples filtered through a 1.2 μm membrane, results are similar to those in the presence of Na^+ and Na^+ & SRHA only at the lowest pH of 3.8

(56% of the total Y concentration was measured in this filtrate) (Fig. 8.6). At all the remaining analysed pH values, the amount of yttrium passing through a 1.2 μm filter is considerably smaller in the presence of Ca^{2+} (0 – 4 % of the total). Ultrafiltration results for all three sets of samples (with Na^+, with Na^+ and SRHA, with Ca^{2+}) are similar and very little yttrium is found in the 1 kDa filtrate (up to 5% in the presence of Ca^{2+}). However, the DGT results significantly differ in the presence of Ca^{2+} than in the two previous sets of samples, where no yttrium was detected. Here, consistently in all analysed pH values, 18 - 22 % of the total yttrium concentration is DGT available.

Chromium concentrations found in the 1.2 μm filtrates in the presence of Ca^{2+} (Fig. 8.7) are similar to those in the presence of Na^+ and SRHA (Fig. 8.5). At lower pH (3.8 and 4.8) more chromium is retained on the filter (21 % and 14 % respectively). For other pH values (6.4, 7.8 and 9) 95 – 100 % of the total chromium passes though the membrane. Very similar concentration versus pH dependence was plotted for ultrafiltrated samples: 71 % and 80 % of the total chromium was found in the ultrafiltrates at pH 3.8 and 4.8 respectively, and ~ 100% for the remaining pH values (6.4, 7.8 and 9). Filtration and ultrafiltration results suggest that there is little Cr effectively bound to CNTs (especially at higher pH values). DGT measurements revealed ~ 30 % of the total chromium at lower pH. At the highest analysed pH (i.e. 9), the biggest fraction of the total chromium amount was detected by the DGT technique (46 %). Similarly to the previous samples only a fraction of dissolved Cr dissociates in the DGT deployment time.

Filtration and ultrafiltration of the samples in the presence of Ca^{2+} produced very similar concentration versus pH curves for copper (Fig. 8.7). At acidic pH values (3.8 and 4.8) significant amounts of copper pass through a 1.2 μm filter (75 % and 30 % of

the total Cu concentration respectively) and through a 1kDa membrane (69 % and 37 % of the total Cu concentration respectively). Very little copper was measured at pH above 6 for the 1.2 μm filtrates (1 – 3 % of the total concentration). In the case of ultrafiltrates
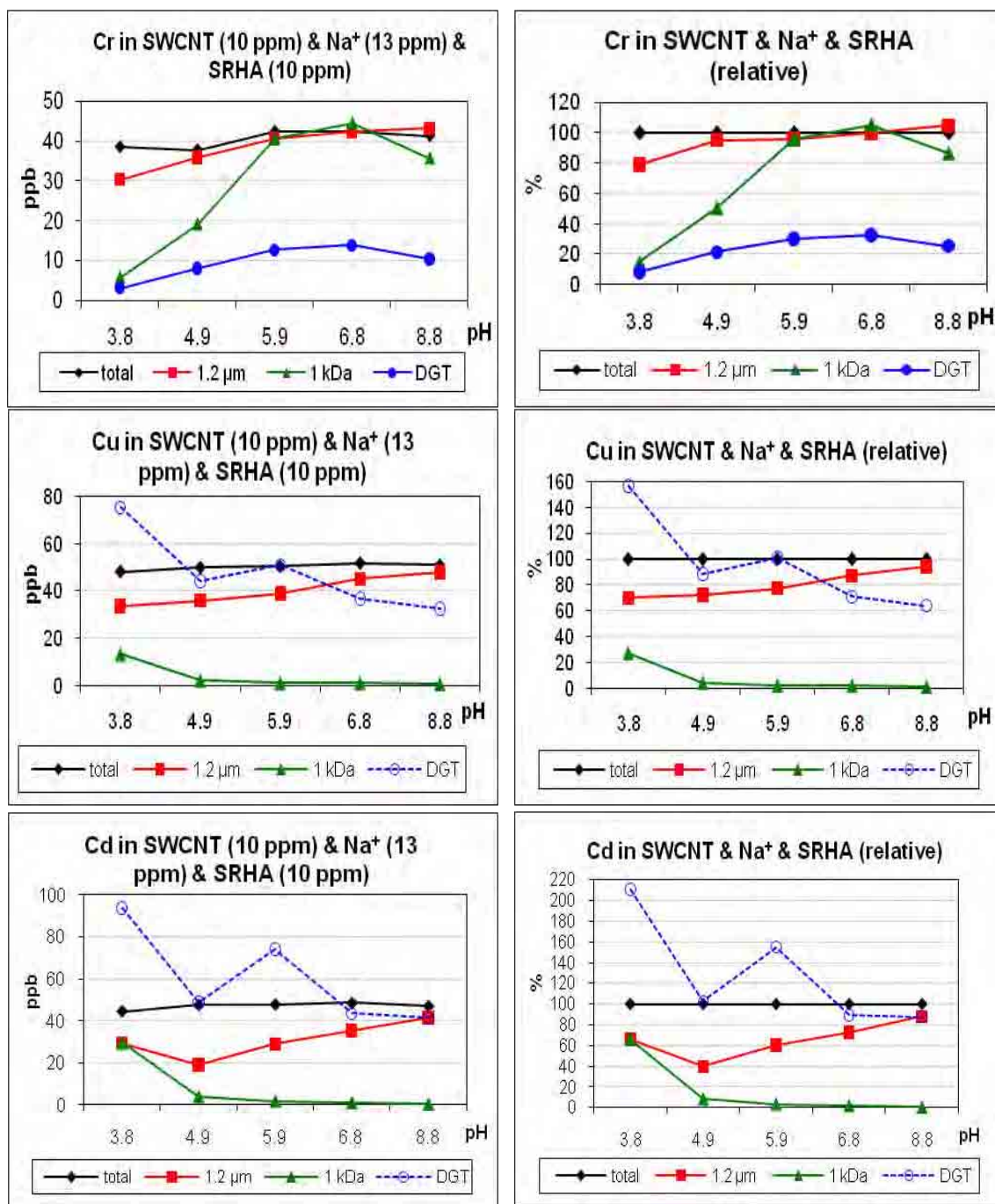

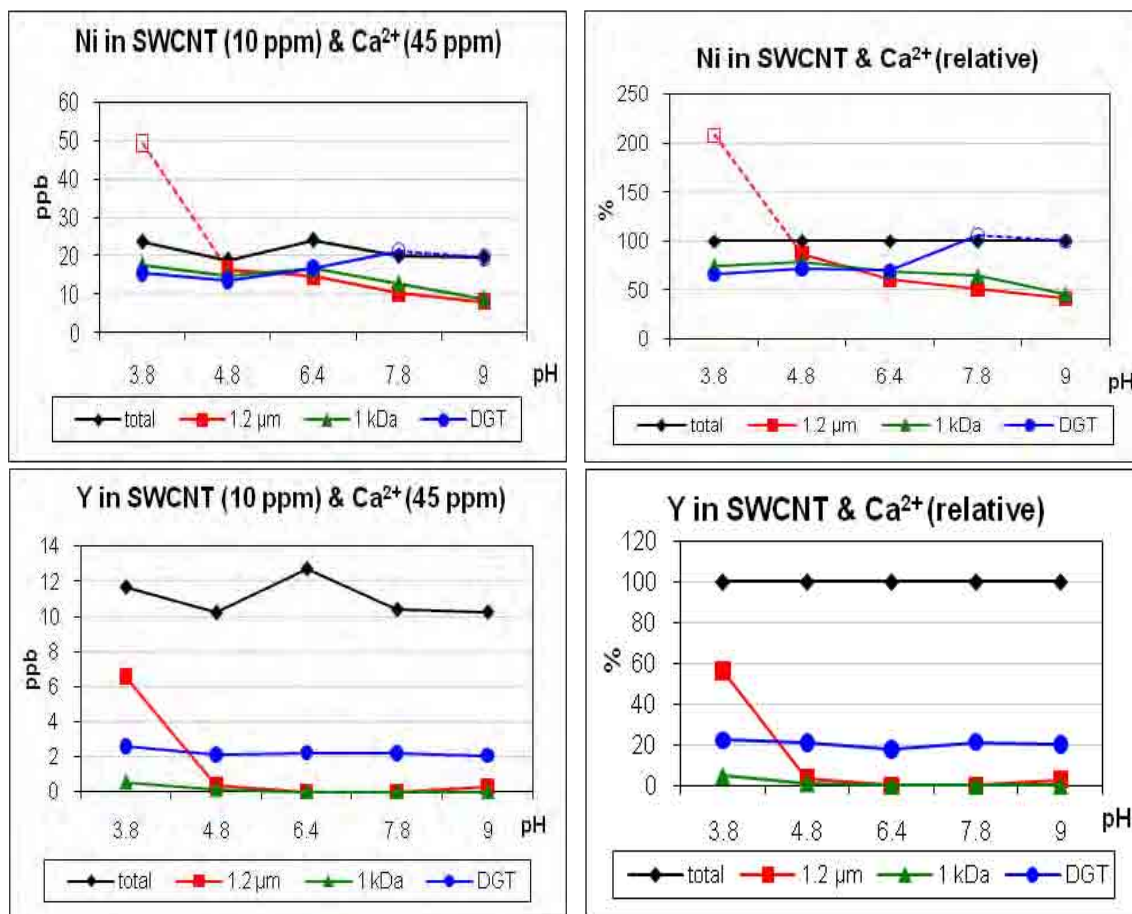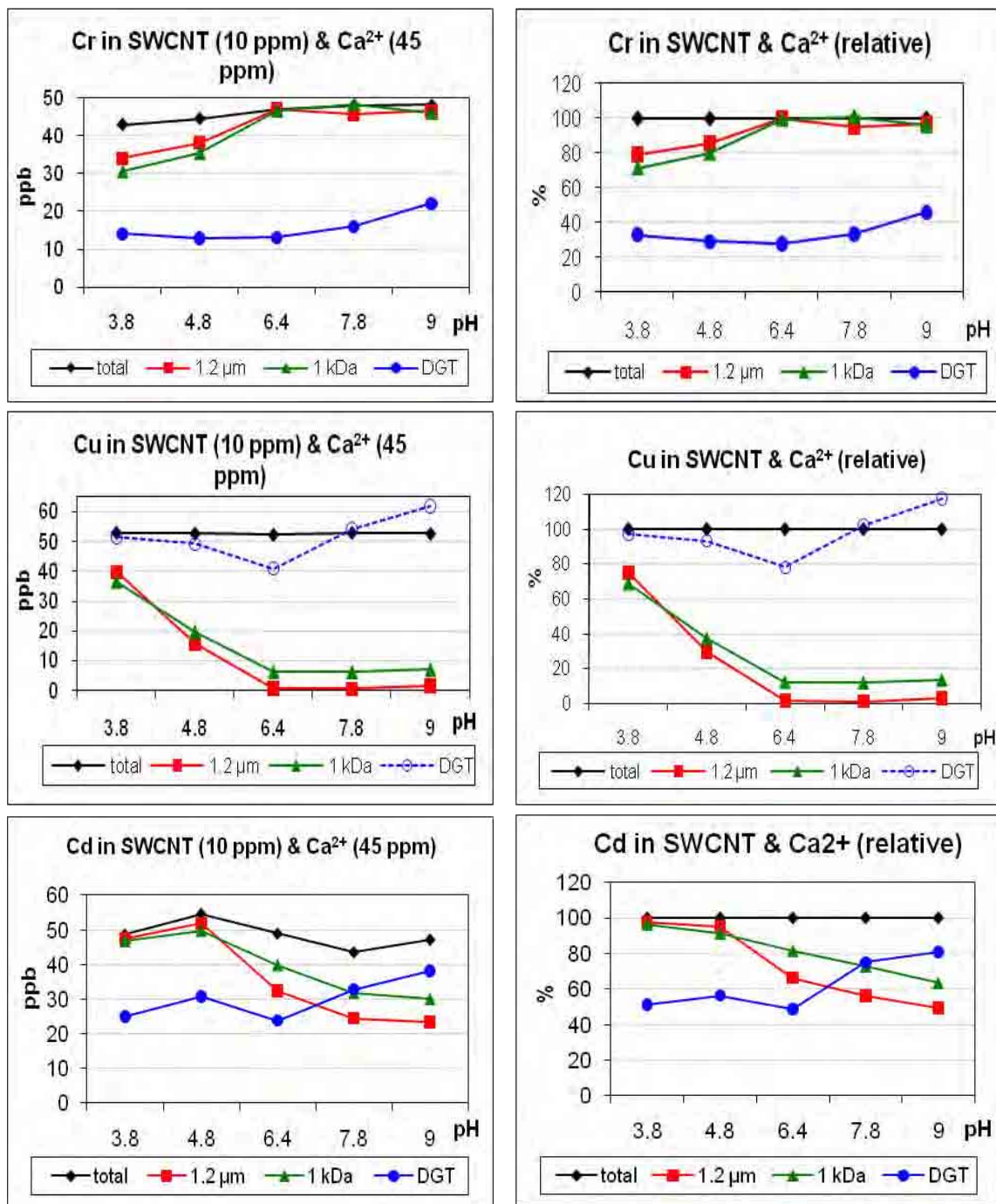Figure 8.7. Chromium, copper and cadmium speciation in aqueous suspensions of SWCNTs in the presence of calcium cations in a pH range ~ 4-9 (in ppb and related to the total concentration) (dashed line used for contaminated samples).

189

at the same pH values (above 6) the copper fraction was found to be $12 - 13$ % of the total concentration. The presence of Ca^{2+} significantly increased the amount of Cu retained on the 1.2 µm filter (due to higher aggregate dimensions). The DGT results, as for previous sets of samples, are implausibly high, which can be regarded as evidence for significant contamination of samples.

The presence of Ca^{2+} significantly alters Cd partitioning between size fractions <1.2 µm and > 1.2 µm (Fig. 8.7). In previous samples the amount of Cd in the 1.2 µm filtrate was higher at alkaline pH values (Fig. 8.3 and 8.5), in this sample, however, the trend is the opposite; at low pH more cadmium passes through the 1.2 µm membrane. Almost all cadmium passes through the 1.2 µm and 1 kDa membranes at pH lower than 5 (Fig. 8.7). At higher pH these values decrease: for the 1.2 µm filtrates to 66 % at pH 6.4, 56 % at pH 7.8, down to 49 % at pH 9 and for the ultrafiltrates to 82 % at pH 6.4, 73 % at pH 7.8, down to 64 % at pH 9. Very similar DGT results were obtained in the presence of Ca^{2+} (Fig. 8.7) and Na^{+} (Fig. 8.3).

8.7   **Summary of the results for the three analysed sets of samples**

In the previous three sections (8.4 − 8.6) metal speciation results were presented for three sets of samples:

1) SWCNT (10 ppm) in the presence of Na$^+$ (13 ppm)

2) SWCNT (10 ppm) in the presence of Na$^+$ (13 ppm) and SRHA (10 ppm)

3) SWCNT (10 ppm) in the presence of Ca^{2+} (45 ppm)

at a pH range 4-9 for two metals, which are carbon nanotubes powder contaminants (Ni and Y) and three metals, which the suspensions were spiked with (Cr, Cu, Cd). Metal concentration was measured to determine the total metal content, the amounts of metals that are bound to particulate matter (< 1.2 μm size fraction), the amounts of dissolved metals (in the 1 kDa ultrafiltrates) and labile (DGT) metal concentrations.

Oxidised CNTs have been known for their excellent sorptive properties towards trace metals and their complexes and are proposed as sorbents in water treatment plants as well as in analytical methods for metal speciation [Lu and Liu, 2006; Rao et al., 2007; Tuzen and Soylak, 2007; Chen et al., 2009; Duran et al., 2009; Pyrzynska, 2010]. The binding mechanisms include two main phenomena: electrostatic attraction between negatively charged oxidised CNT surface and metal cations and chemical complexation of metals by functional groups. In most cases the sorption onto CNTs strongly depends on pH. Where an electrostatic mechanism prevails, sorption efficiency increases with pH. This effect is caused by stronger negative charge on the CNT surface at higher pH and decreased competition between metal cations and H$^+$ (e.g. Ni, Cu, Co, Pb [Lu and Liu, 2006; Chen et al., 2009; Duran et al., 2009]). In a situation when the sorption

mechanism depends on redox reactions (surface complexation), adsorption is significantly more efficient at low pH values (e.g. Ni [Hu et al., 2009]).

In this study, yttrium, which is a residue of the catalyst used to produce SWCNT by the electric-arc technique, shows distinctively different behaviour to that displayed by other analysed metals in all sets of samples, i.e. it is mostly strongly bound to SWCNTs in all studied conditions. It is also possible that yttrium occurs in an oxidised particulate form, which results in high retention on the filters. $46 - 88$ % of the total yttrium passed through the 1.2 µm filter in the presence of SRHA and/or Na$^+$. At the same time no yttrium was found to be dissolved or DGT available, which implies that almost all yttrium in these samples is strongly bound to CNTs. However, in the presence of calcium cations little yttrium was found in the filtrates and ultrafiltrates but a relatively significant proportion of ca. 20 % was detected by DGT.

Although nickel, similarly to yttrium, is the catalyst residue and contaminates the SWCNTs powder, this metal exhibits different and considerably less distinctive behaviour when compared with the metals added to the suspensions. In the sample with Na$^+$ it produces similar results to copper, in the sample with Na$^+$ & SRHA and Ca^{2+} similar to cadmium. Relatively large fractions of nickel are dissolved and DGT available. Fraction of particle-bound nickel increases in the presence of humic acid and by acidic conditions. The presence of Ca^{2+} cations, which compete for binding sites, has the opposite effect (more Ni in the dissolved fraction).

At least 79 % of the total chromium passes through the 1.2 µm filter in all of the samples. In most of the samples well over 50% also passes through the 1 kDa membrane. DGT measurements for chromium are consistent in all samples (ca. 30 % chromium was detected by DGT). Chromium is the only metal analysed in this study,

which is more efficiently absorbed onto SWCNT at lower pH values. This effect is more profound in the presence of HA.

Copper was the only metal that did not produce any credible DGT results. In the presence of SRHA and/or Na$^+$ and at lower pH in the presence of Ca^{2+}, significant amounts of copper were measured in the 1.2 µm filtrates (at least 55 % of the total). The most dissolved copper was found in the presence of Ca^{2+} (especially at acidic pH) and the least at pH > 5 in the presence of Na$^+$ and SRHA.

In most samples less than 50 % of the total cadmium is retained on the 1.2 µm filter. Very little cadmium was found in the ultrafiltrate at pH > 5 in the presence of humic acid. On the other hand, the presence of Ca^{2+} resulted in almost 100 % cadmium recovery in acidic conditions in case of both filtration and ultrafiltration. DGT results suggest that considerable amounts of cadmium are labile, especially at more alkaline conditions.

It should be noted, however, that these are preliminary results and should be confirmed by further experiments. Additionally, trace metal measurements require strict and meticulous protocols to ensure there is no contamination from external sources. There is strong evidence to suggest that many samples in this work were contaminated, especially in case of DGT and copper and nickel. At the time of the experiment the ultrapure water system was faulty and produced water contaminated with copper at 0.29 ppb.

9 RESULTS: CHARACTERISATION OF WATER-STIRRED C$_{60}$ FOR TOXICOGENOMICS FISH EXPOSURE STUDY

9.1 Summary

Water-stirred fullerene C$_{60}$ in concentrations of 0.1 and 0.5 ppm was used in a three-spined stickleback exposure experiment. Liver, brain and gill tissues were analysed by gene expression profiling (chapter 9.7). This work was carried out by Takeshi Kitano, Tim D. Williams, Ioanna Katsiadaki, Matthew B. Sanders and James K. Chipman as part of a collaborative project between Birmingham University, Kumamoto University (Japan) and Cefas Weymouth Laboratory.

Stock suspension of nC$_{60}$ with nominal concentration of 500 ppm was characterised by a number of suitable techniques. To determine size distribution, the solution was filtered through 3 membranes with different pore sizes: 1.2, 0.45 and 0.1 μm. In section 9.3, UV-Vis spectra were used to further quantify and characterise the filtrates, supernatant and stock. Calibration curve was prepared with diluted stock samples. Light absorbance at 280 nm wavelength was measured for all the samples to determine estimated concentrations. After 4 days about 65% of the fullerene mass remains suspended (supernatant concentration was found to be 320 ppm) (chapter 9.4).

TEM imaging was applied to study morphologies of different aggregate size fractions and to calculate size distributions. The results are presented in section 9.5. Using TEM micrographs number concentrations for 0.1 and 0.45 μm filtrates were estimated (chapter 9.6). Quantification of fullerenes in exposure media was inconclusive because of low concentrations.

9.2   Filtration and visual inspection

A protocol involving extended water-stirring was applied to suspend C_{60} in water and this is described in more detail in chapter 3.1.2. The apparently insoluble powder produces dark brown suspension after 65 days of non-stop stirring. Fig. 9.1 shows the suspension of C_{60} at the start (a) and at the end (b) of mixing. However, most of the suspended particles sediment relatively quickly, within hours/days. After about a week the suspension turns orange and becomes very stable (no visual change even after 12-18 months). The stable final product, i.e. supernatant of unknown concentration, is shown in Fig. 9.1 c. Sedimented particles can be easily resuspended by vigorous shaking.
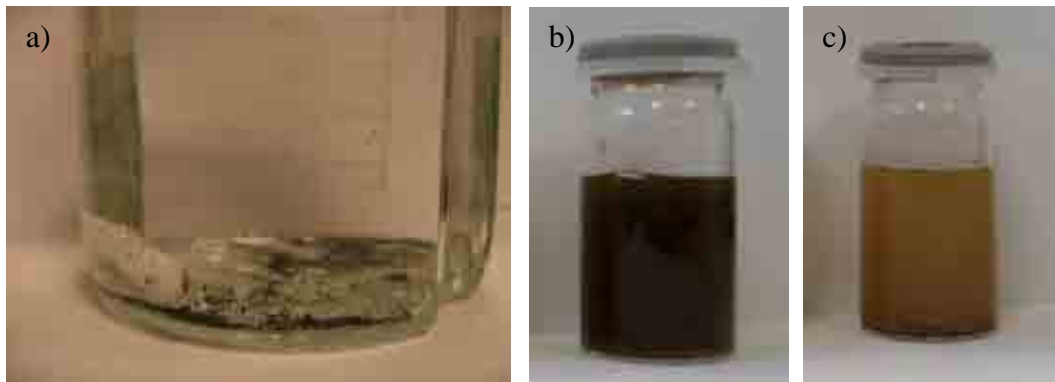
Figure 9.1. Suspension of C_{60} at the start (a) and at the end (b) of 65 day mixing.
Stable final product after a week of quiescent settling (c).

To establish the size range of particles which remain suspended, and thus become available to fish, the stock solution was filtered through a number of different pore size membranes:

- 0.1 μm cellulose nitrate membrane (Whatman)

- 0.45 μm mixed cellulose membrane (Advantec)

- 1.2 μm white RAWP membrane (Millipore).

Photographic images of the stock and filtered samples are shown in Table 9.1. As has been mentioned above, the dark brown, opaque stock solution, sediments within hours/days to produce stable brown-orange supernatant with intensive colouration. It is noticeably more concentrated than 1.2 μm filtrate, which suggests that particles with dimensions > 1.2 μm remain stably suspended. No visible changes can be observed for the opaque orange 1.2 μm filtrate. The bright orange 0.45 μm filtrate is noticeably more transparent. Very few particles pass through a 0.1 μm membrane and the filtrate from the smallest pore size is colourless and transparent.

Dark brown suspensions of nC$_{60}$ produced according to the water-stirred protocol have been previously reported in the literature [Spohn et al., 2009]. In most studies the mixing step is followed by decanting and/or filtration/centrifugation [Lyon et al., 2006; Oberdorster et al., 2006; Hyung and Kim, 2009]. To the best of my knowledge, no study has previously characterised different fractions of water-stirred fullerene C$_{60}$.

Table 9.1. Stock solution and filtrates in time from 0 to 4 weeks.

9.3   UV-Vis measurements

To compare the stock, supernatant and filtrates more qualitatively, UV-Vis measurements were performed on a WPA lightwave UV-VIS Spectrophotometer in the wavelength range of 200-825. The stock solution and the supernatant collected after 4 days settling time had elapsed had to be diluted 5 fold to enable measurement due to their high opacity. The results are shown in Fig. 9.2. Consistent with previous reports [Markovic et al., 2007; Chang and Vikesland, 2009], there are four visible peaks in the spectra for all studied samples: at about 225, 280, 370 and 500 nm wavelength.
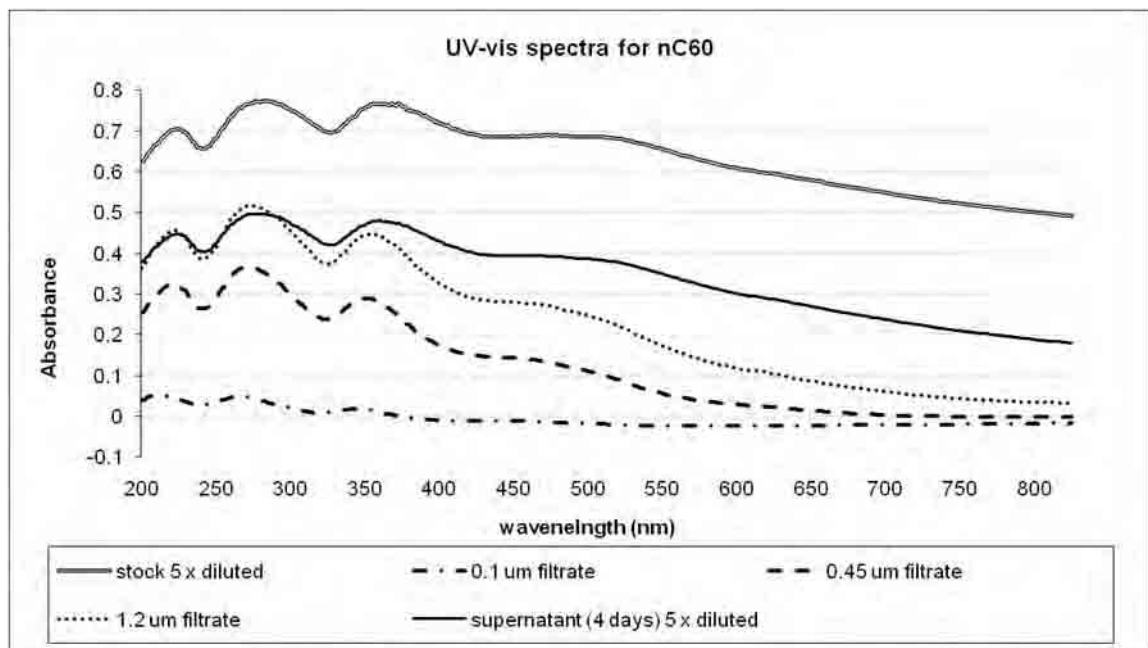
Figure 9.2. UV-Vis absorbance spectra for the stock, its 4 days supernatant and 0.1, 0.45 and 1.2 μm filtrates.

9.4   Concentration of filtrates and supernatant

Although the nominal concentration of the suspension is known (500 ppm), it is important to determine the concentration of particles that remain suspended, i.e. the concentration of nC$_{60}$ that fish are exposed to. To establish approximate concentrations of filtered samples and the supernatant a calibration curve was prepared from samples diluted from stock with the following dilutions based on the nominal concentration:

- 100 x diluted, i.e. 5 ppm,

- 20 x diluted i.e. 25 ppm,

- 10 x diluted i.e. 50 ppm and

- 5 x diluted i.e. 100 ppm

with instrument response to the analyte taken as light absorbance values at the wavelength of 280 nm (the highest peak). Any losses due to sedimentation were minimised by vigorous shaking immediately before the measurement. From the calibration curve and measured absorbance at 280 nm, concentrations of filtered samples and the supernatant were calculated and presented in Table 9.2.

Since the calibration curve was plotted using diluted stock suspension, the calculated concentrations should be treated as approximate. Diluted stock suspensions differ from the sedimented and stable supernatant (and filtrates). Although the total mass of the particles present might be similar, diluted stock have different properties. Visually diluted stock suspensions are always of brown colour with varied intensity depending on the dilution degree and supernatant similarly to filtrates is orange and this fact alone suggests different light absorbance properties. The difference can be explained by a different size distribution of the same C$_{60}$ total mass: diluted stock

suspensions contain a fraction of extremely large (visible to the eye) aggregates, which settle down within minutes or hours; stable supernatant and filtrates contain much smaller particles, which stay suspended for long periods of time.

nom. Conc.	5	25	50	100
absorbance at 280 nm	-0.001	0.162	0.416	0.773
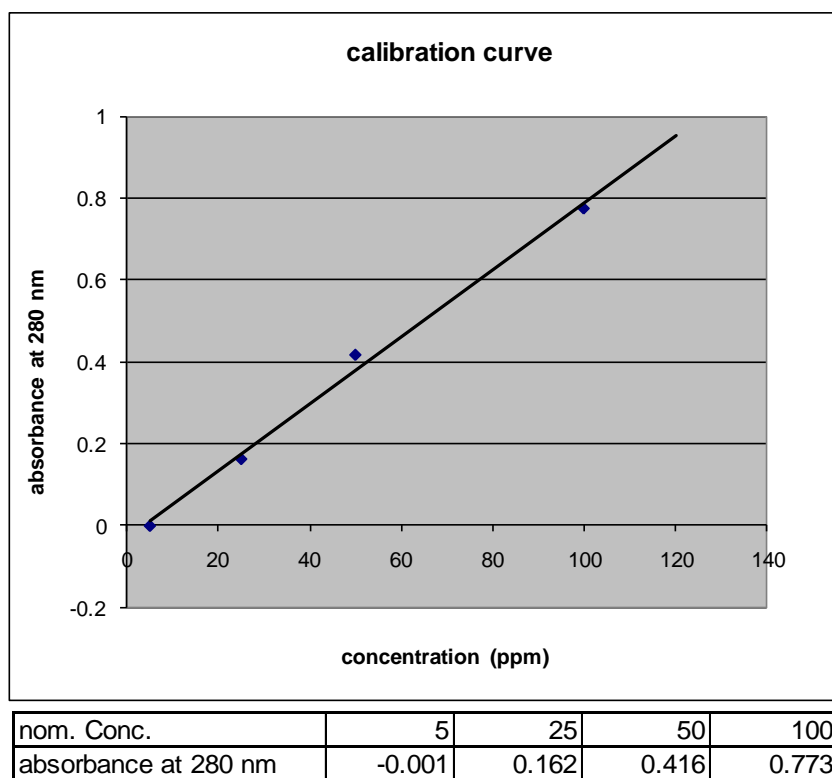
Figure 9.3. Calibration data and plot for concentration calculations.

Consistently with visual observation, only about 2 % of the total mass of suspended C$_{60}$ constitutes the smallest size fraction with diameters of 1- 100 nm (i.e. the nano-fraction) and concentration of these particles is about 9 ppm. Particles with sizes < 0.45 µm and < 1.2 µm are considerably more concentrated, ca. 48 ppm and 64 ppm respectively. Concentrations in the supernatant after a 4-day settling period are estimated from the measurement for the 5 times diluted sample (64.4 ppm, Table 9.2) at 322 ppm, thus after 4 days about 65% of the total mass remains suspended.

Sample	absorbance measured at 280 nm	Concentration read from the calibration curve in ppm
0.1 µm filtrate	0.04	8.9
0.45 µm filtrate	0.358	47.5
1.2 µm filtrate	0.511	66.0
supernatant (4 days) 5 x diluted	0.497	64.4

Table 9.2. UV-Vis absorbance at wavelength of 280 nm and concentration read from the calibration curve for the filtrates and the 4 days supernatant.

9.5   TEM imaging and analysis

Samples were imaged on a FEI Philips TECNAI F20 TEM operating at 200 kV (Fig. 3.8). Microscopic specimens were prepared according to the ultracentrifugation protocol (described in detail in chapter 6.2). 10 mL samples with an optimal dilution (to obtain optimal film coverage) were ultracentrifuged onto a holey carbon film on 400 copper mesh. Analysed samples were:

- 0.1 μm filtrate – no dilution needed

- 0.45 μm filtrate – 5 x diluted

- 1.2 μm filtrate – 10 x diluted

- supernatant (4 days) – 25 x diluted

- stock – 100 x diluted.

A Beckman L7-65 Ultracentrifuge with SW40 swinging bucket rotor was used at the following ultracentrifugation parameters: speed: 30.000 rpm, relative centrifugal field at r$_{av}$: 114.000 x g, temperature: 15° C, time: 60 min.

There are a few reports of water-stirred fullerenes C$_{60}$ imaged with electron microscopy [Brant et al., 2006; Lyon et al., 2006; Labille et al., 2009; Spohn et al., 2009]. They produced a wide size range with the majority of crystalline faceted aggregates with diameters of a few hundreds nm (Fig. 9.4).
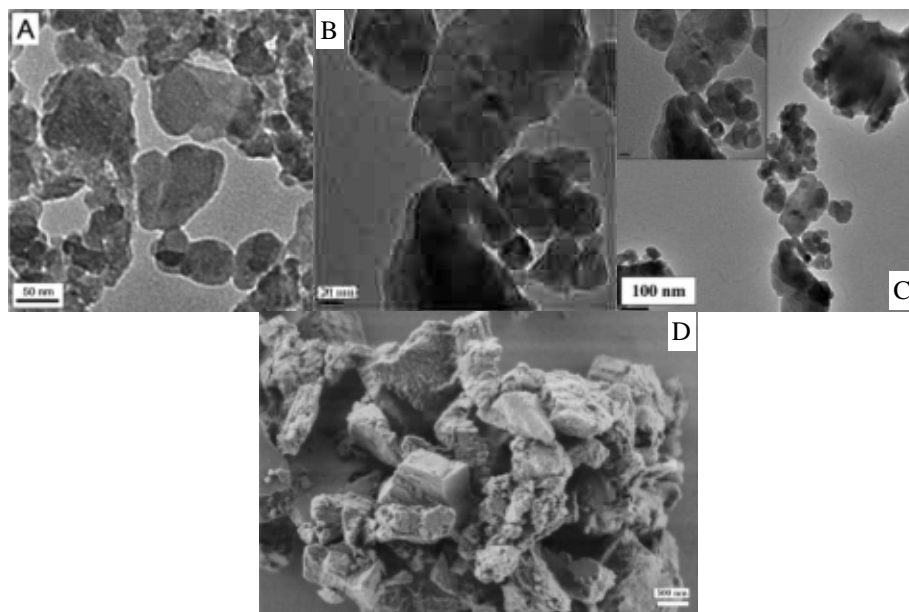
Figure 9.4. Previously reported electron microscopy imaging of water-stirred nC$_{60}$ A. TEM micrograph by Lyon et al., 2006; B. TEM micrograph by Labille et al., 2009; C. TEM micrograph by Brant et al., 2006; D. SEM micrograph by Spohn et al., 2009.

Figure 9.5 shows TEM micrographs of the stock suspension. Consistent with the filtration results (chapter 9.2) and with previous reports [Brant et al., 2006; Spohn, 2009] a wide size range of roughly spherical or cubical nC$_{60}$ aggregates can be observed. Smaller clusters with nanoscale dimension tend to have more oval, smooth edges (Fig. 9.5 c), whereas larger agglomerates show angular, rough-edged morphologies (Fig. 9.5 b). Some of the biggest aggregates occur in the absence of the smaller material (Fig. 9.5 b), some are surrounded with numerous nanoscale clusters (Fig. 9.5 a and d). TEM images where used to calculate particle size distribution based on 370 measurements (Fig. 9.6). The wide size range is confirmed by a high standard deviation, which is 1.6 times higher than the average particle size (369 nm v 605 nm). The smallest particle measured was 12 nm, the biggest over 5.2 µm. About half of the particles by number (50.3 %) have sizes within the nano-size range (i.e. less than 100

nm). This corresponds with the estimated 2 % of the total fullerene mass in the 0.1 μm filtrate (chapter 9.4).
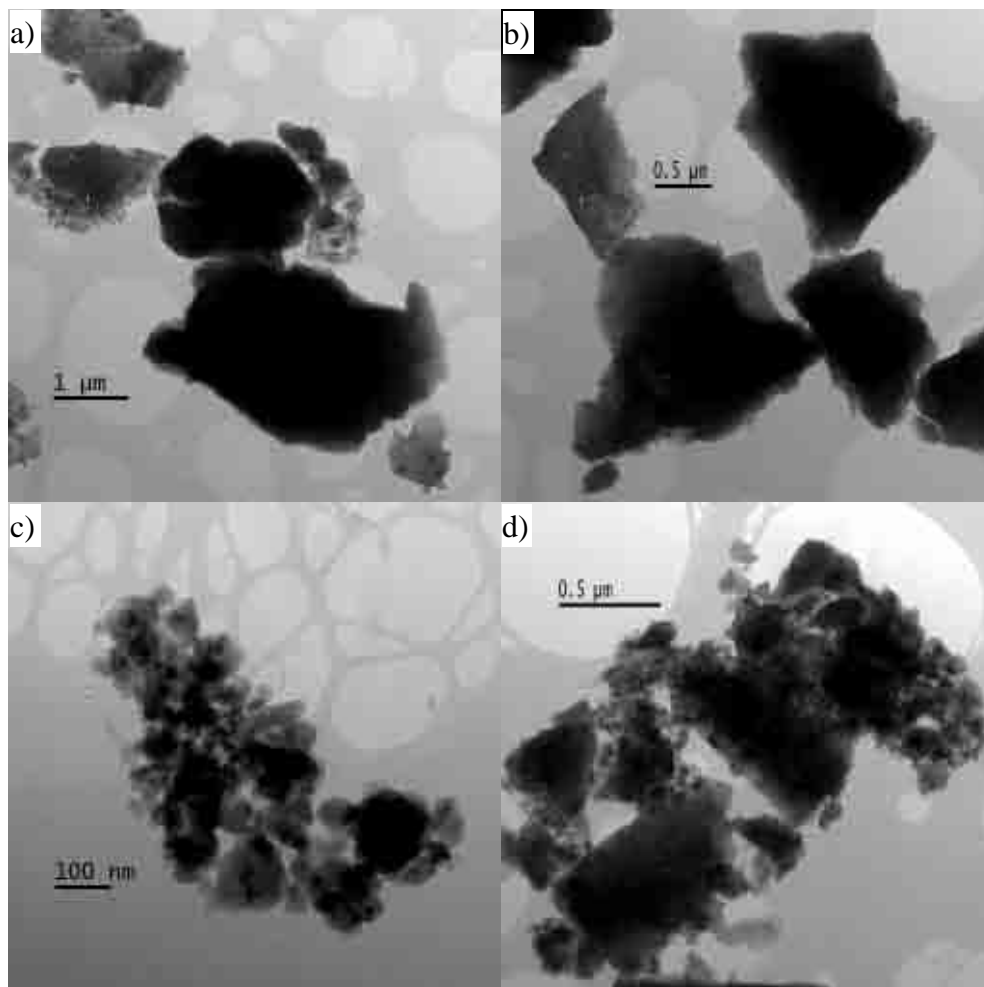
Figure 9.5. TEM micrographs of the nC$_{60}$ stock suspension.

As expected, smaller cluster sizes and narrower size distribution are reported for the supernatant sample (Fig 9.7 and 9.8). Similarly to the stock sample, there are two major types of morphologies: bigger angular microparticles and nanoscale clusters with smoother edges. Again, some of the big clusters are imaged with few nano-clusters around them (Fig. 9.6 a) and some are incorporated in dense aggregates of small particles (Fig. 9.6 b and c) or evenly coated with them (Fig. 9.6 d). A very important
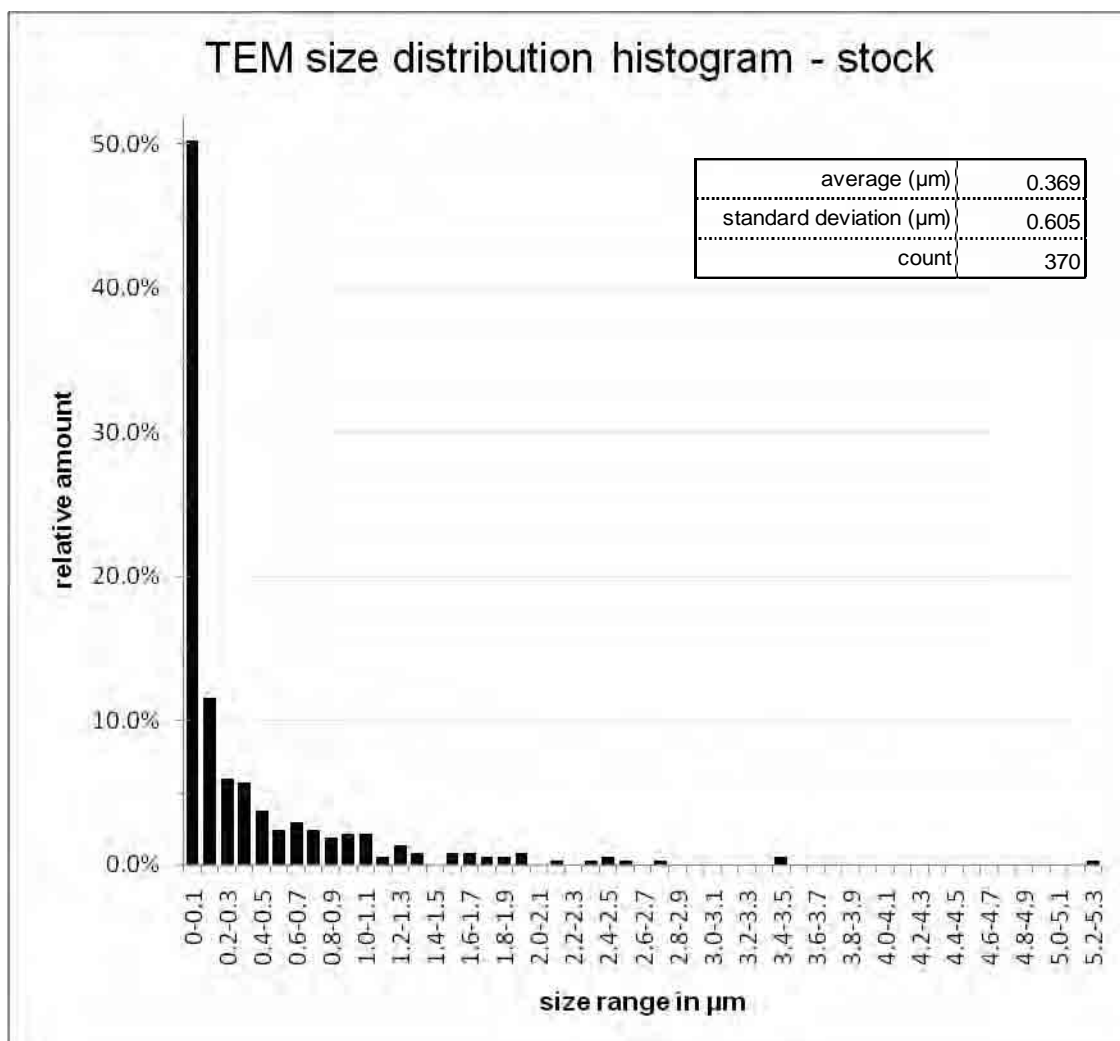
Figure 9.6. TEM size distribution histogram for nC_{60} stock suspension.

morphological characteristic consistent to all TEM images is a flaky (especially noticeable on the edges) and multilayer structure (e.g. Fig. 9.7 b and d). The largest dimensions measured for this sample are up to 1.55 μm. The number of particles increases steeply with decreasing particle sizes for fractions smaller than 250 nm (Fig. 9.8). Particles with dimensions below 100 nm constitute 55.5 %. Average particle size is significantly smaller than in the stock suspension (231 nm v 369 nm). Standard deviation too is lower although still bigger than the average particle size (231 nm v 309 nm).
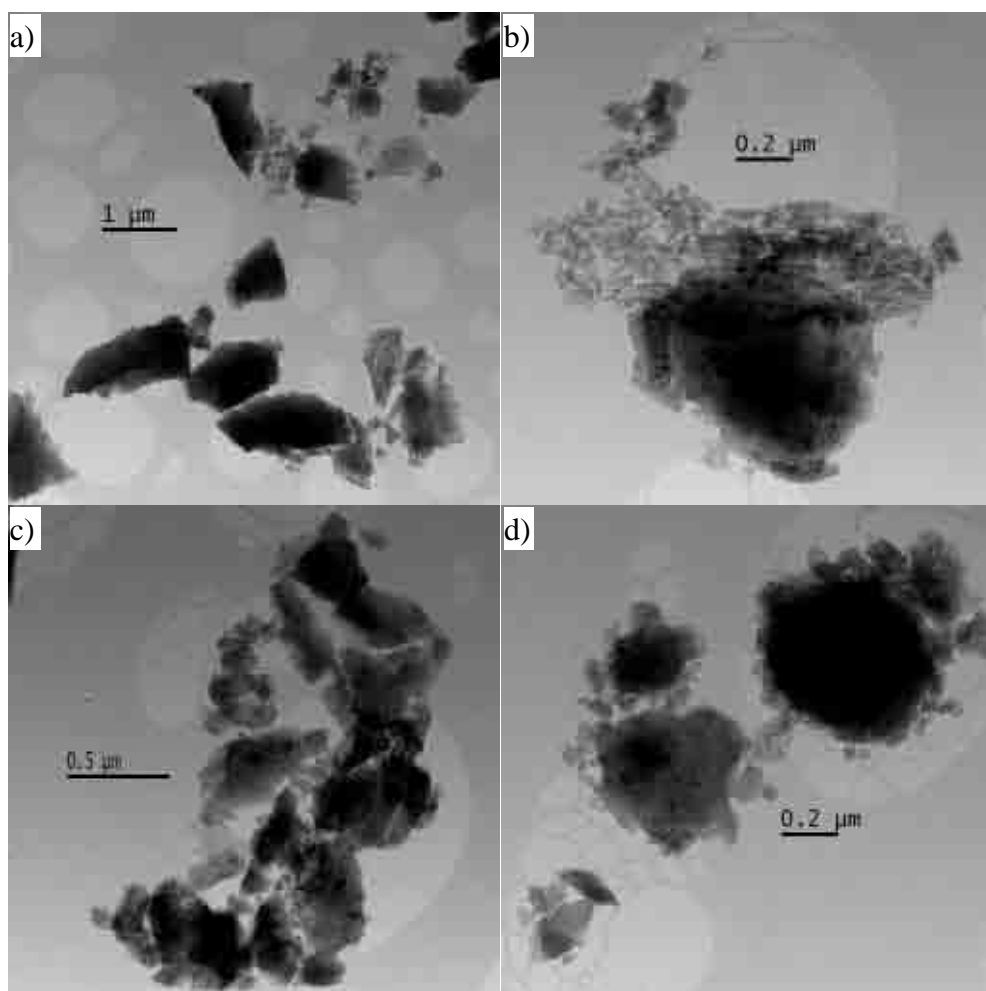
Figure 9.7. TEM micrographs of the 4 day nC$_{60}$ supernatant suspension.
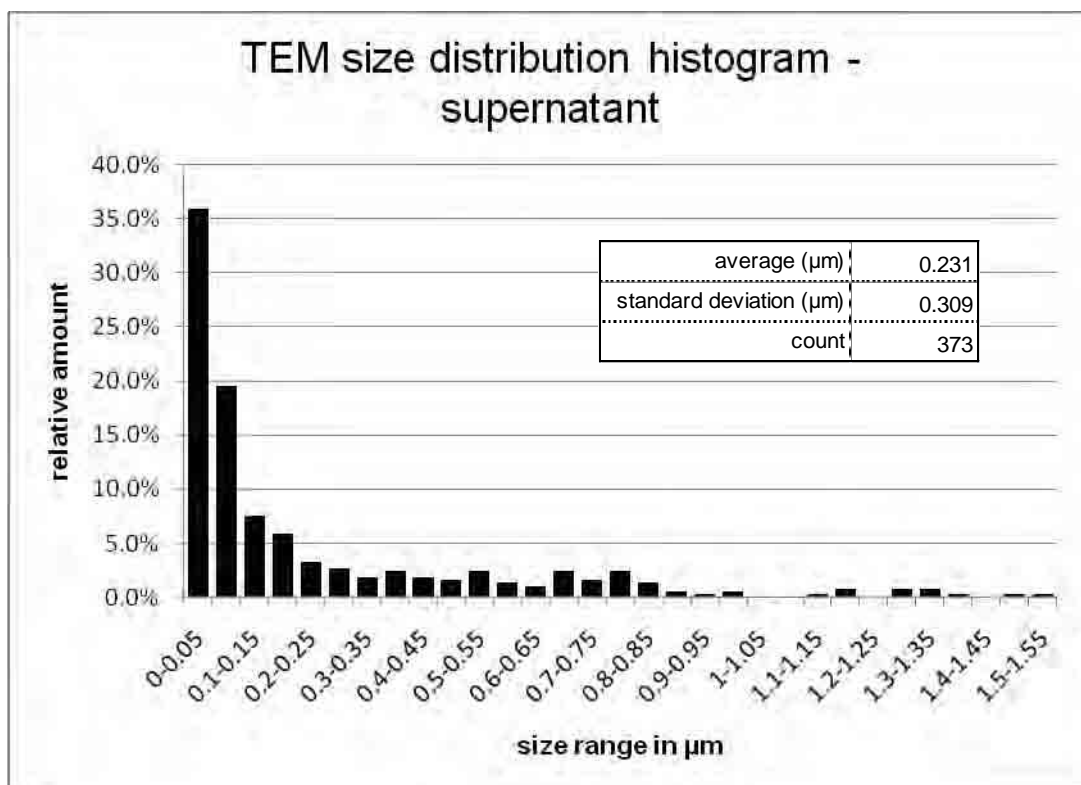
Figure 9.8. TEM size distribution histogram for 4 day nC$_{60}$ supernatant suspension.

TEM micrographs collected for the 1.2 μm filtrate are shown in Fig. 9.9. Similarly to previous samples two main types of morphologies are present: angular microparticles and NPs with smoother edges. However, in this sample the small particles occur also as clearly separate entities (9.9 b), not only surrounding bigger nC$_{60}$ clusters (as in the stock and supernatant samples). Measurements from the TEM images confirm very good performance of the filter membrane: contamination with particles bigger than the nominal pore size constitutes only 0.5 % of the 375 particles measured.
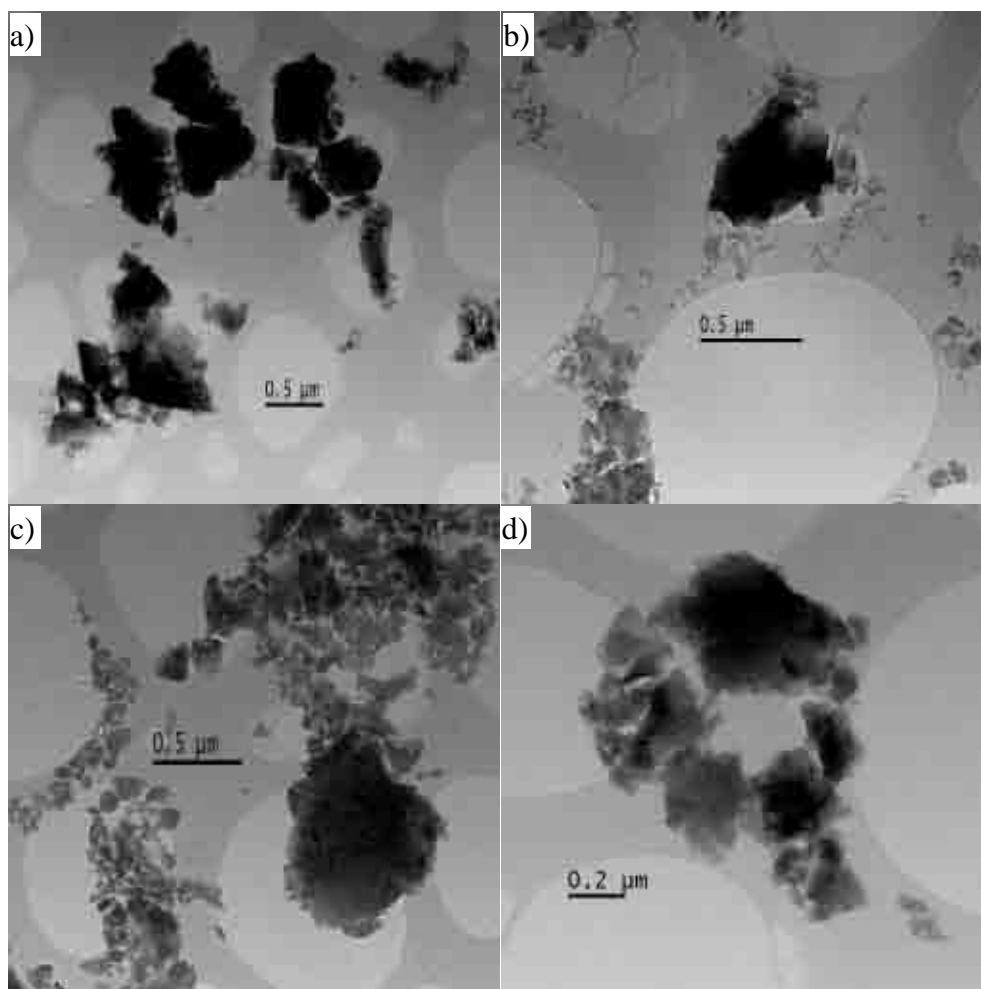
Figure 9.9. TEM micrographs of the nC$_{60}$ 1.2 µm filtrate.
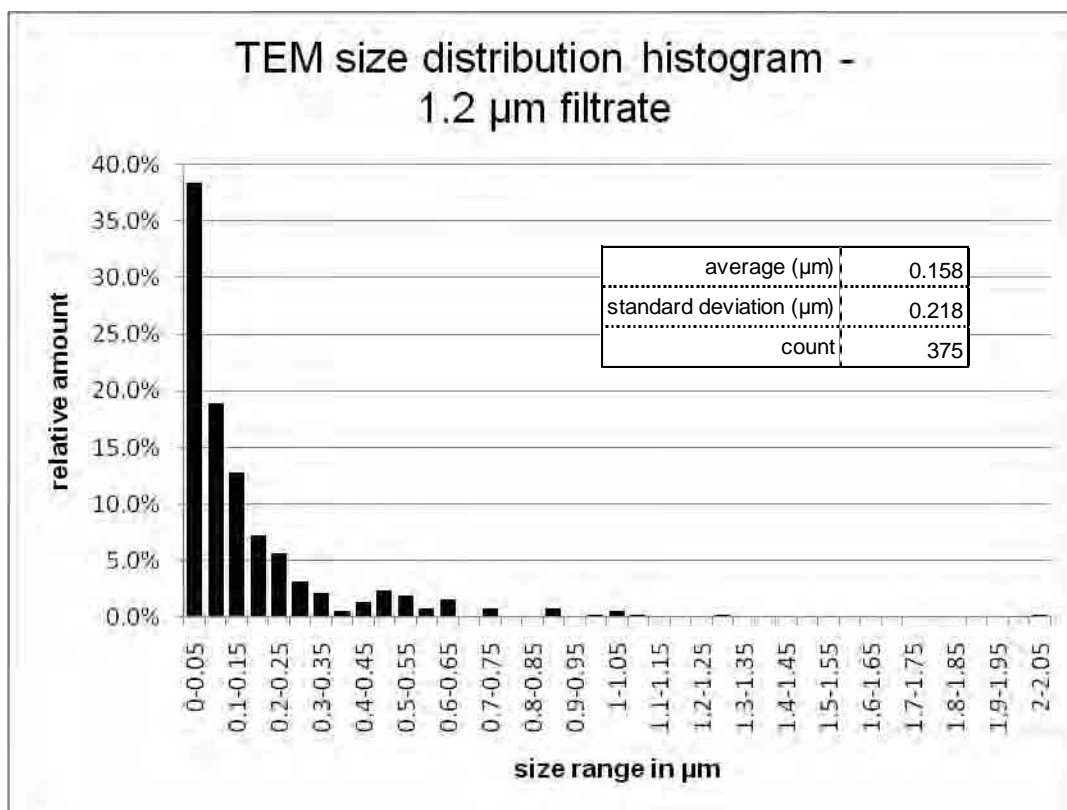
Figure 9.10. TEM size distribution histogram for nC$_{60}$ 1.2 µm filtrate.

Aggregates found in the 0.45 µm filtrate are shown in Fig. 9.11. Morphologies do not differ significantly from reported in the previous samples (stock, supernatant and 1.2 µm filtrate). With higher magnification multilayer and flaky morphologies are more profound. 0.45 µm filtrate produced narrower size distribution histogram with all particles within the filter cut-off (Fig. 9.12). It is the first of the analysed samples, for which standard deviation (77.2 nm) is not higher than the average particle size (100.5 nm). 59.7 % of 365 measured particles have sizes smaller than 100 nm. It should be noted, however, that no particles with sizes 1-10 were found. 4.4 % of particles are in the 10-20 nm fraction but the particle number peak occurs for sizes 20-60 nm (33. 7 % cumulatively).
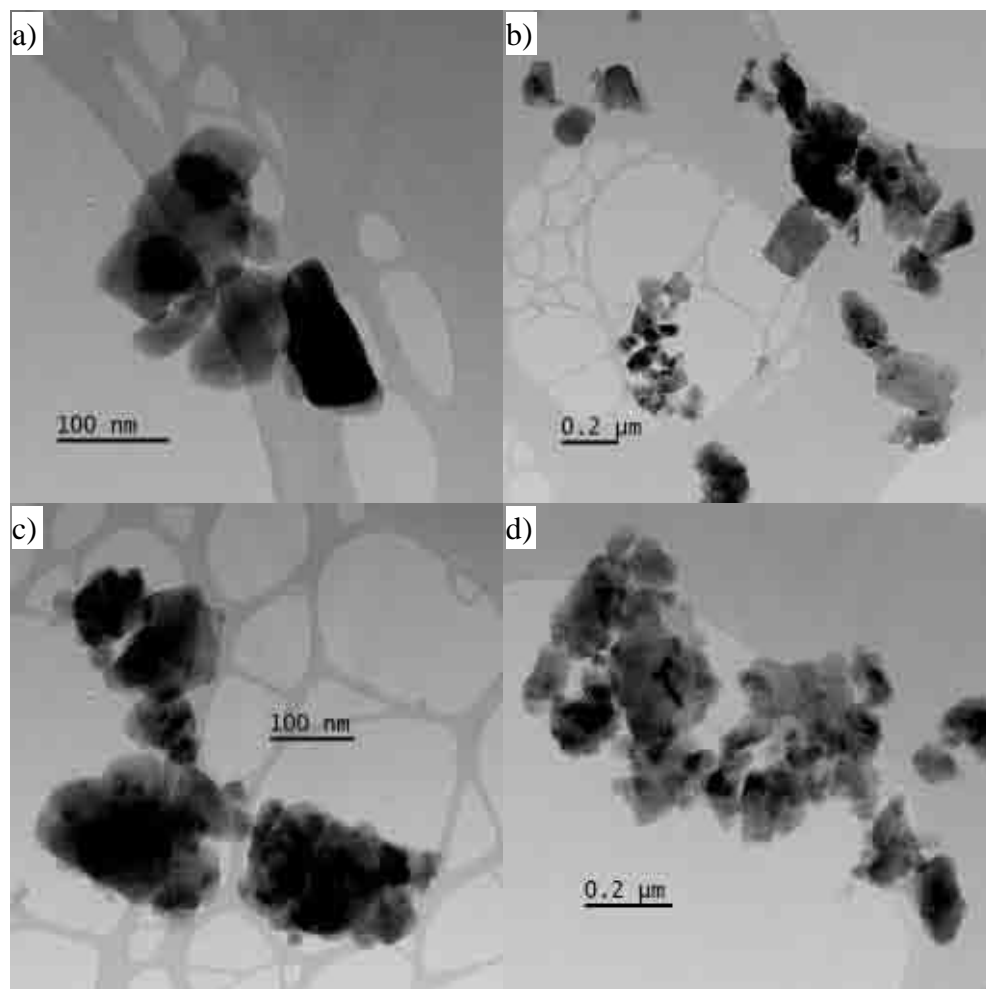
Figure 9.11. TEM micrographs of the nC$_{60}$ 0.45 μm filtrate.
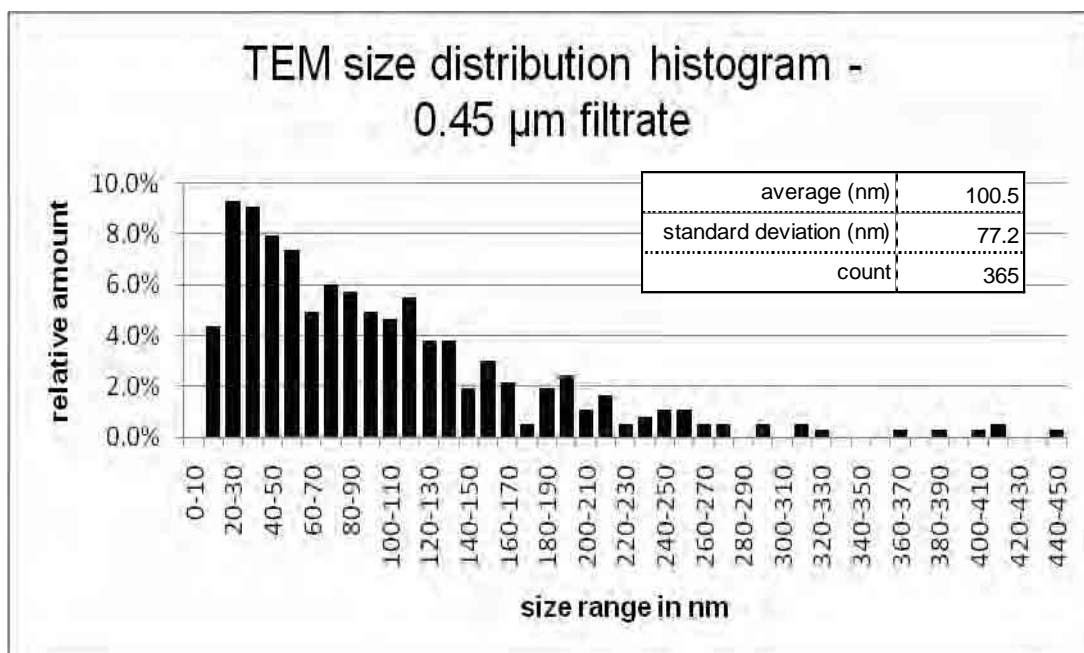
Figure 9.12. TEM size distribution histogram for nC$_{60}$ 0.45 µm filtrate.

Fig. 9.13 presents representative images of the 0.1 µm filtrate. It is the only sample that did not require dilution prior to centrifugation (i.e. the concentration of nC$_{60}$ in the ultracentrifuged 0.1 µm filtrate is the same as in the stock solution). Observed morphologies were abundant on the whole studied grid surface. Only spherical particles with smooth edges can be found. Angular big nC$_{60}$ aggregates (reported for all previously discussed suspensions) are absent in this sample. The roughly spherical or oval nC$_{60}$ particles in the 0.1 µm filtrate form loose conglomerates (Fig. 9.13 red arrows). Such morphologies were also found in the previous samples(e.g. Fig. 9.5 c), where they are considerably less abundant, which can be explained by sample dilution, 5-100 fold, needed in the case of all the other samples. Sizes of these conglomerate structures are well above the nominal pore size of the filter membrane (mostly 100-200 nm), only 15.6 % of the conglomerates measured are smaller than 100 nm (Fig. 9.14 a). However, owing to the loose structure of the conglomerates it is conceivable that these

nC$_{60}$ particles were squeezed through the pores and reformed in the time between filtration and ultracentrifugation. This hypothesis is supported by the size distribution of conglomerate constituents, i.e. nC$_{60}$ single clusters (Fig. 9.13 green arrows). Average size of the clusters in the 0.1 µm filtrate is 33.6 nm with standard deviation of 17.8 and dimensions of all 215 measured particles are below the membrane pore size (Fig. 9.14 b).
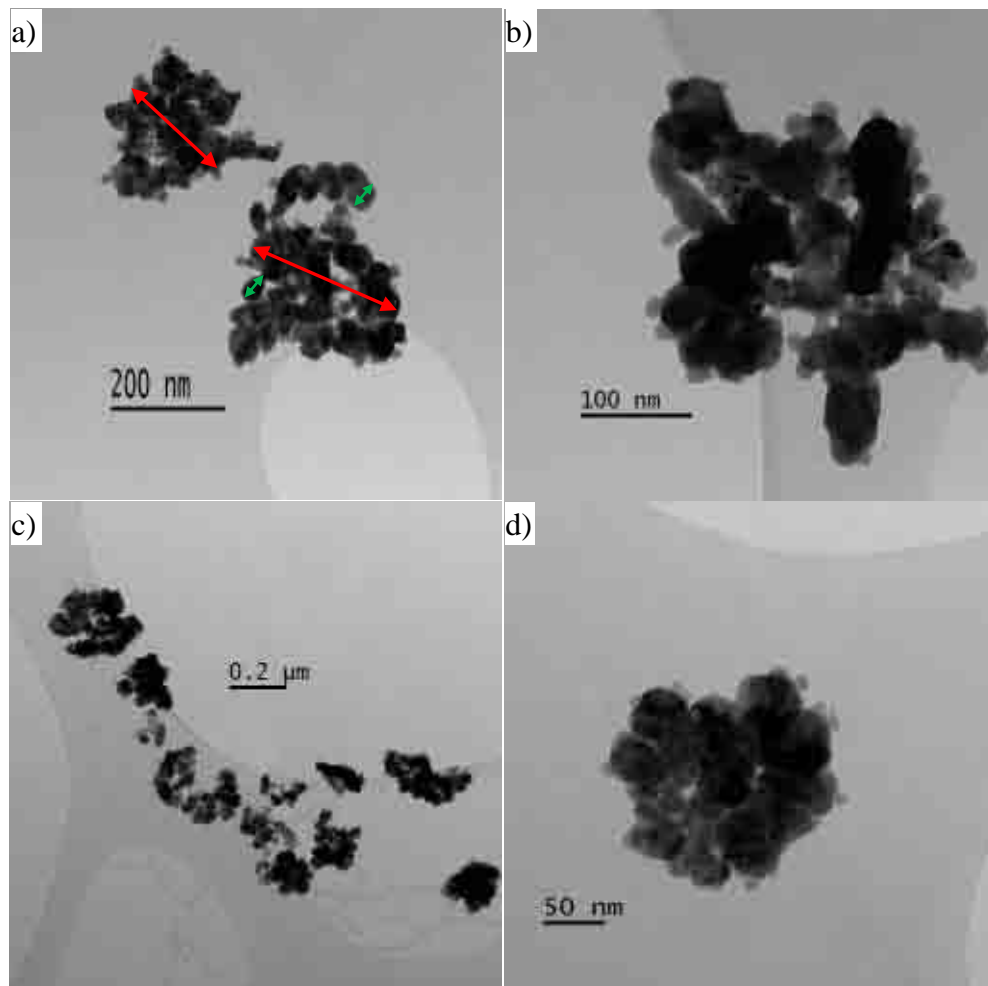
Figure 9.13. TEM micrographs of the nC$_{60}$ 0.1 µm filtrate (red arrow – conglomerate dimension, green arrow – single cluster dimension).
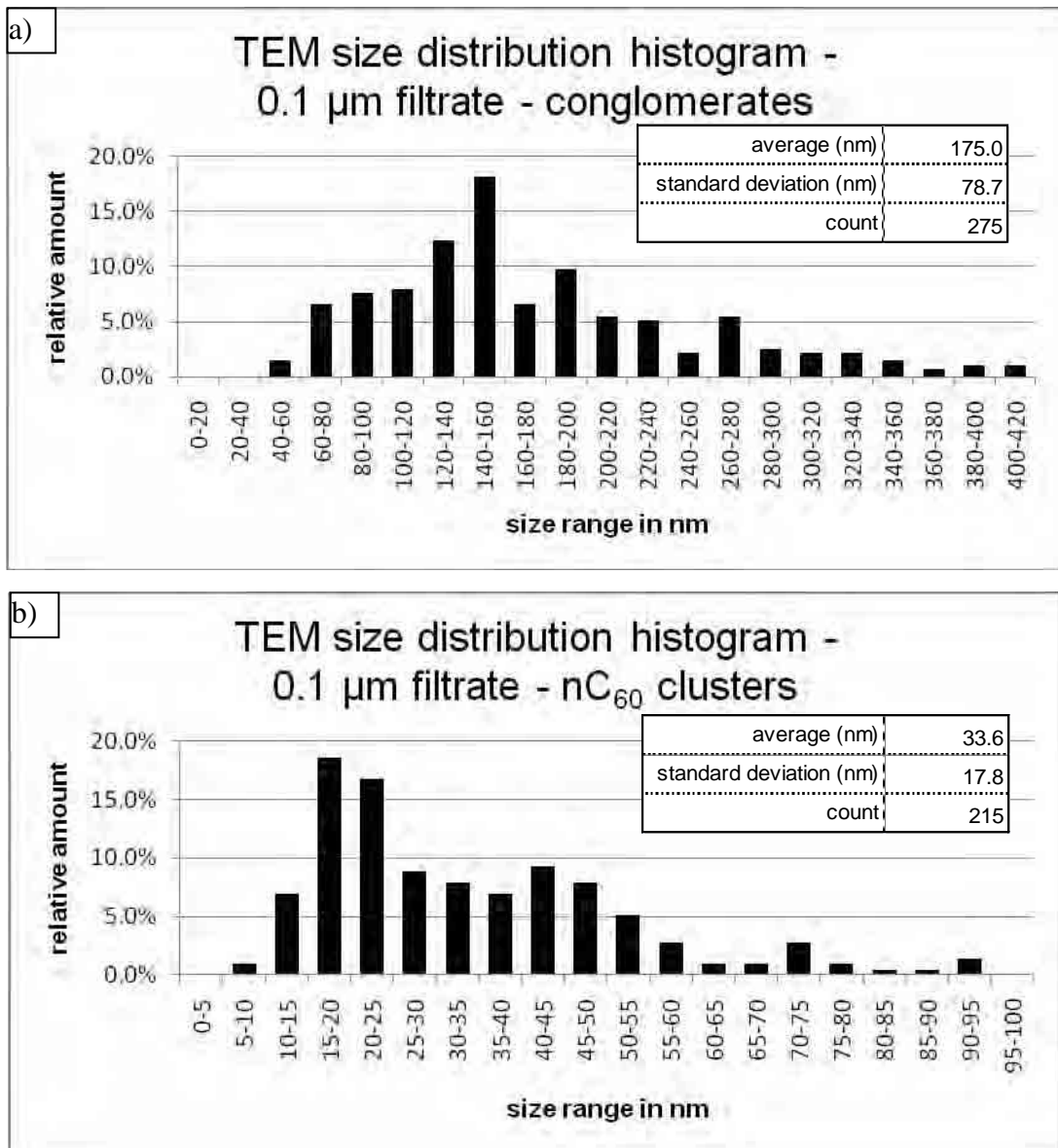
Figure 9.14. TEM size distribution histogram for nC$_{60}$ 0.1 μm filtrate; a) conglomerates, b) nC$_{60}$ clusters).

9.6   Number concentrations

Fig. 9.15 explains how number concentrations were estimated from the centrifuged samples analysed with TEM. The number of particles counted on a TEM grid surface was related to the volume of the sample above it to arrive at the number of particles per unit of volume. This algorithm assumes that all particles in the given volume of sample are effectively deposited on the grid during the centrifugation, i.e. that the centrifugation time is sufficient for the smallest particles to travel from the top of the sample to the bottom.
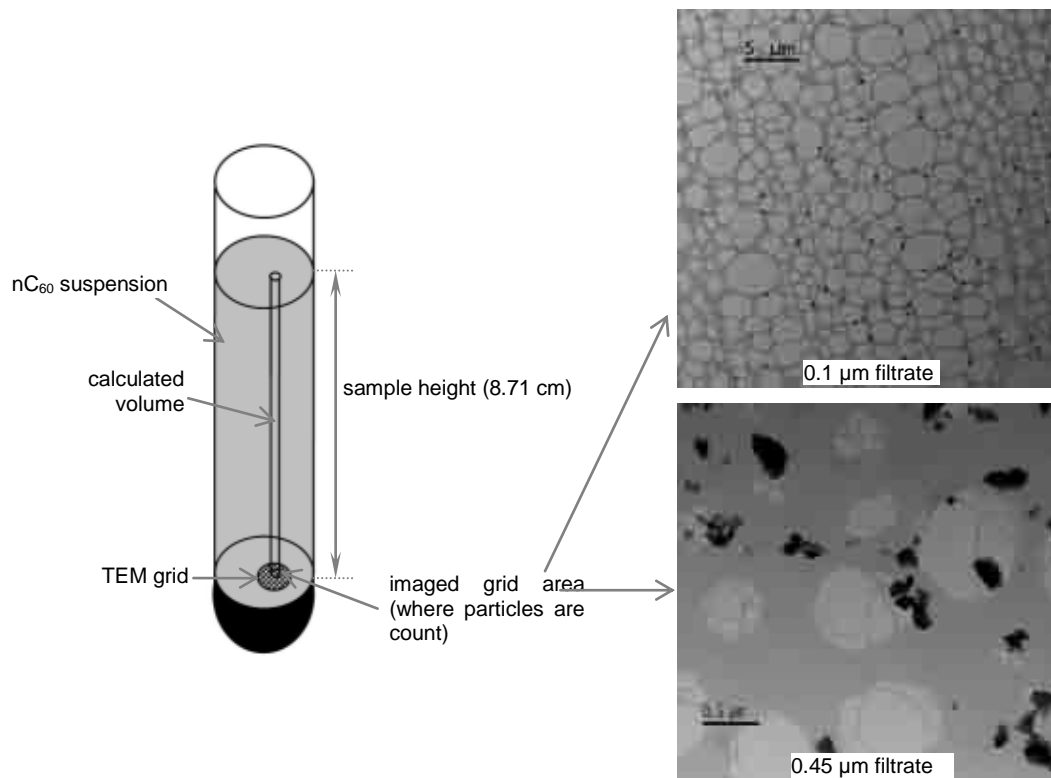
Figure 9.15. Schematic explanation of number concentration calculations using centrifugation and TEM imaging.

With the assumption that centrifuged particles are ideally spherical, the centrifugation time, *t*, (in seconds) can be calculated according to the following formula:

$$t = \frac{18\ \eta\ \ln(r_{max}/r_{min})}{d^2\ (\rho - \rho_0)\ \omega^2}$$

where:

ŋ – solution viscosity assumed to be equal to the viscosity of water at 15 ° C (11. 39 10^{-3} g $s^{-1}cm^{-1}$)

d – particle diameter (cm)

ǫ – particle density (1.65 g cm^{-1}) [Yadav and Ritesh, 2008]

$ǫ_0$ – solution density assumed to be equal to the density of water at 10 ° C (0.99 g cm^{-3})

ω – rotational speed (rad s^{-1}) calculated as 2 π rpm/60

r_{max} – distance from the centre of centrifuge rotor to the bottom of the suspension (14.88 cm)

r_{min} – distance from the centre of centrifuge rotor to the top of the suspension (6.17 cm)

particle diameter (nm)	settling time from top to bottom (min)
10	462
20	115
27.5	**60**
30	51
50	18
100	5
200	1

Table 9.3. Theoretical settling times for ultracentrifuged C_{60} particles with different diameters.

Using this equation, settling times for different nC_{60} particles have been calculated and presented in Table 9.3. The centrifugation time of 60 min, used in the experiments

presented here, is sufficient to settle out all particles with diameters exceeding 27.5 nm. Consequently, it can be assumed that the majority of material even from the smallest fraction (0.1 µm filtrate) is deposited on the TEM grid.

Particles were counted in available lower resolution TEM images, i.e. on surfaces big enough to exhibit roughly homogenous particle distribution (with surface area of either 40.96 µm^2 or 1024 µm^2). In case of 0.1 µm filtrate, 6 different images were analysed and a total number of 388 nC$_{60}$ conglomerates (as discussed in chapter 9.5) were counted. No calculation was feasible for single nC$_{60}$ clusters because it is impossible to distinguish all separate components of the conglomerates in any grid area suitable for number concentration calculations.

For the 0.45 µm filtrate, four images were suitable for the calculations and a total of 156 particles counted. The number of particles found on the given grid surface was related to the volume of liquid above this surface with known height of the sample and then related to 1 mL. The results are summarised in Table 9.4.

	x10^6 aggregates ml^{-1}
0.1 µm filtrate	3.7
0.45 µm filtrate	126.2

Table 9.4. Estimated aggregate number concentrations for nC$_{60}$ 0.1µm and 0.45 µm filtrates.

This method was applied to 0.1 and 0.45 µm filtrates only since for the other samples it was impossible to distinguish separate aggregates of nC$_{60}$ and thus unfeasible to count them. To calculate number concentrations for the other samples (stock, supernatant and 1.2 µm filtrate) additional experiments were needed (further dilution before

ultracentrifugation to reduce grid coverage), which could not be undertaken due to lack of time.

It should be noted, however, that figures presented in Table 9.4 are rough estimates due to limited availability of TEM images suitable for the number concentration calculations, which might not accurately represent the whole grid surface and the bulk suspensions. Additionally, for deposition time calculations it was assumed that all particles are ideally spherical, which is not the case as can be seen in the TEM micrographs.

Comparing these results with mass concentration estimates (Table 9.2) it can be concluded that the smallest fraction (i.e. 0.1 μm filtrate), which constitutes ca. 2 % of the total mass (concentration of 8.9 ppm of the nominal total 500 ppm concentration) contains about 3.7 million particles (nC$_{60}$ conglomerates) per ml. The 0.45 μm filtrate with estimated concentration of 47.5 ppm (9.5 %) contains considerably higher number of particles, ca. 126.2 million per ml.

9.7   Summary of the fish exposure experiment [Chipman et al., 2008]

The data discussed in this section is included for completeness as the fullerene characterisation was performed in order to aid understanding the exposure to fish conducted by Takeshi Kitano, Tim D. Williams, Ioanna Katsiadaki, Matthew B. Sanders and James K. Chipman (Kumamoto University (Japan), University of Birmingham, and Cefas Weymouth Laboratories).

The stock suspension of water-stirred fullerenes C$_{60}$ was diluted accordingly to prepare fish exposure media with two nominal concentrations: 0.1 ppm and 0.5 ppm. Apart from water-stirred fullerenes, other types of carbonaceous particles were included in the exposure experiments: fullerol C$_{60}$OH (hydroxyl-fullerene) suspended directly in water and through an intermediate solvent (THF). A 48 h exposure experiment to female three-spined stickleback (*Gasterosteus aculeatus*) was performed by CEFAS Weymouth Laboratory (I. Katsiadaki, M. N. Sanders). Transcriptomic responses were assessed in the liver, gill and brain tissue of the fish in the School of Biosciences, University of Birmingham (J. K. Chipman, T. D. William). Gene expression profiling is used to underpin toxic effects and their possible mechanisms.

Two different batches of aqueous nC$_{60}$ were used in the experiments, both prepared according to the same protocol. The characterisation of fullerenes improved over time. Results presented in chapters 9.2 -9.6 were obtained for the second batch of water-stirred fullerenes C$_{60}$.

The fish exposure assay was repeated three times: twice with the first batch of fullerene suspension and once with the second batch. In case of the lower dose of water-stirred C$_{60}$, no response was found in any of the analysed tissues compared to the

218

untreated controls. However, the first exposure to the 0.5 ppm concentration resulted in gene expression changes in brain and gill in a variety of gene ontology classes. Obtained results suggested that toxicity mechanisms might include membrane effects and inflammatory response. The other two repeats of the fish exposure (one with the same batch of NP suspension and one with the newer batch) did not find any toxic response. No hypothesis was proposed to explain this inconsistency.

10 CONCLUSIONS AND FUTURE WORK

Two different microscopy techniques (TEM and AFM) were used to image aqueous suspensions of SWCNTs and both proved suitable for the characterisation of engineered NPs in the aquatic environment at the test concentrations. Both techniques provide sufficient spatial resolution (sub-nanometre) to produce valuable information on morphologies and interactions of synthetic NPs with natural ones. Quantitative analysis of TEM (measurements of nanotube bundle thicknesses) and AFM (measurements of nanotube bundle heights) micrographs produced a good agreement within experimental uncertainty and polydispersity of the samples. Other morphological features, such as homogeneity of the surface coating or the presence of nano-scale surface films where clearly present in the samples with natural aquatic colloids although they were more difficult to quantify and compare statistically.

Substantial evidence that carboxylic acid functionalised SWCNTs form very stable aqueous suspensions has been presented in this work. Dispersion in water is facilitated by carboxylic groups giving the nanotubes a negative surface charge (the stabilising mechanism is provided by the electrostatic repulsion). Visual observation and TEM analysis show a slightly stabilising effect of humic acid on suspended SWCNTs due to surface coating formation (i.e. the mechanism of the steric repulsion) whereas the presence of natural water caused instant and profound aggregation and sedimentation. Under most experimental conditions, both the SWCNTs and humic substances were negatively charged, indicating non-charge interactions, e.g. the hydrophobic effect was important and sufficient in magnitude to overcome repulsive electrostatic effects. Further experiments imply that such behaviour is at least partly

attributable to bridging between HS and SWCNTs by divalent cations such as Ca^{2+}, although this evidence is inconclusive. The stability of aqueous SWCNTs depends on their negative surface charge, which if neutralised by divalent cations, results in efficient aggregation and rapid losses from the water column. It can be thus expected that SWCNTs may be persistent in soft waters rich in organic material and efficiently transferred to sediments in hard estuarine or marine waters.

By ensuring even TEM grid coverage, ultracentrifugation used for TEM specimen preparation can significantly shorten the analysis time and improve the reproducibility of the results. It is recommended whenever characterisation of NPs requires a series of TEM analyses for a number of samples. Additionally, by controlling the parameters of NP deposition on the substrate, quantitative data, such as particle number concentrations, can be obtained.

Prolonged stirring produces extremely stable suspensions of fullerene aggregates nC_{60}. The results presented in chapter 9, are the first to address morphologies and dimensions of different size fractions of water-stirred fullerene, which is one of the most common protocol to disperse fullerene in water for toxicity testing. From the conducted experiments there is evidence that very little material (by mass) is dispersed below the diameter size of < 100 nm, i.e. in the nanoscale size range.

TEM analysis of fullerene aqueous suspensions in the presence of natural aquatic colloids (SRFA, succinoglycan and the lake water) revealed some changes in the observed morphologies, i.e. coating of C_{60} aggregates with colloidal material. However, the interaction was clearly not as strong as in the case of SWCNTs with most morphologies undistinguishable from fullerenes in the absence of NAC.

A protocol for analysing metal speciation in aqueous suspensions of SWCNTs was tested in a pilot study and proved suitable for this purpose, although many samples were contaminated with external sources of metals.

The objectives for this thesis listed in chapter 1.2 have largely been met. However, future work is needed to validate and confirm some of the results and further address the knowledge gaps in the field. Further validation of the results is especially relevant in the case of atmospheric NPs analysis with AFM. Size distribution histograms proved inconsistent with the technical specifications for the impactor they were collected with. Further investigation is needed to quantify smallest material by mass and number to assess the significance and implications of the contamination with NPs with diameters below 10 nm.

AFM specimen preparation protocol for SWCNTs requires development (to overcome scarce and patchy particle distribution on mica). Poor nanotube adhesion to mica and significant sample heterogeneity resulted in too few nanotubes available for the height measurements and thus undermined statistical representativeness of the samples and sample comparison. It would be advisable to develop a new method for the AFM specimen preparation. Ultracentrifugation, which has proved successful in the case of TEM, would be a first choice optimisation approach to be tested.

The protocol for metal speciation presented and tested in chapter 8 needs improvement to avoid sample contamination. Also reproducibility of the measurements should be verified.

More generally, microscopy protocols for NP sizing need further optimisation to allow rapid and statistically reliable size characterisation (e.g. automated algorithms for

particle measurement). There is also an urgent need to develop analytical techniques to detect and measure NPs in water, air and soil to advance the knowledge beyond the laboratory conditions and address realistic exposure scenarios in order to conduct risk assessment of nanotechnologies to human health and ecosystems.

APPENDIX

In the results chapters which concerned microscopy analysis (4, 5, 6, 7 and 9) some images were selected to represent studied samples. These and remaining TEM and AFM images used throughout the experimental work have been gathered on a CD, which is attached to the back cover of the thesis. The images are presented in TIFF format suitable for viewing. The main folders are organised and named according to the chapters to which they are relevant:

- Chapter 4 (Atmospheric NPs with AFM)

- Chapter 5 (SWCNTs with TEM)

- Chapter 6 (Ultracentrifugation for TEM)

- Chapter 7 (SWCNTs with AFM)

- Chapter 9 (Characterisation of aqueous C_{60})

All subfolders are named after the samples whose images they contain (e.g. SWCNT +NW). Acronyms used in the subfolder titles are the same as used throughout the text (and as listed in the Nomenclature section). If an image (or images) of a sample were presented within the text, the subfolder titles also contain a relevant figure number in the brackets. AFM images are grouped into the three different output signals they are based on (amplitude, phase and topography). The topography images are saved as raw data (i. e. as collected), however, the selected images that were presented in the thesis had to be processed (flattened or filtered) to enhance their suitability for viewing without the XEI software. These are presented in the "processed" folders. Additionally, in case of Chapter 7, AFM images are grouped according to the mode they were obtained with (i.e. non-contact and tapping). TEM images used for comparison in

Chapter 7 are placed in the folder with the images from Chapter 5 (SWCNTs with TEM), which they were primarily taken for.

REFERENCES

Aitken, R.J., M.Q. Chaudhry, A. B. A. Boxall, M. Hull (2006). "Manufacture and use of nanomaterials: current status in the UK and global trends." Occupational Medicine-Oxford, 56: 300-306.

Alexa, N., H. Zhang, J. R. Lead (2009). "Development of a miniaturized diffusive gradients in thin films (DGT) device." Analytica Chimica Acta, 655: 80-85.

Allianz Group and OECD International Futures Programme (2005). "Small sizes that matter: Opportunities and risks of Nanotechnologies."

Alonso, J. L., W. H. Goldmann (2003). "Feeling the forces: atomic force microscopy in cell biology." Life Sciences, 72(23): 2553-2560.

Alvarez, P. J. J., V. Colvin, J. Lead, V. Stone (2009). "Research Priorities to Advance Eco-Responsible Nanotechnology." ACS Nano, 3(7): 1616–1619.

Anastasio, C., S. T. Martin (2001). "Atmospheric nanoparticles." In: J.F. Banfield and A. Navrotsky, Editors, Nanoparticles and the Environment, pp. 293–349.

Andelman, T., Y. Gong, M. Polking, M. Yin, I. Kuskovsky, G. Neumark, S. O'Brien (2005). "Morphological Control and Photoluminescence of Zinc Oxide Nanocrystals." J. Phys. Chem. B, 109: 14314-14318.

Andrievsky, G. V., V. Klochkov, L. Derevyanchenko (2005). "Is the C60 Fullerene Molecule Toxic?!" Fullerenes, Nanotubes and Carbon Nanostructures 13(4): 363-376.

Andrievsky, G. V., V. I. Bruskov, A. A. Tykhomyrov, S. V. Gudkov (2009). "Peculiarities of the antioxidant and radioprotective effects of hydrated C60 fullerene nanostuctures in vitro and in vivo." Free Radical Biology and Medicine, 47(6): 786-793.

ASTM (American Society for Testing and Materials) (2006). "Standard Terminology Relating to Nanotechnology." E 2456 – 06.

ATSDR (1990). Agency for Toxic Substance and Disease Registry, U. S., "Toxicological Profile for Silver." Public Health Service, Washington, D.C.

Azzazy, H. M. E., M. M. H. Mansour, S. C. Kazmierczak (2007). „From diagnostics to therapy: Prospects of quantum dots." Clinical Biochemistry, 40(13-14): 917-927.

Baalousha, M., M. Motelica-Heino, S. Galaup, P. Le Coustumer (2005 A). "Supramolecular structure of humic acids by TEM with improved sample preparation and staining." Microscopy Research and Technique, 66(6): 299-306.

Baalousha, M., F. Von der Kammer, M. Motelica-Heino, P. Le Coustumer (2005 B). "Natural sample fractionation by FlFFF–MALLS–TEM: Sample stabilization, preparation, pre-concentration and fractionation." Journal of Chromatography A, 1093(1-2): 156-166.

Baalousha, M., M. Motelica-Heino, P. Le Coustumer (2006). "Conformation and size of humic substances: Effects of major cation concentration and type, pH, salinity, and residence time." Colloids and Surfaces A: Physicochemical and Engineering Aspects, 272(1-2): 48-55.

Baalousha, M., J. R. Lead (2007). "Size fractionation and characterization of natural aquatic colloids and nanoparticles." Science of The Total Environment 386(1-3): 93-102.

Baalousha, M. (2009). "Aggregation and disaggregation of iron oxide nanoparticles: Influence of particle concentration, pH and natural organic matter." Science of The Total Environment, 407(6): 2093-2101.

Balnois, E., K. J. Wilkinson, J. R. Lead, J. Buffle (1999). "Atomic Force Microscopy of Humic Substances: Effects of pH and Ionic Strength." Environmental Science & Technology 33(21): 3911-3917.

Balnois, E., G. Papastavrou, K. J. Wilkinson (2007). "Force microscopy and force measurements of environmental colloids." Chapter 9. "Environmental colloids behaviour, structure and characterisation." (K. J. Wilkonson and J. R. Lead, Eds), John Wiley and Sons.

Barkay, Z., A. Teller, E. Ganor, Z. Levin, Y. Shapira (2005). "Atomic force and scanning electron microscopy of atmospheric particles." Microsc Res Tech., 68(2): 107-114.

Barna, A., B. Pecz, M. Menyhard (1998). „Amorphisation and surface morphology development at low-energy ion milling." Ultramicroscopy, 70(3): 161-171.

Barnett, B. P., A. Arepally, P. V. Karmarkar, D. Qian, W. D. Gilson, P. Walczak, V. Howland, L. Lawler, C. Lauzon, M. Stuber, D. L. Kraitchman, J. W. M. Bulte (2007). "Magnetic resonance-guided, real-time targeted delivery and imaging of magnetocapsules immunoprotecting pancreatic islet cells." Nature Medicine, 13: 986-991.

Barone, T. L., Y. Zhu (2008). „The morphology of ultrafine particles on and near major freeways." Atmospheric Environment, 42(28): 6749-6758.

Batson, P. E., N. Dellby, O. L. Krivanek (2002). "Sub-angstrom resolution using aberration corrected electron optics." Nature, 418(6898): 617-620.

Baun, A., S. N. Sorensen, R. F. Rasmussen, N. B. Hartmann, C. B. Koch (2008). "Toxicity and bioaccumulation of xenobiotic organic compounds in the presence

of aqueous suspensions of aggregates of nano-C60." Aquatic Toxicology, 86(3): 379-387.

BCC Research (2005). Market research reports and technical publications. BCC Research, Wellesley, MA.

Beck-Speier, I., N. Dayal, E. Karg, K. L. Maier, G. Schumann, H. Schulz, M. Semmler, S. Takenaka, K. Stettmaier, W. Bors, A. Ghio, J. M. Samet, J. Heyder (2005). "Oxidative stress and lipid mediators induced in alveolar macrophages by ultrafine particles." Free Radical Biology and Medicine, 38(8): 1080-1092.

Bendersky, L. A., F. W. Gayle (2001). "Electron Diffraction Using Transmission Electron Microscopy." J. Res. Natl. Inst. Stand. Technol., 106(6): 997–1012.

Benedetti, M. F., J. F. Ranville, T. Allard, A. J. Bednar, N. Menguy (2003). "The iron status in colloidal matter from the Rio Negro, Brasil." Colloids and Surfaces A: Physicochemical and Engineering Aspects, 217(1-3): 1-9.

Bing-she, X. (2008). "Prospects and research progress in nano onion-like fullerenes." New Carbon Materials, 23(4): 289-301.

Binnig, G., C. Gerber, E. Stoll, T. R. Albrecht, C. F. Quate (1987). "Atomic resolution with atomic force microscope." Surface Science, 189-190: 1-6.

Boxall, A. B., K. Tiede, Q. Chaudhry (2007). "Engineered nanomaterials in soils and water: How do they behave and could they pose a risk to human health?" Nanomedicine, 2: 919-927.

Brandt, D., B. Park, M. Hoang, H. T. Jacobe (2005). "Argyria secondary to ingestion of homemade silver solution." Journal of the American Academy of Dermatology, 53(2): S105-S107.

Brant, J. A., H. Lecoanet, M. Wiesner (2005). "Aggregation and Deposition Characteristics of Fullerene Nanoparticles in Aqueous Systems." Journal of Nanoparticle Research, 7: 545-553.

Brant, J. A., J. Labille, J. Y. Bottero, M. R. Wiesner (2006). "Characterizing the Impact of Preparation Method on Fullerene Cluster Structure and Chemistry." Langmuir 22: 3878-3885.

Brook, R. D., B. Franklin, W. Cascio, Y. Hong, G. Howard, M. Lipsett, R. Luepker, M. Mittleman, J. Samet, S. C. Smith, I. Tager (2004). "Air pollution and cardiovascular disease." Circulation, 109: 2655–2671.

Buffle, J., K. J. Wilkinson, S. Stoll, M. Filella, J. Zhang (1998). "A Generalized Description of Aquatic Colloidal Interactions: The Three-colloidal Component Approach." Environ. Sci. Technol., 32(19): 2887–2899.

Buffle, J. (2006). "The key role of environmental colloids/nanoparticles for the sustainability of life." Environ. Chem., 3: 155–158.

Butt, H. J., B. Cappella, M. Kappl (2005). "Force measurements with the atomic force microscope: Technique, interpretation and applications." Surface Science Reports, 59(1-6): 1-152.

Campbell, C. T. (2004). "The Active Site in Nanoparticle Gold Catalysis." Science, 306(5694): 234-235.

Capek, I. (2004). "Preparation of metal nanoparticles in water-in-oil (w/o) microemulsions." Advances in Colloid and Interface Science, 110: 49-74.

Carnes, C. L., K. J. Klabunde (2000). "Synthesis, Isolation, and Chemical Reactivity Studies of Nanocrystalline Zinc Oxide." Langmuir, 16: 3764-3772.

Casuccio, G. S., S. F. Schlaegle, T. L. Lersch, G. P. Huffman, Y. Chen, N. Shah (2004). "Measurement of fine particulate matter using electron microscopy techniques." Fuel Processing Technology, 85(6-7): 763-779.

Cha, K., H. W. Hong, Y. G. Choi, M. J. Lee, J. H. Park, H. K. Chae, G. Ryu, H. Myung (2008). "Comparison of acute responses of mice livers to short-term exposure to nano-sized or micro-sized silver particles." Biotechnol Lett, 30: 1893–1899.

Chalupa, D. C., P. E. Morrow, G. Oberdorster, M. J. Utell, M. W. Frampton (2004). "Ultrafine Particle Deposition in Subjects with Asthma." Environmental Health Perspectives, 112(8): 879-882.

Chang, X., P. J. Vikesland (2009). "Effects of carboxylic acids on nC60 aggregate formation." Environmental Pollution, 157(4): 1072-1080.

Chanudet, V., M. Filella (2008). "Size and composition of inorganic colloids in a peri-alpine, glacial flour-rich lake." Geochimica et Cosmochimica Acta, 72(5): 1466-1479.

Chappell, M. A., A. J. George, K. M. Dontsova, B. E. Porter, C. L. Price, P. Zhou, E. Morikawa, A. J. Kennedy, J. A. Steevens (2009). "Surfactive stabilization of multi-walled carbon nanotube dispersions with dissolved humic substances." Environmental Pollution, 157(4): 1081-1087.

Checco, A., Y. Cai, O. Gang, B. M. Ocko (2006). "High resolution non-contact AFM imaging of liquids condensed onto chemically nanopatterned surfaces." Ultramicroscopy, 106(8-9): 703-708.

Chen, Q. Z., C. W. Thomas, D. M. Knowles (2004A). "Characterisation of 20Cr32Ni1Nb alloys in as-cast and Ex-Service conditions by SEM, TEM and EDX." Materials Science and Engineering A, 374(1-2): 398-408.

Chen, Q., C. Saltiel, S. Manickavasagam, L. S. Schadler, R. W. Siegel, H. Yang (2004B). "Aggregation behavior of single-walled carbon nanotubes in dilute aqueous suspension." Journal of Colloid and Interface Science, 280: 91–97.

Chen, J., S. Patil , S. Seal, J. F. McGinnis (2006). "Rare earth nanoparticles prevent retinal degeneration induced by intracellular peroxides." Nature Nanotechnology, 1(2): 142–150.

Chen, C., X. Wang, H. Jiang, W. Hu (2007A). "Direct observation of macromolecular structures of humic acid by AFM and SEM." Colloids and Surfaces A: Physicochemical and Engineering Aspects, 302(1-3): 121-125.

Chen, K. L., M. Elimelech (2007B). "Influence of humic acid on the aggregation kinetics of fullerene (C60) nanoparticles in monovalent and divalent electrolyte solutions." Journal of Colloid and Interface Science, 309(1): 126-134.

Chen, W., C. M. Li, L. Yu, Z. Lu, Q. Zhou (2008). "In situ AFM study of electrochemical synthesis of polypyrrole/Au nanocomposite." Electrochemistry Communications, 10(9): 1340-1343.

Chen, S., C. Liu, M. Yang, D. Lu, L. Zhu, Z. Wang (2009). "Solid-phase extraction of Cu, Co and Pb on oxidized single-walled carbon nanotubes and their determination by inductively coupled plasma mass spectrometry." Journal of Hazardous Materials, 170(1): 247-251.

Cheng, X., A. T. Kan, M. B. Tomson (2004.) "Naphthalene adsorption and desorption from aqueous C60 fullerene." J. Chem. Eng. Data, 49(3): 675–683.

Cheng, J. P., E. Flahaut, S. H. Cheng (2007). "Effect of carbon nanotubes on developing zebrafish (Danio rerio) embryos." Environmental Toxicology and Chemistry, 26(4): 708-716.

Chipman, J. K., T. D. Williams, T. Kitan, I. Katsiadaki, M. N. Sanders, J. Lead, M. Baalousha, E. Cieslak (2008). "Toxicogenomics as an "open" system to detect tissue-specific responses to toxicants: Nanoparticles as a proof of principle in fish." Comparative Biochemistry and Physiology - Part A: Molecular & Integrative Physiology, 151(1): S37.

Cho, H. H., B. A. Smith, J. D. Wnuk, D. H. Fairbrother, W. P. Ball (2008). "Influence of surface oxides on the adsorption of naphthalene onto multiwalled carbon nanotubes." Environmental Science and Technology, 42: 2899–2905.

Choi, O., Z. Q. Hu (2008). "Size dependent and reactive oxygen species related nanosilver toxicity to nitrifying bacteria." Environmental Science & Technology, 42: 4583-4588.

Choi, O., K. K. Deng, N. J. Kim, L. Ross, R. Y. Surampalli, Z. Q. Hu (2008). "The inhibitory effects of silver nanoparticles, silver ions, and silver chloride colloids on microbial growth." Water Research, 42: 3066-3074.

Chopra, I. (2007). "The increasing use of silver-based products as antimicrobial agents: a useful development or a cause for concern?" Journal of Antimicrobial Chemotherapy, 59: 587–590.

Christian, P., F. Von der Kammer, M. Baalousha, T. Hofmann (2008). "Nanoparticles: structure, properties, preparation and behaviour in environmental media." Ecotoxicology, 17: 326-343.

Conibeer, G., M. Green, E.-C. Cho, D. König, Y.-H. Cho, T. Fangsuwannarak, G. Scardera, E. Pink, Y. Huang, T. Puzzer, S. Huang, D. Song, C. Flynn, S. Park, X. Hao, D. Mansfield (2008). "Silicon quantum dot nanostructures for tandem photovoltaic cells." Thin Solid Films, 516(20): 6748-6756.

Cornfield, A. H. (1977). "Effects of addition of 12 metals on carbon-dioxide release during incubation of an acid sandy soil." Geoderma, 19(3): 199-203.

Cortie, M. B. (2004). " The weird world of nanoscale gold." Gold Bulletin, 37: 12-19.

Council for Science and Technology (2007). "Nanosciences and Nanotechnologies: A Review of Government's Progress on its policy Commitments."

Covert, D. S., A. Wiedensohler, P. Aalto, J. Heintzenberg, P. H. McMurry, C. Leck (1996). "Aerosol number size distributions from 3 to 500 nm diameter in the arctic marine boundary layer during summer and autumn." Tellus, B48: 197–212.

Cozzi, F., W. H. Powell, C. Thilgen (2005) "Numbering of fullerenes (IUPAC Recommendations)". Pure Appl. Chem., 77(5): 843–923.

Cui, N. Y., N. M. D. Brown, A. McKinley (1999). "An exploratory study of the topography of a CdI2 single crystal using AFM." Applied Surface Science, 152(3-4): 266-270.

Cundy, A. B., L. Hopkinson, R. L. D. Whitby (2008). " Use of iron-based technologies in contaminated land and groundwater remediation: A review." Science of The Total Environment, 400(1-3): 42-51.

Cushing, B. L., V. L. Kolesnichenko, C. J. O'Connor (2004). "Recent advances in the liquid-phase syntheses of inorganic nanoparticles." Chem Rev, 104(9):3893–946.

Daigle, C. C., D. C. Chalupa, F. R. Gibb, P. E. Morrow, G. Oberdorster, M. J. Utell, M. W. Frampton (2003). "Ultrafine particle deposition in humans during rest and exercise." Inhal Toxicol., 15(6): 539-52.

Daniel, M. C., D. Astruc (2004). „Gold nanoparticles: assembly, supramolecular chemistry, quantum-size-related properties, and applications toward biology, catalysis, and nanotechnology." Chem Rev, 104: 293–346.

Das, M., S. Patil, N. Bhargava, J. F. Kang, L. M. Riedel, S. Seal, J. J. Hickman (2007). "Auto-catalytic ceria nanoparticles offer neuroprotection to adult rat spinal cord neurons." Biomaterials, 28: 1918–1925.

Defra (Department for Environment, Food and Rural Affirs) (2007). "Characterising the Potential Risks posed by Engineered Nanoparticles. A Second UK Government Research Report." London.

De Momi, A., J. R. Lead (2008). "Behaviour of environmental aquatic nanocolloids when separated by split-flow thin-cell fractionation (SPLITT)." Science of The Total Environment, 405(1-3): 317-323.

Deguchi, S., R. G. Alargova, K. Tsujii (2001). "Stable Dispersions of Fullerenes, C60 and C70, in Water. Preparation and Characterization." Langmuir, 17:6013-6017.

Delgado, G. C. (2010). "Economics and governance of nanomaterials: potential and risks." Technology in Society, In Press, Corrected Proof, Available online 22 April 2010.

Demanet, C. M. (1995). "Atomic force microscopy determination of the topography of fly-ash particles." Applied Surface Science, 89(1): 97-101.

Deng, B., X. Yan, Q. Wei, W. Gao (2007). "AFM characterization of nonwoven material functionalized by ZnO sputter coating." Materials Characterization, 58(10): 854-858.

Derfus, A. M., W. C. W. Chan, S. N. Bhatia (2004). "Probing the Cytotoxicity of Semiconductor Quantum Dots." Nano Letters, 4(1): 11-18.

Derjaguin, B. V., L. D. Landau (1941). "Theory of stability of strongly charged lyophobic sols and of the adhesion of strongly charged particles in solutions of electrolytes." Acta Physicochimica URSS, 14: 733–762.

Dhawan, A., J. S. Taurozzi, A. K. Pandey, W. Shan, S. M. Miller, S. A. Hashsham, V. V. Tarabara (2006). "Stable Colloidal Dispersions of C60 Fullerenes in Water: Evidence for Genotoxicity." Environ. Sci. Technol., 40(23): 7394–7401.

Dickinson, M., T. B. Scott (2010). "The application of zero-valent iron nanoparticles for the remediation of a uranium-contaminated waste effluent." Journal of Hazardous Materials, 178(1-3): 171-179.

Diegoli, S., A. L. Manciulea, S. Begum, I. P. Jones, J. R. Lead, J. A. Preece (2008). "Interaction between manufactured gold nanoparticles and naturally occurring organic macromolecules." Science of The Total Environment, 402(1): 51-61.

Dobrovolskaia, M. A., A. K. Patri, J. Zheng, J. D. Clogston, N. Ayub, P. Aggarwal, B. W. Neun, J. B. Hall, S. E. McNeil (2009). "Interaction of colloidal gold nanoparticles with human blood: effects on particle size and analysis of plasma protein binding profiles." Nanomedicine: Nanotechnology, Biology and Medicine, 5(2): 106-117.

Dockery, D. W., P. H. Stone (2007). "Cardiovascular Risks from Fine Particulate Air Pollution." N Engl J Med, 356: 511-513.

Dohnálek, Z., G. A. Kimmel, D. E. McCready, J. S. Young, A. Dohnálková, R. Scott Smith, B. D. Kay (2002). "Structural and Chemical Characterization of Aligned Crystalline Nanoporous MgO Films Grown via Reactive Ballistic Deposition." J. Phys. Chem. B., 106(14): 3526-3529.

Domingos, R. F., N. Tufenkji, K. J. Wilkinson (2009A). "Aggregation of Titanium Dioxide Nanoparticles: Role of a Fulvic Acid." Environmental Science & Technology, 43: 1282-1286.

Domingos, R. F., C. Peyrot, K. J. Wilkinson (2009B). "Aggregation of titanium dioxide nanoparticles: role of calcium and phosphate." Environmental Chemistry, 7(1): 61-66.

Domingos, R. F., M. A. Baalousha, Y. Ju-Nam, M. M. Reid, N. Tufenkji, J. R. Lead, G. G. Leppard, K. J. Wilkinson (2009C). "Characterizing Manufactured Nanoparticles in the Environment: Multimethod Determination of Particle Sizes." Environ. Sci. Technol., 43(19): 7277–7284.

Donaldson, K., X. Y. Li, W. MacNee (1998). "Ultrafine (nanometre) particle mediated lung injury." Journal of Aerosol Science, 29(5): 553-560.

Donaldson, K., V. Stone, A. Seaton, W. MacNee (2001). "Ambient particle inhalation and the cardiovascular system: potential mechanisms." Environmental Health Perspectives, 109(suppl. 4): 523–527.

Donaldson, K., R. Aitken, L. Tran, V. Stone, R. Duffin, G. Forrest, A. Alexander (2006). "Carbon nanotubes: a review of their properties in relation to pulmonary toxicology and workplace safety." Toxicol Sci, 92: 5–22.

Dong, P., Z.-L. Cao (2009). "Quantum computation with quantum-dot spin qubits inside a cavity." Physics Letters A, 373(17): 1527-1530.

Doucet, F. J., L. Maguire, J. R. Lead (2004). "Size fractionation of aquatic colloids and particles by cross-flow filtration: analysis by scanning electron and atomic force microscopy." Analytica Chimica Acta, 522(1): 59-71.

Dubochet, J., J. Lepault (1984). "Cryo-electron microscopy of vitrified water." Journal de Physique Colloques, 45(C7): 85-94.

233

Duguet, E., S. Vasseur, S. Mornet, J. M. Devoisselle (2006)." Magnetic nanoparticles and their applications in medicine." Nanomedicine, 1: 157-168.

Dumortier, H., S. Lacotte, G. Pastorin, R. Marega, W. Wu, D. Bonifazi, J. P. Briand, M. Prato, S. Muller, A. Bianco (2006). "Functionalized carbon nanotubes are non-cytotoxic and preserve the functionality of primary immune cells." Nanoletters, 6:1522-1528.

Duran, A., M. Tuzen, M. Soylak (2009). "Preconcentration of some trace elements via using multiwalled carbon nanotubes as solid phase extraction adsorbent." Journal of Hazardous Materials, 169(1-3): 466-471.

Dykman, L. A., L. Y. Matora, V. A. Bogatyrev (1996). "Use of colloidal gold to obtain antibiotin antibodies." Journal of Microbiological Methods, 24(3): 247-248.

Egerton, R. F. (2005). "Physical principles of electron microscopy: an introduction to TEM, SEM, and AEM." Springer.

Eiguren-Fernandez, A., A. H. Miguel, P. A. Jaques, C. Sioutas (2003). "Evaluation of a Denuder-MOUDI-PUF Sampling System to Measure the Size Distribution of Semi-Volatile Polycyclic Aromatic Hydrocarbons in the Atmosphere." Aerosol Science and Technology, 37(3): 201-209.

El Feninat, F., T. H. Ellis, E. Sacher, I. Stangel (2001). "A tapping mode AFM study of collapse and denaturation in dentinal collagen." Dental Materials, 17(4): 284-288.

Endoh, S., J. Maru, K. Uchida, K. Yamamoto, J. Nakanishi (2009). "Preparing samples for fullerene C60 hazard tests: Stable dispersion of fullerene crystals in water using a bead mill." Advanced Powder Technology, 20(6): 567-575.

EPA (Environment Protection Agency) (1998). "Permeable reactive barrier technologies for contaminant remediation." EPA 600/R-98/125, U.S. Environmental Protection Agency, Washington.

EPA (Environment Protection Agency) (2007). "Nanotechnology White Paper." Washington, USA.

Esawi, A. M. K., M. M. Farag (2006). "Carbon Nanotube Reinforced Composites: Potential and Current Challenges." Materials and Design, 28: 2394–2401.

Eslami, A., S. Nasseri, B. Yadollahi, A. Mesdaghinia, F. Vaezi, R. Nabizadeh, S. Nazmara (2008). "Photocatalytic degradation of methyl tert-butyl ether (MTBE) in contaminated water by ZnO nanoparticies." Journal of Chemical Technology and Biotechnology, 83: 1447-1453.

Fabrega, J., S. R. Fawcett, J. C. Renshaw, J. R. Lead (2009A). "Silver Nanoparticle Impact on Bacterial Growth: Effect of pH, Concentration, and Organic Matter." Environ. Sci. Technol., 43(19): 7285–7290.

Fabrega, J., J. C. Renshaw, J. R. Lead (2009B). "Interactions of Silver Nanoparticles with Pseudomonas putida Biofilms." Environ. Sci. Technol., 43(23): 9004–9009.

Fang, J., D. Y. Lyon, M. R. Wiesner, J. Dong, P. J. Alvarez (2007). "Effect of a fullerene water suspension on bacterial phospholipids and membrane phase behaviour." Environ. Sci. Technol., 41: 2636–2642.

Faraday, M. (1857). "Philosophical Transactions of the Royal Society of London." 147, p. 36.

Figuerola, A., R. Di Corato, L. Manna, T. Pellegrino (2010). "From iron oxide nanoparticles towards advanced iron-based inorganic materials designed for biomedical applications." Pharmacological Research, In Press, Corrected Proof, Available online 4 January 2010.

Firme, C. P., P. R. Bandaru (2010). "Toxicity issues in the application of carbon nanotubes to biological systems." Nanomedicine: Nanotechnology, Biology and Medicine, 6(2): 245-256.

Foldvari, M., M. Bagonluri (2008). "Carbon nanotubes as functional excipients for nanomedicines: I. pharmaceutical properties." Nanomedicine: Nanotechnology, Biology and Medicine, 4(3): 173-182.

Fortner, J. D., D. Y. Lyon, C. M. Sayes, A. M. Boyd, J. C. Falkner, E. M. Hotze, L. B. Alemany, Y. J. Tao, W. Guo, K. D. Ausman, V. L. Colvin, J. B. Hughes (2005). "C60 in water: nanocrystal formation and microbial response." Environ Sci Technol., 39(11): 4307-16.

Fotiadis, D., S. Scheuring, S. A. Müller, A. Engel, D. J. Müller (2002). "Imaging and manipulation of biological structures with the AFM." Micron, 33(4): 385-397.

Freitag, B., G. Knippels, S. Kujawa, P. C. Tiemeijer, M. Van der Stam, D. Hubert, C. Kisielowski, P. Denes, A. Minor, U. Dahmen (2008). "First performance measurements and application results of a new high brightness Schottky field emitter for HR-S/TEM at 80-300kV acceleration voltage." EMC, Vol. 1: Instrumentation and Methods (M. Luysberg, K. Tillmann, T. Weirich, Eds.), pp. 55–56, Springer-Verlag Berlin Heidelberg.

French, R. A., A. R. Jacobson, B. Kim, S. L. Isley, R. L. Penn, P. C. Baveye (2009). "Influence of Ionic Strength, pH, and Cation Valence on Aggregation Kinetics of Titanium Dioxide Nanoparticles." Environmental Science & Technology, 43: 1354-1359.

Friedbacher, G., M. Grasserbauer, Y. Meslmani, N. Klaus, M. J. Higatsberger (1995). "Investigation of Environmental Aerosol by Atomic Force Microscopy." Anal. Chem., 67(10): 1749–1754.

Friess, H., H. O. Muller (1939). Gasmaske 11: 1.

Gagne, F., J. Auclair, P. Turcotte, M. Fournier, C. Gagnon, S. Sauve, C. Blaise (2008). "Ecotoxicity of CdTe quantum dots to freshwater mussels: Impacts on immune system, oxidative stress and genotoxicity." Aquat. Toxicol., 86(3): 333-340.

Gan, Y. (2009). "Atomic and subnanometer resolution in ambient conditions by atomic force microscopy." Surface Science Reports, 64(3): 99-121.

Geys, J., A. Nemmar, E. Verbeken, E. Smolders, M. Ratoi, M. F. Hoylaerts, B. Nemery, P. H. M. Hoet (2008). "Acute Toxicity and Prothrombotic Effects of Quantum Dots: Impact of Surface Charge." Environmental Health Perspectives, 116(12): 1607-1613.

Gharbi, N., M. Pressac, M. Hadchouel, H. Szwarc, S. R. Wilson, F. Moussa (2005). "Fullerene is a powerful antioxidant in vivo with no acute or subacute toxicity." Nano Lett., 5(12): 2578–2585.

Giannuzzi, L. A., F. A. Stevie (1999). "A review of focused ion beam milling techniques for TEM specimen preparation." Micron, 30(3): 197-204.

Giasuddin, A. B. M., S. R. Kanel, H. Choi (2007). "Adsorption of humic acid onto nanoscale zerovalent iron and its effect on arsenic removal." Environmental Science & Technology, 41(6): 2022-2027.

Giessibl, F. J. (2005). "AFM's path to atomic resolution." Materials Today, 8(5): 32-41.

Giorgio, S., S. Sao Joao, S. Nitsche, D. Chaudanson, G. Sitja, C. R. Henry (2006). "Environmental electron microscopy (ETEM) for catalysts with a closed E-cell with carbon windows." Ultramicroscopy, 106(6): 503-507.

Global Industry Analysts, Inc. (2008). "Nanotechnology: a global strategic industry report." Global Industry Analysts, Inc., San Jose, CA.

Godehardt, R., W. Lebek, R. Adhikari, M. Rosenthal, C. Martin, S. Frangov, G. H. Michler (2004). "Optimum topographical and morphological information in AFM tapping mode investigation of multicomponent polyethylene." European Polymer Journal, 40(5): 917-926.

Grichko, V. P., O. A. Shenderova (2006). "Nanodiamond: Designing the Bio-Platform." Ultrananocrystalline Diamond, 529-557.

Griffitt, R. J., K. Hyndman, N. D. Denslow, D. S. Barber (2009). "Comparison of Molecular and Histological Changes in Zebrafish Gills Exposed to Metallic Nanoparticles." Toxicological Sciences, 107: 404-415.

Guo, L., P. H. Santschi (1997). "Composition and cycling of colloids in marine environments." Rev Geophys., 35: 17–40.

Guo, J., J. Ma (2006). "AFM study on the sorbed NOM and its fractions isolated from River Songhua." Water Research, 40(10): 1975-1984.

Guzman, K. A. D., M. P. Finnegan, J. F. Banfield (2006). "Influence of surface potential on aggregation and transport of titania nanoparticles." Environmental Science & Technology, 40: 7688-7693.

Gwaze, P., H. J. Annegarn, J. Huth, G. Helas (2007). "Comparison of particle sizes determined with impactor, AFM and SEM." Atmospheric Research, 86(2): 93-104.

Hamada, N., S. Sawada, A. Oshiyama (1992). „New one-dimensional conductors: graphitic microtubules." Physical Review Letters, 68: 1579-1581.

Handy, R. D., F. von der Kammer, J. R. Lead, M. Hassellov, R. Owen, M. Crane (2008). "The ecotoxicology and chemistry of manufactured nanoparticles." Ecotoxicology, 17: 287-314.

Hannah, D. M., D. Muirhead, J. R. Lead (2003). "Imaging of suspended macromolecules and colloids in glacial and alpine streams by atomic force microscopy." Journal of Glaciology, 49(167): 607-609.

Hardman, R. (2006). "A toxicologic review of quantum dots: Toxicity depends on physicochemical and environmental factors." Environmental Health Perspectives, 114: 165-172.

Hassellov, M., J. Readman, J. Ranville, K. Tiede (2008). "Nanoparticle analysis and characterization methodology in environmental risk assessment of engineered nanoparticles." Ecotoxicology, 17: 344–361.

He, Q. H., G. G. Leppard, C. R. Paige, W. J. Snodgrass (1996). "Transmission electron microscopy of a phosphate effect on the colloid structure of iron hydroxide." Water Research, 30(6): 1345-1352.

Helland, A., H. Kastenholz, A. Thidell, P. Arnfalk, K. Deppert (2006). "Nanoparticulate materials and regulatory policy in Europe: an analysis of stakeholder perspectives." J. Nanopart. Res., 8: 709–719.

Hennrich, F., R. Krupke, K. Arnold, J. A. R. Stutz, S. Lebedkin, T. Koch, T. Schimmel, M. M. Kappes (2007). "The mechanism of cavitation-induced scission of single-walled carbon nanotubes." Journal of Physical Chemistry B, 111(8): 1932-1937.

Hernández-Santos, D., M. B. González-García, A. Costa-García (2000). "Electrochemical determination of gold nanoparticles in colloidal solutions." Electrochimica Acta, 46(4): 607-615.

Hetherington, C. (2004). "Aberration correction for TEM." Materials Today, 7(12): 50-55.

Heymann, D., L. P. F. Chibante, R. E. Smalley (1995). "Determination of C60 and C70 fullerenes in geologic materials by high-performance liquid-chromatography." J. Chromatogr., A 689: 157–163.

Heymann, D. (1996). "Solubility of C60 and C70 in seven normal alcohols and their deduced solubility in water." Fuller. Nanotub. Carbon Nanostruct., 4: 509–515.

Hingston, T. J., M. R. Sambrook, K. Porfyrakis, G. A. D. Briggs (2006). "Synthesis of a short-chain fullerene dimer." Tetrahedron Letters, 47(42): 7413-7415.

Hu, H., A. Yu, E. Kim, B. Zhao, M. E. Itkis, E. Bekyarova, R. C. Haddon (2005). "Influence of the Zeta Potential on the Dispersability and Purification of Single-Walled Carbon Nanotubes." J. Phys. Chem. B, 109: 11520-11524.

Hu, N., G. Dang, H. Zhou, J. Jing, C. Chen (2007). "Efficient direct water dispersion of multi-walled carbon nanotubes by functionalization with lysine." Materials Letters, 61(30): 5285-5287.

Hu, J., C. Chen, X. Zhu, X. Wang (2009). "Removal of chromium from aqueous solution by using oxidized multiwalled carbon nanotubes." Journal of Hazardous Materials, 162(2-3): 1542-1550.

Huang, H.-C., G. L. Huang, H.-L. Chen. Y-D. Lee (2006). "Immobilization of TiO2 nanoparticles on Fe-filled carbon nanocapsules for photocatalytic applications." Thin Solid Films, 515: 1033-1037.

Huang, Q., X. Shi, R. A. Pinto, E. J Petersen, W. J. Weber (2008). "Tunable Synthesis and Immobilization of Zero-Valent Iron Nanoparticles for Environmental Applications." Environmental Science & Technology, 42: 8884-8889.

Huang, X., M. A. El-Sayed (2010). "Gold nanoparticles: Optical properties and implementations in cancer diagnosis and photothermal therapy." Journal of Advanced Research, 1(1): 13-28.

Hughes, G. A., (2005). "Nanostructure-mediated drug delivery." Nanomedicine: Nanotechnology, Biology and Medicine, 1(1): 22-30.

Hunter, K. A., P. S. Liss (1982). "Organic matter and the surface charge of suspended particles in estuarine waters." Limnology and Oceanography, 27: 322-335.

Hyung, H., J. D. Fortner, J. B. Hughes, J. H. Kim (2007). "Natural Organic Matter Stabilizes Carbon Nanotubes in the Aqueous Phase." Environ. Sci. Technol., 41(1): 179 -184.

Hyung, H., J.-H. Kim (2009). "Dispersion of C60 in natural water and removal by conventional drinking water treatment processes." Water Research, 43(9): 2463-2470.

IPCC (2001). J. T. Houghton, Y. Ding, D. J. Griggs, M. Noguer, J. van der Linden,X. Dai, K. Maskell, C. A. Johnson (Eds.). "Climate Change 2001: The Scientific Basis. Contribution of Working Group I to the Third Assessment Report of the Intergovernmental Panel on Climate Change." Cambridge University Press, Cambridge, UK.

Islam, M. F., E. Rojas, D. M. Bergey, A. T. Johnson, A. G. Yodh (2003). "High weight fraction surfactant solubilization of single-wall carbon nanotubes in water." Nano Letters, 3: 269–273.

ISO/TS 27687:2008, Nanotechnologies - Terminology and definitions for nano-objects.

Jalili, N., K. Laxminarayana (2004). "A review of atomic force microscopy imaging systems: application to molecular metrology and biological sciences." Mechatronics, 14(8): 907-945.

Jallouli, Y., A. Paillard, J. Chang, E. Sevin, D. Betbeder (2007). "Influence of surface charge and inner composition of porous nanoparticles to cross blood–brain barrier in vitro." International Journal of Pharmaceutics, 344(1-2): 103-109.

Jamieson, T., R. Bakhshi, D. Petrova, R. Pocock, M. Imani, A. M. Seifalian (2007). "Biological applications of quantum dots." Biomaterials, 28(31): 4717-4732.

Jandt, K. D., M. Finke, P. Cacciafesta (2000). "Aspects of the physical chemistry of polymers, biomaterials and mineralised tissues investigated with atomic force microscopy (AFM)." Colloids and Surfaces B: Biointerfaces, 19(4): 301-314.

Jiang, L., L. Gao, J. Sun (2003). "Production of aqueous colloidal dispersions of carbon nanotubes." Journal of Colloid and Interface Science, 260: 89–94.

Jiang, J. K., G. Oberdorster, P. Biswas (2009). "Characterization of size, surface charge, and agglomeration state of nanoparticle dispersions for toxicological studies." Journal of Nanoparticle Research, 11: 77-89.

Journet, C., W. K. Maser, P. Bernier, A. Loiseau, M. Lamy de La Chapelle, S. Lefrant, P. Deniard, R. Lee, J. E. Fischer (1997). "Large-scale production of single-walled carbon nanotubes by the electric-arc technique." Nature, 388(6644): 756-758.

Ju-Nam, Y., J. R. Lead (2008). „Manufactured nanoparticles: An overview of their chemistry, interactions and potential environmental implications." Science of the Total Environment, 400: 396-414.

Kang, B., M. A. Mackey, M. A. El-Sayed (2010). "Nuclear Targeting of Gold Nanoparticles in Cancer Cells Induces DNA Damage, Causing Cytokinesis Arrest and Apoptosis." J. Am. Chem. Soc., 132(5): 1517–1519.

Karajanagi, S. S., H. C. Yang, P. Asuri, E. Sellitto, J. S. Dordick, R. S. Kane (2006). "Protein-assisted solubilization of single-walled carbon nanotubes." Langmuir, 22: 1392–1395.

Keller, D. (1991). "Reconstruction of STM and AFM images distorted by finite-size tips." Surface Science, 253(1-3): 353-364.

Kim, J. S., E. Kuk, K. N. Yu, J. H. Kim, S. J. Park, H. J. Lee, S. H. Kim, Y. K Park, Y. H. Park, C. Y. Hwang, Y. K. Kim, Y. S. Lee, D. H. Jeong, M. H. Cho (2007). "Antimicrobial effects of silver nanoparticles." Nanomedicine-Nanotechnology Biology and Medicine, 3: 95-101.

Kittelson, D. B. (1998). "Engines and nanoparticles - a review." Journal of Aerosol Science, 29(5): 575-588.

Kittelson, D. B., W. Watts, J. Johnson (2001). "Fine Particle (nanoparticle) emissions on Minnesota highways." MN/RC Report No. 2001-12 for Minnesota Department of Transportation.

Ko, W.-B., J.-Y. Heo, J.-H. Nam, K.-B. Lee (2004). „Synthesis of a water-soluble fullerene [C60] under ultrasonication." Ultrasonics, 41(9): 727-730.

Köllensperger, G., G. Friedbacher, A. Krammer, M. Grasserbauer (1999). "Application of atomic force microscopy to particle sizing." Fresenius J Anal Chem, 363(4): 323 – 332.

Koukal, B., C. Gueguen, M. Pardos, J. Dominik (2003). "Influence of humic substances on the toxic effects of cadmium and zinc to the green alga Pseudokirchneriella subcapitata." Chemosphere, 53(8):953-961.

Koukal, B., P. Rosse, A. Reinhardt, B. Ferrari, K. J. Wilkinson, J.-L. Loizeau, J. Dominik (2007). "Effect of Pseudokirchneriella subcapitata (Chlorophyceae) exudates on metal toxicity and colloid aggregation." Water Research, 41(1): 63-70.

Kulmala, M., H. Vehkamaki, T. Petaja, M. Dal Maso, A. Lauri, V. M. Kerminen, W. Birmili, P. H. McMurry (2004). "Formation and growth rates of ultrafine atmospheric particles: a review of observations." Journal of Aerosol Science, 35(2): 143-176.

Kumar, A. P., D. Depan, N. S. Tomer, R. P. Singh (2009). "Nanoscale Particles for Polymer Degradation and Stabilization – Trends and Future Perspectives." Progress in Polymer Science In Press.

Kvitek, L., M. Vanickova, A. Panacek, J. Soukupova, M. Dittrich, E. Valentova, R. Prucek, M. Bancirova, D. Milde, R. Zboril (2009). "Initial Study on the Toxicity of Silver Nanoparticles (NPs) against Paramecium caudatum." Journal of Physical Chemistry C, 113: 4296-4300.

Kwon, J., Y.-S. Kim, K. Yoon, S.-M. Lee, S. Park (2005). "Advanced nanoscale metrology of pole-tip recession with AFM." Ultramicroscopy, 105(1-4): 51-56.

Labar, J. L., R. Egerton (1999). "Special issue on Ion Beam Techniques." Micron, 30(3): 195-196.

Labille, J., A. Masion, F. Ziarelli, J. Rose, J. Brant, F. Villieras, M. Pelletier, D. Borschneck, M. R. Wiesner, J.-Y. Bottero (2009). "Hydration and Dispersion of C-60 in Aqueous Systems: The Nature of Water-Fullerene Interactions." Langmuir, 25(19): 11232-11235.

Lam, C. W., J. T. James, R. McCluskey, R. L. Hunter (2003). "Pulmonary Toxicity of Single-Wall Carbon Nanotubes in Mice 7 and 90 Days After Intratracheal Instillation." Toxicological Sciences, 77: 126–134.

Lead, J. R., J. Hamilton-Taylor, W. Davison, M. Harper (1999). "Trace metal sorption by natural particles and coarse colloids." Geochimica et Cosmochimica Acta, 63(11/12): 1661-1670.

Lead, J. R., D. Muirhead, C. T. Gibson (2005). "Characterisation of freshwater natural aquatic colloids by atomic force microscopy (AFM)." Environ. Sci. and Technol., 39: 6930-6936.

Lead, J. R., K. J. Wilkinson (2006A). "Aquatic Colloids and Nanoparticles: Current Knowledge and Future Trends." Environ. Chem., 3: 159–171.

Lead, J. R., K. J. Wilkinson (2006B). "Environmental Colloids and Particles: Behaviour, Structure and Characterisation." (Eds K. J. Wilkinson, J. R. Lead), Vol. 10, John Wiley and Sons: Chichester.

Lecoanet, H. F., J. Y. Bottero, M. R. Wiesner (2004). "Laboratory assessment of the mobility of nanomaterials in porous media." Environ. Sci. Technol., 38: 5164–5169.

Lee, J., M. Kim, C. K. Hong, S. E. Shim (2007). "Measurement of the dispersion stability of pristine and surface-modified multiwalled carbon nanotubes in various nonpolar and polar solvents." Measurement Science and Technology, 18: 3707–3712.

Leppard, G. G., B. K. Burnison, J. Buffle (1990). "Transmission electron microscopy of the natural organic matter of surface waters."Analytica Chimica Acta, 232: 107-121.

Li, Y., Y. Huang, S. Du, R. Liu (2001). „Structures and stabilities of C60-rings." Chemical Physics Letters, 335(5-6): 524-532.

Li, Y. H., S. Wang, J. Wei, X. Zhang, C. Xu, Z. Luan, D. Wu, B. Wei (2002). "Lead adsorption on carbon nanotubes." Chem. Phys. Lett., 357: 263–266.

Li, W., H. Zhao, P. R. Teasdale, R. John, F. Wang (2005). "Metal speciation measurement by diffusive gradients in thin films technique with different binding phases." Analytica Chimica Acta, 533(2): 193-202.

Li, J. J., L. Zou, D. Hartono, C. N. Ong, B. H. Bay, L. Y. L. Yung (2008A). "Gold nanoparticles induce oxidative damage in lung fibroblasts in vitro." Advanced Materials, 20: 138-+.

Li, M., M. Boggs, T. P. Beebe, C. P. Huang (2008B). "Oxidation of single-walled carbon nanotubes in dilute aqueous solutions by ozone as affected by ultrasound." Carbon, 46(3): 466-475.

Li, Q. L., S. Mahendra, D. Y. Lyon, L. Brunet, M. V. Liga, D. Li, P. J. J. Alvarez (2008C). "Antimicrobial nanomaterials for water disinfection and microbial control: Potential applications and implications." Water Research, 42: 4591-4602.

Li, Y., Q. Yue, B. Gao, Q. Li, C. Li (2008D). "Adsorption thermodynamic and kinetic studies of dissolved chromium onto humic acids." Colloids and Surfaces B: Biointerfaces, 65(1): 25-29.

Liang, P., Y. Liu, L. Guo, J. Zeng, H. B. Lu (2004). "Multiwalled carbon nanotubes as solid-phase extraction adsorbent for the preconcentration of trace metal ions and their determination by inductively coupled plasma atomic emission spectrometry." J. Anal. At. Spectrom., 19: 1489–1492.

Liang, P., Q. Ding, F. Song (2005). "Application of multiwalled carbon nanotubes as solid phase extraction sorbent for preconcentration of trace copper in water samples." J. Sep. Sci., 28: 2339–2343.

Lienemann, C. P., M. Taillefert, D. Perret, J. Gaillard (1997). "Association of cobalt and manganese in aquatic systems: Chemical and microscopic evidence." Geochimica et Cosmochimica Acta, 61(7): 1437-1446.

Lienemann, C. P., A. Heissenberger, G. G. Leppard, D. Perret (1998). "Optimal preparation of water samples for the examination of colloidal material by transmission electron microscopy." Aquat. Microb. Ecol., 14: 205-213.

Lin, W., Y.-W. Huang, X.-D. Zhou, Y. Ma (2006). "Toxicity of cerium oxide nanoparticles in human lung cancer cells." Int. J. Toxicol., 25: 451–457.

Liu, A., R. C. Wu, E. Eschenazi, K. Papadopoulos (2000). „AFM on humic acid adsorption on mica." Colloids and Surfaces A: Physicochemical and Engineering Aspects, 174(1-2): 245-252.

Liu, W. (2005). "Catalyst technology development from macro-, micro- down to nanoscale." China Particuology, 3(6): 383-394.

Liu, Y., P. Liang, H. Y. Zhang, D. S. Guo (2006). "Cation-controlled aqueous dispersions of alginic-acid-wrapped multi-walled carbon nanotubes." Small, 2: 874–878.

Lok, C. N., C. M. Ho, R. Chen, Q. Y. He, W. Y. Yu, H. Sun, P. K. H. Tam, J. F. Chiu, C. M. Che. (2007). "Silver nanoparticles: partial oxidation and antibacterial activities." Journal of Biological Inorganic Chemistry, 12: 527-534.

Long, R. Q., R. T. Yang (2001). "Carbon nanotubes as superior sorbent for dioxin removal." J. Am. Chem. Soc., 123: 2058–2059.

Lopez, N., T. V. W. Janssens, B. S. Clausen, Y. Xu, M. Mavrikakis, T. Bligaard, J. K. Nørskov (2004). "On the origin of the catalytic activity of gold nanoparticles for low-temperature CO oxidation." Journal of Catalysis, 223: 232–235

Lovern, S. B., R. Klaper (2006). "Daphnia magna mortality when exposed to titanium dioxide and fullerene (C60) nanoparticles." Environ. Toxicol. Chem., 25: 1132–1137.

Lu, C., C. Liu (2006). "Removal of nickel(II) from aqueous solution by carbon nanotubes." J Chem Technol Biotechnol, 81: 1932–1940.

Lu, Y., X. Lu, B. T. Mayers, T. Herricks, Y. Xia (2008A). "Synthesis and characterization of magnetic Co nanoparticles: A comparison study of three different capping surfactants." Journal of Solid State Chemistry, 181(7): 1530-1538.

Lu, Z. S., C. M. Li, H. F. Bao, Y. Qiao, Y. H .Toh, X. Yang (2008B). "Mechanism of antimicrobial activity of CdTe quantum dots." Langmuir, 24(10): 5445-5452.

Lyon, D. Y., J. D. Fortner, C. M. Sayes, V. L. Colvin, J. B. Hughe (2005). "Bacterial cell association and antimicrobial activity of a C60 water suspension." Environ. Toxicol. Chem., 24(11): 2757–2762.

Lyon, D. Y., L. K. Adams, J. C. Falkner, P. J. Alvarez (2006). "Antibacterial activity of fullerene water suspensions: effects of preparation method and particle size." Environ. Sci. Technol., 40(14): 4360-6.

Lyon, D. Y., L. Brunet, G. W. Hinkal, M. R. Wiesner, P. J. Alvarez (2008). "Antibacterial activity of fullerene water suspensions (nC60) is not due to ROS-mediated damage." Nano Lett., 8: 1539–1543.

Lyubchenko, Y. L., L. S. Shlyakhtenko (2009). "AFM for analysis of structure and dynamics of DNA and protein–DNA complexes." Methods, 47(3): 206-213.

Lyven, B., M. Hassellov, D. R. Turner, C. Haraldsson, K. Andersson (2003). "Competition Between Iron- and Carbon-Based Colloidal Carriers for Trace Metals in a Freshwater Assessed Using Flow Field-Flow Fractionation Coupled to ICPMS." Geochim. Cosmochim. Acta, 67: 3791-3802.

Markovic, Z., B. Todorovic-Markovic, D. Kleut, N. Nikolic, S. Vranjes-Djuric, M. Misirkic, L. Vucicevic, K. Janjetovic, A. Isakovic, L. Harhaji, B. Babic-Stojic, M. Dramicanin, V. Trajkovic (2007). "The mechanism of cell-damaging reactive oxygen generation by colloidal fullerenes." Biomaterials, 28: 5437–5448.

Marple, V. A., K. L. Rubow, S. M. Behm (1991). "Amicroorifice uniform deposit impactor (MOUDI): Description, calibration, and use." Aerosol Science and Technology, 14: 434–446.

Marple, V. A., K. L. Rubow, B. A. Olson (1992). "Inertial, Gravitational, Centrifugal and Thermal Collection Techniques, Chapter 12: Aerosol Measurement: Principles, Techniques and Applications." (Eds. K. Willeke and P. A. Baron).

Martin, Y., C. C. Williams, H. K. Wickramasinghe (1987). "Atomic Force Microscope - force mapping and profiling on a sub 100-A scale." Journal of Applied Physics, 61(10): 4723-4729.

Martin, J. M., M. H. Dai (1995). "Significance of colloids in the biogeochemical cycling of organic carbon and trace metals in the Venice Lagoon (Italy)." Limnol. Oceanogr., 40(1): 119-131.

Maury, P. A., D. N. Reinhoudt, J. Huskens (2008). "Assembly of nanoparticles on patterned surfaces by noncovalent interactions." Current Opinion in Colloid & Interface Science, 13(1-2): 74-80.

Mavrocordatos, D., R. Kaegi, V. Schmatloch (2002). "Fractal analysis of wood combustion aggregates by contact mode atomic force microscopy." Atmospheric Environment, 36(36-37): 5653-5660.

McMurry, P. H., K. S. Woo, R. Weber, D.-R. Chen, D. Y. H. Pui (2000). "Size distributions of 3-10 nm atmospheric particles: implications for nucleation mechanisms." Phil Trans Roy Soc of London A, 358(1775): 2625-2642.

Medarova, Z., W. Pham, C. Farrar, V. Petkova, A. Moore (2007). "In vivo imaging of siRNA delivery and silencing in tumors." Nature Medicine, 13: 372-377.

Michalowski, J., P. Halaburda, A. Kojlo (2001). "Determination of humic acid in natural waters by flow injection analysis with chemiluminescence detection." Analytica Chimica Acta, 438(1-2): 143-148.

Mitchnick, M. A., D. Fairhurst, S. R. Pinnell (1999). "Microfine zinc oxide (Z-cote) as a photostable UVA/UVB sunblock agent." Journal of the American Academy of Dermatology, 40: 85–90.

Moleski, R., E. Leontidis, F. Krumeich (2006). "Controlled production of ZnO nanoparticles from zinc glycerolate in a sol–gel silica matrix." Journal of Colloid and Interface Science, 302(1): 246-253.

Mondain-Monval, O. (2005). "Freeze fracture TEM investigations in liquid crystals." Current Opinion in Colloid & Interface Science, 10(5-6): 250-255.

Morita, S., R. Wiesendanger, E. Meyer (2002). "Noncontact Atomic Force Microscopy." vol. 2, Springer.

Mornet, S., S. Vasseur, F. Grasset, P. Veverka, G. Goglio, A. Demourgues, J. Portier, E. Pollert, E. Duguet (2006). "Magnetic nanoparticle design for medical applications." Progress in Solid State Chemistry, 34(2-4): 237-247.

Morones, J. R., J. L. Elechiguerra, A. Camacho, K. Holt, J. B. Kouri, J. T. Ramírez, M. J. Yacaman (2005). "The bactericidal effect of silver nanoparticles." Nanotechnology, 16: 2346-2353.

Mouchet, F., P. Landois, E. Sarremejean, G. Bernard, P. Puech, E. Pinelli, E. Flahaut, L. Gauthier (2008). "Characterisation and in vivo ecotoxicity evaluation of double-wall carbon nanotubes in larvae of the amphibian Xenopus laevis." Aquatic Toxicology, 87(2): 127-137.

Mueller, N. C., B. Nowack (2008). "Exposure Modeling of Engineered Nanoparticles in the Environment." Environmental Science & Technology, 42: 4447-4453.

Muller, J., M. Delos, N. Panin, V. Rabolli, F. Huaux, D. Lison (2009). "Absence of Carcinogenic Response to Multiwall Carbon Nanotubes in a 2-Year Bioassay in the Peritoneal Cavity of the Rat." Toxicological Sciences, 110(2): 442-448.

Murr, L. E. (2009). "Imaging systems and materials characterization." Materials Characterization, 60(5): 397-414.

Murr, L. E., K. M. Garza (2009). "Natural and anthropogenic environmental nanoparticulates: Their microstructural characterization and respiratory health implications." Atmospheric Environment, 43(17): 2683-2692.

Murray, A. R., E. Kisin, S. S. Leonard, S. H. Young, C. Kommineni, V. E. Kagan, V. Castranova, A. A. Shvedova (2009). "Oxidative stress and inflammatory response

in dermal toxicity of single-walled carbon nanotubes." Toxicology, 257(3): 161-171.

Nagarajan, R., T. Alan Hatton (2008). "Nanoparticles Synthesis, Stabillization, Passivation and Functionalization." Oxford University Press, USA.

National Nanotechnology Initiative (2006). "Environmental, Health and Safety Research Needs for Engineered Nanoscale Materials." US National Science and Technology Council, Arlington, VA, USA.

Navarro, E., F. Piccapietra, B. Wagner, F. Marconi, R. Kaegi, N. Odzak, L. Sigg, R. Behra (2008). "Toxicity of Silver Nanoparticles to Chlamydomonas reinhardtii." Environmental Science & Technology, 42: 8959-8964.

Nemmar, A., H. Vanbilloen, M. F. Hoylaerts, P. H. M. Hoet, A. Verbruggen, B. Nemery (2001). "Passage of Intratracheally Instilled Ultrafine Particles from the Lung into the Systemic Circulation in Hamster." Am. J. Respir. Crit. Care Med., 164(9): 1665-1668.

Nemmar, A., P. H. Hoet, B. Vanquickenborne, D. Dinsdale, M. Thomeer, M. F. Hoylaerts, H. Vanbilloen, L. Mortelmans, B. Nemery (2002). "Passage of inhaled particles into the blood circulation in humans." Circulation, 105(4): 411-4.

Newman, M. D., M. Stotland, J. I. Ellis (2009). "The safety of nanosized particles in titanium dioxide– and zinc oxide–based sunscreens." Journal of the American Academy of Dermatology, 61(4): 685-692.

Niu, J. L., A. Azfer, L. M. Rogers, X. H. Wang, P. E. Kolattukudy (2007). "Cardioprotective effects of cerium oxide nanoparticles in a transgenic murine model of cardiomyopathy." Cardiovasc. Res., 73: 549–559.

Nohynek, G. J., E. K. Dufour, M.S Roberts (2008). "Nanotechnology, cosmetics and the skin: Is there a health risk?" Skin Pharmacology and Physiology, 21(3): 136-149.

Noubactep, C. (2009). "Metallic iron for environmental remediation: Learning from the Becher process." Journal of Hazardous Materials, 168(2-3): 1609-1612.

Nowack, B., T. D. Bucheli (2007). „Occurrence, behavior and effects of nanoparticles in the environment." Environmental Pollution, 150: 5-22.

NPCA (2008). Norwegian Pollution Control Authority, "Environmental fate and ecotoxicity of engineered nanoparticles." Report no. TA 2304/2007. Eds.: E. J. Joner, T. Hartnik and C. E. Amundsen. Bioforsk.

Oberdorster, G. (1996). "Significance of particle parameters in the evaluation of exposure – dose response relationships of inhaled particles." Inhalation Toxicology, 8: 73–89.

Oberdorster, E. (2004). "Manufactured nanomaterials (fullerenes, C60) induce oxidative stress in brain of juvenile largemouth bass." Environ. Health Persp., 112: 1058–1062.

Oberdorster, G., E. Oberdorster, J. Oberdorster (2005). "Nanotoxicology: An Emerging Discipline Evolving from Studies of Ultrafine Particles." Environmental Health Perspectives, 113(7): 823-839.

Oberdörster, E., S. Zhu, T. M. Blickley, P. McClellan-Green, M. Haasch (2006). "Ecotoxicology of carbon-based engineered nanoparticles: effects of fullerene (C60) on aquatic organisms." Carbon, 44: 1112–1120.

Obst, M., P. Gasser, D. Mavrocordatos, M. Dittrich (2005). "Title: TEM-specimen preparation of cell/mineral interfaces by Focused Ion Beam milling." American Mineralogist, 90(8-9): 1270-1277.

O'Connell, M. J., S. M. Bachilo, C. B. Huffman, V. C. Moore, M. S. Strano, E. H. Haroz, K. L. Rialon, P. J. Boul, W. H. Noon, C. Kittrell, J. Ma, R. H. Hauge, R. B. Weisman, R. E. Smalley (2002). "Band gap fluorescence from individual single-walled carbon nanotubes." Science, 297: 593-596.

Padmavathy, N., R. Vijayaraghavan (2008). "Enhanced bioactivity of ZnO nanoparticles-an antimicrobial study." Science and Technology of Advanced Materials, 9: 1-7.

Pal, S., Y. K. Tak, J. M. Song (2007). "Does the antibacterial activity of silver nanoparticles depend on the shape of the nanoparticle? A study of the gram-negative bacterium Escherichia coli." Applied and Environmental Microbiology, 73: 1712-1720.

Paloniemi, H., T. Aaritalo, T. Laiho, H. Liuke, N. Kocharova, K. Haapakka, F. Terzi, R. Seeber, J. Lukkari (2005). „Water-soluble full-length single-wall carbon nanotube polyelectrolytes: Preparation and characterization." Journal of Physical Chemistry B, 109(18): 8634-8642.

Panyala, N. R., E. M. Pena-Mendez, J. Havel (2009). "Gold and nano-gold in medicine: overview, toxicology and perspectives." J Appl Biomed, 7: 75–91.

Papastefanou, C. (2007) "Radioactive aerosols." "Radioactivity in the environment, v 12." (M. Baxter, Ed) Elsevier.

Paradise, M., T. Goswami (2007). "Carbon nanotubes – Production and industrial applications." Materials and Design, 28(5): 1477-1489.

Park, J., K. J. An, Y. S. Hwang, J. G. Park, H. J. Noh, J. Y. Kim, J. H. Park, N. M. Hwang, T. Hyeon (2004). "Ultra-large-scale syntheses of monodisperse nanocrystals." Nature Materials, 3(12): 891–895.

Park, J.-H., J.-G. Park (2006). "Synthesis of ultrawide ZnO nanosheets." Current Applied Physics, 6(6): 1020-1023.

Park, E.-J., J. Choi, Y.-K. Park, K. Park (2008). "Oxidative stress induced by cerium oxide nanoparticles in cultured BEAS-2B cells." Toxicology, 245(1-2): 90-100.

Park, K., J. Y. Park, S. Lee, J. Cho (2009). "Measurement of size and number of suspended and dissolved nanoparticles in water for evaluation of colloidal fouling in RO membranes." Desalination, 238(1-3): 78-89.

PAS 71:2005, Vocabulary - Nanoparticles.

Patil, S., A. Sandberg, E. Heckert, W. Self, S. Seal (2007). "Protein adsorption and cellular uptake of cerium oxide nanoparticles as a function of zeta potential." Biomaterials, 28(31): 4600-4607.

Patra, H. K., S. Banerjee, U. Chaudhuri, P. Lahiri, A. K. Dasgupta (2007). "Cell selective response to gold nanoparticles." Nanomedicine-Nanotechnology Biology and Medicine, 3: 111-119.

PCAST (The President's Council of Advisors on Science and Technology) (2010). "Report to the President and Congress on the Third Assessment of the National Nanotechnology Initiative."

Peng, G., U. Tisch, O. Adams, M. Hakim, N. Shehada, Y. Y. Broza, S. Billan, R. Abdah-Bortnyak, A. Kuten, H. Haick (2009). "Diagnosing lung cancer in exhaled breath using gold nanoparticles." Nature Nanotechnology, 4: 669-673.

Percival, S. L., P. G. Bowler, D. Russell (2005). "Bacterial resistance to silver in wound care." Journal of Hospital Infection, 60(1): 1-7.

Perez, S., M. la Farre, D. Barcelo (2009). „Analysis, behavior and ecotoxicity of carbon-based nanomaterials in the aquatic environment." Trends in Analytical Chemistry, 28(6): 820-832.

Perret, D., G. G. Leppard, M. Müller, N. Belzile, R. De Vitre, J. Buffle (1991). "Electron microscopy of aquatic colloids: Non-perturbing preparation of specimens in the field." Water Research, 25(11): 1333-1343.

Peters, A., H. E. Wichmann, T. Tuch, J. Heinrich, J. Heyder (1997). "Respiratory effects are associated with the number of ultrafine particles." Am J Respir Crit Care Med., 155(4): 1376-83.

Plaschke, M., J. Römer, R. Klenze, J. I. Kim (1999). "In situ AFM study of sorbed humic acid colloids at different pH." Colloids and Surfaces A: Physicochemical and Engineering Aspects, 160(3): 269-279.

Poland, C. A., R. Duffin, I. Kinloch, A. Maynard, W. A. Wallace, A. Seaton, V. Stone, S. Brown, W. MacNee, K. Donaldson (2008). "Carbon nanotubes introduced into the abdominal cavity of mice show asbestos-like pathogenicity in a pilot study." Nat Nanotechnol, 3: 423-8.

Posfai, M., H. F. Xu, J. R. Anderson, P. R. Buseck (1998). "Wet and dry sizes of atmospheric aerosol particles: An AFM-TEM study." Geophysical Research Letters, 25(11): 1907-1910.

Pourret, O., M. Davranche, G. Gruau, A. Dia (2007). "Rare earth elements complexation with humic acid." Chemical Geology, 243(1-2): 128-141.

Powell, M., M. Griffin, S. Tai (2008). "Bottom-Up Risk Regulation? How Nanotechnology Risk Knowledge Gaps Challenge Federal and State Environmental Agencies." Environmental Management, 42: 426-443.

Pyrzynska, K. (2010). "Carbon nanostructures for separation, preconcentration and speciation of metal ions." TrAC Trends in Analytical Chemistry, In Press, Corrected Proof, Available online 4 May 2010.

Qiu, S., S. J. Kalita (2006). "Synthesis, processing and characterization of nanocrystalline titanium dioxide." Materials Science and Engineering: A, 435-436: 327-332.

Quate, C. F. (1994). "The AFM as a tool for surface imaging." Surface Science, 299-300: 980-995.

Quintana, C. (1997). "Ultramicrotomy for cross-sections of nanostructure." Micron, 28(3): 217-219.

Rai, M., A. Yadav, A. Gade (2009). "Silver nanoparticles as a new generation of antimicrobials." Biotechnology Advances, 27(1): 76-83.

Ramirez-Aguilar, K. A., D. W. Lehmpuhl, A. E. Michel, J. W. Birks, K. L. Rowlen (1999). "Atomic force microscopy for the analysis of environmental particles." Ultramicroscopy, 77(3-4): 187-194.

Rao, C. N. R., A. Govindaraj, G. Gundiah, S. R. C. Vivekchand (2004). "Nanotubes and nanowires." Chemical Engineering Science, 59(22-23): 4665-4671.

Rao, G. P., C. Lu, F. Su (2007). "Sorption of divalent metal ions from aqueous solution by carbon nanotubes: A review." Separation and Purification Technology, 58(1): 224-231.

Ratte, H. T. (1999). "Bioaccumulation and toxicity of silver compounds: A review." Environmental Toxicology and Chemistry, 18: 89-108.

Rejeski, D. (2009 A). "Nanotech-enabled Consumer Products Top the 1,000 Mark." Project on Emerging Nanotechnologies (PEN), 25 August (http://www.nanotechproject.org/pressroom/).

Rejeski, D. (2009 B). "Nanotechnology and Consumer Products." Project on Emerging Nanotechnologies (PEN), 25 August (http://www.nanotechproject.org/pressroom/).

Renwick, L. C., K. Donaldson, A. Clouter (2001). "Impairment of Alveolar Macrophage Phagocytosis by Ultrafine Particles." Toxicology and Applied Pharmacology, 172: 119–127.

Reyes-Gasga, J., R. Garcia-Garcia (2002). "Analysis of the electron-beam radiation damage of TEM samples in the acceleration energy range from 0.1 to 2 MeV using the standard theory for fast electrons." Radiation Physics and Chemistry, 64(5-6): 359-367.

Roberts, K. A., P. H. Santschi, G. G. Leppard, M. M. West (2004). "Characterization of organic-rich colloids from surface and ground waters at the actinide-contaminated Rocky Flats Environmental Technology Site (RFETS), Colorado, USA." Colloids and Surfaces A: Physicochemical and Engineering Aspects, 244(1-3): 105-111.

Roberts, A. P., A. S. Mount, B. Seda, J. Souther, R. Qiao, S. Lin, P. C. Ke, A. M. Rao, S. J. Klaine (2007). "In vivo biomodification of lipid-coated carbon nanotubes by Daphnia magna." Environ Sci Technol, 41(8): 3025–3029.

Roco, M. C. (2005). "Environmentally responsible development of nanotechnology." Environ. Sci. Technol., 39: 106A–112A.

Roco, M. C. (2006). "Nanotechnology's Future." Sientific American, Forum, August issue.

Royal Society & The Royal Academy of Engineering (2004). "Nanoscience and nanotechnologies: opportunities and uncertainties."

Rugar, D., P. Hansma (1990). "Atomic Force Microscopy." Phys. Today, 43(10): 23.

Ruiz, T., I. Erk, J. Lepault (1994). "Electron cryo-microscopy of vitrified biological specimens: towards high spatial and temporal resolution." Biology of the Cell, 80(2-3): 203-210.

Sambhy, V., M. M. MacBride, B. R. Peterson (2006). "Silver bromide nanoparticle/polymer composites: dual action tunable antimicrobial materials." J. Am. Chem. Soc., 128: 9798–9808.

Samet, J. M., F. Dominici, F. C. Curriero, I. Coursac, S. L. Zeger (2000). "Fine Particulate Air Pollution and Mortality in 20 U.S. Cities, 1987–1994." N Engl J Med, 343: 1742-1749.

San Paulo, A., R. García (2000). "High-Resolution Imaging of Antibodies by Tapping-Mode Atomic Force Microscopy: Attractive and Repulsive Tip-Sample Interaction Regimes." Biophysical Journal, 78: 1599–1605.

Sano, M., J. Okamura, S. Shinkai (2001). "Colloidal nature of single-walled carbon nanotubes in electrolyte solution: the Schulze–Hardy rule." Langmuir, 17: 7172–7173.

Savolainen, K., H. Alenius, H. Norppa, L. Pylkkänen, T. Tuomi, G. Kasper (2010). "Risk assessment of engineered nanomaterials and nanotechnologies—A review." Toxicology, 269(2-3): 92-104.

Sayes, C. M., A. M. Gobin, K. D. Ausman, J. Mendez, J. L. West, V. L. Colvin (2005). "Nano-C60 cytotoxicity is due to lipid peroxidation." Biomaterials, 26: 7587–7595.

Sayes, C. M., F. Liang, J. L. Hudson, J. Mendez, W. Guo, J. M. Beach, V. C. Moore, C. D. Doyle, J. L. West, W. E. Billups, K. D. Ausman, V. L. Colvin (2006). "Functionalization density dependence of single-walled carbon nanotubes cytotoxicity in vitro." Toxicol Lett, 161: 135-142.

Sayes, C. M., A. A. Marchione, K. L. Reed, D. B. Warheit (2007). "Comparative pulmonary toxicity assessments of C60 water suspensions in rats: few differences in fullerene toxicity in vivo in contrast to in vitro profiles". Nano Lett., 7(8): 2399–2406.

SCENIHR (2006). Scientific Committee on Emerging and Newly Identified Health Risks, European Commission, Health and Consumer Protection Directorate-General. "Opinion on the appropriateness of existing methodologies to assess the potential risks associated with engineered and adventitious products of nanotechnologies." modified opinion (after public consultation).

SCENIHR (2009). Scientific Committee on Emerging and Newly Identified Health Risks. European Commission, Health and Consumer Protection Directorate-General. "Risk Assessment of Products of Nanotechnologies." European Commission, Brussels, Belgium.

Schierz, A., H. Zaenker (2009) "Aqueous suspensions of carbon nanotubes: Surface oxidation, colloidal stability and uranium sorption." Environmental Pollution, 157: 1088–1094.

Schmitz, I., M. Schreiner, G. Friedbacher, M. Grasserbauer (1997). "Phase imaging as an extension to tapping mode AFM for the identification of material properties on humidity-sensitive surfaces." Applied Surface Science, 115(2): 190-198(9).

Schneider, R. (2002). "High-resolution analytical TEM of nanostructured materials." Anal Bioanal Chem, 374: 639–645.

Schubert, D., R. Dargusch, J. Raitano, S. W. Chan (2006). "Cerium and yttrium oxide nanoparticles are neuroprotective." Biochem. Biophys. Res. Commun., 342: 86–91.

Sealy, C. (2008). "Carbon nanotubes could be as harmful as asbestos: Nanotechnology." Materials Today, 11(7-8): 10.

Seaton, A., W. MacNee, K. Donaldson, D. Godden (1995). "Particulate air pollution and acute health effects." The Lancet, 345: 176–178.

Seinfeld, J. H., S. N. Pandis (1998). "Atmospheric Chemistry and Physics: From Air Pollution to Climate Change." Wiley-Interscience, New York, p. 1326.

Service, R. F. (1998). "Nanotubes: The next asbestos?" Science, 281(5379): 941.

Service, R. F. (2005). "Nanotechnology Takes Aim at Cancer." Science, 310: 1132 – 1134.

Shi, J. P., A. A. Khan, R. M. Harrison (1999). "Measurements of ultrafine particle concentration and size distribution in the urban atmosphere." The Science of The Total Environment, 235(1-3): 51-64.

Shi, J. P., D. E. Evans, A. A. Khan, R. M. Harrison (2001). "Sources and concentration of nanoparticles (<10nm diameter) in the urban atmosphere." Atmospheric Environment, 35(7): 1193-1202.

Shmaefsky, B. R. (2006). "Science 101. Biotechnology 101." 1 edition, Greenwood.

Shukla, R., V. Bansal, M. Chaudhary, A. Basu, R. R. Bhonde, M. Sastry (2005). "Biocompatibility of gold nanoparticles and their endocytotic fate inside the cellular compartment: A microscopic overview." Langmuir, 21: 10644-10654.

Shvedova, A. A., V. Castranova, E. R. Kisin, D. Schwegler-Berry, A. R. Murray, V Z. Gandelsman, A. Maynard, P. Baron (2003). "Exposure to carbon nanotube material: assessment of nanotube cytotoxicity using human keratinocyte cells." J Toxicol Environ Health A, 66(20): 1909-26.

Shvedova, A. A., E. Kisin, A. R. Murray, V. J. Johnson, O. Gorelik, S. Arepalli, A. F. Hubbs, R. R. Mercer, P. Keohavong, N. Sussman, J. Jin, J. Yin, S. Stone, B. T. Chen, G. Deye, A. Maynard, V. Castranova, P. A. Baron, V. E. Kagan (2008). "Inhalation vs. aspiration of single-walled carbon nanotubes in C57BL/6 mice: inflammation, fibrosis, oxidative stress, and mutagenesis." Am J Physiol Lung Cell Mol Physiol, 295: L552–L565.

Siegrist, M., A. Wiek, A. Helland, H. Kastenholz (2007). "Risks and nanotechnology: the public is more concerned than experts and industry." Nat. Nanotechnol., 2: 67.

Singh, G., L. F. Song (2007). "Experimental correlations of pH and ionic strength effects on the colloidal fouling potential of silica nanoparticles in crossflow ultrafiltration." J. Membr. Sci., 303: 112-118.

Sioutas, C., R. J. Delfino, M. Singh (2005). "Exposure Assessment for Atmospheric Ultrafine Particles (UFPs) and Implications in Epidemiologic Research." Environ Health Perspect, 113(8): 947–955.

Slayter, E. M., H. S. Slayter (1992). "Light and electron microscopy." Cambridge University Press.

Smith, C. J., B. J. Shaw, R. D. Handy (2007). "Toxicity of Single Walled Carbon Nanotubes on Rainbow Trout, (Oncorhynchus mykiss): Respiratory Toxicity, Organ Pathologies, and Other Physiological Effects." Aquatic Toxicology, 82: 94–109.

Smith, B., K. Wepasnick, K. E. S., H.-H. Cho, W. P. Ball, D. H. Fairbrother (2009). "Influence of Surface Oxides on the Colloidal Stability of Multi-Walled Carbon Nanotubes: A Structure−Property Relationship." Langmuir, 25(17): 9767–9776.

Sobanska, S., C. Couer, B. Pauwels, W. Maenhaut, F. Adams (2000). "Micro-characterisation of tropospheric aerosols from the Negev Desert, Israel." Journal of Aerosol Science, 31(1): 344-345.

Sondi, I., B. Salopek-Sondi (2004). "Silver nanoparticles as antimicrobial agent: a case study on E-coli as a model for Gram-negative bacteria." Journal of Colloid and Interface Science, 275: 177-182.

Song, X., P. Qu, H.-M. Yang, G.-Z. Qiu (2006). "Synthesis of ZnO doped ceria nanoparticles via azeotropic distillation processing." Transactions of Nonferrous Metals Society of China, 16(1): s350-s355.

Soto, K. F., A. Carrasco, T. G. Powell, L. E. Murr, K. M. Garza (2006). "Biological effects of nanoparticulate materials." Materials Science and Engineering: C, 26(8): 1421-1427.

Spatz, J. P., S. Sheiko, M. Moller, R. G. Winkler, P. Reineker, O. Marti (1995). "Forces affecting the substrate in resonant tapping force microscopy." Nanotechnology, 6: 40-44.

Spence, J. (2002). "Achieving atomic resolution." Materials Today, 5(3): 20-33.

Spohn, P., C. Hirsch, F. Hasler, A. Bruinink, H. F. Krug, P. Wick (2009). "C60 fullerene: A powerful antioxidant or a damaging agent? The importance of an in-depth material characterization prior to toxicity assays." Environmental Pollution, 157: 1134–1139.

Stach, E. A. (2008). "Real-time observations with electron microscopy." Materials Today, 11: 50-58.

Star, A., D. W. Steuerman, J. R. Heath, J. F. Stoddart (2002). "Starched carbon nanotubes." Angewandte Chemie International Edition, 41: 2508–2512.

Stolpe, B., M. Hassellov (2007). "Changes in size distribution of fresh water nanoscale colloidal matter and associated elements on mixing with seawater." Geochim. Cosmochim. Acta, 71: 3292-3301.

Stone, V., B. Nowack, A. Baun, N. van den Brink, F. von der Kammer, M. Dusinska, R. Handy, S. Hankin, M. Hassellov, E. Joner, T. F. Fernandes (2010). "Nanomaterials for environmental studies: Classification, reference material issues, and strategies for physico-chemical characterisation." Science of the Total Environment, 408(7): 1745-1754.

Sugimoto, Y., P. Pou, M. Abe, P. Jelinek , R. Perez, S. Morita, O. Custance (2007). "Chemical identification of individual surface atoms by atomic force microscopy." Nature, 446(7131): 64-67.

Suh, W. H., K. S. Suslick, G. D. Stucky, Y. H Suh (2009). "Nanotechnology, nanotoxicology, and neuroscience." Progress in Neurobiology, 87(3): 133-170.

Sun, X., Y. Li (2005). "Hollow carbonaceous capsules from glucose solution." Journal of Colloid and Interface Science, 291(1): 7-12.

Sun, Y.-P., X.-Q. Li, J. Cao, W.-X. Zhang, H. P. Wang (2006). "Characterization of zero-valent iron nanoparticles." Advances in Colloid and Interface Science, 120(1-3): 47-56.

Sun, H. W., X. Z. Zhang, Q. Niu, Y. S. Chen, J. C. Crittenden (2007). "Enhanced accumulation of arsenate in carp in the presence of titanium dioxide nanoparticles." Water Air Soil Pollut., 178: 245–254.

Sundahl, M., T. Andersson, K. Nilsson, O. Wennerstrom, G. Westman (1993). "Clusters of C60-fullerene in a water solution containing γ-cyclodextrin; A photophysical study." Synthetic Metals, 56(2-3): 3252-3257.

Sung, J. H., J. H. Ji, J. U. Yoon, D. S. Kim, M. Y. Song, J. Jeong, B. S. Han, J. H. Han, Y. H. Chung, J. Kim, T. S. Kim, H. K. Chang, E. J. Lee, J. H. Lee, I. J. Yu (2008). "Lung function changes in Sprague-Dawley rats after prolonged inhalation exposure to silver nanoparticles." Inhalation Toxicology, 20: 567-574.

Swartz, C. H., A. L. Ulery, P. M. Gschwend (1997). "An AEM-TEM study of nanometer-scale mineral associations in an aquifer sand: Implications for colloid mobilization." Geochimica et Cosmochimica Acta, 61(4): 707-718.

Templeton, D. M., F. Ariese, R. Cornelis, L. G. Danielsson, H. Muntau, H. P. Van Leeuwen, R. Lobinski (2000). "Guidelines for terms related to chemical speciation and fractionation of elements. Definitions, structural aspects, and methodological approaches (IUPAC Recommendations 2000)." Pure Appl Chem, 72(8): 1453-1470.

Templeton, R., P. Leeferguson, K. Washburn, W. Scrivens, G. Thomaschandler (2006). "Life-cycle effects of singlewalled carbon nanotubes (SWNTs) on an estuarine meiobenthic copepod." Environ Sci Technol, 40(23): 7387–7393.

TGA (2006). Therapeutic Goods Administration, Department of health and Ageing. "A review of the scientific literature on the safety of nanoparticulate titanium dioxide or zinc oxide in sunscreens."
Available at http://www.tga.govau/npmeds/sunscreen-zotd.pdf.

Thill, A., O. Zeyons, O. Spalla, F. Chauvat, J. Rose, M. Auffan, A. M. Flank (2006). "Cytotoxicity of CeO2 nanoparticles for Escherichia coli, physico-chemical insight of the cytotoxicity mechanism." Environ. Sci. Technol., 40: 6151–6156.

Tiede, K., M. Hassellov, E. Breitbarth, Q. Chaudhry, A. B. A. Boxall (2009). "Considerations for environmental fate and ecotoxicity testing to support environmental risk assessments for engineered nanoparticles." J Chromatogr A, 1216: 503-509.

Tipping, E., C. Rey-Castro, S. E. Bryan, J. Hamilton-Taylor (2002). "Al(III) and Fe(III) binding by humic substances in freshwaters, and implications for trace metal speciation." Geochimica et Cosmochimica Acta, 66(18): 3211–3224.

Tran, P. A., L. Zhang, T. J. Webster (2009). "Carbon nanofibers and carbon nanotubes in regenerative medicine." Advanced Drug Delivery Reviews, 61(12): 1097-1114.

Trouiller, B., R. Reliene, A. Westbrook, P. Solaimani, R. H. Schiestl (2009). "Titanium Dioxide Nanoparticles Induce DNA Damage and Genetic Instability In vivo in Mice." Cancer Res, 69(22): 8784-8789.

Tsoli, M., H. Kuhn, W. Brandau, H. Esche, G. Schmid (2005). "Cellular Uptake and Toxicity of Au55 Clusters." Small, 1(8-9): 841–844.

Tuzen, M., M. Soylak (2007). "Multiwalled carbon nanotubes for speciation of chromium in environmental samples." Journal of Hazardous Materials, 147(1-2): 219-225.

Tykhomyrov, A. A., V. S. Nedzvetsky, V. K. Klochkov, G. V. Andrievsky (2008). "Nanostructures of hydrated C60 fullerene (C60HyFn) protect rat brain against alcohol impact and attenuate behavioral impairments of alcoholized animals." Toxicology, 246(2-3): 158-165.

Van Leer, B., L. A. Giannuzzi (2008). "Advances in TEM Sample Preparation using a Focused Ion Beam." Microsc Microanal, 14(Suppl 2): 380-381.

Van Leeuwen, H. P., R. M. Town, J. Buffle, R. F. M. J. Cleven, W. Davison, J. Puy, W. H. van Riemsdijk, L. Sigg (2005). "Dynamic Speciation Analysis and Bioavailability of Metals in Aquatic Systems." Environ. Sci. Technol., 39(22): 8545–8556.

Verwey, E. J. W., J. T. G. Overbeek (1948). "Theory of the Stability of Lyophobic Colloids." (Elsevier, New York).

Wang, W.-Z., M. L. Brusseau, J. F. Aftiola (1997). "The use of calcium to facilitate desorption and removal of cadmium and nickel in subsurface soils." Journal of Contaminant Hydrology, 25(3-4): 325-336.

Wang, C. T., C.-L. Wu, I-C. Chen, Y.-H. Huang (2005A). "Humidity sensors based on silica nanoparticle aerogel thin films." Sensors and Actuators B: Chemical, 107(1): 402-410.

Wang, X., J. Zhuang, Q. Peng, Y. Li (2005B). "A general strategy for nanocrystal synthesis." Nature, 437: 121–124.

Wang, Y., X. Chen (2007). "Carbon nanotubes: A promising standard for quantitative evaluation of AFM tip apex geometry." Ultramicroscopy, 107(4-5): 293-298.

Wang, X., Q. Li, J. Xie, Z. Jin, J. Wang, Y. Li, K. Jiang, S. Fan (2009). "Fabrication of Ultralong and Electrically Uniform Single-Walled Carbon Nanotubes on Clean Substrates." Nano letters, 9(9): 3137 -3141.

Warheit, D. B., B. R. Laurence, K. L. Reed, D. H. Roach, G. A. M. Reynolds, T. R. Webb (2004). "Comparative Pulmonary Toxicity Assessment of Single-wall Carbon Nanotubes in Rats." Toxicological Sciences, 77: 117–125.

Warheit, D. B. (2006). "What is currently known about the health risks related to carbon nanotube exposures?" Carbon, 44(6): 1064-1069.

Weber, R. J., J. J. Marti, P. H. McMurry, F. L. Eisele, D. J. Tanner, A. Jefferson (1997). "Measurements of new particle formation and ultrafine particle growth rates at a clean continental site." J. Geophys. Res., 102: 4375–4385.

Weber, R. J., P. H. Mcmurry, F. L. Eisele, D. J Tanner (1995). "Measurement of expected nucleation precursor species and 3-500-nm diameter particles at Mauna-Loa-Observatory, Hawaii." Journal of the Atmospheric Sciences, 52(12): 2242-2257.

Wetzig, K., J. Thomas, H. D. Bauer, M. Hecker, A. John (2001). "TEM–EELS investigations of nanoscale multilayers in the linescan mode." Journal of Electron Spectroscopy and Related Phenomena, 114-116: 1019-1023.

Wigginton, N. S., K. L. Haus, M. F. Hochella (2007). "Aquatic environmental nanoparticles." Journal of Environmental Monitoring, 9: 1306-1316.

Wilkinson, K. J., S. Stoll, J. Buffle (1995). "Characterization of NOM colloid aggregates in surface waters: Coupling transmission electron microscopy staining techniques and mathematical modelling." Fresenius J. Anal. Chem., 351: 54–61.

Wilkinson, K. J., E. Balnois, G. G. Leppard, J. Buffle (1999). "Characteristic features of the major components of freshwater colloidal organic matter revealed by transmission electron and atomic force microscopy." Colloids and Surfaces A: Physicochemical and Engineering Aspects, 155(2-3): 287-310.

Wilkinson, K. J., J. R. Lead, Eds. (2007). "Environmental Colloids and Particles: Behaviour, Separation and Characterisation.", Wiley, Chichester, Vol. 10.

Willeke, K., P. A. Baron (eds) (1993). "Aerosol Measurement, Principles, Techniques and Applications." Van Nostrand Reinhold, New York.

Williams, D. B., C. B. Carter (2009). "Transmission Electron Microscopy. A Textbook for Materials Science." Springer US.

Wilson, M. A., L. S. K Pang, G. D. Willett, K. J. Fisher, I. G. Dance (1992). "Fullerenes—preparation, properties, and carbon chemistry." Carbon, 30(4): 675-693.

Worms, I., D. F. Simon, C. S. Hassler, K. J. Wilkinson (2006). "Bioavailability of trace metals to aquatic microorganisms: importance of chemical, biological and physical processes on biouptake." Biochimie, 88: 1721–1731.

Wu, A., Z. Li, L. Yu, H. Wang, E. Wang (2002). "A relocated technique of atomic force microscopy (AFM) samples and its application in molecular biology." Ultramicroscopy, 92(3-4): 201-207.

Wu, W., Q. G. He, C. Z. Jiang (2008). "Magnetic Iron Oxide Nanoparticles: Synthesis and Surface Functionalization Strategies." Nanoscale Research Letters, 3(11): 397-415.

Xiong, Y., Y. Jing, G. Xiaoyu, C. Qianwang (2008). "Synthesis and magnetic properties of iron oxide nanoparticles/C and α-Fe/iron oxide nanoparticles/C composites." Journal of Magnetism and Magnetic Materials, 320(3-4): 107-112.

Xue, C.-H., R. J. Zhou, M. M. Shi, Y. Gao, G. Wu, X.-B. Zhang, H.-Z. Chen, M. Wang (2008). "A green route to water soluble carbon nanotubes and in situ loading of silver nanoparticles." Nanotechnology, 19(32): 325605.

Yabe, S., T. Sato (2003). "Cerium oxide for sunscreen cosmetics." Journal of Solid State Chemistry, 171(1-2): 7-11.

Yadav, B. C., K. Ritesh (2008). "Structure, properties and applications of fullerenes." International Journal of Nanotechnology and Applications, 2(1): 15–24.

Yang, D. Q., J. F. Rochette, E. Sacher (2005). "Functionalization of multiwalled carbon nanotubes by mild aqueous sonication." Journal of physical chemistry. B, 109(16): 7788-7794.

Yang, J., J. Y. Lee, H.-P. Too, G.-M. Chow, L. M. Gan (2006A). "Single stranded DNA stabilization and assembly of Au nanoparticles of different sizes." Chemical Physics, 323(2-3): 304-312.

Yang, K., L. Zhu, B. Xing (2006B). "Adsorption of polycyclic aromatic hydrocarbons by carbon nanomaterials." Environ. Sci. Technol., 40: 1855–1861.

Yang, X. Y., R. E. Edelmann, J. T. Oris (2009). "Suspended C60 nanoparticles protect against short-term UV and fluoranthene photo-induced toxicity, but cause long-term cellular damage in Daphnia magna." Aquatic Toxicology, In Press, Corrected Proof, Available online 1 October 2009.

Yao, X., N. T. Lau, M. Fang, C. K. Chan (2005). "Real-Time Observation of the Transformation of Ultrafine Atmospheric Particle Modes." Aerosol Science and Technology, 39: 831–841.

Yeo, M. K., S. W. Pak (2008). "Exposing Zebrafish to Silver Nanoparticles during Caudal Fin Regeneration Disrupts Caudal Fin Growth and p53 Signaling." Molecular and Cellular Toxicology, 4: 311-317.

Yih, T. C., V. K. Moudgil (2007). "Nanotechnology comes of age to trigger the third industrial revolution." Nanomedicine: Nanotechnology, Biology and Medicine, 3(4): 245.

Yih, T. C., I. Talpasanu (2008). "Micro and Nano Manipulations for Biomedical Applications." Artech House, Norwood, USA.

Yu, M. F., O. Lourie, M. J. Dyer, K. Moloni, T. F. Kelly, R. S. Ruoff (2000). "Strength and Breaking Mechanism of Multiwalled Carbon Nanotubes Under Tensile Load." Science, 287: 637-640.

Zar, J. H. (1999). "Biostatistical Analysis. 4th Edition." Pearson Prentice-Hall, Upper Saddle River, New Jersey 07458.

Zhang, W. (2003). "Nanoscale iron particles for environmental remediation: An overview." Journal of Nanoparticle Research, 5: 323–332.

Zhang, B., M. Cho, J. B. Hughes, J.-H. Kim (2009). "Translocation of C60 from Aqueous Stable Colloidal Aggregates into Surfactant Micelles." Environ. Sci. Technol., 43(24): 9124–9129.

Zhang, H., W. Davison, G. W. Grime (1995). "New In-Situ Procedures for Measuring Trace Metals in Pore Waters." ASTM STP 1293: 170-181.

Zhang, W. X. (2003). "Nanoscale iron particles for environmental remediation: an overview." J. Nanopart. Res., 5: 323–332.

Zhang, L. W., L. Zeng, A. R. Barron, N. A. Montiero-Riviere (2007). "Biological interactions of functionalized single-wall carbon nanotubes in human epidermal keratinocytes." Int J Toxicol, 26: 103-113.

Zhang, L., Q. Q. Ni, Y. Fu, T. Natsuki (2009). "One-step preparation of water-soluble single-walled carbon nanotubes." Applied Surface Science, In Press.

Zhou, Q. X., J. P. Xiao, W. D. Wang (2006). "Using multi-walled carbon nanotubes as solid phase extraction adsorbents to determine dichlorodiphenyltrichloroethane and its metabolites at trace level in water samples by high performance liquid chromatography with UV detection." J. Chromatogr., A 1125: 152–158.

Zhu, Y., W. C. Hinds, S. Kim, S. Shen, C. Sioutas (2002). "Study of ultrafine articles near a major highway with heavy-duty diesel traffic." Atmospheric Environment, 36(27): 4323-4335.

Zhu, S., E. Oberdorster, M. L. Haasch (2006). "Toxicity of an engineered nanoparticle (fullerene, C60) in two aquatic species, Daphnia and fathead minnow." Mar. Environ. Res., 62(Suppl.): S5–S9.

Zhu, X., L. Zhu, Y. Li, Z. Duan, W. Chen, P. J. Alvarez (2007). "Developmental toxicity in zebrafish (Danio rerio) embryos after exposure to manufactured nanomaterials: buckminsterfullerene aggregates (nC60) and fullerol." Environ. Toxicol. Chem., 26: 976–979.